# Monumental olive trees of Lebanon : drought history, pollution traceability and lessons for the future

Nagham Tabaja

# THÈSE POUR OBTENIR LE GRADE DE DOCTEUR DE L'UNIVERSITÉ DE MONTPELLIER ET DE L'UNIVERSITÉ LIBANAIS

**En EERGP- Écologie, Evolution, Ressources Génétique, Paléobiologie**

**École doctorale GAIA-Biodiversite, Agriculture, Alimentation, Environment, Terre, Eau**

**Unité de recherche Institut des Sciences de l'Evolution de Montpellier (ISEM)**

# Monumental olive trees of Lebanon : drought history, pollution traceability and lessons for the future


**Présentée par Nagham TABAJA**


**Le 16 Décembre 2022**


**Sous la direction de Dr. Ilham BENTALEB et Prof. Lamis CHALAK**


**Devant le jury composé de**

| | |
|---|---|
| Mme Magda BOU DAGHER KHARRAT, Professeure, Saint-Joseph University | Rapporteure |
| M. Paolo CHERUBINI, Professeur, WSL Swiss Federal Institute for Forests | Rapporteur |
| Mme Patricia GHANIME, Head of Department of Arts & Archeology, Université Libanaise | Examinatrice |
| Pierre-Olivier Antoine, Professeur, Université de Montpellier | Président/Examinateur |
| Mme Ilham BENTALEB, Professeure Adjoint, Université de Montpellier | Membre invité |
| Mme Lamis CHALAK, Professeure, Université Libanaise | Membre invité |

UNIVERSITÉ DE MONTPELLIER

Université Libanaise
École Doctorale
Sciences et Technologies

UNIVERSITÉ DE MONTPELLIER

**THESE de doctorat en Cotutelle**

Pour obtenir le grade de Docteur délivré par

**L'Université Libanaise**

**L'Ecole Doctorale des Sciences et Technologie**

**Spécialité : Agriculture**

Présentée et soutenue publiquement par

**TABAJA Nagham**

**Le 16 Décembre 2022**

# Monumental olive trees of Lebanon : drought history, pollution traceability and lessons for the future

## Membres du Jury

| | |
|---|---|
| Mme Magda BOU DAGHER KHARRAT, Professeure, Saint-Joseph University | Rapporteure |
| M. Paolo CHERUBINI, Professeur, WSL Swiss Federal Institute for Forests | Rapporteur |
| Mme Patricia GHANIME, Head of Department of Arts & Archeology, Université Libanaise | Examinatrice |
| Pierre-Olivier Antoine, Professeur, Université de Montpellier | Président/Examinateur |
| Mme Ilham BENTALEB, Professeure Adjoint, Université de Montpellier | Membre invité |
| Mme Lamis CHALAK, Professeure, Université Libanaise | Membre invite |

**Acknowledgement**

This PhD thesis is a summary of the work, time and effort carried over the course of four years. It is a sample of my fruitful journey.

I am beyond grateful to have explored this chapter, which was supported by a PhD scholarship from the National Council for Scientific Research of Lebanon and Montpellier University. Also, to the Franco-Lebanese Hubert Curien Partnership (PHC-CEDRE) project 44559PL for the funding provided.

Foremost, I would like to thank my thesis supervisors; Dr. Ilham Bentaleb and Prof. Lamis Chalak, your constant support, wisdom and guidance kept me motivated throughout my thesis. It is under your supervision that I was able to grow on many levels, both professionally and personally. Thank you for sharing your knowledge and awakening my interest and for giving me the opportunity to open the doors to a world of challenges, but also a world of solutions.

I extend my sincere gratitude to all my collaborators, co-authors, and thesis committee members for contributing to this work. Thank you for being an inspiration and a great support.

Furthermore, I would like to thank ISEM at Montpellier University and PRASE at the Lebanese University, led by Dr. Fouad Haj Hassan. Thank you for your constant support of the laboratory work. I warmly thank Mr. R. Geagea, Bchaaleh mayor, and Ms. Mira Khoury, Kawkaba mayor deputy, for the support and hospitality. Both Bchaaleh and Kawkaba have a special and dear place in my heart.

I am extremely thankful to the great support group and new friendships that I made during my journey at Montpellier University. Additionally, a special mention to my friends in my home country, Lebanon. I couldn’t have done it without your continuous motivation and encouraging words.

Also, I would like to express my sincerest gratitude to my family, for whom I dedicate this work to. To my dearest Mom, Dad, and brother, thank you for your unconditional love, endless support and warmest video calls. Thank you for believing in me and for always being there no matter what.

Lastly, thank you Montpellier University for being my home away from home. I am extremely grateful to everyone I crossed path with. I am very much looking forward to my next chapter!

“A little knowledge that acts is worth infinitely more than much knowledge that is idle.” Khalil Gibran

**Table of Contents**

**Table of figures**

**Table of Tables**

## Résumé

**Les anciennes oliveraies du Liban : un des points-chauds du Levant**

Considérés parmi les plus anciens arbres du bassin méditerranéen, les oliviers monumentaux sont présents dans de nombreux pays de la rive orientale de la Méditerranée. Leur longévité témoignant de l'importance historique, culturelle et écologique (Terral et al. 2004; Chalak et al., 2015), questionne sur leur capacité à surmonter des chocs climatiques, environnementaux et anthropiques. Depuis des millénaires comme aujourd'hui, l'olivier est considéré comme élément clé de l'agriculture. Les changements climatiques globaux sont inquiétants dans la rive sud de la Méditerranée surtout en termes de réduction des précipitations. Afin de mieux anticiper leur impact sur les oliviers, il est important de comprendre les adaptations des oliviers actuels et ceux du passé aux sécheresses extrêmes. Cette problématique est bien entendu très complexe et la compréhension des impacts des changements globaux (climats, Homme) sur les oliviers du présent et du passé doit faire appel à différentes disciplines car seule l'approche holistique peut nous laisser espérer comprendre le fonctionnement de ces agro-écosystèmes. Dans le cadre de ma thèse, j'apporte une nouvelle pierre à l'édifice en utilisant des méthodes empruntées à la biogéochimie des isotopes stables et radiogéniques et que j'applique en dendrologie.

Le Levant est aujourd'hui confronté à de nombreux facteurs tels que la croissance démographique, les conflits armés, les caractéristiques géographiques, la transition sociale et économique (Giorgi, 2006; Lange, 2018). L'impact du changement climatique qui se traduit par l'augmentation des vagues de chaleur, la sécheresse, la disponibilité de l'eau et la sécurité énergétique dans les pays du Levant (Giorgi, 2006; Lange, 2018) nous amène à qualifier cette région comme un point chaud du changement climatique ou des changements globaux. Les modèles de climat suggèrent un réchauffement de 3,5°C à 7°C pour la période entre 2070 et 2099, une augmentation de la température diurne et des étés très chauds au milieu et à la fin du 21e siècle (Lange, 2018). Une diminution des précipitations est prévue, avec une baisse de plus de 20% au Liban, en Syrie, à Chypre et en Turquie, alors qu'une augmentation des précipitations est attendue dans la région du Golfe (Lelieveld et al., 2012; Lange, 2018). L'augmentation de la durée de la saison sèche prédite par les modèles, pourrait être responsable de la diminution des zones agricoles, réduisant les pâturages pour les animaux. Ces reconstructions des précipitations sont toutefois caractérisées par une grande incertitude (Telelis, 2000). A ces conditions climatiques inquiétantes, s'ajoutent les changements liés aux pratiques globales (ie. Industrielles, agriculture, utilisation des terres) qui causent des transformations de la qualité de l'air et des écosystèmes terrestres et marins. Compte tenu de cette situation difficile, il est nécessaire de comprendre comment les oliviers qui ont régné au Levant sous différents climats au cours des derniers millénaires (ie. Début de l'Holocène, fin de la période humide Africaine, des évènements d'aridification

autour de 4200 ans BP, période dite de « réchauffement médiéval », ou le « Petit Age de Glace » (Telelis, 2000).

**L'olivier comme indicateur des taxons méditerranéens**

L'olivier (*Olea europea* L.) est considéré comme l'arbre le plus emblématique de la Méditerranée (Besnard et Rubio de Casas, 2016) et l'un des premiers arbres fruitiers à avoir été cultivé par l'homme et utilisé pour ses fruits comestibles et son huile. L'exploitation des oliviers sauvages a commencé avant leur culture comme le suggèrent des morceaux carbonisés de bois d'olivier ou de noyaux d'olives trouvés dans les colonies levantines au moins depuis le Paléolithique (Oflaz et al., 2019), alors qu'ils ont été présents depuis le Néolithique, du Proche-Orient à l'Espagne, et que la domestication a commencé au Proche-Orient il y a environ 6000 ans (Besnard et al., 2013). Fuller, (2018) montre une augmentation du nombre de noyaux d'olives dans le sud du Levant lui permettant d'énoncer l'hypothèse de la domestication de l'olivier à partir de la fin du Néolithique/Calcolithique. Ces données corroborent les résultats de Langgut et al., (2019) obtenues à partir de données palynologiques et archéologiques montrant que le sud du Levant a servi de lieu de domestication et développement de l'horticulture de l'olivier dès ~6500 ans BP. Ces travaux sont corroborés par Langgut & Garfinkel (2022) démontrant que l'horticulture de l'olive (Olea europaea) et de la figue (Ficus carica) était pratiquée dès 7000 ans dans la vallée centrale du Jourdain, en Israël. Ces auteurs suggèrent une gestion précoce des oliviers et qu'ils attachent à la mise en place d'une « économie villageoise méditerranéenne » mettant fin à la période plus ancienne faisant l'usage des produits des oliviers « révolution des produits secondaires ». La domestication de l'olivier en Crête en Mer Egée suivra quelques 500 ans après. À partir de ces zones d'origine, la culture de l'olivier dans le sud du Levant et en Égée s'est répandue dans toute la Méditerranée (Langgut et al., 2019, 2022).

De nombreux oliviers monumentaux ont été étudiés dans la région méditerranéenne pour leur âge et leur résilience au stress climatique. Les oliviers sont connus pour leur adaptation aux conditions extrêmes, leur capacité à pousser sur des sols rocheux et arides, et leur capacité à survivre dans des conditions de sécheresse et de vents forts (Cherubini & Lev-Yadun, 2014; Yazbeck et al., 2018).

Les oliviers sont également connus pour leur tronc creusé dû au pourrissement du bois avec le temps, et des cernes irréguliers et difficilement détectables. De nouveaux troncs peuvent se développer autour de la base de l'arbre d'origine et comme ils grandissent à proximité, une pression physique finira par s'exercer entre eux. Cette pression peut provoquer la rupture de l'écorce, exposant ainsi les cellules vivantes du parenchyme, qui peuvent créer des "ponts tissulaires" pour finalement former un anneau de cambium continu (Ehrlich et al., 2017). La disponibilité en eau a un effet positif sur la taille des vaisseaux et la circonférence dans le bois d'olivier, montrant que le bois initial et le bois final sont détectés dans les arbres pluviaux contrairement aux arbres irrigués (Ehrlich et al., 2017).

**Les oliviers monumentaux au Liban**

Le Liban fait partie de la région du Levant où la culture de l'olivier remonte à une époque ancienne (Mahfoud, 2007). Le pays bénéficie d'un climat méditerranéen modéré et d'abondantes réserves d'eau qui permettent aux oliviers de pousser et de prospérer. Des oliviers centenaires poussent encore dans différentes localités du Liban, témoignant de la longue histoire de cette espèce dans le pays. Certains d'entre eux ont actuellement une importante valeur historique et ornementale et sont déjà classés comme monumentaux. La conservation des oliviers monumentaux libanais devient une tâche prioritaire tandis que des études sont recommandées pour comprendre comment ces arbres ont survécu au cours des siècles à divers stress (Chalak et al., 2015). Les études évaluant les âges des oliviers monumentaux du Liban sont rares. Yazbeck et al. (2018) ont estimé l'âge de certains oliviers centenaires poussant dans le Nord à 1400 ans, mais ont suggéré d'utiliser des méthodes plus adéquates pour estimer l'âge des centenaires libanais.

**Isotopes climatiques et dendrochimie**

Afin de comprendre comment les oliviers ont été affectés par les changements climatiques dans le passé, il faut d'abord comprendre la réaction de ces arbres aux paramètres climatiques au présent. L'analyse des isotopes stables du carbone sur les oliviers peut aider à comprendre la réponse physiologique des oliviers à la variation de la disponibilité en eau, qui serait principalement affectée par le niveau de conductance stomatique et la capacité photosynthétique (Basheer-Salimia et Ward, 2014). Les arbres plus anciens semblent avoir un rapport isotopique différent de celui des plus jeunes, ce qui reflète une adaptation au climat passé qui n'est plus dans la région méditerranéenne (Basheer-Salimia and Ward, 2014). $\delta^{13}C$ et $\delta^{15}N$ dans le feuillage des arbres ont été utilisés afin d'identifier l'efficacité d'utilisation de l'eau. Aussi, les isotopes stables de l'hydrogène et de l'oxygène sont de bons outils pour étudier le chemin de l'eau dans les plantes et pour identifier la source d'eau utilisée par ces plantes (Barbeta et al., 2019; Amin et al., 2021).

En outre, la dendrochimie de certains éléments comme le mercure peut aider à étudier les impacts passés du mercure sur les écosystèmes terrestres et peut également aider à prédire les changements futurs dans le cycle du mercure dans les forêts (Yanai et al., 2020). Les études récentes sur l'absorption du Hg par la végétation ont mis en évidence le rôle important de différents paramètres tels que le déficit de pression de vapeur, la teneur en eau du sol, les conditions climatiques, la date d'échantillonnage, la surface de la masse foliaire, les groupes fonctionnels de l'arbre et la conductance stomatique affectant potentiellement l'absorption par les racines du Hg dissous dans l'eau du sol et le taux d'absorption par les stomates et finalement la teneur en Hg des feuilles (Wohlgemuth et al., 2021). Il est donc important de comprendre le comportement sur place de l'olivier à la pollution par le Hg dans son environnement naturel de culture méditerranéen.

**Estimation de l'âge des oliviers**

L'un des principaux problèmes de la datation à l'aide des cercles d'arbres en Méditerranée est que les arbres ne forment pas toujours des cercles de croissance annuels distincts et peuvent produire des fluctuations de densité intra-annuelles supplémentaires lors de changements de température ou de périodes de sécheresse. La structure anatomique du bois de l'olivier est caractérisée par une disposition diffuse de vaisseaux poreux, ce qui entraîne des limites de cercles de croissance plutôt indistinctes, en plus d'une croissance cambiale asymétrique qui est problématique pour l'identification des cercles annuels (Cherubini et al. 2013; Ehrlich et al. 2017). L'utilisation à la fois de la datation au radiocarbone et l'estimation du nombre de cernes manquants dans la cavité interne du tronc a permis d'estimer les dates de plantation de trois oliviers anciens à Jerusalem autour des années 1200, 1109 et 1184 respectivement (Bernabei, 2015). Plus récemment, Ehrlich et al. (2021) ont pu identifier l'âge d'une branche de bois moderne en combinant la datation au radiocarbone avec l'imagerie micro-CT à haute résolution tout en se référant au bois annuel identifié par le schéma des isotopes stables du carbone (Ehrlich et al. 2021).

## Objectifs de cette étude

Cette étude a été menée sur l'olivier, arbre le plus emblématique de la Méditerranée (Kaniewski et al., 2012 ; Besnard et al., 2013) et composante majeure de l'agriculture d'aujourd'hui et de demain. Il est donc important, non seulement de préserver ce patrimoine, mais aussi de comprendre le comportement sur place de l'olivier aux différents changements environnementaux et climatiques, en se basant sur deux temporalités : étudier le présent pour comprendre le passé qui nous apprendra l'adaptation de cet arbre aux chocs climatiques et anthropiques. La combinaison des différentes méthodologies de cette thèse, la concentration en Hg et l'analyse isotopique (C, N, S, H, O) à différentes méthodes d'études dendrologiques (radiocarbone, microtomographie), a été appliquée sur des oliveraies monumentales libanaises, comme une approche multi-proxy pour mieux comprendre comment ces arbres fonctionnent et construisent leur résilience à différents stress climatiques et environnementaux.

## Principaux résultats

Le chapitre I a introduit les oliviers monumentaux objet de cette étude dans l'oliveraie village de Bchaaleh au Nord Liban, 1300 m a.s.l. et l'oliveraie village de Kawkaba au Sud Liban, 673 m a.s.l., avec les différentes méthodes utilisées dans cette étude, depuis les analyses isotopiques jusqu'à la dendrologie.

**Suivi mensuel des isotopes stables du carbone, azote et souffre des oliviers du Liban**

Le chapitre II étudie la saisonnalité de la concentration en mercure (Hg) du feuillage des oliviers, un arbre emblématique du bassin méditerranéen. Les concentrations de Hg du feuillage, des tiges, de la surface du sol et de la litière ont été analysées mensuellement chez des oliviers centenaires poussant dans deux bosquets au Liban, Bchaaleh et Kawkaba (respectivement 1300 et 672 m a.s.l). Une concentration significativement plus faible a été enregistrée dans les tiges (~7-9 ng/g) par rapport au

feuillage (~35-48 ng/g) dans les deux sites avec la plus forte concentration de Hg dans le feuillage à la fin de l'hiver et au début du printemps et la plus faible en été. Il convient de noter que les olives ont également une faible concentration en Hg (~ 7-11 ng/g). Le sol a la teneur en Hg la plus élevée (~62-129 ng/g) probablement héritée de la biomasse cumulée de la litière (~63-76 ng/g). Une bonne covariation observée entre notre analyse des séries chronologiques de Hg du feuillage et celles des concentrations atmosphériques de Hg disponibles pour le sud de l'Italie dans le bassin ouest de la Méditerranée confirme que la pollution au mercure peut être étudiée à travers les oliviers. L'échantillonnage printanier est recommandé si l'objectif est d'évaluer la susceptibilité de l'arbre à l'absorption de Hg. Notre étude établit une base de référence adéquate pour la Méditerranée orientale et la région avec des inventaires climatiques similaires sur l'absorption de Hg par la végétation. En plus d'être une base de référence pour de nouvelles études sur les oliviers en Méditerranée pour reconstituer les concentrations régionales de pollution au mercure dans le passé et le présent.

Le chapitre III se concentre sur la Méditerranée orientale au Liban. Deux sites d'oliveraies sont l'intérêt principal de notre étude, Bchaaleh au Nord et Kawkaba au Sud. Les techniques isotopiques stables du carbone, de l'azote, du soufre, de l'hydrogène et de l'oxygène dans l'écologie végétale se sont développées au cours des dernières années, servant de technique non radioactive et non destructive importante pour étudier comment les plantes du présent et du passé interagissaient et répondaient aux milieu biotique et abiotique. Afin de comprendre comment nos oliviers ont été affectés par les changements climatiques dans le passé, il faut d'abord comprendre comment ces arbres sont aujourd'hui affectés par les paramètres environnementaux et climatiques. Cette étude est la première à étudier toutes les différentes compositions isotopiques ($\delta^{13}C$, $\delta^{15}N$, $\delta^{34}S$, $\delta D$ et $\delta^{18}O$) chez les oliviers monumentaux. Tout d'abord, il a abordé la façon dont les différentes compositions isotopiques du feuillage, des tiges, de la litière et du sol des oliviers varient entre elles. Deuxièmement, comment les compositions isotopiques du feuillage et $\delta D$, $\delta^{18}O$ des précipitations varient annuellement et saisonnièrement entre Bchaaleh et Kawkaba et entre chaque site étudié. Troisièmement, la réponse du feuillage aux paramètres climatiques en utilisant les différents marqueurs isotopiques stables comme indicateurs du climat.

Dans cette étude, nous pouvons voir que $\delta^{13}C$ dans les deux sites a montré une corrélation entre le feuillage et les tiges, contrairement à $\delta^{15}N$ et $\delta^{34}S$ du feuillage et des tiges qui n'avaient aucune corrélation. Un effet altitudinal est enregistré pour la plupart des compositions isotopiques ($\delta^{13}C$, $\delta^{15}N$, $\delta D$ et $\delta^{18}O$) des tissus végétaux, de la litière et du sol. Alors que $\delta^{34}S$ a montré un effet géologique sur les éléments aériens et souterrains. L'année 2020 à Bchaaleh et Kawkaba a montré des valeurs plus appauvries dans les compositions isotopiques étudiées du feuillage. Tandis qu'une légère saisonnalité est montrée pour les $\delta^{13}C$ et $\delta^{15}N$ du feuillage, et une plus forte saisonnalité pour le feuillage $\delta D$. A Bchaaleh et Kawkaba, les paramètres climatiques variaient dans leur corrélation significative avec les compositions isotopiques du feuillage. $pCO_2$ a montré une corrélation négative avec $\delta^{13}C$ du feuillage, les précipitations ont montré une corrélation négative significative avec $\delta^{15}N$, $\delta^{34}S$ n'a montré aucune

corrélation significative avec aucun des paramètres climatiques, tandis que le feuillage δD à Bchaaleh a montré une corrélation significative avec tous les paramètres climatiques contrairement à Kawkaba. Ces résultats peuvent principalement indiquer que les oliviers étudiés au Liban sont tolérants toute l'année à tous les changements des paramètres climatiques sans être radicalement affectés. En plus de cela, nous pouvons voir que les tiges et le feuillage $\delta^{13}C$ et δD ont une bonne corrélation là où il y a un transport de la composition isotopique du sol vers le feuillage à travers le bois et les tiges et vice versa. Cela peut confirmer que les tiges peuvent nous aider à comprendre le bois des oliviers monumentaux et indique que les noyaux de bois peuvent, espérons-le, être un bon indicateur des données climatiques passées grâce à des études isotopiques. Nous avons également montré dans cette étude que la matière organique en vrac du feuillage, des tiges, de la litière et du sol peut être une technique fiable et moins coûteuse pour récupérer des données sur la saisonnalité et la composition isotopique du feuillage.

Feuillage et tiges de Bchaaleh $\delta^{13}C$ valeurs moyennes (-26.6 ± 0.7 ‰, -25.7 ± 0.9 respectivement) par rapport à celles de Kawkaba (-28.1 ± 1.2 ‰, -26.7 ± 0.6 ‰ respectivement) significativement plus élevées. Pour le feuillage de Bchaaleh, les valeurs moyennes de $\delta^{15}N$ (2.4 ± 1.0 ‰) sont significativement plus élevées par rapport à celles de Kawkaba (0.2 ± 1.2 ‰). Alors que les tiges de Bchaaleh $\delta^{15}N$, les valeurs moyennes (1.5 ± 3.4 ‰) comparées à celles de Kawkaba (5.4 ± 2.8 ‰) sont nettement inférieures. La valeur moyenne $\delta^{34}S$ du feuillage de Bchaaleh (6.2 ± 5.7 ‰) par rapport à celle de Kawkaba (9.9 ± 2.4 ‰) est significativement différente, tandis que les valeurs moyennes de $\delta^{34}S$ des tiges de Bchaaleh (11.3 ± 3.7 ‰) et de Kawkaba (11.4 ± 1.6 ‰) sont similaires. Le feuillage signifie des valeurs de δD et $\delta^{18}O$ à Bchaaleh (-79.7 ± 3.6 ‰ et 26.1 ± 3.3 ‰ respectivement) et Kawkaba (-74.8 ± 4.9 ‰ et 31.2 ± 1.6 ‰) sont significativement différentes, tandis que les tiges signifient des valeurs de δD et $\delta^{18}O$ de Bchaaleh (-69.2 ± 5.9 ‰ et 28.0 ± 7.7 ‰ respectivement) et de Kawkaba (-68.4 ± 4.2 ‰ et 25.3 ± 1.1 ‰ respectivement) ne sont pas significativement différents.

Annuellement, les valeurs annuelles moyennes de $\delta^{13}C$ du feuillage de Bchaaleh et Kawkaba montrent une différence significative entre les années 2019 et 2020 avec des valeurs plus enrichies en 2019 (-26.4 ± 0.8 ‰ et -27.8 ± 1.0 ‰ respectivement) qu'en 2020 (-27.0 ± 0.5 ‰ et – 28.4 ± 1.3 ‰ respectivement). Les valeurs de $\delta^{15}N$ du feuillage à Bchaaleh et Kawkaba ne montrent pas de variations significatives entre les périodes étudiées 2019 (2.5 ± 1,1 ‰ et 0.3 ± 1.0 ‰ respectivement) et 2020 (2.4 ± 0.9 ‰ et 0.07 ± 1.5 ‰ respectivement). La valeur moyenne annuelle du feuillage de Bchaaleh $\delta^{34}S$ a enregistré une différence significative entre 2019 (7.7 ± 7.4 ‰) et 2020 (4.4 ± 1.3 ‰). Les valeurs annuelles moyennes de δD des feuillages de Bchaaleh et Kawkaba n'ont enregistré aucune différence significative entre 2019 (-80.0 ± 3.3 ‰ et -75.3 ± 5.6 ‰ respectivement) et 2020 (-79.2 ± 4.0 ‰ et -74.1 ± 3.4 ‰ respectivement).

**Dendrologie**
**Approche multi-proxy et résultats préliminaires des isotope**

Après ces chapitres centrés sur le présent, le chapitre IV est venu examiner le passé à travers un ensemble de carottes de bois prélevées à l'intérieur des oliviers monumentaux pour évaluer l'âge et les éventuels changements climatiques, en utilisant différentes techniques de dendrochronologie, densitométrie, tomographie à rayons X, datation radiocarbone et analyse isotopique du carbone. L'utilisation de la tomographie à rayons X a permis d'identifier un grand nombre de cernes annuelles dans les carottes échantillonnées, ce qui a facilité la sélection des échantillons pour la datation radiocarbone et l'évaluation des différentes dates en fonction du nombre et de l'orientation des cernes. L'application de la tomographie à rayons X dans le cas de cernes très complexes, comme c'est le cas pour les oliviers, s'est avérée être un grand succès et un pas en avant dans l'identification des cernes de croissance annuelle (bois précoce et tardif). Cette technique a été une clé principale pour comprendre les structures des pièces de bois (différentes branches) et pour la sélection des échantillons de datation radiocarbone. Ainsi, la tomographie à rayons X et le radiocarbone combinés ensemble ont permis d'améliorer nos connaissances sur l'âge des oliviers au Liban. Nos résultats préliminaires du 13C ont montré une variabilité à l'échelle interannuelle. Ces résultats semblent confirmer le potentiel de reconstruction du paléoenvironnement et du paléoclimat à partir des isotopes stables des cernes de croissance de l'olivier, bien que des analyses plus poussées du 13C soient encore nécessaires. Nous avons obtenu un âge minimum plus ancien de 7400 ans BP à partir du bois existant échantillonné sur le tronc de l'un des oliviers monumentaux de KW, et d'environ 1800 ans pour BC. Ces âges devraient être confirmés en élargissant le nombre de carottes analysées par la tomographie à rayons X et le radiocarbone.

## Conclusion

Cette thèse est la première recherche dans la région du Levant rapportant l'utilisation de l'analyse multi-proxies sur les oliviers monumentaux pour comprendre la résilience présente et passée de ces arbres aux stress climatiques et environnementaux dans les conditions agroclimatiques libanaises. Des résultats majeurs ont conclu que les oliviers monumentaux au Liban sont tolérants toute l'année à tous les changements des paramètres climatiques sans être radicalement affectés. D'autre part, la saisonnalité a été enregistrée dans la concentration de Hg du feuillage, tandis que les faibles valeurs de concentration de Hg enregistrées dans les deux sites d'étude confirment l'absence de contamination. En comprenant comment le présent enregistre les compositions isotopiques dans les tissus végétaux, nous pourrions comprendre le passé en étudiant les compositions isotopiques dans le vieux bois. Les analyses de carottes de bois ont indiqué que la tomographie aux rayons X et la datation au radiocarbone sont des proxies complémentaires pour dater les oliviers centenaires indiquant un âge de 7400 avant JC à Kawkaba, ce qui en fait l'âge le plus ancien enregistré a priori dans la région du Levant.

Des recommandations peuvent être considérées comme un pas en avant pour améliorer la compréhension de l'état actuel et passé des oliviers monumentaux, notamment : Poursuivre l'analyse

isotopique sur une plus grande échelle de temps afin de confirmer l'effet du climat sur les différents marqueurs isotopiques ; augmenter la résolution de la datation au radiocarbone en analysant un grand nombre de carottes de bois suffisamment anciennes pour déterminer avec précision l'âge des arbres monumentaux ; augmenter la résolution du $\delta^{13}C$ sur le bois massif afin de permettre l'évaluation de la relation entre la largeur des cernes et le $\delta^{13}C$ et comprendre l'impact des données climatiques sur la croissance des arbres.

**Mots-clés :** Oliviers monumentaux, $\delta^{13}C$, $\delta^{15}N$, $\delta^{34}S$, $\delta D$, $\delta^{18}O$ Hg concentration, Dendrologie, Densitométrie, Tomographie par rayons X, Datation au radiocarbone

# General Introduction

The Mediterranean basin which represents 1.5% of the earth surface is considered one of the hotspots to climate change in the northern hemisphere region (Giorgi, 2006; Tuel and Eltahir, 2020). It is a home to almost all catastrophic issues facing the planet such as global warming, change to soil and vegetation functions, natural risks, change in the water cycle, biodiversity damages and unequal distribution of resources. The Mediterranean was the first to register the greenhouse effect, with scenarios predicting that these changes will continue to exist due to various anthropological pressures (Tuel and Eltahir, 2020).

## Challenges in the Mediterranean basin

The Mediterranean is known to be one of the regions with the strongest human occupation and the oldest too. The region can provide information on the resilience capacity and the ability to take benefit of environmental requirements. Human activities and occupation, in addition to the climate variation caused a degradation in the ecological and biological resources. Due to the intense use of these resources, there was a strong pressure on the hydrological and biogeochemical cycle of the Mediterranean which in return increased to a greater extent the degradation of the environment (Alliance nationale de recherche pour l'environnement and Nations Unies, 2016).

Climatic disasters such as droughts, floods and hurricanes, accompanying the Earth's atmosphere warming shows the need for understanding the future climatic scenarios and its impact on the environment and human (Telelis, 2000). Two recent climatic periods have been of an interest, the Medieval Warm Period (A.D 1000-1200) and the Little Ice Age (A.D 1550-1850) for their relation to modern climatic trends and the response of the societies to the climatic shifts now and in the future. Those two phases build the second millennium A.D background, where the human activity had an effect on the globe and on the ecosystem balance (Wigley et al., 1981; Telelis, 2000). Both physical and anthropogenic data can support the hypothesis that the Eastern Mediterranean and Middle East were also affected by the Medieval Warm Period and the Late Ice Age period (Telelis, 2000).

The different models used to predict the changes in the Mediterranean area during this century suggest an increase of greenhouse gases causing an overall warming in all the seasons in addition to a decrease in the annual precipitation about 20-25 % of winter precipitation which will accentuate the limitation of water resources (Gibelin and Déqué, 2003; Giorgi, 2006; Tuel and Eltahir, 2020). The Mediteranean basin is presently facing important climatic challenges and anthropogenic pressures mainly caused by the increase in temperature. There was a temperature change between 1975-2005 and 2070 - 2100 for the four seasons. Where an increase of up to 3.5 °C over the Eastern sub-basin of the Mediterranean Sea is recorded (Hawkins, 2018; Drobinski et al., 2020). In Lebanon, in the recent years there is a rapid heating. IPCC, 2021 predicts a rise in temperature up to 5 °C by 2100, associated to a decrease in precipitation of about 4% which will be reflected in an increase in drought and water scarcity and food stress and extreme weather events.

## The Levant region as a hot spot

The Levant region (Figure 1) is normally characterized by the importance of its rainfall seasonality. Southern Greece, Libya and the Middle East contributes to an annual total of more than 50% of the winter precipitation. Lebanon, Jordan, Egypt and other countries contributes to 60 to 80% of winter precipitation (Xoplaki, 2002; Lelieveld et al., 2012). Today the Levant is challenged by many factors such as population growth, armed conflicts, geographical characteristics, social and economic transition. The impact of climate change is high due to the increase in heat waves and decline in water availability due to drought (Giorgi, 2006; Lange, 2018). The region is predicted to face climatic changes in the future leading it to be considered as a climate change hot spot on a global scale. This climate change will have an effect on the water availability and energy security in the Levant countries (Giorgi, 2006; Lange, 2018). A strong warming of 3.5°C to 7°C between 2070 and 2099 is expected, with an increase in daytime temperature and very hot summers occurring by the mid and end of the 21$^{st}$ century, while the highest temperature increases are to be in the northeastern Mediterranean countries (Zhang et al., 2005; Lelieveld et al., 2012; Lange, 2018). Also a decrease in the overall precipitation is predicted with more than 20% decrease in Lebanon, Syria, Cyprus and Turkey *vs.* an increase in precipitation expected in the Gulf area (Lelieveld et al., 2012; Lange, 2018). In addition to water scarcity, drying and poor air quality will be prevalent in the Levant (IPCC, 2007; Kitoh et al., 2008; Lelieveld et al., 2012). A decrease in the rainfed agricultural areas will take place, with an increase in dry seasons reducing graze lands for animals (Evans, 2009; Lelieveld et al., 2012). Taking into account this challenging situation, it would be interesting to have a clear understanding of the climatic conditions that revived in the Levant during the Medieval Warm Period and the Late Ice Age (Telelis, 2000).


**Figure 1** Map of the Levant region (Rashid's Blog: An Educational Portal).

## Olive tree as an indicator of the Mediterranean taxa

Olive tree (*Olea europea* L.) has been a big indicator of the expansion of the Mediterranean taxa which is mainly used to define the boundaries of the Mediterranean region (Carrión et al., 2010; Oflaz et al., 2019). It is considered the most iconic tree in the Mediterranean (Besnard and Rubio de Casas, 2016). Cultivated olive trees are an important element in the lives of human race which made it a symbol in the ancient literature and being a controversies subject concerning its origin (Kaniewski et al., 2012; Besnard et al., 2013). Olive is said to be one of the first fruit trees to be cultivated by man and used for its edible fruit and oil although hard to know when its cultivation actually began since it is hard to distinguish between wild and cultivated olive trees (Liphschitz et al., 1991). It is a symbol of the Mediterranean world (Newton et al., 2014). Although there is no specific agreement on the development of the olive cultivation or domestication, botanical data shows archeological evidence since the Bronze age and onwards, where olive has been extensively used and economically significant (Oflaz et al., 2019). Olive is a long lived evergreen that is tolerant to drought, poor soil and salinity stress (Maldonado et al., 2016.; Oflaz et al., 2019). Today it has spread beyond its natural range (altitude, latitude), and its pollen is considered one of the most abundant air-born pollen in the Mediterranean region (Tormo-Molina et al., 2010; Mercuri, 2015; Oflaz et al., 2019). It is assumed that wild olives exploitation began before their cultivation due to the appearance of olive wood charred pieces or olive stones found in the Levantine settlements at least since the Palaeolithic (Oflaz et al., 2019). It is also said that wild olive trees has been there since the Neolithic from the Near East to Spain and the domestication started in the Near East around 6000 years ago (Kaniewski et al., 2012; Besnard et al., 2013). Starting the late Neolithic/Calcolithic, the number of olive stones increased in the southern Levant making the assumption that the olive domestication began afterwards this period (Fuller, 2018; Oflaz et al., 2019). Other studies through genetic evidence showed that the primary domestication in the eastern Mediterranean was on the north-eastern Levant territory on the Syrian-Turkish borders (Besnard et al., 2013; Besnard & Rubio de Casas, 2016; Oflaz et al., 2019). In the Early Bronze age (3300-2200 BCE), timber and olive stones were recorded with higher frequency in the Near East in dry farming regions (Liphschitz et al., 1991). For the northern Levant, there is not much archaeobotanical or archeological or genetic evidence supporting that the olive domestication originated in the eastern Mediterranean, leading to the assumption that before the Bronze age olive had a minor economical and alimentary role (Janick, 2010; de Gruchy et al., 2016; Oflaz et al., 2019). It was also presented that the earliest evidence of table olive production was from the mid 7$^{th}$ millennium BP at the Carmel coast (Galili et al., 2021) . Olive tree is a good indicator of climate change for all the Mediterranean basin due to the good relation between the Mediterranean climate and the olive growing areas, in addition to no existence of any competition with other species and the human role in reducing the time lag between the crop distribution and the spatial changes in climate (Moriondo et al., 2008). Adding to that, in the coming decades the olive is predicted to face much greater climatic changes, yet it is expected to adapt to these changes (Moriondo et al., 2013). During the last two millennia, the olive tree cultivated area changed most

probably due to the climate (Moriondo et al., 2008), where it was observed that with warmer climatic conditions there is an increase in olive tree cultivation. This was noticed for example in Northern Italy, and was also confirmed by the use of fossil pollen data analysis (Neumann, 1985).

Many monumental olive trees have been studied in the Mediterranean region throughout the years for their age and climatic resilience. Olive trees are known for their adaptation to extreme conditions, ability to grow in rocky and arid soil, and ability to survive under drought conditions and strong winds (Cherubini & Lev-Yadun, 2014; Yazbeck et al., 2018). Olive trees are also known for their un-existing pith that rots with time, and irregular and not easily detected tree rings. New trunks may develop around the base of the original tree and as they grow in close proximity, physical pressure will eventually be exerted between them (Lavee, 1996). This pressure can cause bark breakage, exposing live parenchyma cells, which can create "tissue bridges" eventually forming a continuous cambium ring (Ehrlich et al., 2017). Water availability has a positive effect on the vessel size and the girth in olive wood, showing that the earlywood and latewood are detected in rainfed trees unlike in irrigated ones (Ehrlich et al., 2017).

### Monumental olive trees in Lebanon

Lebanon is a part of the Levant region where olive cultivation dates back to an old era (Thalmann, 2000; Beayno et al., 2002; Mahfoud, 2007). The country has a moderate Mediterranean climate and is blessed with plentiful supplies of water that allow olive tree to grow and flourish. Monumental olive trees are still growing in different localities in Lebanon witnessing to the long history of this species in the country. Some of them currently have an important historical and ornamental value and are already classified as monumental (Chalak et al., 2015). Many of them are still producing and exploited for family consumption. Unfortunately, some ancient groves are threatened due to various human pressures particularly to their progressive transformation into new commercial orchards with varieties originating from Greece, Spain and Italy. Hence, the conservation of the Lebanese monumental olive trees become a priority task while studies are recommended to understand how these trees have survived over centuries to diverse stresses (Chalak et al., 2015).

Studies assessing the ages of monumental olive trees of Lebanon are rare. Yazbeck et al. (2018) estimated the age of some centennial olive trees growing in the North to 1400 years, but suggested to further investigate more adequate methods to estimate the age of the Lebanese centennials.

## Integrative methodological approaches

### Hg concentration

The studies of the Hg cycle in forest ecosystems showed that gaseous elemental Hg(0) is the main source taken up by plants (Bishop et al. 2020; Zhou et al. 2021). The atmospheric deposition that has declined in recent decades can be shown in the declining concentration from the older to newer tree rings suggesting a more important uptake through the foliage than the roots. Hg dendrochemistry can help investigate Hg past impacts on terrestrial ecosystems and can also help predict future changes in

the cycle of Hg in forests (Yanai et al., 2020a). The recent studies on Hg uptake by vegetation have highlighted the important role of different parameters as vapor pressure deficit, soil water content, climatic conditions, date of sampling, leaf mass area, tree functional groups, and stomatal conductance affecting potentially the root uptake of Hg dissolved in soil water and the absorption rate via stomata and eventually the Hg leaf content (Rea et al., 2002; Blackwell and Driscoll, 2015; Yang et al., 2018; Wohlgemuth et al., 2021).

It is important to understand the on-site behavior of the olive tree to Hg pollution in its natural Mediterranean growing environment. The Hg source in foliage varies with respect to the amount of contamination. In polluted sites the soil is the main source of Hg, while away from those sites the atmosphere is the most important source (Naharro et al. 2018).

**Isotopic analysis (C, N, S, H, O)**

In order to understand how were olive trees affected by the climatic changes in the past, first it should be understood how are those trees affected today by the climatic parameters. This is usually studied using isotopic analysis of carbon, nitrogen, oxygen, hydrogen, and sulfur which is rarely studied (Amin et al., 2021b). Using stable carbon isotope analysis on olive trees can help understand the physiological response of olive trees to the water availability variation, which is said to be mainly affected by the stomatal conductance level and the photosynthetic capacity (Gonzàlez-Meler et al., 2009; Rossi et al., 2013; Basheer-salimia & Ward, 2014). Older trees seem to have a different isotopic ratio from the younger trees, which reflects an adaptation to the past climate that is no longer in the Mediterranean region (Basheer-Salimia and Ward, 2014). $\delta^{13}C$ and $\delta^{15}N$ in tree foliage have been used in order to identify the water use efficiency. The hydrogen and oxygen stable isotopes are good tools investigating the water pathway in plants and to identify the water source that is used by those plants (Barbeta et al., 2019; Amin et al., 2021b).

**Age estimation of olive trees**

There is a number of methods used around the Mediterranean basin to detect the age of the monumental olive trees, starting with the most classical (dendrochronology) to the newest (densitometry), and moving to the most up to date and effective method (X-ray tomography and radiocarbon dating) (Friedrich et al., 2006; Arnan et al., 2012; Ehrlich et al., 2017; Yazbeck et al., 2018). One main problem for dating using tree rings in the Mediterranean, is that the trees do not always form distinct annual growth rings and may produce extra intra-annual density fluctuation during changes in temperature or drought periods. These conditions lead to the formation of false rings which are mainly common in olive tree rings due to their ability of forming wood after being affected by an induced stress of radial growth(Cherubini & Lev-Yadun, 2014). The wood-anatomical structure of olive trees is characterized by a diffuse porous vessel member arrangement resulting in rather indistinct growth-ring boundaries, in addition to an asymmetric cambial growth which is problematic for identifying the annual rings (Cherubini et al. 2013, Ehrlich et al. 2017). Olive trees in Santorini were sampled and dendrochronology and wood density by Neutron-Imaging Radiography were used and resulted in unsuccessful counting

of tree rings due to their anatomical nature and inability to easily distinguish between the annual growth rings and the false rings (Cherubini et al. 2013).

Eleven samples of radiocarbon were extracted from a cross section of an olive tree in Zippori that was cut down post-mortem in 2013. These samples were visually analyzed for annual rings counting (dendrochronology) and radiocarbon dated at different points, taking into consideration the growth pattern. Multiple piths were identified which indicated a new branching within the same trunk. The cross section was dated to 200 years old which was in agreement with most internal wood radiocarbon dates of living olive trees that was not much older than 300 years. The datable wood of the Zippori tree was not older than 1879 CE (Ehrlich et al., 2017).

The Jerusalem Gethsemane's olive trees age was analyzed and estimated using both radiocarbon dating and the estimation of the number of missing rings from the inner cavity of the trunk. The three ancient dated olive trees were estimated to be planted around the years 1200, 1109 and 1184 (Bernabei, 2015). Modern wood branch was obtained from Zipporini in 2013 and was used for radiocarbon dating, high resolution micro-CT imaging, and $\delta^{13}C$, and was compared with a reference pine species. This analysis confirmed that annual wood is produced by olive trees and that it can be identified by stable carbon isotope pattern (Ehrlich et al. 2021).

## Objectives

Considered among the oldest trees in the Mediterranean basin, monumental olive trees are still growing in many countries along both the eastern and western shore, surviving to various stresses and witnessing the historical, cultural and ecological importance of this tree (Terral et al. 2004; Chalak et al., 2015). Furthermore, the olive tree remains a key component of agriculture today and in the future. Therefore, it is important to understand the present on-site behavior of the olive tree to the different environmental and climatic changes.

This study is conducted in Lebanon, this small country at the Eastern Mediterranean that is facing important anthropogenic pressure within a changing environment (Gérard and Nehmé 2020) and where monumental olive trees are still growing. Our main objective is to understand how are these trees overcoming the climatic, environmental and anthropogenic shocks in order to understand how they faced the past circumstances. The main challenging problematic is the cavity and irregular tree rings of old olive trees requesting the use of multiproxy analysis. Our methodology is based on two timeframes: studying the present to understand the past which will teach us about adaptation of this tree to climatic and anthropogenic shocks. Stable isotopes of carbon, nitrogen, oxygen and hydrogen are used to construct the present climatic and environmental changes recorded by the tree, mercury content is studied to trace the impact of pollution in the trees, X-Ray tomography and radiocarbon dating are used to assess the structure and date the tree rings while dendro-isotopy measurements are considered to assist in reconstructing the dynamics recorded by trees (Figure 2).

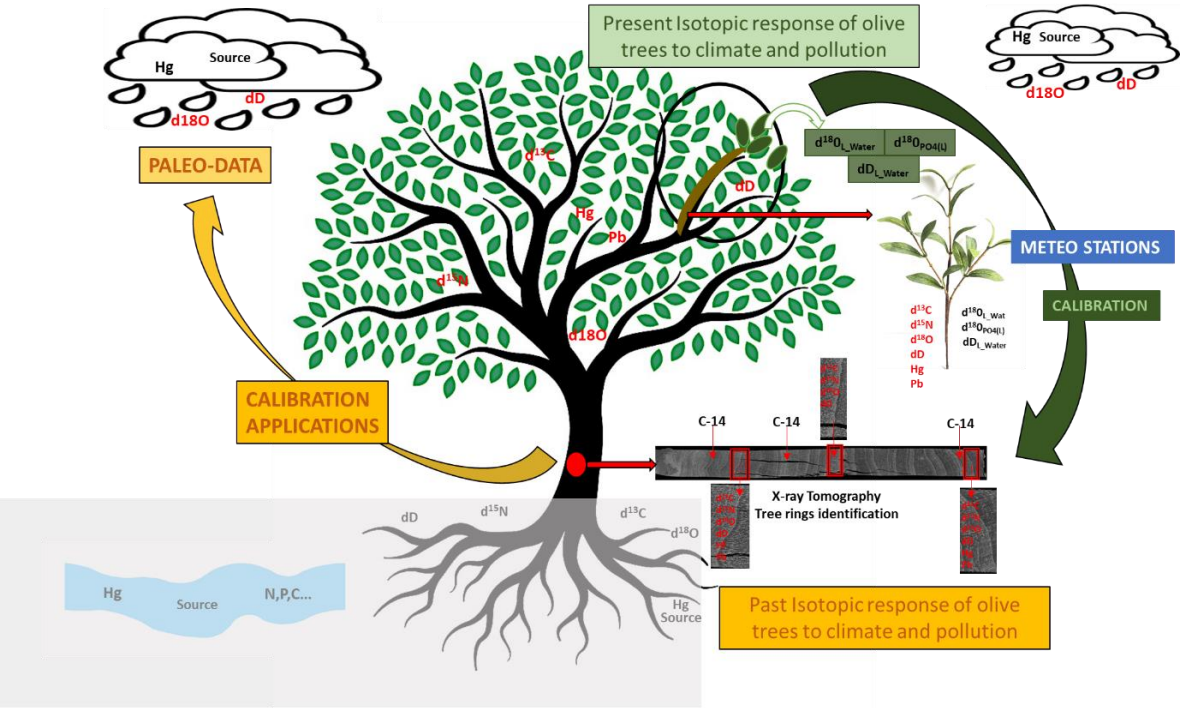


**Figure 2** Scheme showing inter complementarity of the multi proxie approachapplied to the olive tree and their inter-relation with climate and pollution parameters for present and their potential applications for the past.

As to the structure of this manuscript, and after the "Introduction", the manuscript continues with Chapter I which is a general presentation of the "Materials and Methods" where the two study groves sites are described in addition to the different techniques used in the different parts of this study. Then, three chapters are presented in the form of articles followed by a general discussion and conclusion.

Chapter II examines the possible Hg contamination in the two study olive groves sites by following the monthly concentrations variation of Hg during 2019 and 2020 in the foliage and stems of olive trees, soils and litter. The main objectives of this study are to examine and compare Hg levels measured in the foliage, stems, fruits, litter, and soil in each of these two olive groves, which we monitored monthly for 18 months. The second objective is to analyze the relative importance of Hg uptake by the soil and foliage in comparison with the atmospheric mercury.

Chapter III investigates how does the olive tree foliage respond to climatic parameters using C,N,S,H and O stable isotopic markers as indicators of the climate, and how the fractionation of the different isotopic compositions are exchanged between foliage, stems, litter and soil, aiding in grasping the wood isotopic composition to allow studying the wood of monumental olive trees and understand the past. In addition to confirming that bulk dry matter of the plant tissues can be good candidate for less time consuming and cost-effective analysis giving similar and reliable information on foliage and stem isotopic compositions in comparison to cellulose.

Chapter IV studies the wood cores of the monumental olive trees in order to estimate their age and to analyze the possible climatic changes, in addition to comparing the different used techniques and technologies of dendrochronology, densitometry, X-Ray tomography, radiocarbon dating and $\delta^{13}C$ of tree rings.

Chapter V consists of a general discussion and conclusion of the results achieved in the different parts of this thesis with the major outcomes relevant to the Hg concentration and the different isotopic compositions (C, N, S, H and O). Finally, the efficiency of X-Ray tomography along with radiocarbon for dating irregular olive tree rings is discussed and $\delta^{13}C$ of tree rings to understand the past, while recommendations for future steps are formulated.

# Chapter I. General Materials and Methods

## I. Monumental olive groves and sites major characteristics

This study is focusing on two monumental olive groves in Lebanon, where trees are believed to be thousands of years old with respect to their important foot circumference and cavity diameter and also as to the information given by the elderly villagers and municipalities. Bchaaleh monumental trees are called the "sisters" or the Olive trees of Noah with a biblical origin (LEBANONUNTRAVELLED, 2021). Kawkaba with its monumental olive trees, is said to be the land of Christ and his apostles and the prophets (discover Lebanon, 2020). Figure 1a presents the two groves on Lebanon map while Figure 1b and 1c shows an overview of the monumental olive trees considered in the study.

Geologically, Lebanon consists mainly of limestones of Cretaceous origin and Jurassic limestones in some areas. In the North basaltic rocks may appear (Faour, 2004).

Monumental olive groves were targeted for Hg concentration and isotopic analyses in order to understand the climatic and environmental changes registered in the present through the plant tissues (Foliage and stems), soil and litter and the past using the wood cores of the monumental olive trees, in addition to the different dendrology and radiocarbon dating approaches to identify the tree rings and date the monumental olive trees.

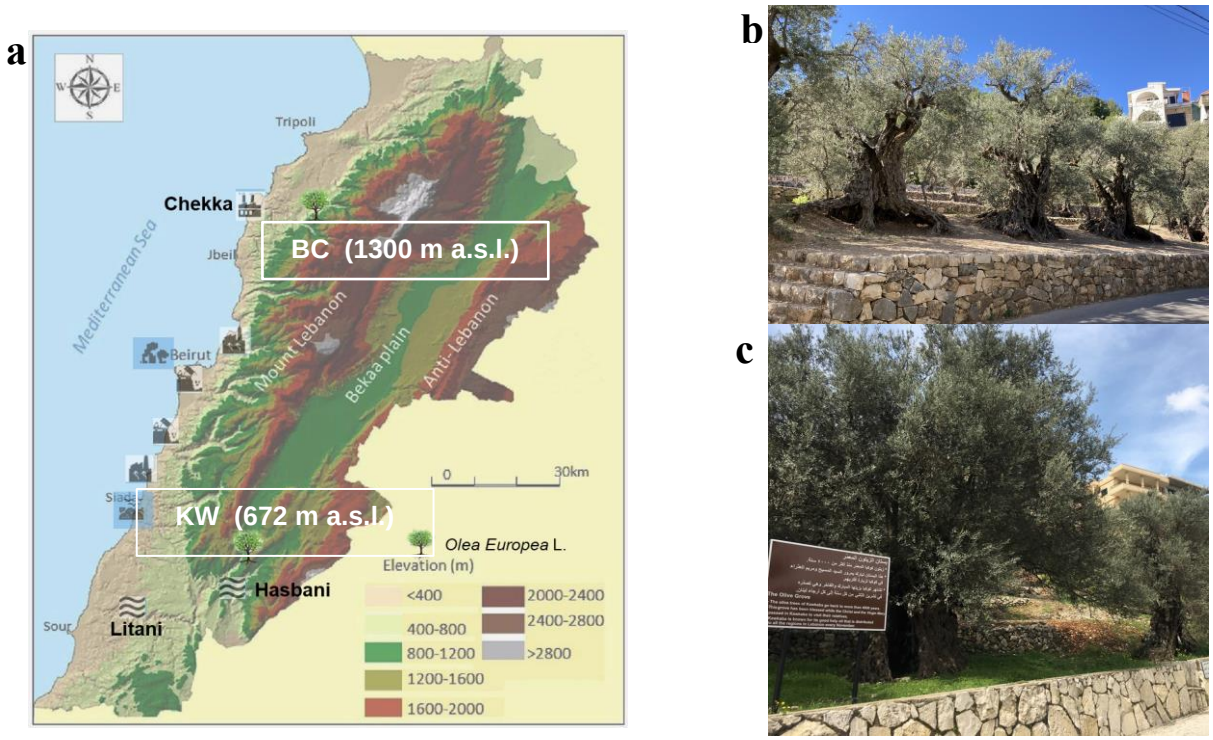


**Figure 1 (a)** Site locations of the two selected focus areas (modified after Shared Water Resources of Lebanon, Nova Science Publishers 2017). (**b)** Bchaaleh (BC) and **(c)** Kawkaba (KW).

**Bchaaleh site- North Lebanon**

Bchaaleh grove is situated in Batroun district with a latitude 34°12'06''N, longitude 35º49'23''E, and altitude of 1300 m a.s.l (Figure 1a). The olive trees are grown in a sandy loam texture soil with grain size analysis of sand, silt, and clay percentages of 52.8%, 38.7%, and 10.7% respectively. The soil pH is 7.07 ± 0.26 with organic matter and calcium. The carbonate contents are 1.7% and 38.3% respectively (Yazbeck et al. 2018). An analysis of the carbon and nitrogen contents in the soil profiles show that organic carbon contents decreased with soil depth from about 4 % at 0-1 cm (Soil surface) to 2.7% at 30-60 cm. The total nitrogen is about 0.3% at 1cm depth and 0.2 % at 30-60 cm depth.

Average precipitation ranged between 0 and 426 mm/year, while the average temperature 4.1 and 24 °C between 2019 and 2021. Relative humidity averaged between 40 and 83% per year between 2019 and 2021 (data extracted from LARI climatic data) (Table 1).

**Kawkaba site - South Lebanon**

KW grove is situated in South Lebanon at latitude 33°23'856''N, longitude 35°38'588''E, altitude 672 m a.s.l. (Figure 1a). The soil is characterized as clay loam with pH of 7.5 ±0.5. Soil organic material and calcium carbonate average are 1.7 % and 59.0 % respectively (Al-Zubaidi et al., 2008). The sand, silt and clay percentage of the grain size analysis are 6%, 28% and 66% respectively. The organic carbon and nitrogen analysis at the 0-1 cm and at 0-30 cm decrease from about 9.0 % to 2.2% and from 0.9 % to 0.3 % for the carbon and nitrogen respectively (Tabaja et al., 2022).

The annual average precipitation from 2019 to 2021 ranges between zero and 398 mm/year while the annual average temperature is between 7 and 27 °C, while annual average relative humidity is between 38 and 81% (data extracted from LARI climatic data) (Table 1).

**Table 1** Study sites geographic location and climatic data collected from the meteo stations installed by LARI.

| Village name | Location (Lebanon) | Latitude (N) | Longitude (E) | Altitude (m.a.s.l) | Temperature min-max (°C) | Annual mean Temperature (°C) | SD (±) | Annual mean rainfall (mm) | SD (±) |
|---|---|---|---|---|---|---|---|---|---|
| **Bchaaleh** | North | 34°12'06″ | 35°49'23″ | 1300 | 4-23 | 14 | 6.81 | 1631 | 110.17 |
| **Kawkaba** | South | 33°23'85″ | 35°38'58″ | 672 | 7-27 | 17 | 6.76 | 1311 | 295.29 |

## II. Trees of the study

A total of 21 olive trees from Bchaaleh were sampled of which 16 are monumental olive trees, three medium young olive size trees measuring up to 1 m and two young olive trees (40-80 cm circumference) from Bchaaleh were selected for sampling. In Kawkaba, a total of 20 olive trees were selected, among

which 16 are monumental olive trees, three medium sized olive trees (40-60 cm circumferance), while only one young olive tree (40 cm circumference) was sampled. In Bchaaleh, Tree 1 to 16 are sampled (BCO1, BCO2, BCO3, BCO4, BCO5, BCO6, BCO7, BCO9, BCO10, BCO11, BCO12, BCO13, BCO14, BCO15, BCO16, BCOY1, BCOY2, BCOY3, BCOY4 and BCOY5; Figure 2a and Table SI 1). In Kawkaba grove, the following trees are sampled (KWO1, KWO2, KWO3, KWO4, KWO4, KWO6, KWO7, KWO8, KO12, KWO13, KWO14 and KWO15, KWO16, KWO17, KWO18, KWO18, KWOY1, KWOY2, KWOY3 and KWOY4; Figure 2b and Table SI 1).

**a**

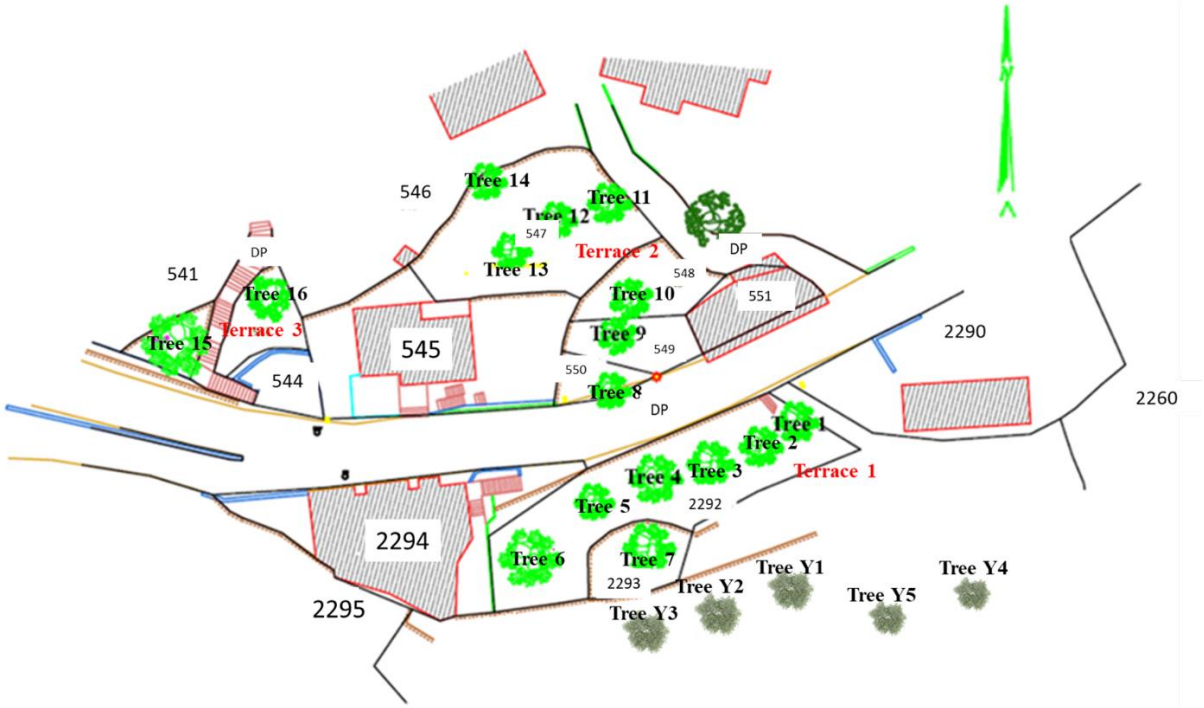


**b**

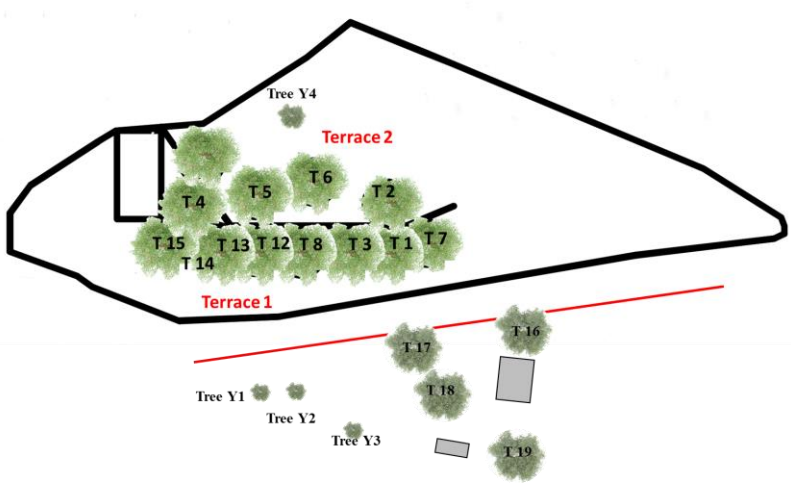


**Figure 2** Map of **(a)** Bchaaleh site and sampled tree locations. Upper terrace plot 2292 are under the endowment of the church. While Lower terrace plot 549 and 547 are a private property. (Y for young trees) **(b)** Map of Kawkaba site and sampled tree locations. (T for Tree, Y for young).

## III. Hg concentration and isotopic analyses

### III.1 Sampling plant tissues, soil, litter and rain

Four trees from each site were selected as a representative of the studied sites. In Bchaaleh, the selected trees were BCO1, BCO4, BCO9 and BCO12 where these trees are spread along the different terraces (Figure 2a). In Kawkaba, the selected trees were KWO1, KWO2, KWO3 and KWO4 (Figure 2b). Foliage, stems and fruits were collected from the trees, while litter and soil were sampled directly under the trees, starting from February 2019 and ending by May 2021. For each monumental olive, both sun exposed and shaded foliage (olive tree bears foliage from three different years) and stems (terminal portions of 20 cm) with no evidence of pathogens were randomly taken and merged from the upper, middle, and lower canopy position of the olive trees on a monthly basis using a manual pruner. The litter and soil surface were separately collected on the whole surface area of the olive groves and stored in different paper bags once every four months (Figure 3). Collected foliage and stems were rinsed with distilled water and then dried for 48 hours in an oven at a temperature of 50°C. The dried foliage, stems, litter, and olive fruits samples were grinded using an electrical stainless grinding machine with no heating system for 5-10 minutes (Figure 4). Soil samples were dried using the same mentioned procedure and prepared with a manual natural agate grinder. All samples were later sieved using an inox stainless-steel 125-micron sieve mesh to collect homogeneous powders for analysis (Pleijel et al., 2021). These samples were used for Hg analysis and isotopic analysis (C,N,S,H and O).

In parallel, soil sampling was performed using a bucket auger to a maximum depth of 60 cm. In both sites, the soil showed uniform color and texture. Soil cores were fractioned in soil surface (0-1 cm), 0 to 30 cm depth and from 30 to 60 cm depth. To avoid contamination, gloves were worn while collecting samples, and the equipment was rinsed with methanol between every sample. Thus, a set of

453 powder samples, prepared for Hg concentration and C,N,S,H and O isotopic analyses were prepared.


**Figure 3** Collected foliage, stems, litter and soil samples from Bchaaleh and Kawkaba olive groves.

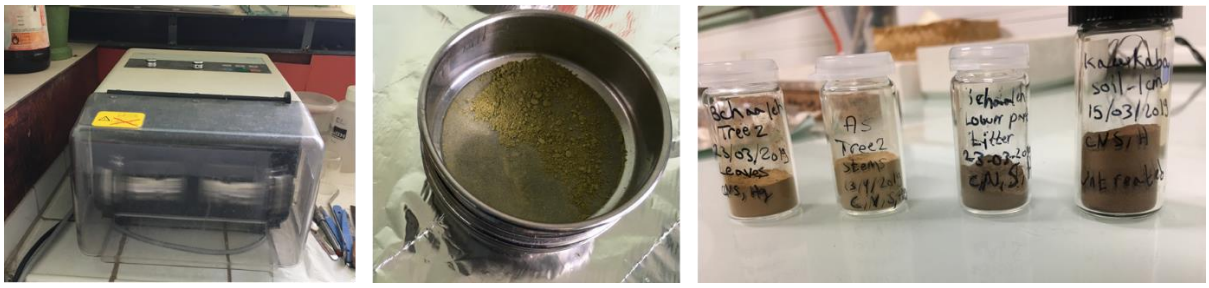

**Figure 4** Sample preparation of foliage, stems, litter and soil for Bchaaleh and Kawkaba.

As for rain collection, a specific collector was installed underground in Bchaaleh and Kawkab to be able to collect rainwater from both sites during raining seasons that ranges between November and May for the three-year study (2019-202)1. The collector was filled with paraffin in order to separate the water from any other elements inside the collector and during the sampling. A duplicate for oxygen and hydrogen samples were collected in a 5ml bottle. These samples where then sealed using parafilm and stored at a temperature of 4°C.

### III.2 Analytical method for Hg analysis

A total of 150 mg for dried grinded foliage and soil (50 mg/analysis), and 300 mg of litter and stems (100 mg/analysis) were considered in triplicates for the analysis of Hg concentration. Hg elemental analysis was performed using an advanced Hg analyzer AMA 254 (Altec) as described in previous works (Barre et al. 2018; Duval et al. 2020). An amount of 50 to 100 mg is weight using a nickel boat and a $10^{-6}$ g precision balance was used. Samples are first dried for 60 seconds at 120°C and thereafter pyrolyzed for 150 seconds at 750°C, under oxygen flow. The resulting gaseous Hg produced during the sample decomposition is amalgamated on a gold trap and then released to an Atomic Absorption spectrometer after a thermal desorption step at 950°C (Figure 5). The AMA 254 instrument was calibrated using several external matrix-matched calibration procedures using the following certified

reference materials: IAEA-456 sediment (77 ± 5 ng/g), NIST-1575A pine needles (39,9 ± 0,7 ng/g) and IAEA336 (200 ± 40 ng/g). The QA/QC evaluation of the analytical procedure was completed after every 15 analyzed samples, using a continuous monitoring of the blank's values (Nickel boat Hg background noise). The measurement precision was assessed using replicated analyses (n=2) of 13% of the total amount of samples (n=453). Average relative standard deviations of 5% and 2.5% are thus associated to the reported Hg concentrations for the 2019 and 2020 samples batches, respectively. The detection limit of the analytical method has been assessed to 0.7 ng/g, for analytical sessions.

**Figure 5** Advanced mercury analyzer AMA 254 at (IPREM).

### III.3 Isotopic analysis

Soil samples were decarbonated overnight using HCL 0.5 ml followed by a second overnight treatment with HCL 0.1 ml then rinsed five times using distilled water before being dried in oven for 48 hours at 50°C, grind again and seized into 125-micron mesh.

Powder samples of 2 mg foliage and stems and 5 mg of decarbonated soil and litter powders were weighed into tin capsules and then sent to LEHNA to be measure C,N,S by dry combustion in Pyrocube Elemental Analyser (EA, Elementar GmbH) connected on line in continuous flow mode to an Isoprime 100 IRMS (Elementar) (Figure 6), and following the analytical approach of Fourel et al., (2014).

Data for soil C and N content and isotopic ratio of carbon were calibrated against international reference material IAEA-601. $\delta^{13}C$ values are expressed in δ notation, deviation from standards in parts per thousand (‰), relative to Vienna Pee Dee Belemnite (V-PDB), using the conventional delta (δ) notation: δ (‰) = [(Rsample/Rstandard) – 1] x 1000, where R sample and R standard are the 13C/12C ratios of the sample and standard, respectively. Results of elemental analysis are expressed as C, and N,S in % and C/N ratios.

For O and H isotopic analysis, samples of 2 mg bulk, foliage, stems, soil and litter powders into tin capsules were sent to LEHNA for the measurement of the oxygen and hydrogen stable isotope ratio,

using an Isoprime 100 isotopic mass spectrometer (IRMS). Four international standards were used giving a precision for δD better than 0.73‰ (B2203, B2205, IAEA 601 and IAEA CH7).

Rainwater collected samples were analyzed at ECOTRON using A Picarro L2140i laser spectrometer as well as Delta V Plus IRMS to access δD values of liquid water. Hydrogen stable isotopic in rain water was analyzed using $\delta D = [(2H/1H_{sample})/(2H/1H_{standard}) - 1] * 1000$ (Edwards & Vandenabeele, 2016).

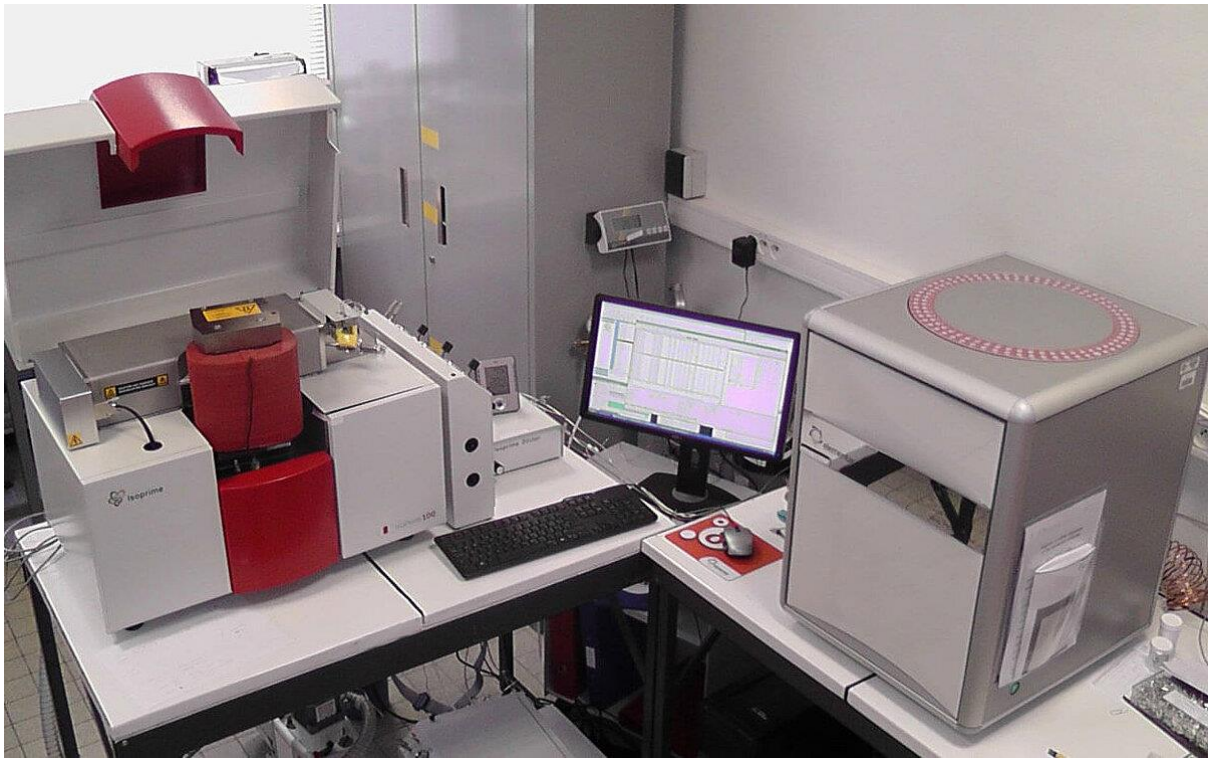

**Figure 6** Isoprime 100 IRMS (Elementar).

## IV. Dendrology analyses

### IV.1 Wood collection

Monumental olive trees were sampled in both Bchaaleh and Kawkaba. Additionally, olive trees of 80-100 years old (according to the owners), growing in young plantations next to the ancient groves, were also considered in both sites. Olive tree's wood coring was conducted in March - May 2019. A coring strategy was designed using an electric drill (Bosch GSB 18 VE-2-LI Combi Drill with two batteries) with a mech of 22 cm length and diameter of 0.7 cm diameter which is a non-destructive sampling method (Tenzin & Dukpa, 2017). The sampling was based on the accessibility through the tree and the visual investigation of the wood anatomy and potential core depth from the inner to the outer side of the tree for trees with accessible cavity. Trees with no direct access to the cavity were sampled from the outside of the trunk towards the center of the tree. About three to six cores per tree were taken in different positions. For monumental trees, three main cores were taken in positions to be accessible and

continues in terms of the width of the available trunk with a duplicate of each of these three main samples taken right above or under the main core in order to widen the precision of the collected data and overlapping of rings. While from younger olive trees three cores were sampled covering the full trunk, at breast height from the trunk towards the center of the tree. A total of 216 cores were collected from 32 monumental olive trees and nine young trees (Figure 7).


**Figure 7** Wood core sampling using electrical driller.

Wood cores are fragile and need to be handled carefully. Before pulling the sample out of the mesh, a piece of paper is prepared to place the core slowly and carefully when extracted from the mesh. After the extraction, the core is left to dry in case of any moist, the cores are then inserted and secured in a transparent straw, closed and labelled with the necessary information to represent the core. Label includes the site name, tree number and core number, the length of the core, the bark and center side, in addition to the collection date (Dendro Manual., 2003.) The location of the sampled core is labelled on the tree to be able to go back to the source of the core. The opening is closed using an organic wax to protect the tree from any infection. Wood samples preparation was dependent on the analysis procedure and technique used.

### IV.2 Dendrology methods for dating and ring identification

A multi-proxy analysis was done to study the wood cores tree rings, dating the monumental olive trees and understanding the past climate.

**X-Ray tomography**. This technique was used, in a non-destructive way, using an EasyTom 150KV machine core at ISEM plateform. Thirty-one wood cores with 9 to 22 cm length and 0.7 cm width were selected from 13 trees in Bchaaleh and 11 trees in Kawkaba (Figure 8a). For data analysis, “Xact” was used for the tomographic reconstruction in order to have an image post processing which help us do corrections for our samples such as bad pixels, contrast, geometry form and 3D optimization of the reconstruction volume. This was followed by FIJI/IMAGESJ for complete reconstruction of the X-

rayed images tree rings for the best ring detection, counting and width measurements depending on the late and earlywood boundaries.

**Densitometry.** This technique required a first treatment of the samples for microdensitometer analysis, a very time-consuming step and destructive for the wood cores, where cores were cut with a double-bladed saw to a thickness of 1.4 mm to be scanned. Two olive cores, one from Bchaaleh and the other from Kawkaba with a length of 7 cm for the first and 14.4 cm for the second (Figure 8b)**,** afterwards, the rings were identified and rings width were measure.

**Dendrochronology**. This required a wood base to support the wood core and a sanding machine (Seheppach bsm 2000) and three sand papers (300, 600, 1000nm) to get a good visual ring detection. Three cores from Bchaaleh site were selected for the trial of this method, including two young and one monumental olive wood core of length ranging between 19 and 21 cm (Figure 8c). Microscopic and Coorecorder were used for tree ring reading and double checking to ensure the correct results of the ring detection and counting, followed by TSAP-win and COFECHA programs.

**Radiocarbon dating ($^{14}$C).** Five wood core samples of 10 mg each were prepared using a manual cutting blade, a microtome machine with a resolution of 11 µg and an electrical driller depending on the accessibility of the core length (Figure 8d). The samples are sent to the Carbon 14 Measurements Laboratory (LMC14) that performs measurements of $^{14}$C using accelerator mass spectrometry (SMA ARTEMIS) (Figure 8e). The samples are transformed into $CO_2$ gas and transported in sealed tubes. The raw form is mechanically or chemically treated in the laboratory to remove any contaminations. Afterwards, the carbon is extracted in $CO_2$ form (LMC14, n.d.). For radiocarbon data analysis, the OxCal 4.4 Project program was used to calibrate the results of C14 dates retrieved. This program used for application has different ranges of chronological research, it performs simple calculations on ordinary numbers and on different parameters such as R_Date function that calibrates the radiocarbon dates.

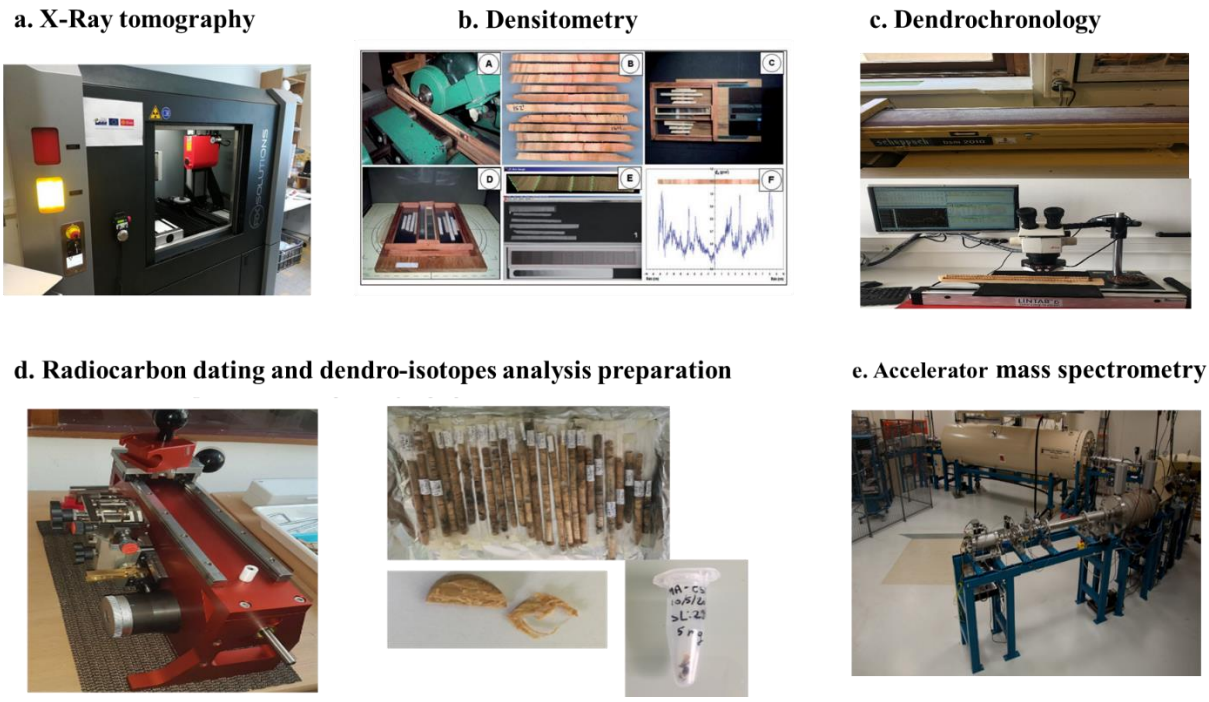


**Figure 8** multi-proxy analysis and dendrositopes for dating and studying the climatic and environmental data on tree rings using **(a)** X-Ray tomography, **(b)** Densitometry, **(c)** Dendrochronology, **(d)** Radiocarbon dating and dendro-isotopes analysis preparation, **(e)** Accelerator mass spectrometry.

**Dendro-isotopes**. Wood rings from the monumental olive trees in Bchaaleh (BCO4.4 and BCO9.1D) were cut using the microtome machine with 20 µg resolution to extract samples used for a high resolution isotopic analysis of Carbon with a weight ranging between 1-2 mg (Figure 8d) in order to analyse the climatic and environmental data in the past using the Isoprime 100 IRMS (Elementar).This approach will allow to compare the past climatic and environmental data and compare it to the present isotopic data extracted for plant tissues.

## Supplimentary Information

**Table SI 1** Bchaaleh and Kawkaba sampled trees, age class and cored samples.

| **Site** | **Bchaaleh** | **Olive** | **Altitude** | **1300 m a.s.l.** |
|---|---|---|---|---|
| **Tree no.** | **Core reference no.** | **Height core position (cm)** | **Length of Core (cm)** | **Age class** |
| **Tree 1** | O1.1 | 60 | 10.2 | Monumental |
| | O1.1D | 64 | 10.5 | |
| | O1.2 | 70 | 15.6 | |
| | O1.2D | 64 | 17.3 | |
| | O1.3 | 56 | 7.9 | |
| | O1.3D | 72 | 9.5 | |
| | | | | |
| **Tree 2** | O2.1 | 147 | 9.6 | Monumental |
| | O2.1D | 143 | 11.2 | |
| | O2.2 | 127 | 11.8 | |
| | O2.2D | 119 | 7 | |
| | O2.3 | 73 | 15.8 | |

| | | | | |
|---|---|---|---|---|
| | O2.4 | 133 | 6.8 | |
| | | | | |
| **Tree 3** | O3.1 | 55 | 7.1 | Monumental |
| | O3.1D | 57 | 11.3 | |
| | O3.2 | 140 | 8.4 | |
| | O3.2D | 143 | 12 | |
| | O3.3 | 141 | 18 | |
| | O3.3D | 148 | 13.7 | |
| | | | | |
| **Tree 4** | O4.1 | 124 | 19.5 | Monumental |
| | O4.1D | 132 | 14.8 | |
| | O4.2 | 132 | 11.4 | |
| | O4.3 | 105 | 5.5 | |
| | O4.3D | 110 | 13 | |
| | O4.4 | 124 | 17.4 | |
| | | | | |
| **Tree 5** | O5.1 | 40 | 7.7 | Monumental |
| | O5.1D | 47 | 6.3 | |
| | O5.2 | 90 | 7.9 | |
| | O5.2D | 95 | 9.4 | |
| | O5.3 | 24 | 8.8 | |
| | O5.3D | 43 | 10.3 | |
| | | | | |
| **Tree 6** | O6.1 | 28 | 12 | Monumental |
| | O6.1D | 35 | 10.8 | |
| | O6.2 | 40 | 3.9 | |
| | O6.2D | 37 | 6 | |
| | O6.3 | 100 | 17.2 | |
| | O6.3D | 106 | 12.5 | |
| | | | | |
| **Tree 7** | O7.1 | 115 | 3.5 | Monumental |
| | O7.1D | 97 | 9.4 | |
| | O7.2 | 94 | 15.1 | |
| | O7.2D | 74 | 6.2 | |
| | O7.3 | 60 | 11 | |
| | O7.3D | 75 | 13.9 | |
| | | | | |
| **Tree 8** | O8.1 | 117 | 8.2 | Monumental |
| | O8.1D | 105 | 9.4 | |
| | O8.2 | 104 | 18.3 | |
| | O8.2D | 105 | 15.7 | |
| | O8.3 | 120 | 12.5 | |
| | O8.3D | 107 | 12.6 | |
| | | | | |
| **Tree 9** | O9.1 | | 12.5 | Monumental |
| | O9.1D | 120 | 12.2 | |
| | O9.2 | 130 | 12.6 | |
| | O9.2D | 120 | 8 | |
| | O9.3 | 40 | 9.4 | |
| | O9.3D | 50 | 6.1 | |
| | | | | |
| **Tree 10** | O10.1 | 63 | 6.9 | Monumental |
| | O10.1D | 70 | 6.1 | |
| | O10.2 | 112 | 13 | |
| | O10.2D | 117 | 18 | |
| | O10.3 | 67 | 12.7 | |

| | | | | |
|---|---|---|---|---|
| | O10.3D | 65 | 16.8 | |
| | | | | |
| **Tree 11** | O11.1 | 105 | 17.8 | Monumental |
| | O11.1D | 110 | 18 | |
| | O11.2 | 175 | 16 | |
| | O11.2D | 180 | 15.8 | |
| | O11.3 | 150 | 12.6 | |
| | O11.3D | 130 | 10.5 | |
| | | | | |
| **Tree 12** | O12.1 | 35 | 11 | Monumental |
| | O12.1D | 30 | 9.8 | |
| | O12.2 | 50 | 17.1 | |
| | O12.2D | 45 | 10 | |
| | O12.3 | 130 | 17.9 | |
| | O12.3D | 122 | 15.5 | |
| | | | | |
| **Tree 13** | O13.1 | 60 | 15.1 | Monumental |
| | O13.1D | 56 | 10.2 | |
| | O13.2 | 55 | 9.2 | |
| | O13.2D | 40 | 16.8 | |
| | O13.3 | 145 | 13.5 | |
| | O13.3D | 140 | 12.3 | |
| | | | | |
| **Tree 14** | O14.1 | 80 | 17 | Monumental |
| | O14.1D | 86 | 12.3 | |
| | O14.2 | 38 | 16.3 | |
| | O14.2D | 46 | 11.8 | |
| | O14.3 | 78 | 11.8 | |
| | O14.3D | 70 | 14.1 | |
| | | | | |
| **Tree 15** | O15.1 | 53 | 13.2 | Monumental |
| | O15.1D | 55 | 10.5 | |
| | O15.2 | 57 | 16.2 | |
| | O15.2D | 56 | 17.8 | |
| | O15.3 | 110 | 17.2 | |
| | O15.3D | 97 | 15.2 | |
| | | | | |
| **Tree 16** | O16.1 | 57 | 17.9 | Monumental |
| | O16.1D | 56 | 14.8 | |
| | O16.2 | 125 | 16.7 | |
| | O16.2D | 130 | 13 | |
| | O16.3 | 55 | 15.4 | |
| | O16.3D | 50 | 16.3 | |
| | | | | |
| **Tree 1** | YO1.1 | 94 | 18.4 | Medium |
| | YO1.2 | 90 | 20.5 | |
| | YO1.3 | 77 | 16.2 | |
| | | | | |
| **Tree 2** | YO2.1 | 70 | 21.2 | Medium |
| | YO2.2 | 75 | 19.8 | |
| | YO2.3 | 62 | 17.3 | |
| | | | | |
| **Tree 3** | YO3.1 | 75 | 17 | Medium |
| | YO3.2 | 85 | 15.2 | |
| | YO3.3 | 88 | 19 | |
| | | | | |

| | | | | |
|---|---|---|---|---|
| **Tree 4** | YO4 | 20 | 16 | Young |
| | | | | |
| **Tree 5** | YO5 | 20 | 19 | Young |

| **Site** | **Kawkaba** | **Olive** | **Altitude** | **672 m a.s.l.** |
|---|---|---|---|---|
| **Tree no.** | **Core reference no.** | **Height core position (cm)** | **Length of Core (cm)** | **Age class** |
| **Tree 1** | O1.1 | 60 | 21.5 | Monumental |
| | O1.1D | 55 | 15.8 | |
| | O1.2 | 73 | 14.4 | |
| | O1.2D | 72 | 10.6 | |
| | O1.3 | 103 | 12.9 | |
| | O1.3D | 100 | 14 | |
| | | | | |
| **Tree 2** | O2-Trial | 100 | 2.3 | Monumental |
| | O2.1 | 100 | 6.5 | |
| | O2.2 | 93 | 9.7 | |
| | O2.2D | 103 | 12.8 | |
| | O2.3 | 130 | 10.9 | |
| | O2.3D | 135 | 3.5 | |
| | O2.4 | 130 | 18 | |
| | O2.4D | 125 | 13 | |
| | | | | |
| **Tree 3** | O3.1 | 90 | 17.3 | Monumental |
| | O3.1D | 80 | 17.4 | |
| | O3.2 | 102 | 16.3 | |
| | O3.2D | 98 | 13.1 | |
| | O3.3 | 70 | 20.5 | |
| | O3.3D | 69 | 6.8 | |
| | | | | |
| **Tree 4** | O4.1 | 60 | 17.3 | Monumental |
| | O4.1D | 55 | 5.6 | |
| | O4.2 | 40 | 16.2 | |
| | O4.2D | 37 | 11.7 | |
| | O4.3 | 114 | 13.1 | |
| | O4.3D | 110 | 8.5 | |
| | | | | |
| **Tree 5** | O5.1 | 143 | 13.7 | Monumental |
| | O5.1D | 135 | 9.5 | |
| | O5.2 | 131 | 13.8 | |
| | O5.2D | 127 | 18.6 | |
| | O5.3 | 108 | 16.5 | |
| | O5.3D | 98 | 15.7 | |
| | | | | |
| **Tree 6** | O6.1 | 110 | 11.7 | Monumental |
| | O6.1D | 98 | 16.2 | |
| | O6.2 | 130 | 8.5 | |
| | O6.2D | 124 | 11.6 | |
| | O6.3 | 76 | 12.5 | |
| | O6.3D | 70 | 15.7 | |
| | | | | |
| **Tree 7** | O7.1 | 57 | 16.1 | Monumental |
| | O7.1D | 63 | 16.9 | |
| | O7.2 | 105 | 11.5 | |

| | | | | |
|---|---|---|---|---|
| | O7.2D | 100 | 5.5 | |
| | O7.3 | 130 | 10.6 | |
| | O7.3D | 127 | 18.2 | |
| | | | | |
| **Tree 8** | O8.1 | 114 | 19.5 | Monumental |
| | O8.1D | 108 | 18 | |
| | O8.2 | 98 | 20.3 | |
| | O8.2D | 90 | 18 | |
| | O8.3 | 103 | 12 | |
| | O8.3D | 95 | 13.6 | |
| | | | | |
| **Tree 12** | O12.1 | 24 | 17.3 | Monumental |
| | O12.1D | 30 | 15.2 | |
| | O12.2 | 120 | 4 | |
| | O12.2D | 140 | 8.8 | |
| | O12.3 | 130 | 12.3 | |
| | O12.3D | 115 | 13.5 | |
| | O12.4 | 120 | 10 | |
| | | | | |
| **Tree 13** | O13.1 | 126 | 14.7 | Monumental |
| | O13.1D | 122 | 14.8 | |
| | O13.2 | 138 | 5.9 | |
| | O13.2D | 135 | 9.2 | |
| | O13.3 | 138 | 19 | |
| | O13.3D | 129 | 13.3 | |
| | | | | |
| **Tree 14** | O14.1 | 70 | 17.5 | Monumental |
| | O14.1D | 74 | 12.3 | |
| | O14.2 | 108 | 19.7 | |
| | O14.2D | 101 | 15.3 | |
| | O14.3 | 122 | 10.5 | |
| | O14.3D | 118 | 9.5 | |
| | | | | |
| **Tree 15** | O15.1 | 115 | 7.4 | Monumental |
| | O15.1D | 108 | 16.3 | |
| | O15.2 | 111 | 17.4 | |
| | O15.2D | 106 | 19 | |
| | O15.3 | 108 | 17.5 | |
| | O15.3D | 105 | 16.8 | |
| | | | | |
| **Tree 16** | O16.1 | 50 | 16.7 | Monumental |
| | O16.1D | 47 | 18 | |
| | O16.2 | 70 | 16.5 | |
| | O16.2D | 63 | 20.2 | |
| | O16.3 | 87 | 18 | |
| | O16.3D | 91 | 14.3 | |
| | | | | |
| **Tree 17** | O17.1 | 83 | 20.5 | Monumental |
| | O17.1D | 84 | 15 | |
| | O17.2 | 103 | 10.5 | |
| | O17.2D | 95 | 20 | |
| | O17.3 | 112 | 18.3 | |
| | O17.3D | 106 | 10.6 | |

| | | | | |
|---|---|---|---|---|
| **Tree 18** | O18.1 | 85 | 20 | Monumental |
| | O18.1D | 78 | 13.9 | |
| | O18.2 | 95 | 21 | |
| | O18.2D | 88 | 20 | |
| | O18.3 | 60 | 20 | |
| | O18.3D | 54 | 19 | |
| | | | | |
| **Tree 19** | O19.1 | 67 | 15.8 | Monumental |
| | O19.1D | 68 | 20 | |
| | O19.2 | 80 | 19.5 | |
| | O19.2D | 73 | 20 | |
| | O19.3 | 58 | 20.6 | |
| | O19.3D | 50 | 21 | |
| | | | | |
| **Tree 1** | YO1.1 | 75 | 9.5 | Medium |
| | YO1.2 | 68 | 20 | |
| | YO1.3 | 42 | 17.5 | |
| | | | | |
| **Tree 2** | YO2.1 | 55 | 15.8 | Medium |
| | YO2.2 | 62 | 12.4 | |
| | YO2.3 | 82 | 18.2 | |
| | | | | |
| **Tree 3** | YO3.1 | 70 | 14.9 | Medium |
| | YO3.2 | 70 | 20 | |
| | YO3.3 | 71 | 19.5 | |
| | | | | |
| **Tree 4** | YO4 | 20 | 12.2 | Young |

Biogeosciences, 20, 619–633, 2023 https://doi.org/10.5194/bg-20-619-2023 

## Chapter II: Seasonal variation of mercury concentration of ancient olive groves of Lebanon.

Nagham Tabaja[1,2,3], David Amouroux[4], Lamis Chalak[2], François Fourel[5], Emmanuel Tessier[4], Ihab Jomaa[6], Milad El Riachy[7], Ilham Bentaleb[1]

[1] ISEM, Université de Montpellier, CNRS, IRD, Montpellier, France
[2] Faculty of Agronomy, Plant Production Department, The Lebanese University, Dekwaneh, Lebanon
[3] Plateforme de Recherche et d'Analyses en Sciences de l'Environnement (PRASE), Ecole Doctorale de Sciences et Technologie, Université Libanaise, Hadath, Liban
[4] Université de Pau et des Pays de l'Adour, E2S/UPPA, CNRS, Institut des Sciences Analytiques et de Physico-Chimie pour l'Environnement et les Matériaux (IPREM), PAU, France
[5] UMR CNRS 5023 LEHNA, Université Claude Bernard Lyon 1, Villeubanne, France
[6] Department of Irrigation and Agrometeorology, Lebanese Agricultural Research Institute (LARI), P.O. box 287, Zahle, Lebanon
[7] Department of Olive and Olive Oil, Lebanese Agricultural Research Institute (LARI), P.O. box 287, Zahle, Lebanon

*Correspondence to*: Ilham Bentaleb (Email: ilham.bentaleb@umontpellier.fr, Tel: +33(0) 6 38 61 57 69)

**Abstract.** This study invistigates the seasonality of the mercury (Hg) concentration of olive trees foliage, an iconic tree of the Mediterranean basin. Hg concentrations of foliage, stems, soil surface, and litter were analyzed on monthly basis in ancient olive trees growing in two groves in Lebanon, Bchaaleh and Kawkaba (1300 and 672 m.a.s.l respectively). A significantly lower concentration was registered in stems (~7-9 ng/g) with respect to foliage (~35-48 ng/g) in both sites with the highest foliage Hg concentration in late winter-early spring and the lowest in summer. It is noteworthy that olive fruits also have low Hg concentration (~7-11 ng/g). The soil has the highest Hg content (~62-129 ng/g) likely inherited through the cumulated litter biomass (~ 63-76 ng/g). A good covariation observed between our foliage Hg time-series analysis and those of atmospheric Hg concentrations available for southern Italy in the western Mediterranean basin confirms that mercury pollution can be studied through olive trees. Spring sampling is recommended if the objective is to assess the tree's susceptibility to Hg uptake. Our study draws an adequate baseline for Eastern Mediterranean and the region with similar climatic inventories on Hg vegetation uptake. In addition to being a baseline to new studies on olive trees in the Mediterranean to reconstruct regional Hg pollution concentrations in the past and present.
**Keywords:** Eastern Mediterranean, ancient groves, *Olea europaea* L., mercury pollution, plant tissues, soil and litter

## I. Introduction

Mercury (Hg) is among the most widely distributed potentially toxic metals polluting the Earth (Briffa et al. 2020). It is found as all heavy metals naturally on the Earth's crust reservoir and in the atmosphere through the natural long-term Hg biogeochemical cycle (i.e., volcanic activities, geological weathering). This metal is easily modified into several oxidation states and it can also be spread through many ecosystems (Boening 2000). The natural Hg cycle has been modified due to anthropogenic activities (i.e., mining, smelting, soil erosion due to deforestation, gold extraction, agriculture-fertilizers, manure) (Patra and Sharma 2000). Among natural and anthropogenic Hg emissions, inorganic elemental Hg (Hg(0)) is the most dominant chemical form. It is primarily transferred through the atmosphere by air mass movement and can undergo long-range transport. Because of its high volatility and susceptibility to oxidation, elemental Hg(0) is the predominant form of Hg in the atmosphere that can be accumulated into foliage. This highly diffusive Hg can easily pass biological barriers (i.e. cell membranes, foliage, skin). Mercury has three oxidation states, namely, Hg(0) (elemental mercury), Hg(I) (mercurous), or Hg(II) (mercuric), although Hg(I) mercurous form is not stable under typical environmental conditions and, therefore, is rarely observed. It is likely that the Hg(II) high binding affinities bind covalently with organic groups (Du and Fang, 1983; Clarkson and Magos 2006; Pleijel et al., 2021). The exchange of Hg between the soil and plants is not stable and is variable dependent (e.g. cation-exchange capacity, soil pH, soil aeration, and plant species) (Patra and Sharma 2000). Forests are known to act as a sink of atmospheric Hg. Plant foliage takes up of Hg deposited on leaf surfaces through the stomata (i.e. Leaf gas exchange) and leaf cuticles (Hanson et al. 1995; Jiskra et al. 2018; Li et al. 2017; Lodenius et al. 2003; Maillard et al. 2016; Rea et al. 2002; Yanai et al. 2020) where it accumulates with minimal mobility and small portions released back into the atmosphere or transferred to other plant organs (Cavallini et al. 1999; Hanson et al. 1995; Li et al. 2017; Lodenius et al. 2003; Schwesig and Krebs 2003). All together these authors contributed to highlight the dynamic role of the foliar surfaces in terrestrial forest landscapes acting as a source or sink dependent on the magnitude of current Hg concentrations. Hanson et al. (1995) suggested a species-specific compensation concentrations (or compensation points) for Hg deposition.

Hg is redistributed to the forest floor through litter and throughfall and hence passes to the soil (Rea et al. 1996). The Hg input through the litter is greater than the input from that of the wet deposition (Wang et al., 2016). Litter has been estimated to constitute 30 to 60 % of the Hg atmospheric deposition in Europe and North America forests (Rea et al. 1996; Blackwell and Driscoll 2015; Zhou et al. 2018). According to Wright et al., (2016) the litter Hg is the dominant pathway in forests where it contributes 53 to 90 % of the dry deposition to the forest. In terrestrial ecosystem, soils have the highest Hg reservoir (Obrist et al., 2018; O'Connor et al., 2019) followed by trees (Yang et al., 2018). This Hg is provided by natural geological sources and natural events such as forest fires, volcanic eruptions (Ermolin et al. 2018; Obrist et al. 2018; O′Connor et al. 2019) and anthropogenic sources (UNEP, 2019). Though

variable from year to year, Hg emission to the atmosphere from biomass burning is considered as an important driver of the global Hg biogeochemical cycle (Friedli et al., 2009; De Simone et al., 2015; McLagan et al., 2021; Dastoor et al., 2022). Soil can also release Hg to the atmosphere (Luo et al., 2016; Assad, 2017; Yang et al., 2018; Schneider et al., 2019; Gworek et al., 2020; Pleijel et al., 2021) and also behave as a source of Hg to the plants. Hg of the soil is is taken up by the roots along with the water , it is translocated to other parts (ie. Stems, Leaves) of the plant using the xylem sap (Bishop et al., 1998; Li et al., 2017). This pathway ~~have~~ has been described on several plant species in Hg contaminated sites (Assad et al. 2017). Trees are hence considered as important drivers of Hg exchange between the atmosphere and the soil (Yang et al. 2018). The recent studies on Hg uptake by vegetation have highlighted the importance of the role of different parameters as vapor pressure deficit, soil water content, climatic conditions, date of sampling, leaf mass area, tree functional groups, stomatal conductance, affecting potentially the root uptake of Hg dissolved in soil water and the absorption rate via stomata and eventually the Hg leaf content (Rea et al., 2002; Obrist et al., 2011; Blackwell & Driscoll, 2015; Yang et al., 2018; Wohlgemuth et al., 2021). In polluted sites the soil is the main source of Hg to the vegetation while away from those sites the atmosphere is the most important source (Naharro et al., 2018). The Hg source in foliage varies with respect to the amount of contamination (Hanson et al., 1995).

The studies of the Hg cycle in forest ecosystems show that gaseous elemental Hg(0) is the main source taken up by plants (Bishop et al. 2020; Zhou et al. 2021). Analysis of long term atmospheric Hg(0) and $CO_2$ concentrations are very informative to understand the role of the vegetation in the global Hg cycle (Jiskra et al., 2018). Emission reduction measures adopted in Europe and North America since the 70s are corroborated by Hg dendrochemistry analysis showing a declining Hg concentration trend from the older to newer tree rings. Indeed, tree ring Hg (dendrochronology) is a powerful archiving tool for atmospheric Hg(0). After Hg(0) oxidation inside the leaves, Hg(II) bind to organic compounds and then is transported to the bole wood via the phloem (Beauford et al., 1977; Lindberg et al., 1979). This is corroborated by the recent study of McLagan et al., (2022) showing the benefit of the stable Hg isotope analysis on dendrochemistry. Several studies have evidenced seasonal variations of the atmospheric Hg(0) contents (ie. in temperate Northern Hemisphere by Jiskra et al., 2018; in Western Mediterranean Basin in South Italy (Martino et al. 2022) with high values in winter and low values in summer. Interinstingly, Jiskra et al., (2018) show also a significant positive correlation between the monthly Hg(0) and $CO_2$ concentrations. They highlighted a one-month offset in Hg(0) summer time minima happening in September in comparison to the $CO_2$ minima value occurring in August, this trend is not observed in winter time. The uptake of Hg(0) by the vegetation continues during $CO_2$ respiration periods during the fall and night when the ecosystem exchange of $CO_2$ turns from being a sink to becoming a source (Wofsy et al., 1993; Jiskra et al., 2018).

The total gaseous Hg (TGM) in the Mediterranean atmosphere is similar to Northern Europe (1.3 to 2.4 ng $m^{-3}$) (Kotnik et al. 2014). In the case of a semi-closed sea such as the Mediterranean basin with warm

summers, high sea-water evaporation, solar radiations and Hg anthropogenic sources, the Mediterranean Sea acts as a net source of Hg to the global atmosphere (Kotnik et al. 2014) making the Mediterranean an air-pollution emission area (Baayoun et al. 2019; Borjac et al. 2019).

The olive tree (*Olea europaea* L.) is one of the most distinctive Mediterranean agro-ecosystems tree species (Besnard et al., 2013), and is adapted to drought (Sghaier et al. 2019). Considered to be among the oldest trees in the Mediterranean basin, centennial olive trees are still growing in many countries along both the eastern and western shore, surviving numerous stresses and are of considerable historical, cultural and ecological importance (Terral et al. 2004). The olive tree still remains a key component of agriculture today and will be into the future. Therefore, genetic characterization of olive varieties and genetic resources (Khadari et al., 2019; Galatali et al., 2021), description based on morphological characters and phenology of growth stages of olive trees (Sanz-Cortés et al., 2002), experimentation through field irrigation and/or more rarely through drought stress treatments (Alcaras et al., 2016) have been conducted to avoid genetic erosion, optimize the water use for irrigation and hence improve orchard management, and solely to better understand the biodiversity. Only few studies have focused on the response of the olive tree to Hg pollution in its natural Mediterranean environment (Higueras et al., 2012; Higueras et al., 2016; Guarino et al., 2021; Labdaoui et al., 2021).

Lebanon, a small country at the Eastern Mediterranean, is facing important anthropogenic pressure within a changing environment (Gérard and Nehmé 2020). The air quality in Lebanon all over the country is noted to be moderately unsafe with an annual mean concentration of 31 $\mu g/m^3$ of PM2.5 (Particulate Matter) which is above the maximum recommended value (10 $\mu g/m^3$) (Lebanon: Air Pollution IAMAT 2020). Adding to that, soil samples collected from different areas in southern Lebanon showed values of Hg concentration ranging between 160-6480 ng/g showing a high contamination levels (Borjac et al. 2020) as indicated by World reference Senesil et al., 1999; Kabata-Pendias & Pendias, 2000. The main contributors of the air pollution include cement industries, mineral and chemical factories, vehicles emissions, food processing and oil refining. Ancient olive groves are found across different agroclimatic areas at different altitudinal belts, still producing olives and oil for consumption with these various pollution pressures.

In this study two sites, known for their century-old olive groves and located at two different altitudes in Lebanon, were selected to assess the Hg contents. In these remote areas, no direct sources of mercury contamination are reported and hence we expect very low Hg concentrations. However, due to atmospheric transport of Hg, dry or wet deposition of Hgcan be expected in remote areas (Grigal, 2003). The main objectives of this study are to examine and compare Hg levels in foliage, stems, fruits, litter and soil measured in each of these two olive groves, which we monitored monthly for 18 months. The second objective is to analyze the relative importance of Hg uptake by the soil and foliage in comparison with the atmospheric Hg. Since the distribution of Hg pollution is by nature geographically widespread, and given the extent of Hg pollution in the Mediterranean and the transfer of pollution by wind and the Mediterranean Sea, long-distance contamination occurs over large areas. This study may draw an

adequate baseline for Eastern Mediterranean and region of similar climates inventories on Hg vegetation uptake and new studies on olive trees in the Mediterranean to reconstruct regional Hg pollution concentrations in the past and present.

## II. Materials and methods

Two monumental olive groves were chosen in the context of their historical and agricultural importance, since these two sites are considered to contain olive trees more than 1400 years old and are still productive.

### II.1.1 Bchaaleh site - North Lebanon

This grove is situated in Batroun district (Latitude 34°12'06'' N, Longitude 35º49'23'' E, Altitude 1300 m.a.s.l.) (Figure 1). Olive trees are growing rainfed in a sandy loam texture soil of grain size analysis of sand, silt and clay percentages are 52.8 %, 38.7 % and 10.7 % respectively. Soil pH is 7.07 ± 0.26 with organic matter and calcium carbonate contents are 1.7 % and 38.3 % respectively (Yazbeck et al. 2018). In this study, soil profiles of carbon and nitrogen contents were analyzed. Organic carbon contents decreased with soil depth from about 4 % at 0-1 cm (Soil surface) to 2.7 % at 30-60 cm. The total nitrogen is about 0.3 % at 1cm depth and 0.2 % at 30-60 cm depth. The olive trees are located on two terraces. The first terrace is at 1.5 meter above the road level while the second is at the road level. They are maintained by the municipality for the last four decades as an endowment property. Precipitation average ranges between 229 and 392 mm in winter and between zero and less than 2 mm/season in summer, while average temperature is between 4 and 8 °C in winter and between 20 and 23 °C in summer and average relative humidity of 63% (data extracted from LARI climatic data) (Table S1, Figure S1).

The village is at about 36 km from Chekka town located at a lower altitude (0-200 m.a.s.l.) nearby the sea (Figure 1), and which is classified as a source of air pollution (EJOLT 2017)**.** Chekka is the site of an important national cement factory responsible of carbon dioxide, sulfur dioxide, nitrous oxides, carbon monoxide and particulate material emissions causing respiratory and health issues (Kobrossi et al. 2002) and water pollution (Nassif et al. 2016). At 28 km from Bchaaleh, the small commercial port of Selaata (0-37 m.a.s.l.) emits many pollutants (ie. Phosphogypssum, heavy metals, radionuclides) expanding via water and air pathways (Petrlik et al. 2013; Yammine et al. 2010). To our knowledge no direct Hg pollution is reported at Chekka and Selaata sites. However a dissolved gaseous Hg from natural and human activities is saturated in the upper Eastern Mediterranean Sea, Gårdfeldt et al., (2003) have evidenced that Mediterranean Sea is a source of airborne elemental Hg.

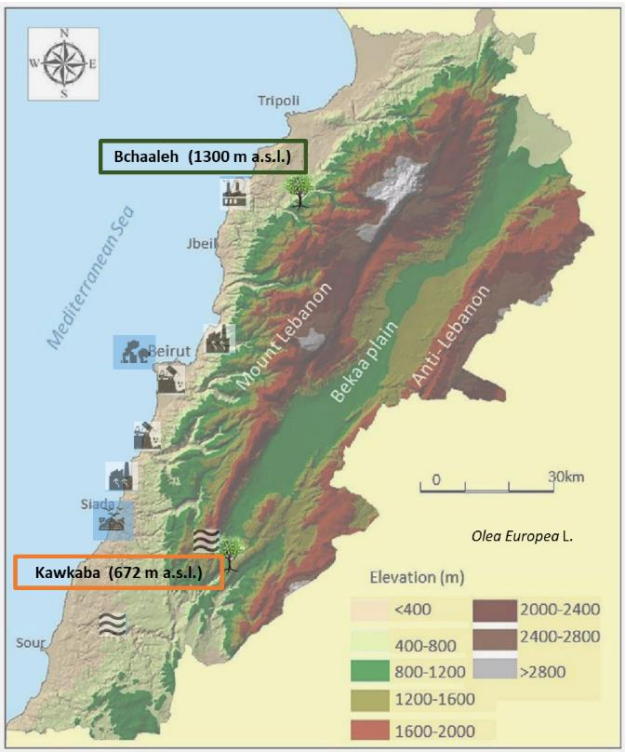


**Figure 3** Site locations of the two selected focus areas (modified after Shared Water Resources of Lebanon, Nova Science Publishers 2017).

### II.1.2 Kawkaba site - South Lebanon

The second grove is located in the village of Kawkaba, South Lebanon (Latitude 33°23'856'' N, Longitude 35°38'588'' E, Altitude 672 m.a.s.l. (Figure 1). Kawkaba soil is characterized as clay loam soil of pH 7.5 ± 0.5. Soil organic material and calcium carbonate average are 1.7 % and 59.0 % respectively (Al-Zubaidi et al., 2008) and grain size analysis of sand, silt and clay percentages are 6 %, 28 % and 66 % respectively. The analysis of organic carbon and nitrogen at the 0-1 cm and at 0-30 cm decrease from about 9.0 % to 2.2 % and from 0.9 % to 0.3 % for the carbon and nitrogen respectively. Average precipitation ranges between 215 and 374 mm in winter and drop to almost zero mm in summer, while average temperature is between 7 and 11 °C in winter and between 21 and 27 °C in summer and relative humidity of 61% (data extracted from LARI climatic data) (Table S1, Figure S1). The village has to its east the Hasbani river, originated from the north-western slopes of Mount Hermon in Hasbaya (36 km away from Kawkaba and located at 750 m.a.s.l.) (Badr et al. 2014; Jurdi et al. 2002). On the other hand, the Litani River (170 km long and located at 800 to 1000 m.a.s.l) (Figure 1) rising in the south of the Bekaa valley is about 29 km away from Kawkaba (Abou Habib et al. 2015, Khatib et al. 2018). These two rivers are polluted and for these reasons they are not used for irrigating crops in Kawkaba and surrounding areas while the olive trees are growing rainfed as per indicated by the municipality of Kawkaba. Here as well, we did not find indication of direct Hg pollution.

Climatic data in both Bchaaleh and Kawkaba were collected from meteorological station and manual rain gauge installed in the villages by LARI (Lebanese Agricultural Research Institute). $CO_2$ data used in this study are from NOAA Global Monitoring Laboratory (https://gml.noaa.gov/webdata/ccgg/trends/co2/co2_trend_gl.txt ).

## II.2 Field sampling

For the Hg concentration analysis, four olive trees (3-5 m in diameter and an average height of 4-6 m) were sampled in each of the two groves from February 2019 to September 2020. Within Bchaaleh two trees were selected from the upper terrace (BCO1-Bchaaleh-Tree 1, BCO4-Bchaaleh-Tree 4) and two other trees were sampled from a lower terrace located 1.5 m below the upper one (BCO9-Bchaaleh-Tree 9, BCO12-Bchaaleh-Tree 12) (Figure S2). In Kawkaba, four trees were selected and sampled (KWO1-Kawkaba-Tree 1, KWO2-Kawkaba-Tree 2, KWO3-Kawkaba- Tree 3, KWO4-Kawkaba-Tree 4). For each olive tree, both sun exposed and shaded foliage and stems (terminal portions of 20 cm) with no evidence of pathogens were randomly taken and merged from the upper, middle, and lower canopy position of the olive trees on a monthly basis using a manual pruner. The phenological growth stages of olive trees described by Sanz-Cortés et al.,( 2002) in Spain suggest leaf development from March to November. Hence it should be mentioned that the Hg concentration measured on monthly collected foliage represents an average of Hg accumulated in young foliage (year N of collection where N is equal to 2019 and 2020) and older foliage (N-1 year and N-2 years). Fruits were collected in April 2019. Litter and soil surface were separately collected on the whole top surface area of the olive groves and stored in different paper bags once every four months. In parallel, soil sampling was performed using a bucket auger to a maximum depth of 60 cm. In both sites Bchaaleh and Kawkaba, the soil showed uniform color and texture. Soil cores were fractioned in soil surface (0-1 cm), 0 to 30 cm depth and from 30 to 60 cm depth in order to study the effect and accumulation of Hg concentration on the different depth layers. To avoid contamination, gloves were worn while collecting samples, and the equipment was rinsed with methanol between every sample. A set of 453 samples were collected and stored in paper bags until further preparation for the Hg analysis.

## II.3 Sample preparation for Hg analysis

Collected foliage and stems were rinsed with distilled water and then dried for 48 hours in an oven at a temperature of 50°C at maximum (Demers et al., 2013; Li et al., 2017; Pleijel et al., 2021). This procedure likely eliminate any Hg(0) present in the samples. The dried foliage, stems, litter and olive fruits samples were grinded using an electrical stainless grinding machine with no heating system for 5-10 minutes, while soil samples were prepared with a manual natural agate grinder. All samples were later sieved using an inox stainless-steel 125-micron sieve mesh to collect homogeneous powders for

analysis. A total of 150 mg for foliage and soil (50 mg/analysis), and 300 mg of litter and stems (100 mg/analysis) were considered in triplicates for analysis of Hg concentrations.

## II.4 Analytical method

For the Hg elemental analysis, a total of 453 powder samples from foliage, stem, grain, litter and soil were analyzed using an advanced Hg analyzer AMA 254 (Altec) as described elsewhere (Barre et al. 2018; Duval et al. 2020). A known amount of sample (50-100 mg) is weight in a nickel boat, using a $10^{-6}$ g precision balance. The sample aliquot is first dried at 120°C for 60s and subsequently pyrolyzed at 750°C for 150s, under oxygen flow. The resulting gaseous Hg produced during the sample decomposition is amalgamated on a gold trap and then released to an Atomic Absorption spectrometer after a thermal desorption step at 950°C. The AMA 254 instrument was calibrated through several external matrix-matched calibration procedures using the following certified reference materials: IAEA-456 sediment (77 ± 5 ng Hg/g), NIST-1575A pine needles (39,9 ± 0,7 ng Hg/g) and IAEA336 (200 ± 40 ng Hg/g). The QA/QC evaluation of the analytical procedure was completed with a continuous monitoring of the blank's values (Nickel boat Hg background noise), every 15 analyzed samples. The precision of the measurements was assessed through replicated analyses (n=2) of 13 % of the total amount of samples (n=453). Average relative standard deviations of 5 % and 2.5 % are thus associated to the reported Hg concentrations for the 2019 and 2020 samples batches, respectively. The absolute detection limit (ADL) of the analytical technique (AMA 254) was estimated at 0.04 ng Hg. As a consequence, the method detection limit (MDL) for samples analyzed were 0.7 ng Hg/g for soil, litter and foliage and 0.4 ng Hg/g for stem and wood. These MDL were much lower than the measured Hg concentration in the various samples.

Susbamples of soil were used for carbon and nitrogen elemental contents (%) analysis. A 2 mg (acid washed soil and bulk soil) of powders were weighed into tin capsules and measured by dry combustion using a Pyrocube Elemental Analyser (EA, Elementar GmbH).

## II.5 Statistical analysis

For the statistical analysis we used the R 4.1.0 program. Our data are not normally distributed, so for the effect of tissue type on Hg concentration, Wilcoxon test was used with the tissue type (foliage and stems) as the main effect. Pearson correlation analysis was used to examine the inter-individual correlation of Hg concentration between the trees. Correlation between Hg concentration of soil surface, litter and foliage was studied using a correlation test. For the seasonal effect (Winter: Mid December till Mid-March, Spring: Mid-March till Mid-June, Summer: Mid-June till Mid-September, Autumn: Mid-September till Mid-December) on Hg concentration, Wilcoxon test was used considering the unequal data available for the different seasons. Finally, the effect of climatic factors (Temperature, precipitation, $pCO_2$) on Hg accumulation was examined using a Wilcoxon test.

## III. Results

### III.1 Hg concentrations in plant tissues, litter and soil at Bchaaleh and Kawkaba groves

Hg concentrations measured in the different sampled materials (plant tissues, litter and soil) varied generally according to both tree tissues and groves agroclimatic conditions (Table 1). Hg values in the foliage varied significantly between the two groves (p-value=$1.581*10^{-6}$), where the highest concentration was recorded in Bchaaleh (48.1 ± 10.6 ng/g) *vs.* (35 ± 12.4 ng/g) in Kawkaba. Soil surface also recorded a difference in Hg concentration between Bchaaleh and Kawkaba, with 61.9 ± 20.0 ng/g in Bchaaleh and 128.5 ± 9.4 ng/g in Kawkaba. Soil 0-30 cm samples taken from Bchaaleh and Kawkaba groves, values ranged between 31.8 ± 4.7 ng/g and 70.2 ± 23.4 ng/g respectively. In soil 30-60 cm Hg concentrations recorded 19.5 ± 6.73 ng/g at Bchaaleh. No significant differences were recorded for litter and stems Hg concentrations (p-value= 0.0915 and p-value=0.2215 respectively) between the groves, with litter values of 62.9 ± 17.8 at Bchaaleh and 75.7 ± 20.3 ng/g at Kawkaba *vs.* stem values of 7.9 ± 2.8 ng/g at Bchaaleh and 9.0 ± 4.7 ng/g at Kawkaba. Positive correlations were observed between soil and litter in Bchaaleh (r=0.60) and Kawkaba (r=0.95) though statistically insignificant (p-value= 0.40 and 0.13 respectively).

The comparison between Bchaaleh and Kawkaba soil surface Hg contents showed significant difference between the two groves (p-value=0.04746). We observe the same significant difference when comparing the soil horizon of 0-30 cm of both groves. In descending order of Hg concentrations and considering the different sites, plant tissue, soil and litter samples, the Hg concentrations could be ranked in Bchaaleh, soil surface > litter> foliage > soil 0-30 cm > soil 30-60 cm > stems > fruits; and in Kawkaba, soil surface > litter > soil 0-30 > foliage > soil 30-60 > stems > fruits (Table 1).

**Table 2** Overall mean values of Hg concentration (ng/g) of the different studied material in both Bchaaleh and Kawkaba olive groves

| Sample material | Bchaaleh (BC) | | | Kawkaba (KW) | | |
|---|---|---|---|---|---|---|
| | Average (ng/g) | SD | N | Average (ng/g) | SD | N |
| **Foliage** | **48.1** | **10.6** | **66** | **35.0** | **12.4** | **67** |
| **Stems** | **7.9** | **2.8** | **66** | **9.0** | **4.7** | **67** |
| **Litter** | **62.9** | **17.8** | **7** | **75.7** | **20.3** | **6** |
| **Soil Surface** | **61.9** | **20.0** | **8** | **128. 5** | **9.4** | **6** |
| **Soil 0-30cm** | **31.8** | **4.7** | **6** | **70.2** | **23.4** | **5** |
| **Soil 30-60cm** | **19.5** | **6.7** | **5** | **28.0** | | **1** |
| **Fruits** | **7.0** | **3.5** | **3** | **11.0** | | **1** |

### III.2 Seasonal variation of Hg concentration in plant tissues, litter and soil

Hg concentrations recorded between February 2019 and September 2020 (Table 2) reflected a significant seasonal variation in both sites (p-value<$2.2*10^{-16}$)

In Bchaaleh grove, foliage registered its highest Hg concentration during winter and spring with 61.8 ± 7.6 ng/g and 55.1 ± 12.5 ng/g respectively, and its lowest Hg amount during summer and autumn with 41.5±12.7 ng/g and 44.4 ± 6.2 ng/g, respectively. A seasonal effect on foliage and stems was registered (p-value<$2.2*10^{-16}$; Figure 2a,c). The stems and soil 0-30cm highest values was registered in autumn. Significant differences were found in foliage Hg values between summer and winter (p-value=0.00020), and autumn and winter (p-value= 0.00014). Similarly, stems Hg values varied significantly between spring and winter (p-value=0.030), autumn and winter (p-value=0.047). Litter highest Hg content occur in summer in Bchaaleh olive groves (79.3 ± 26.5 ng/g) and the lowest in winter (48.6 ± 13.3 ng/g) (p-value = 0.2286). Highest Hg contents in the soil surface of Bchaaleh is recorded in summer (84.5 ± 21.2 ng/g).

In Kawkaba, the highest Hg concentrations for foliage and stems were registered in spring with 51.8 ± 4.5 ng/g, 11.7 ± 6.7 ng/g respectively (Table 2, Figure 2b,d). Significant differences were found in foliage Hg values between summer and winter (p-value=0.013), autumn and winter (p-value= 0.00067), autumn and spring (p-value=$1.589*10^{-05}$), spring and winter (p-value= $9.383*10^{-05}$) and spring and summer (p-value=$2.327*10^{-06}$). Similarly, stem Hg values varied significantly between spring and winter (p-value=0.006), spring and summer (p-value=0.0036) and autumn and spring (p-value=0.011). There is no seasonal variation between the litter different seasons for Bchaaleh nor for Kawkaba. Bchaaleh and Kawkaba groves soil surface, 0-30 cm and 30-60cm Hg values varied significantly between seasons, (p-value < 0.05). A seasonal variation is observed in both olive groves especially in the foliage.

**Table 3** Seasonal mean Hg concentration (ng/g) and standard deviations of the different studied material in both Bchaaleh and Kawkaba olive groves. Grey color indicated the highest Hg concentration values among the different material during the different seasons.

| Hg (ng/g) | | | | | | | | | | | | |
|---|---|---|---|---|---|---|---|---|---|---|---|---|
| **Bchaaleh** | **Spring** | **SD** | **N** | **Summer** | **SD** | **N** | **Autumn** | **SD** | **N** | **Winter** | **SD** | **N** |
| **Foliage** | 55.1 | 12.5 | 16 | 41.5 | 12.7 | 24 | 44.4 | 6.2 | 12 | 61.8 | 7.6 | 18 |
| **Stems** | 7.8 | 3.8 | 16 | 7.61 | 3.9 | 24 | 8.3 | 2.7 | 12 | 6.4 | 2.9 | 18 |
| **Litter** | 79.3 | 26.5 | 3 | 64.7 | 4 | 4 | 55.5 | 3.54 | 2 | 48.6 | 13.3 | 3 |
| **Soil Surface** | 58.3 | 13 | 3 | 84.5 | 21.2 | 4 | 50 | | 1 | 50.6 | 23.5 | 3 |
| **0-30cm** | 33.6 | 6.2 | 2 | 32.2 | 4.3 | 2 | 34.5 | 7.79 | 2 | 27 | 0.7 | 3 |
| **30-60cm** | 23.1 | 9.1 | 2 | 20.7 | 10.32 | 2 | 19.6 | 9.05 | 2 | 11 | | 1 |
| | | | | | | | | | | | | |
| **Kawkaba** | **Spring** | **SD** | **N** | **Summer** | **SD** | **N** | **Autumn** | **SD** | **N** | **Winter** | **SD** | **N** |
| **Foliage** | 51.8 | 4.5 | 16 | 28 | 7.2 | 24 | 28.5 | 7.2 | 16 | 33.9 | 5.6 | 18 |
| **Stems** | 11.7 | 6.7 | 16 | 6.5 | 1.4 | 24 | 7.7 | 2.1 | 16 | 6.9 | 1.6 | 18 |
| **Litter** | 90.1 | 29.3 | 2 | 67 | 24 | 2 | 70 | 1.4 | 2 | | | |
| **Soil Surface** | 132 | 8.5 | 2 | 118 | 4.2 | 2 | 135.6 | 2.2 | 2 | | | |
| **0-30cm** | 57.9 | 11.2 | 2 | 65.8 | | 1 | 84.8 | 36.4 | 2 | | | |
| **30-60cm** | 28 | | 1 | | | | | | | | | |

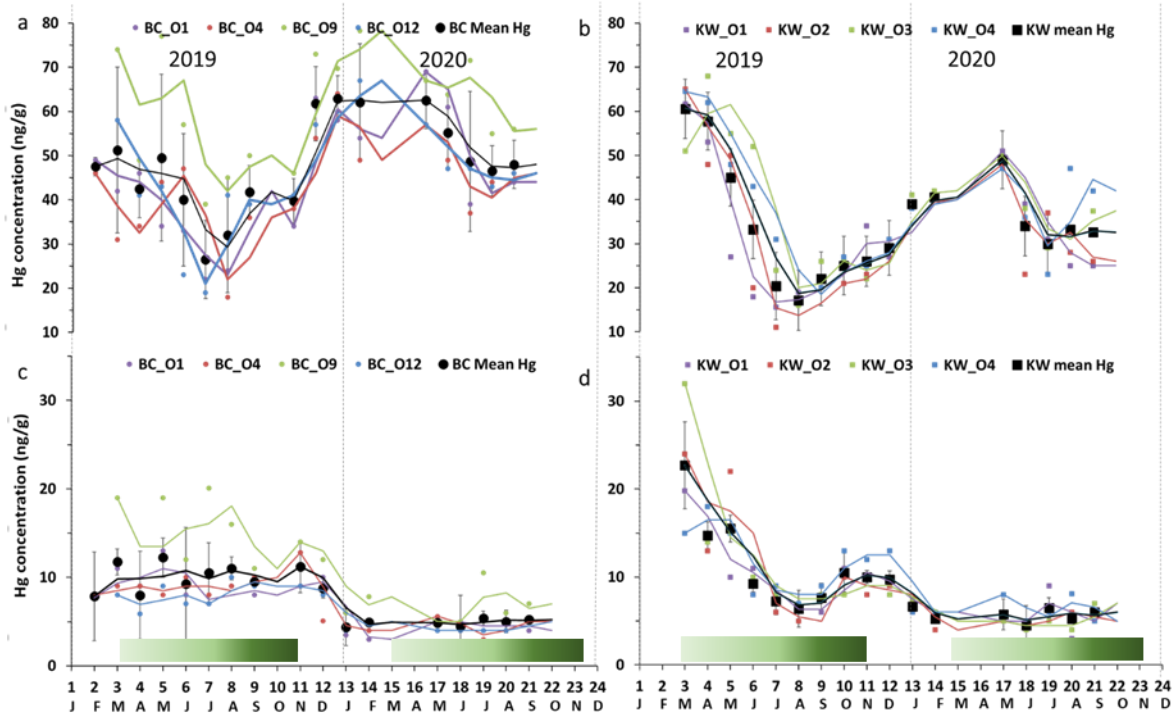


**Figure 4** Seasonal variations of foliage Hg concentration in(**a)** Bchaaleh (BC) and (**b)** Kawkaba (KW) olive groves and stems Hg concentration in **(c)** Bchaaleh and **(d)** Kawkaba olive groves. Shaded green horizontal bars represent the leaf development of olive trees during the growing season of cultivars in Spain according to the BBCH scale (Sanz-Cortès et al., 2002).

### III.3 Inter-individual variability between trees for each site

In the upper terrace of Bchaaleh grove, the foliage average Hg concentration of BCO4 and BCO1 varied between 42.4 ± 11.5 ng/g and 44.6 ± 13.3 ng/g respectively showing no significant difference (p-value = 0.8225). In the lower terrace of the same site, foliage average Hg concentrations of trees BCO12 and BCO9 were found to vary from 45.6 ± 12.7 ng/g to 60.7 ± 12.7 ng/g respectively (Figure 2a) exhibiting a significant difference ((p-value=0.0059). Tree BCO9 is significantly different to each of the three trees (p-value< 0.0059) while BCO1, BCO4 and BCO12 have very similar Hg contents (p-value= 0.46). In the upper terrace of Bchaaleh grove, the stems average Hg concentration of BCO4 and BCO1 varied between 7.0 ± 2.8 ng/g and 7.1 ± 2.9 ng/g respectively showing no significant difference (p-value= 0.94). In the lower terrace, stems average Hg concentrations of BCO12 and BCO9 are 6.4 ± 2.2 ng/g and 11.2 ± 5.2 ng/g respectively showing a significant difference (p-value= 0.0054; Figure 2c). For BCO1 and BCO12 there was no significance difference (p-value= 0.5725), the same goes for BCO4 and BCO12 (p-value= 0.523).

The average concentration per tree in foliage and stems were 32.4 ± 12.2 ng/g and 8.5 ± 4.0 ng/g respectively for KWO1, 32. 8 ± 14.7 ng/g and 8.9 ± 6.0 ng/g for KWO2, 37.6 ± 14.0 ng/g and 9.3 ± 6.7 ng/g for KWO3 and 37.7 ± 13.6 ng/g and 9.6 ± 4.0 ng/g for KWO4 (Figure 2b,d). In Kawkaba grove, comparison of the foliage Hg concentration between the four studied trees shows no significant difference (0.22<p-value<1), neither for the stems (0.21<p-value<0.96).

### III.4 Hg concentration and agro-climatic effect

At first glance, seasonal variations of the Hg concentrations of the foliage of both sites suggest a covariation with climatic parameters (Precipitation amounts, Relative Humidity and Temperature) (Figure SI 1) and atmospheric $pCO_2$. Foliage Hg content increased with higher precipitation and lower temperature (Autumn and Winter) while during the warmer and dryer seasons (May to mid-October), the Hg concentration of foliage decreased (Figure SI 1). However, the Wilcoxon test for a non-normal distribution shows no significant correlation between Hg concentration of foliage and precipitation (p-value= 0.95). While temperature, relative humidity and atmospheric $CO_2$ ($pCO_2$) shows a significant correlation (p-value = $2.2e^{-16}$). For the stems, Hg concentration also showed no significant correlation with precipitation (p-value= 0.1147), and a significant correlation with temperature, relative humidity and $pCO_2$ (p-value= $2.2e^{-16}$).

# IV. Discussion

## IV.1 Hg concentration in plant tissues, soil and litter in the studied groves

In both groves our values showed a higher Hg concentration in the olive foliage (Bchaaleh average of 48.1 ± 10.6 ng/g; Kawkaba average of 35.0 ± 12.4 ng/g), than that of the stems (Bchaaleh average of 7.9 ± 2.8 ng/g; Kawkaba average of 9.0 ± 4.7 ng/g) and that of olive fruits (7 ± 3.5 ng/g at Bchaaleh, n=3 and 11 ng/g in Kawkaba, n=1). Our data corroborates previous studies (Bargagli 1995; Higueras et al. 2016) showing that olive foliage has the highest Hg concentration of plant tissues. Our values are lower than 200 ng/g considered as Hg pollution threshold (Kabata-Pendias & Pendias, 2000) and implying no pollution effect for both Bchaaleh and Kawkaba groves (Table SI 2; Figure SI 3a,b). This suggests that our sites are good remote bioindicators of the uptake of Hg through the plant, although more prolonged time range study is needed. However, in an overview of vegetation uptake of mercury and impacts on global cycling, Zhou et al., (2021) suggested lower values for unpolluted sites (litterfall 43 ng/g > foliage 20 ng/g and branch 12 ng/g). Knowing that our sites correspond to unpolluted areas of Lebanon, the lower values of Zhou et al., (2021) obtained from an ensemble of various species (trees and grasses) and not specifically on olive trees, we considered that the threshold value of 200 ng/g (Kabata-Pendias and Pendias 2000) is more adapted to our comparison.

As described in several studies, Hg in foliage originates predominantly from the atmospheric gaseous Hg(0) through stomatal uptake (Ericksen et al., 2003; Lindberg et al., 1979; Zhou et al., 2021). Adding to that, the atmospheric Hg uptake in foliage excedes Hg stomatal re-emission (Pleijel et al., 2021; J. Zhou et al., 2021). Inside the leaves the oxidized Hg(II) has high affinities to bind covalently with organic groups (Du & Fang, 1983; Clarkson & Magos, 2006; Pleijel et al., 2021). The Hg can be translocated by phloem transport to the stems and eventually into roots and potential release into soils may also be contributing to Hg accumulation in soils (Giesler et al., 2017; Schaefer et al., 2020).

The soil surface and litter registered the highest Hg concentration (62 to 129 ng/g) among all samples (foliage, stems, fruit) in both groves (Table 1) suggesting that the soil is the main Hg reservoir through the Hg throughfall and litter-inputs (Tomiyasu et al., 2005). Our findings are in agreement with studies on evergreen forest ecosystems reporting that soil can hold more than 60 % of Hg input to the forest floor (Wang et al. 2016). Our soil surface sites values (61.9 ± 20.0 ng/g in Bchaaleh and 128.5 ± 9.4 ng/g in Kawkaba) show higher Hg concentration in Kawkaba compared to the general background level of Hg as defined by uncontaminated soil world reference mean Hg contents (20 to 100 ng/g; Kabata-Pendias and Pendias 2000; Senesil et al. 1999; Gworek et al. 2020). However, both sites have significantly lower values compared to known industrial and mining contaminated sites (> 1000 ng/g ; ). Nevertheless, studies conducted in different sites show a wide range of natural background Hg levels (ie. topsoils in Europe, India, Brazil, Norwegian Arctic, New Zealand have values of 40, 50, 80, 110, 230 ng/g respectively) (Gworek et al. 2020) making it difficult to set a specific Hg threshold value for uncontaminated soil (Table S2; Figure SI 3c). Due to the differences registered in different countries

and sites of sampled soil, this indicates a link with chemical and mineralogical soil properties (ie. pH, humic acid, soil grain size distribution, organic matter type and clay percentage) affecting Hg in soil and its transport (Richardson et al., 2013; Chen et al., 2016; O'Connor et al., 2019). Nitrogen can also be a factor affecting the Hg content in soil depending on its characteristics. Nitrogen increase can change the equilibrium of soil solution and the morphology of roots, causing a possible increase in Hg availability in soil and increases the Hg uptake by the plant (Alloway, 1995; Barber, 1995; Carrasco-Gil et al., 2012). The increase in Hg availability in the soil is due to the organic Nitrogen that provides a high absorption capacity, retaining the atmospheric Hg deposition (Obrist et al., 2009). Nitrogen supply prevents oxidative stress in roots, but also can improve root development and increase the uptake of Hg from the soil (Carrasco-Gil et al. 2012). Hence, we suggest that lower values in Bchaaleh soils are likely explained by the low clay, organic carbon and nitrogen contents (10.7 %, 4 % and 0.3 % in soil surface respectively). While Kawkaba higher Hg soil contents can be explained by the higher clay proportion (66 %) and organic carbon and nitrogen contents (9 % and 0.92 %). On such clay loam soils and rich organic matter, Hg binding is facilitated explaining higher content (O'Connor et al. 2019).

The litter showed higher Hg concentration than that in foliage in both Bchaaleh (62.9 ± 17.8 ng/g) and Kawkaba (75.7 ± 20.3 ng/g) (Table 1). This has been also described by Rea et al., (1996) and Zhou et al., (2021) in uncontaminated and contaminated sites where litterfall Hg contents were systematically higher than the foliage Hg contents. The bacterial and chemical decomposition of the litter decrease significantly the amount of C compared to the Hg that conversely may continue to increase due to the continued absorption of Hg from precipitation and throughfall (Obrist et al., 2011; Pokharel & Obrist, 2011; Zhou et al., 2021). Another possible explanation is that the leaves shed as litter are likely to mostly be the oldest leaves which have accumulated Hg during the longest period of time and thus have higher Hg concentrations than the remaining foliage have on average since they consist of both younger and older foliage (Rea et al. 1996; Pleijel et al. 2021).

### IV.2 Seasonal foliage Hg content versus seasonal atmospheric Hg and $CO_2$

The late winter-early spring registered the highest Hg concentration for foliage in both groves, while summer and early fall to a less extent recorded the lowest concentrations. This seasonal change is explained by the seasonal tree physiology variations such as the Hg accumulation in leaves after stomatal uptake (Pleijel et al., 2021; Wohlgemuth et al., 2021). We can suggest that during winter-early spring, water is available and photosynthetic activity is not limited, hence both $CO_2$ and Hg diffuse through opened stomata inside the foliage. As shown on figure 2, Hg in foliage is low in summer-fall and hence act as a sink of Hg. A clear seasonal pattern of Hg concentration in foliage is evident, despite being based on three generation of olive leaves (1-3 years old), with youngest leaves known to have low concentrations (Pleijel et al., 2021), the seasonal signal is still very remarkable. Therefore, one can speculate that the mercury levels would have been higher if we had avoided the recently formed foliage

during spring and early summer. This may also explain the large difference in Hg levels between litter and foliage.

Evergreen olive foliage at our sites show a decrease in Hg contents from end of March to late August, with minimum values centered in August suggesting a decline of the plant Hg uptake likely explained by the reduction of the stomatal conductance (Lindberg et al., 2007; Pleijel et al., 2021). This minimal photosynthetic activity occurs during the driest season (0 mm precipitation) and hottest temperatures (above 25°C) at our sites. For the period 2018-2020, Martino et al. (2022) showed an atmospheric GEM depletion when NDVI values increased (normalized difference vegetation index). This can explain the lower foliage Hg content in 2019 compared to 2020 at our study sites in Lebanon. This was also collaborating Jiskra et al., (2018) for the Northern Hemisphere site. Since no data of atmospheric mercury in Lebanon or surrounding countries are available we used the atmospheric Hg time series data of Martino et al. (2022) (Figure 3a). We observed opposite trends between foliage Hg concentration and air Hg (negative covariation in 2019 and positve covariation in 2020) (Figure a,d,e).

Alternatively other studies reported a positive correlation between atmospheric Hg and crops (Niu et al. 2011) as observed in our study between the $Hg_{foliage}$ and the atmospheric Hg in 2020 (Figure 3a,d,e). This suggest the hypothesis where our groves seasonally exposed to high atmospheric Hg, accumulate Hg in their foliage (Lindberg et al. 2007; Pleijel et al. 2021). According to Hanson et al. (1995), a compensation point for Hg uptake by plant foliage can be considered but no information to our knowledge is available for the specific case of the olive trees. The tight link between foliage Hg uptake and stomatal conductance seasonal variations can be also deduced from the analysis of the partial pressure of the $pCO_{2atm}$ seasonal variation (Obrist, 2007; Jiskra et al., 2018; Obrist et al., 2018; Pleijel et al., 2021) (Figure 3b,d,e). Very good covariation between olive foliage Hg and $pCO_{2atm}$ are shown for Bchaaleh and Kawkaba despite a notable offset of one month at Kawkaba to two months at Bchaaleh can be deduced (Figure SI 4). Taking into account our calculated time lags, we obtained significant correlations between our foliage Hg content and $pCO_{2atm}$ of 0.718 and 0.704 in Bchaaleh and Kawkaba respectively. Interestingly a one month time-lag between atmospheric Hg and $pCO_{2atm}$ is also reported by Jiskra et al. (2018) for most northern hemisphere sites. The offset of one to two months between maxima of Bchaaleh and Kawkaba foliage Hg (March/April) and $pCO_{2atm}$ (May) suggests that the minimum of Hg in the foliage occur during the decreasing phase of the $pCO_{2atm}$ when the global northern hemisphere tend to become a net sink of $CO_2$. When minimum values of $pCO_{2atm}$ are reached at the end of the dry summer (Figure 3b), concomitant to minimum atmospheric Hg (Figure 3a), end of the drought and increase of precipitation (Figure 3c), Bchaleh and Kawkaba olive trees show a recovery in the Hg uptake rates. The photosynthetic activity and the stomatal conductance related to the climatic parameters (temperature, precipitation, humidity, $pCO_2$) as shown by Ozturk et al. (2021) and the atmospheric Hg explain our foliage Hg seasonal cycle. At a regional scale, our sites show different time lags between Bchaaleh and Kawkaba that we cannot explain fully except their altitudinal differences, which can suggest that Bchaaleh grove benefits of less drought in summer.

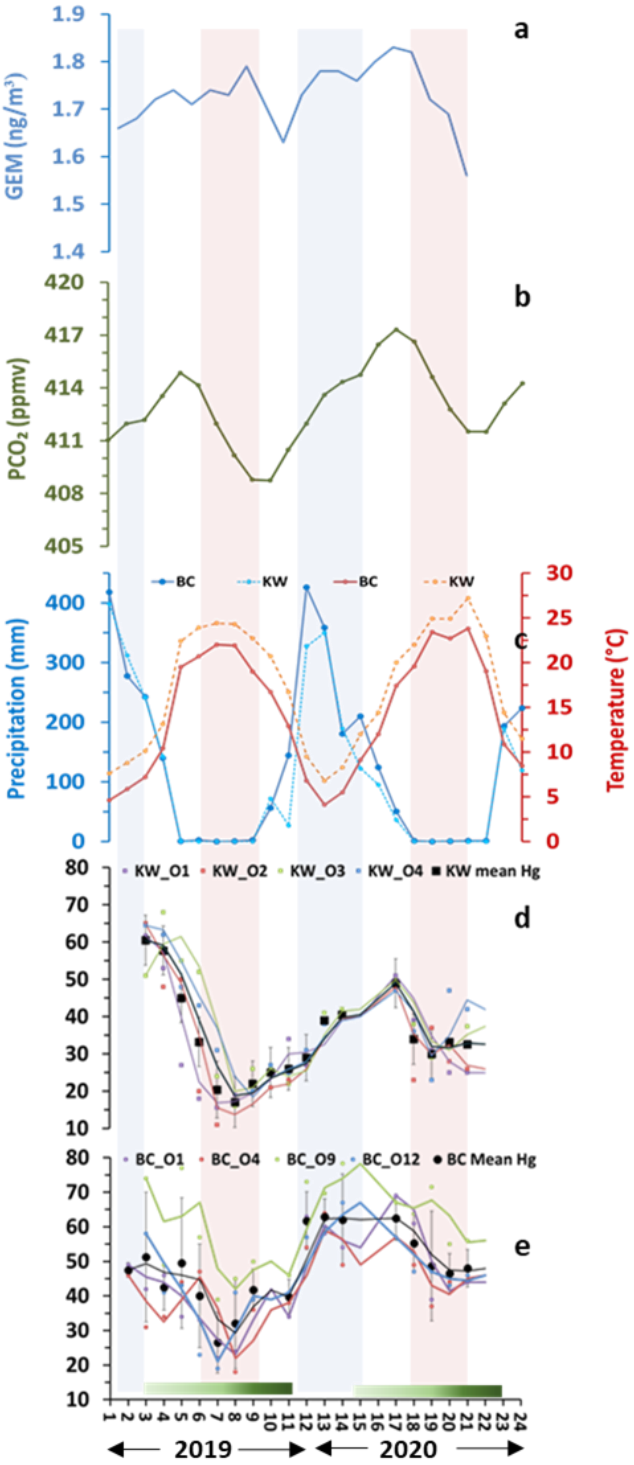


**Figure 5** Seasonal variations of **(a)** atmospheric Hg(0) (Martino et al. 2022), **(b)** $pCO_2$ (NOAA Global Monitoring Laboratory), **(c)** precipitations and temperature of Bchaaleh and Kawkaba respectively and **(d)** and **(e)** foliage Hg concentration in Bchaaleh and Kawkaba olive groves respectively. Shaded green horizontal bars represent the leaf development of olive trees during the growing season of cultivars in Spain according to the BBCH scale (Sanz-Cortès et al., 2002). Shaded colored lines correspond to the Winter (Blue) and Summer (Red).

### IV.3 Hg cycling in the stems, litter and soil system

For each site, Hg contents in stems exhibit a narrow range between the different trees except tree BCO9, which had the highest stem values. We speculate that this higher Hg content is the adjunction of chemical products as fertilizer on the plot 549 belonging to a different owner (Figure SI 2) likely between fall and winter. It was observed by (Zhao & Wang, 2010) that the fertilizer used and its source of phosphorous may affect the Hg content in the product and thus affect the amount of Hg transported into the fertilized soil.

At a seasonal scale, the averaged Hg values of soil system show statisticaly significant differences between the four seasons, while stems show statisticaly significant differences between winter (lowest values) and spring (p-value= 0.030) and winter-autumn (p-value= 0.047) in Bchaaleh grove mostly similar to foliage changes. While litter shows no significant difference between seasons. The same behavior was registered in Kawkaba in litter and soils, while stems showing statistical significance differences between autumn and spring (p-value= 0.011), spring-winter (p-value= 0.006) and spring-summer (p-value= 0.004) (Table 2). Despite the small amount of Hg content in the stems, the statistically significant seasonal changes may suggest that small amount of Hg move from the foliage to the lignified tissues as stems. However, we cannot neglect the Hg transport in xylem sap from the roots to the aboveground plant tissues even if minimal (Yang et al. 2018).

We can suggest the following Hg cycling in the system of the olive grove/soil. In winter-early spring the highest concentrations in foliage continuously feed the litter and can explain the following maximal spring Hg content of the litter. The decomposition of the litter organic matter during the wettest conditions likely liberate Hg in the Hg(0) or Hg(II) forms or MeHg either towards the atmosphere or the surface soil (see Table 2) respectively (Gworek et al., 2020). A fraction of the degraded organic matter is transferred through gaseous evaporative processes towards the atmosphere while another fraction of the Hg is leaching towards the deeper soil in addition to dry Hg deposition during dry season (Teixeira et al. 2017). We can also speculate that the small Hg decrease observed in soil 0-30, 30-60 cm during the winter season in Bchaaleh can be due to the minimal absorption of total Hg and MeHg through the roots and xylem sap to the above ground tissues (Johnson and Lindberg 1995).

## V. Conclusion

This is the first study conducted on monumental olive trees in a-remote site of the MENA region without local contamination and followed at a monthly basis over 18 months. Findings of our study indicate a higher uptake of Hg in the olive foliage compared to stems, fruits items and a remarkable $Hg_{Foliage}$ seasonal variation in both studied groves. Winter and Spring were particularly suitable for Hg accumulation in foliage in both sites. The significant correlation between our $Hg_{Foliage}$ contents and the atmospheric Hg content and $pCO_2$, despite the one to two months' time lag, suggests that the main source of $Hg_{Foliage}$ is the atmospheric Hg as observed in different species and studies (conifers and hardwood).

Hg is absorbed by the foliage, via the open stomata, driven by the interaction of high vegetal activity, temperature, water availability and the processes that control transpiration, which is likely to be seasonal. Hence physiological and climatic processes explain the seasonal Hg accumulation in foliage. Thus, a more intensive study taking account the phenological dynamics of olive tree foliage must be focused on. Further comparison and studies on the seasonal atmospheric Hg in the eastern Mediterranean basin are necessary to test our hypothesis of the reversed seasonality of Hg in 2019 and positive covariation in 2020 since contrary to the global Northern Hemisphere and western Mediteranean region vegetation, our olive groves act as a sink of Hg and $CO_2$ when global Northern and western Mediteranean vegetation is emitting. This relationship $Hg_{Foliage} - Hg_{atm}\text{-}pCO_{2atm}$ should be further investigated along the season and locally to better understand the observed time lags. Soil surface registered the highest Hg concentration among all studied compartments due to well-known processes of litter and throughfall that incorporate Hg to the soil surface. Moreover, this study highlights significant differences between $Hg_{soil}$ in Bchaaleh and Kawkaba groves due to differences in soil characteristics. In this study we worked on the present time samples in order to have a better understanding of the Hg cycle in the olive tree. Our main contribution in this study is to see how the present-day olive trees records some elements such as Hg to better understand how the Hg in tree rings could be used for the past accumulation records.

## Supplementary Information

**Table SI 2** Study sites geographic location and climatic data collected from the meteo stations installed by LARI.

| Village Name | Location | Latitude (N) | Longitude (E) | Altitude (m a.s.l) | Temperature min-max (°C) | Annual mean Temperature (°C) | SD (±) | Annual mean rainfall (mm) | SD (±) |
|---|---|---|---|---|---|---|---|---|---|
| Bchaaleh | North Lebanon | 34°12'06" | 35°49'23" | 1300 | 4-23 | 14 | 6.81 | 1631 | 110.17 |
| Kawkaba | South Lebanon | 33°23'85" | 35°38'58" | 672 | 7-27 | 17 | 6.76 | 1311 | 295.29 |

**Table SI 3** Detailed synthesis of the Hg concentration values in different studies.

**Table S2 in an Excel Format**

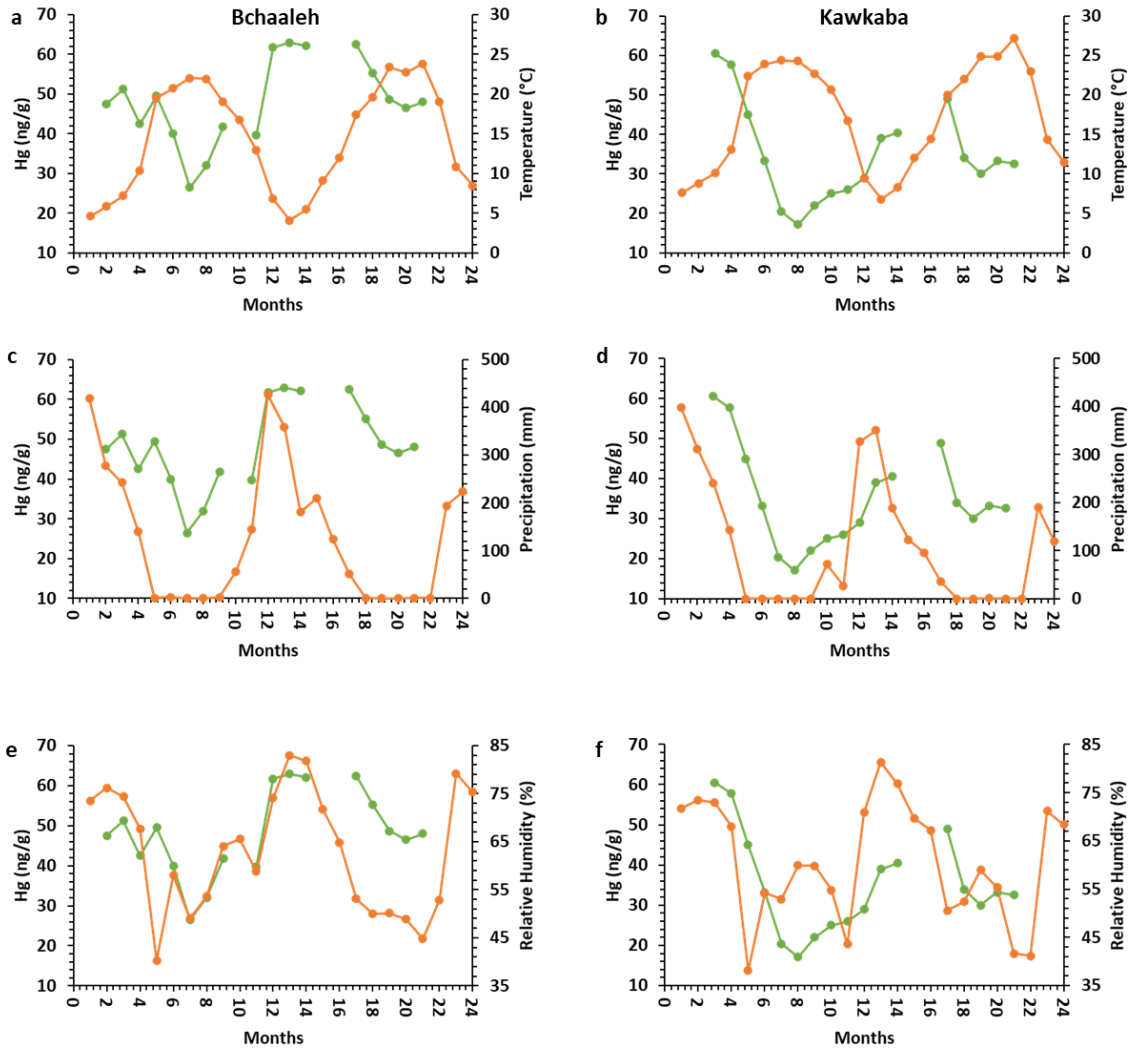


**Figure SI 1** Bchaaleh and Kawkaba **(a) (b)** Hg(ng/g) and Temperature(°C), **(c) (d)** Hg(ng/g) and Precipitation(mm) and **(e)** Hg(ng/g) and Relative Humidity (%).

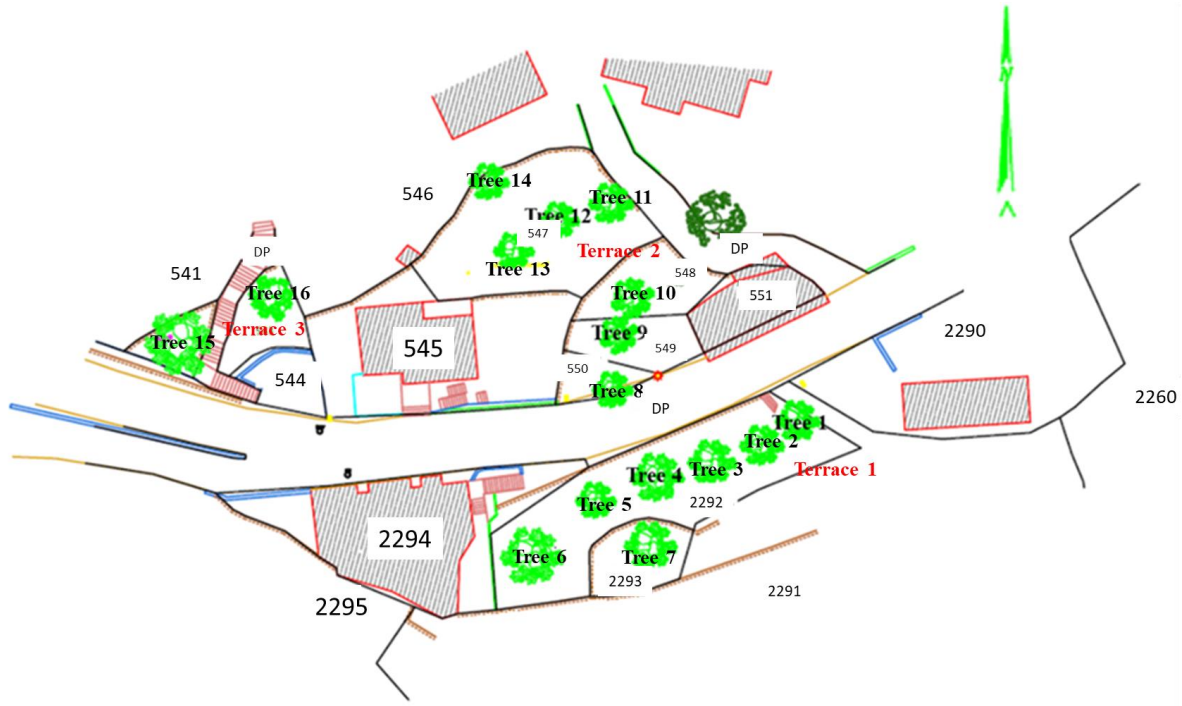


**Figure SI 2** Map of Bchaaleh site and sampled tree locations. Upper terrace plot 2292 are under the endowment of the church. While Lower terrace plot 549 and 547 are a private property.

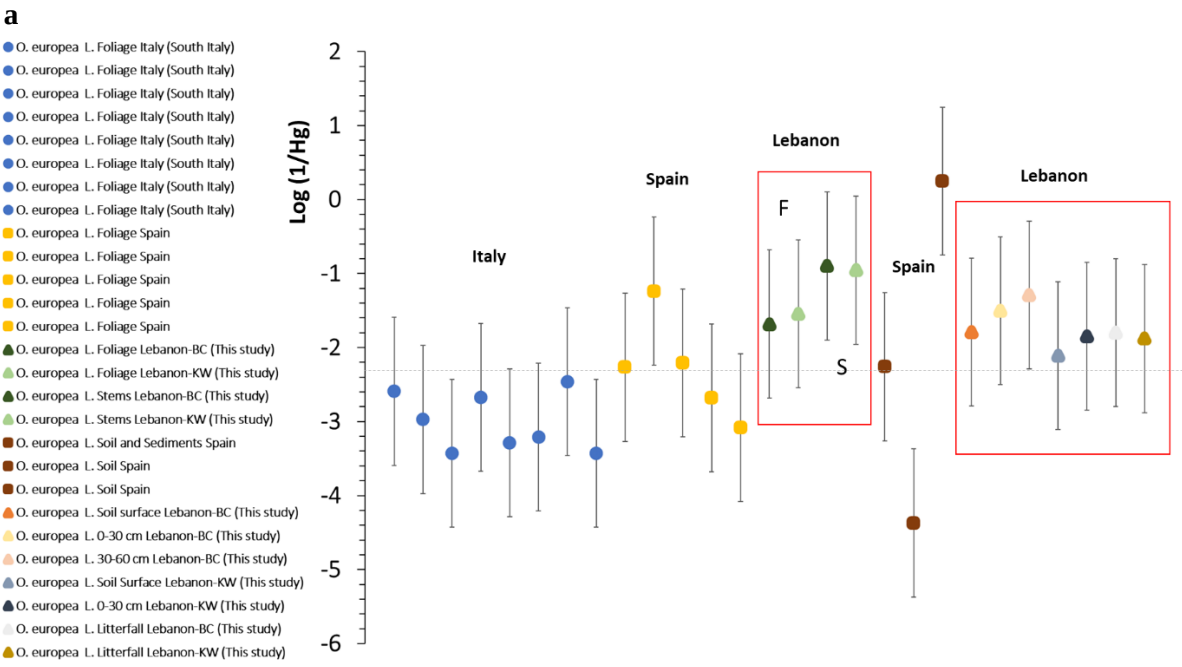

**b**

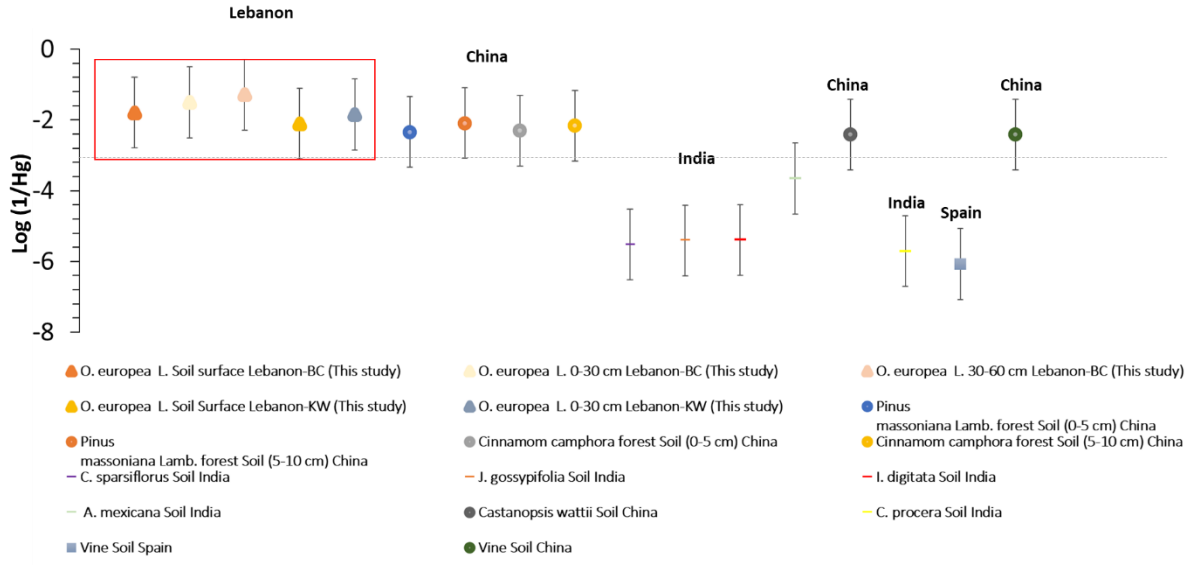
Lebanon
China
China
China
India
India
Spain
0
-2
-4
-6
-8
Log (1/Hg)
O. europea L. Soil surface Lebanon-BC (This study)
O. europea L. 0-30 cm Lebanon-BC (This study)
O. europea L. 30-60 cm Lebanon-BC (This study)
O. europea L. Soil Surface Lebanon-KW (This study)
O. europea L. 0-30 cm Lebanon-KW (This study)
Pinus massoniana Lamb. forest Soil (0-5 cm) China
Pinus massoniana Lamb. forest Soil (5-10 cm) China
Cinnamom camphora forest Soil (0-5 cm) China
Cinnamom camphora forest Soil (5-10 cm) China
C. sparsiflorus Soil India
J. gossypifolia Soil India
I. digitata Soil India
A. mexicana Soil India
Castanopsis wattii Soil China
C. procera Soil India
Vine Soil Spain
Vine Soil China

**c**

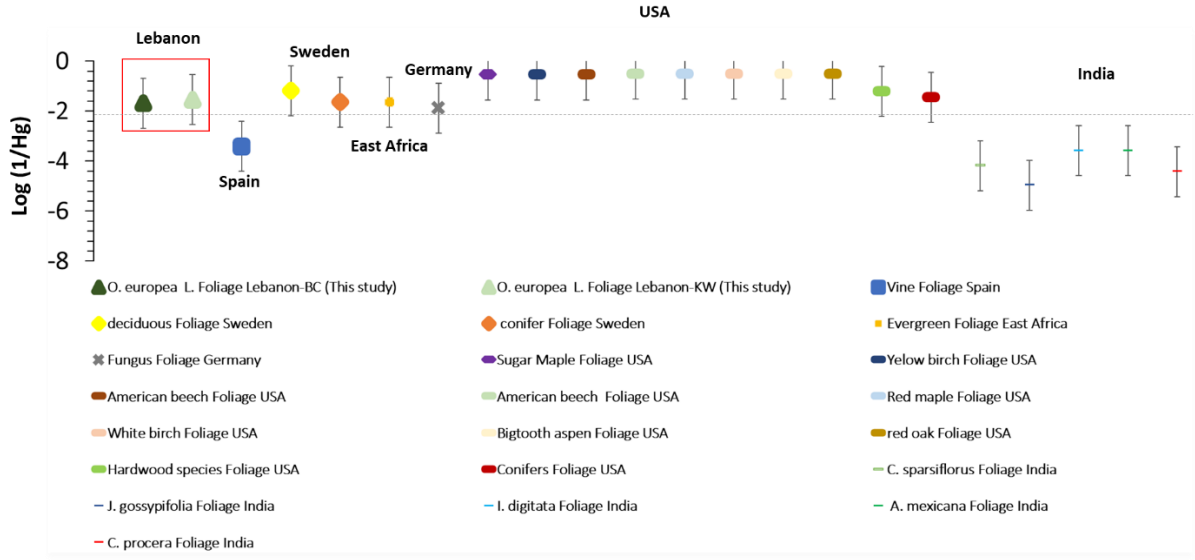
USA
Lebanon
Sweden
Germany
India
East Africa
Spain
0
-2
-4
-6
-8
Log (1/Hg)
O. europea L. Foliage Lebanon-BC (This study)
O. europea L. Foliage Lebanon-KW (This study)
Vine Foliage Spain
deciduous Foliage Sweden
conifer Foliage Sweden
Evergreen Foliage East Africa
Fungus Foliage Germany
Sugar Maple Foliage USA
Yelow birch Foliage USA
American beech Foliage USA
American beech Foliage USA
Red maple Foliage USA
White birch Foliage USA
Bigtooth aspen Foliage USA
red oak Foliage USA
Hardwood species Foliage USA
Conifers Foliage USA
C. sparsiflorus Foliage India
J. gossypifolia Foliage India
I. digitata Foliage India
A. mexicana Foliage India
C. procera Foliage India

**d**

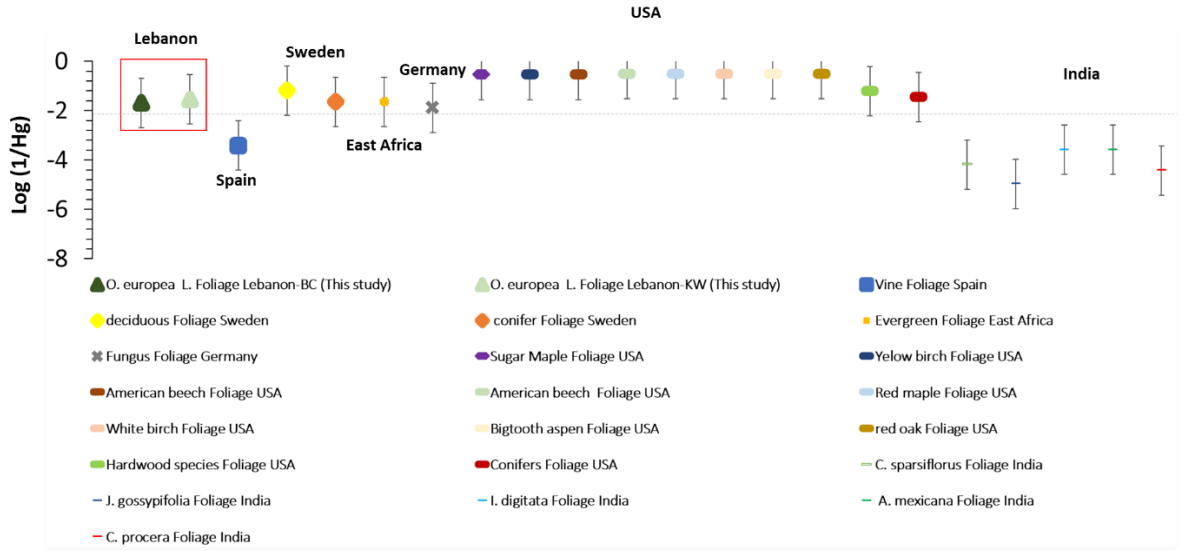


**Figure SI 3** Synthesis of Hg concentration for **a)** the Olive grove of the Mediterranean basin including foliage, stems, litter and soil. Our sites are indicated in red; **b)** the foliage of different species around the world; **c)** soil studies in different countries and **d)** litter, roots and stems of different species and countries. All the references are listed in Table SI 3. The gray dashed lines referrer to the threshold limit above which soil and plants are not contaminated.

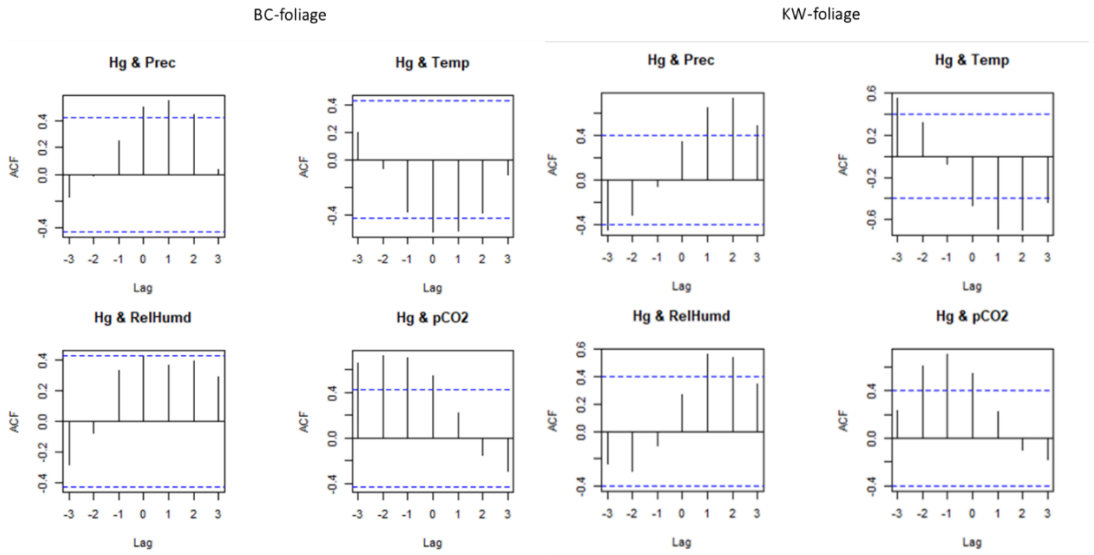


**Figure SI 4** Time lag test (R, Cross correlation) between the dependent variable (Hg) and the independent climatic variables in the foliage of BC and KW.

## References for Supplementary Information

Amorós JA, Esbrí JM, García-Navarro FJ, Pérez-de-los-Reyes C, Bravo S, Villaseñor B, Higueras P (2014) Variations in mercury and other trace elements contents in soil and in vine leaves from the Almadén Hg-mining district. Journal of Soils and Sediments, 14(4), 773–777. https://doi.org/10.1007/s11368-013-0783-2

Bargagli R (1995) The elemental composition of vegetation and the possible incidence of soil contamination of samples. Science of The Total Environment, 176(1–3), 121–128. https://doi.org/10.1016/0048-9697(95)04838-3

Esbrí JM, López-Berdonces MA, Fernández-Calderón, S, Higueras P, Díez S (2015) Atmospheric mercury pollution around a chlor-alkali plant in Flix (NE Spain): An integrated analysis. Environmental Science and Pollution Research, 22(7), 4842–4850. https://doi.org/10.1007/s11356-014-3305-x

Fische RG, Rapsomanikis S, Andreae MO, Baldi F (1995) Bioaccumulation of methylmercury and transformation of inorganic mercury by macrofungi. Environmental Science & Technology 29(4), 993–999. https://doi.org/10.1021/es00004a020

Guarino F, Improta G, Triassi M, Castiglione S, Cicatelli A (2021) Air quality biomonitoring through *Olea europaea* L.: The study case of "Land of pyres." Chemosphere 282, 131052. https://doi.org/10.1016/j.chemosphere.2021.131052

Higueras P, Amorós JA, Esbrí JM, García-Navarro FJ, Pérez de los Reyes C, Moreno G (2012) Time and space variations in mercury and other trace element contents in olive tree leaves from the Almadén Hg-mining district. Journal of Geochemical Exploration 123, 143–151. https://doi.org/10.1016/j.gexplo.2012.04.012

Higueras P, Amorós, JÁ, Esbrí JM, Pérez-de-los-Reyes C, López-Berdonces MA, García-Navarro FJ (2016) Mercury transfer from soil to olive trees. A comparison of three different contaminated sites. Environmental Science and Pollution Research 23(7), 6055–6061. https://doi.org/10.1007/s11356-015-4357-2

Kabata-Pendias A and Pendias H (2000) Trace elements in soils and plants (3rd ed) CRC Press

Llanos W, Kocman D, Higueras P, Horvat M (2011) Mercury emission and dispersion models from soils contaminated by cinnabar mining and metallurgy. Journal of Environmental Monitoring 13(12), 3460. https://doi.org/10.1039/c1em10694e

Naharro R, Esbri J, Amorós J, Higueras P (2018) Atmospheric mercury uptake and desorption from olive-tree leaves. 20(EGU2018-2982,2018), 2

Pleijel H, Klingberg J, Nerentorp M, Broberg MC, Nyirambangutse B, Munthe J, Wallin G (2021) Mercury accumulation in leaves of different plant types – the significance of tissue age and specific leaf area [Preprint]. Biogeochemistry: Air - Land Exchange. https://doi.org/10.5194/bg-2021-117

Rea AW, Lindberg SE, Scherbatskoy T, Keeler GJ (2002) Mercury accumulation in foliage over time in two Northern mixed-hardwood forests. Water, Air, and Soil Pollution 133(1), 49-67

Senesil GS, Baldassarre G, Senesi N, Radina B (1999) Trace element inputs into soils by anthropogenic activities and implications for human health. Chemosphere 39(2), 343–377. https://doi.org/10.1016/S0045-6535(99)00115-0

Shaw BP and Panigrahi AK (1986) Uptake and tissue distribution of mercury in some plant species collected from a contaminated area in India: Its ecological implications. Archives of Environmental Contamination and Toxicology 15(4), 439–446. https://doi.org/10.1007/BF01066412

Teixeira DC, Lacerda LD, Silva-Filho EV (2017) Mercury sequestration by rainforests: The influence of microclimate and different successional stages. Chemosphere, 168:1186–1193. https://doi.org/10.1016/j.chemosphere.2016.10.081

Wang X, Li CJ, Lu Z, Zhang H, Zhang Y, Feng X (2016) Enhanced accumulation and storage of mercury on subtropical evergreen forest floor: Implications on mercury budget in global forest ecosystems: Hg storage on subtropical forest floor. Journal of Geophysical Research: Biogeosciences 121: 2096–2109. https://doi.org/10.1002/2016JG003446

Yang Y, Yanai RD, Driscoll CT, Montesdeoca M, Smith KT (2018) Concentrations and content of mercury in bark, wood, and leaves in hardwoods and conifers in four forested sites in the Northeastern USA. PLOS ONE 13(4): e0196293. https://doi.org/10.1371/journal.pone.0196293

**Data availability**

The datasets generated during and/or analyzed during the current study are available from the corresponding author on reasonable request.

**Author Contributions**

The corresponding author **Ilham Bentaleb** is responsible for ensuring that the descriptions are accurate and agreed upon by all authors. Conceptualization and methodology were done and developed by **Ilham Bentaleb** and **Lamis Chalak**. The material collection was performed by **Nagham Tabaja, Ilham Bentaleb, Lamis Chalak, Ihab Jomaa, and Milad Riachy**. Sample storage and preparation in Lebanon organized by Nagham Tabaja. Material preparation at ISEM by Nagham Tabaja, Data collection and analysis were performed by Nagham Tabaja, Ilham Bentaleb, David Amouroux, and Emmanuel Tessier. The setting of the meteorological stations by Ihab Jomaa. Subsamples of soil were analyzed for carbon and nitrogen elemental contents (%) by **François Fourel.** The first draft of the manuscript was written by **Nagham Tabaja**. **Ilham Bentaleb, Lamis Chalak, David Amouroux, Ihab Jomaa, and Milad Riachy** commented on previous versions of the manuscript. All authors read and approved the final manuscript. Supervision was done by **Ilham Bentaleb and Lamis Chalak**.

**Competing interests**

The authors declare that they have no known competing financial interests or personal relationships that could have appeared to influence the work reported in this paper.

## Acknowledgments

The authors would like to acknowledge the National Council for Scientific Research of Lebanon (CNRS-L) and Montpellier University for granting a doctoral fellowship (CNRS-L/UM) to Nagham Tabaja. The authors would also like to thank the Franco-Lebanese Hubert Curien Partnership (PHC-CEDRE) project 44559PL for the funding provided. Institute of Evolutionary Science of Montpellier (ISEM) at Montpellier University and the Research Platform for Environment and Science- Doctoral School of Science and Technology (PRASE-EDST) at the Lebanese University are also acknowledged for their support of the laboratory work. Credits go to the Lebanese Agriculture Research Institute (LARI) for assuring automated weather stations and manual rain gauges per site. The authors are grateful to the Municipality of Bchaaleh (Mr. Rachid Geagea) and the Municipality of Kawkaba (Ms. Mira Khoury). Acknowledgments are extended to Ms. Amira Yousef at LARI for her kind support and to Mr. Akram Tabaja for helping during fieldwork. We are very greatful to Pleijel Hakan who reviewed this article improving significantly our paper. We deeply aknowledge Andrew Johnston for the English revision.

### Funding

This work was supported and funded by Lebanon and Montpellier University (CNRS-L/UM grant), and PHC-CEDRE-project 44559PL

## References

Abou Habib, N., Taleb, M., and Khoury, R.: Environmental and social safeguard studies for lake qaraoun pollution prevention project, V1(E4749), 2015.

Alcaras, L. M. A., Rousseaux, M. C., and Searles, P. S.: Responses of several soil and plant indicators to post-harvest regulated deficit irrigation in olive trees and their potential for irrigation scheduling, Agricultural Water Management, 171, 10–20, https://doi.org/10.1016/j.agwat.2016.03.006, 2016.

Alloway, B. J.: Heavy Metals in Soils, Springer Science & Business Media, 1995.

Al-Zubaidi, A., Yanni, S., and Bashour, I.: Potassium status in some Lebanese soils, Lebanese Science Journal, 9(1), 81–97, 2008.

Assad, M.: Transfert des éléments traces métalliques vers les végétaux: Mécanismes et évaluations des risques dans des environnements exposés à des activités anthropiques, 218, 2017.

Baayoun, A., Itani, W., El Helou, J., Halabi, L., Medlej, S., El Malki, M., Moukhadder, A., Aboujaoude, L. K., Kabakian, V., Mounajed, H., Mokalled, T., Shihadeh, A., Lakkis, I., and Saliba, N. A.: Emission inventory of key sources of air pollution in Lebanon, Atmospheric Environment, 215, 116871, https://doi.org/10.1016/j.atmosenv.2019.116871, 2019.

Badr, R., Holail, H., and Olama, Z.: Water quality assessment of hasbani river in south lebanon: microbiological and chemical characteristics and their impact on the ecosystem, 3, 16, 2014.

Barber, S. A.: Soil Nutrient Bioavailability: A Mechanistic Approach, John Wiley and Sons, 1995.

Bargagli, R.: The elemental composition of vegetation and the possible incidence of soil contamination of samples, Science of The Total Environment, 176(1–3), 121–128, https://doi.org/10.1016/0048-9697(95)04838-3, 1995.

Barre, J. P. G., Deletraz, G., Sola-Larrañaga, C., Santamaria, J. M., Bérail, S., Donard, O. F. X., and Amouroux, D.: Multi-element isotopic signature (C, N, Pb, Hg) in epiphytic lichens to discriminate atmospheric contamination as a function of land-use characteristics (Pyrénées-Atlantiques, SW France), Environmental Pollution, 243, 961–971, https://doi.org/10.1016/j.envpol.2018.09.003, 2018.

Beauford, W., Barber, J., and Barringer, A. R.: Uptake and Distribution of Mercury within Higher Plants, Physiologia Plantarum, 39(4), 261–265, https://doi.org/10.1111/j.1399-3054.1977.tb01880.x, 1977.

Besnard, G., Khadari, B., Navascues, M., Fernandez-Mazuecos, M., Bakkali, A. E., Arrigo, N., Baali-Cherif, D., de Caraffa, V. B.-B., Santoni, S., Vargas, P., and Savolainen, V.: The complex history of the olive tree: From Late Quaternary diversification of Mediterranean lineages to primary domestication in the northern Levant, Proceedings of the Royal Society B: Biological Sciences, 280(1756), https://doi.org/10.1098/rspb.2012.2833, 2013.

Bishop, K. H., Lee, Y.-H., Munthe, J., and Dambrine, E.: Xylem sap as a pathway for total mercury and methylmercury transport from soils to tree canopy in the boreal forest, Biogeochemistry, 40, 101–113, https://doi.org/10.1023/A:1005983932240, 1998.

Bishop, K., Shanley, J. B., Riscassi, A., de Wit, H. A., Eklöf, K., Meng, B., Mitchell, C., Osterwalder, S., Schuster, P. F., Webster, J., and Zhu, W.: Recent advances in understanding and measurement of mercury in the environment: Terrestrial Hg cycling, Science of The Total Environment, 721, 137647, https://doi.org/10.1016/j.scitotenv.2020.137647, 2020.

Blackwell, B. D., and Driscoll, C. T.: Using foliar and forest floor mercury concentrations to assess spatial patterns of mercury deposition, Environmental Pollution, 202, 126–134, https://doi.org/10.1016/j.envpol.2015.02.036, 2015.

Boening, D. W.: Ecological effects, transport, and fate of mercury: A general review, Jun;40(12):1335-51. doi: 10.1016/s0045-6535(99)00283-0, PMID: 10789973, 2000.

Borjac, J., El Joumaa, M., Kawach, R., Youssef, L., and Blake, D. A.: Heavy metals and organic compounds contamination in leachates collected from Deir Kanoun Ras El Ain dump and its adjacent canal in South Lebanon, Heliyon, 5(8), e02212, https://doi.org/10.1016/j.heliyon.2019.e02212, 2019.

Borjac, J., El Joumaa, M., Youssef, L., Kawach, R., and Blake, D. A.: Quantitative Analysis of Heavy Metals and Organic Compounds in Soil from Deir Kanoun Ras El Ain Dump, Lebanon, The Scientific World Journal, 2020, 1–10, https://doi.org/10.1155/2020/8151676, 2020.

Briffa, J., Sinagra, E., and Blundell, R.: Heavy metal pollution in the environment and their toxicological effects on humans, Heliyon, 6(9), e04691, https://doi.org/10.1016/j.heliyon.2020.e04691, 2020.

Carrasco-Gil, S., Estebaranz-Yuberob, M., Medel-Cuestab, D., Millán, R., and Hernández, L. E.: Influence of nitrate fertilization on Hg uptake and oxidative stress parameters in alfalfa plants cultivated in a Hg-polluted soil, Environmental and Experimental Botany, 75, https://doi.org/10.1016/j.envexpbot.2011.08.013, 2012.

Cavallini, A., Natali, L., Durante, M., and Maserti, B., Mercury uptake, distribution and DNA affinity in durum wheat (Triticum durum Desf.) plants, Science of The Total Environment, 243–244, 119–127, https://doi.org/10.1016/S0048-9697(99)00367-8, 1999.

Chen, X., Ji, H., Yang, W., Zhu, B., and Ding, H. Speciation and distribution of mercury in soils around gold mines located upstream of Miyun Reservoir, Beijing, China, Journal of Geochemical Exploration, 163, 1–9, https://doi.org/10.1016/j.gexplo.2016.01.015, 2016.

Clarkson, T. W., and Magos, L.: The Toxicology of Mercury and Its Chemical Compounds, Critical Reviews in Toxicology, 36(8), 609–662, https://doi.org/10.1080/10408440600845619, 2006.

Dastoor, A., Angot, H., Bieser, J., Christensen, J. H., Douglas, T. A., Heimbürger-Boavida, L.-E., Jiskra, M., Mason, R. P., McLagan, D. S., Obrist, D., Outridge, P. M., Petrova, M. V., Ryjkov, A., St. Pierre, K. A., Schartup, A. T., Soerensen, A. L., Toyota, K., Travnikov, O., Wilson, S. J., and Zdanowicz, C.: Arctic mercury cycling, Nature Reviews Earth & Environment, 3(4), Article 4, https://doi.org/10.1038/s43017-022-00269-w, 2022.

Demers, J. D., Blum, J. D., and Zak, D. R.: Mercury isotopes in a forested ecosystem: Implications for air-surface exchange dynamics and the global mercury cycle: Mercury isotopes in a forested ecosystem, Global Biogeochemical Cycles, 27(1), 222–238, https://doi.org/10.1002/gbc.20021, 2013.

Du, S.-H., and Fang, S. C.: Catalase activity of C3 and C4 species and its relationship to mercury vapor uptake Environmental and Experimental Botany, 23(4), 347–353, https://doi.org/10.1016/0098-8472(83)90009-6, 1983.

Duval, B., Gredilla, A., Fdez-Ortiz de Vallejuelo, S., Tessier, E., Amouroux, D., and De Diego, A.: A simple determination of trace mercury concentrations in natural waters using dispersive Micro-Solid phase extraction preconcentration based on functionalized graphene nanosheets, Microchemical Journal, 154, 104549, https://doi.org/10.1016/j.microc.2019.104549, 2020.

EJOLT: Cimenterie Nationale Factory in Chekaa, Lebanon | EJAtlas, Environmental Justice Atlas, https://ejatlas.org/conflict/chekaa, Acces date: 2019.

Ericksen, J. A., Gustin, M. S., Schorran, D. E., Johnson, D. W., Lindberg, S. E., and Coleman, J. S.: Accumulation of atmospheric mercury in forest foliage, Atmospheric Environment, 37(12), 1613–1622, https://doi.org/10.1016/S1352-2310(03)00008-6, 2003.

Ermolin, M. S., Fedotov, P. S., Malik, N. A., and Karandashev, V. K.: Nanoparticles of volcanic ash as a carrier for toxic elements on the global scale, Chemosphere, 200, 16–22, https://doi.org/10.1016/j.chemosphere.2018.02.089, 2018.

Freeman, M., and Carlson, R. M.: Essential nutrients, Olive Production Manual, 3353, 75, 2005.

Friedli, H. R., Arellano, A. F., Cinnirella, S., and Pirrone, N.: Initial Estimates of Mercury Emissions to the Atmosphere from Global Biomass Burning, Environmental Science and Technology, 43(10), 3507–3513, https://doi.org/10.1021/es802703g, 2009.

Galatali, S., A., N., and Kaya, E.: Characterization of Olive (Olea Europaea L.) Genetic Resources via PCR-Based Molecular Marker Systems, 2, 26–33, https://doi.org/10.24018/ejbio.2021.2.1.146, 2021.

Gårdfeldt, K., Sommar, J., Ferrara, R., Ceccarini, C., Lanzillotta, E., Munthe, J., Wängberg, I., Lindqvist, O., Pirrone, N., Sprovieri, F., Pesenti, E., and Strömberg, D.: Evasion of mercury from coastal and open waters of the Atlantic Ocean and the Mediterranean Sea, Atmospheric Environment, 37, 73–84, https://doi.org/10.1016/S1352-2310(03)00238-3, 2003.

Gérard, J., and Nehmé, C.: Lebanon, Méditerranée, Revue Géographique Des Pays Méditerranéens / Journal of Mediterranean Geography, 131, Article 131, https://journals.openedition.org/mediterranee/11018#, 2020.

Giesler, R., Clemmensen, K. E., Wardle, D. A., Klaminder, J., and Bindler, R.: Boreal Forests Sequester Large Amounts of Mercury over Millennial Time Scales in the Absence of Wildfire, Environmental Science and Technology, 51(5), 2621–2627, https://doi.org/10.1021/acs.est.6b06369, 2017.

Grigal, D.: Mercury Sequestration in Forests and Peatlands: A Review, Journal of Environmental Quality - J ENVIRON QUAL, 32, https://doi.org/10.2134/jeq2003.0393, 2003.

Guarino, F., Improta, G., Triassi, M., Castiglione, S., and Cicatelli, A.: Air quality biomonitoring through Olea europaea L.: The study case of "Land of pyres." Chemosphere, 282, 131052, https://doi.org/10.1016/j.chemosphere.2021.131052, 2021.

Gworek, B., Dmuchowski, W., and Baczewska-Dąbrowska, A. H.: Mercury in the terrestrial environment: A review, Environmental Sciences Europe, 32(1), 128, https://doi.org/10.1186/s12302-020-00401-x, 2020.

Hanson, P. J., Lindberg, S. E., Tabberer, T. A., Owens, J. G., and Kim, K.-H.: Foliar exchange of mercury vapor: Evidence for a compensation point, Water, Air, and Soil Pollution, 80(1–4), 373–382, https://doi.org/10.1007/BF01189687, 1995.

Higueras, P., Amorós, J. A., Esbrí, J. M., García-Navarro, F. J., Pérez de los Reyes, C., and Moreno, G.: Time and space variations in mercury and other trace element contents in olive tree leaves from the Almadén Hg-mining district, Journal of Geochemical Exploration, 123, 143–151, https://doi.org/10.1016/j.gexplo.2012.04.012, 2012.

Higueras, P. L., Amorós, J. Á., Esbrí, J. M., Pérez-de-los-Reyes, C., López-Berdonces, M. A., and García-Navarro, F. J.: Mercury transfer from soil to olive trees, A comparison of three different contaminated sites, Environmental Science and Pollution Research, 23(7), 6055–6061, https://doi.org/10.1007/s11356-015-4357-2, 2016.

Jindrich Petrlik, Kodeih, N., IndyACT, Arnika Association, and IPEN WG.: Mercury in Fish and Hair Samples from Batroun, Lebanon, https://doi.org/10.13140/RG.2.2.12052.40327, 2013.

Jiskra, M., Sonke, J. E., Obrist, D., Bieser, J., Ebinghaus, R., Myhre, C. L., Pfaffhuber, K. A., Wängberg, I., Kyllönen, K., Worthy, D., Martin, L. G., Labuschagne, C., Mkololo, T., Ramonet, M., Magand, O., and Dommergue, A.: A vegetation control on seasonal variations in global atmospheric mercury concentrations, Nature Geoscience, 11(4), 244–250, https://doi.org/10.1038/s41561-018-0078-8, 2018.

Johnson, and Lindberg: The biogeochemical cycling of Hg in forests: Alternative methods for quantifying total deposition and soil emission, 1995, 80: 1069–1077, 9, 1995.

Jurdi, M., Korfali, S. I., Karahagopian, Y., and Davies, B. E.: Evaluation of Water Quality of the Qaraaoun Reservoir, Lebanon: Suitability for Multipurpose Usage, 77(11–30), 20, 2002.

Kabata-Pendias, A., and Pendias, H.: Trace elements in soils and plants (3rd ed), CRC Press, 2000.

Khadari, B., El Bakkali, A., Essalouh, L., Tollon, C., Pinatel, C., and Besnard, G.: Cultivated Olive Diversification at Local and Regional Scales: Evidence From the Genetic Characterization of French Genetic Resources, Frontiers in Plant Science, 10, https://www.frontiersin.org/articles/10.3389/fpls.2019.01593, 2019.

Kobrossi, R., Nuwayhid, I., Sibai, A. M., El-Fadel, M., and Khogali, M.: Respiratory health effects of industrial air pollution on children in North Lebanon, International Journal of Environmental Health Research, 12(3), 205–220, https://doi.org/10.1080/09603/202/000000970, 2002.

Kotnik, J., Sprovieri, F., Ogrinc, N., Horvat, M., and Pirrone, N.: Mercury in the Mediterranean, part I: Spatial and temporal trends, Environmental Science and Pollution Research, 21(6), 4063–4080, https://doi.org/10.1007/s11356-013-2378-2, 2014.

Labdaoui, D., Lotmani, B., and Aguedal, H.: Assessment of Metal Pollution on the Cultivation of Olive Trees in the Petrochemical Industrial Zone of Arzew (Algeria), South Asian Journal of Experimental Biology, 11(3), Article 3, https://doi.org/10.38150/sajeb.11(3).p227-233, 2021.

Lebanon: Air Pollution | IAMAT: https://www.iamat.org/country/lebanon/risk/air-pollution, 2020.

Li, D., Fang, K., Li, Y., Chen, D., Liu, X., Dong, Z., Zhou, F., Guo, G., Shi, F., Xu, C., and Li, Y.: Climate, intrinsic water-use efficiency and tree growth over the past 150 years in humid subtropical China, PLOS ONE, 12(2), e0172045, https://doi.org/10.1371/journal.pone.0172045, 2017.

Li, R., Wu, H., Ding, J., Fu, W., Gan, L., and Li, Y.: Mercury pollution in vegetables, grains and soils from areas surrounding coal-fired power plants, Scientific Reports, 7(1), 46545, https://doi.org/10.1038/srep46545, 2017.

Lindberg, S., Bullock, R., Ebinghaus, R., Engstrom, D., Feng, X., Fitzgerald, W., Pirrone, N., Prestbo, E., and Seigneur, C.: A Synthesis of Progress and Uncertainties in Attributing the Sources of Mercury in Deposition, Ambio, 36(1), 19–32, 2007.

Lindberg, S. E., Jackson, D. R., Huckabee, J. W., Janzen, S. A., Levin, M. J., and Lund, J. R.: Atmospheric Emission and Plant Uptake of Mercury from Agricultural Soils near the Almadén Mercury Mine, Journal of Environmental Quality, 8(4), 572–578, https://doi.org/10.2134/jeq1979.00472425000800040026x, 1979.

Lodenius, M., Tulisalo, E., and Soltanpour-Gargari, A.: Exchange of mercury between atmosphere and vegetation under contaminated conditions, Science of The Total Environment, 304(1–3), 169–174, https://doi.org/10.1016/S0048-9697(02)00566-1, 2003.

Luo, Y., Duan, L., Driscoll, C. T., Xu, G., Shao, M., Taylor, M., Wang, S., and Hao, J.: Foliage/atmosphere exchange of mercury in a subtropical coniferous forest in south China, Journal of Geophysical Research: Biogeosciences, 121(7), 2006–2016, https://doi.org/10.1002/2016JG003388, 2016.

Maillard, F., Girardclos, O., Assad, M., Zappelini, C., Pérez Mena, J. M., Yung, L., Guyeux, C., Chrétien, S., Bigham, G., Cosio, C., and Chalot, M.: Dendrochemical assessment of mercury releases from a pond and dredged-sediment landfill impacted by a chlor-alkali plant, Environmental Research, 148, 122–126, https://doi.org/10.1016/j.envres.2016.03.034, 2016.

McLagan, D. S., Biester, H., Navrátil, T., Kraemer, S. M., and Schwab, L.: Internal tree cycling and atmospheric archiving of mercury: Examination with concentration and stable isotope analyses, Biogeosciences, 19, 4415–4429, 2022, https://doi.org/10.5194/bg-19-4415-2022, 2022.

McLagan, D. S., Stupple, G. W., Darlington, A., Hayden, K., Steffen, A., and Kamp, L.: Where there is smoke there is mercury: Assessing boreal forest fire mercury emissions using aircraft and highlighting uncertainties associated with upscaling emissions estimates, Atmos. Chem. Phys., 19, 2021.

Naharro, R., Esbri, J., Amorós, J., and Higueras, P.: Atmospheric mercury uptake and desorption from olive-tree leaves, 20(EGU2018-2982,2018), 2, 2018.

Nassif, N., Jaoude, L. A., El Hage, M., and Robinson, C. A.: Data Exploration and Reconnaissance to Identify Ocean Phenomena: A Guide for In Situ Data Collection, Journal of Water Resource and Protection, 08(10), 929–943, https://doi.org/10.4236/jwarp.2016.810076, 2016.

Niu, Z., Zhang, X., Wang, Z., and Ci, Z.: Field controlled experiments of mercury accumulation in crops from air and soil, Environmental Pollution, 159(10), 2684–2689, https://doi.org/10.1016/j.envpol.2011.05.029, 2011.

Obrist, D.: Atmospheric mercury pollution due to losses of terrestrial carbon pools? Biogeochemistry, 85(2), 119–123, https://doi.org/10.1007/s10533-007-9108-0, 2011, 2007.

Obrist, D., Johnson, D. W., and Lindberg, S. E.: Mercury concentrations and pools in four Sierra Nevada forest sites, and relationships to organic carbon and nitrogen, 13, 2009.

Obrist, D., Kirk, J. L., Zhang, L., Sunderland, E. M., Jiskra, M., and Selin, N. E.: A review of global environmental mercury processes in response to human and natural perturbations: Changes of emissions, climate, and land use, Ambio, 47(2), 116–140, https://doi.org/10.1007/s13280-017-1004-9, 2018.

Obrist, D., Johnson, D. W., Lindberg, S. E., Luo, Y., Hararuk, O., Bracho, R., Battles, J. J., Dail, D. B., Edmonds, R. L., Monson, R. K., Ollinger, S. V., Pallardy, S. G., Pregitzer, K. S., and Todd, D. E.: Mercury Distribution Across 14 U.S. Forests, Part I: Spatial Patterns of Concentrations in Biomass, Litter, and Soils, Environmental Science and Technology, 45(9), 3974–3981, https://doi.org/10.1021/es104384m, 2011.

O'Connor, D., Hou, D., Ok, Y. S., Mulder, J., Duan, L., Wu, Q., Wang, S., Tack, F. M. G., and Rinklebe, J.: Mercury speciation, transformation, and transportation in soils, atmospheric flux, and implications for risk management: A critical review, Environment International, 126, 747–761, https://doi.org/10.1016/j.envint.2019.03.019, 2019.

Ozturk, M., Altay, V., Gönenç, T. M., Unal, B. T., Efe, R., Akçiçek, E., and Bukhari, A.: An Overview of Olive Cultivation in Turkey: Botanical Features, Eco-Physiology and Phytochemical Aspects, Agronomy, 11(2), 295, https://doi.org/10.3390/agronomy11020295, 2021.

Patra, M., and Sharma, A.: Mercury toxicity in plants, The Botanical Review, 66(3), 379–422, https://doi.org/10.1007/BF02868923, 2000.

Pleijel, H., Klingberg, J., Nerentorp, M., Broberg, M. C., Nyirambangutse, B., Munthe, J., and Wallin, G.: Mercury accumulation in leaves of different plant types – the significance of tissue age and specific leaf area, Biogeosciences, 18, 6313–6328, 2021, https://doi.org/10.5194/bg-18-6313-2021, 2021.

Pokharel, A. K., and Obrist, D.: Fate of mercury in tree litter during decomposition, Biogeosciences, 8(9), 2507–2521, https://doi.org/10.5194/bg-8-2507-2011, 2011.

Rea, A. W., Keeler, G. J., and Scherbatskoy, T.: The deposition of mercury in throughfall and litterfall in the lake champlain watershed: A short-term study, Atmospheric Environment, 30(19), 3257–3263, https://doi.org/10.1016/1352-2310(96)00087-8, 1996.

Rea, A. W., Lindberg, S. E., Scherbatskoy, T., and Keeler, G. J.: Mercury Accumulation in Foliage over Time in Two Northern Mixed-Hardwood Forests. 19, 2002.

Richardson, J. B., Friedland, A. J., Engerbretson, T. R., Kaste, J. M., and Jackson, B. P.: Spatial and vertical distribution of mercury in upland forest soils across the northeastern United States, Environmental Pollution (Barking, Essex : 1987), 182, 127–134, https://doi.org/10.1016/j.envpol.2013.07.011, 2013.

Sanz-Cortés, F., Martinez-Calvo, J., Badenes, M. L., Bleiholder, H., Hack, H., Llacer, G., and Meier, U.: Phenological growth stages of olive trees (Olea europaea), Annals of Applied Biology, 140(2), 151–157, https://doi.org/10.1111/j.1744-7348.2002.tb00167.x, 2002.

Schaefer, K., Elshorbany, Y., Jafarov, E., Schuster, P. F., Striegl, R. G., Wickland, K. P., and Sunderland, E. M.: Potential impacts of mercury released from thawing permafrost, Nature Communications, 11(1), Article 1, https://doi.org/10.1038/s41467-020-18398-5, 2020.

Schneider, L., Allen, K., Walker, M., Morgan, C., and Haberle, S.: Using Tree Rings to Track Atmospheric Mercury Pollution in Australia: The Legacy of Mining in Tasmania. Environmental Science & Technology, 53(10), 5697–5706, https://doi.org/10.1021/acs.est.8b06712, 2019.

Schwesig, D., and Krebs, O.: The role of ground vegetation in the uptake of mercury and methylmercury in a forest ecosystem, Plant and Soil, 11, 2003.

Senesil, G. S., Baldassarre, G., Senesi, N., and Radina, B.: Trace element inputs into soils by anthropogenic activities and implications for human health, Chemosphere, 39(2), 343–377, https://doi.org/10.1016/S0045-6535(99)00115-0, 1999.

Sghaier, A., Perttunen, J., Sievaènen, R., Boujnah, D., Ouessar, M., Ben Ayed, R., and Naggaz, K.: Photosynthetical activity modelisation of olive trees growing under drought conditions, Scientific Reports, 9(1), 15536, https://doi.org/10.1038/s41598-019-52094-9, 2019.

Teixeira, D. C., Lacerda, L. D., and Silva-Filho, E. V.: Mercury sequestration by rainforests: The influence of microclimate and different successional stages, Chemosphere, 168, 1186–1193, https://doi.org/10.1016/j.chemosphere.2016.10.081, 2017.

Terral, J.-F., Alonso, N., Capdevila, R. B. i, Chatti, N., Fabre, L., Fiorentino, G., Marinval, P., Jordá, G. P., Pradat, B., Rovira, N., and Alibert, P.: Historical biogeography of olive domestication (Olea europaea L.) as revealed by geometrical morphometry applied to biological and archaeological material: Historical biogeography of olive domestication (Olea europaea L.), Journal of Biogeography, 31(1), 63–77, https://doi.org/10.1046/j.0305-0270.2003.01019.x, 2004.

Tomiyasu, T., Matsuo, T., Miyamoto, J., Imura, R., Anazawa, K., and Sakamoto, H.: Low level mercury uptake by plants from natural environments—Mercury distribution in Solidago altissima L.-, Environmental Sciences: An International Journal of Environmental Physiology and Toxicology, 12(4), 231–238, 2005.

UNEP: Technical Background Report to the Global Mercury Assessment 2018, IVL Svenska Miljöinstitutet, 2019.

Wang, X., Lin, C.-J., Lu, Z., Zhang, H., Zhang, Y., and Feng, X.: Enhanced accumulation and storage of mercury on subtropical evergreen forest floor: Implications on mercury budget in global forest ecosystems: Hg storage on subtropical forest floor, Journal of Geophysical Research: Biogeosciences, 121(8), 2096–2109, https://doi.org/10.1002/2016JG003446, 2016.

Wofsy, S. C., Goulden, M. L., Munger, J. W., Fan, S.-M., Bakwin, P. S., Daube, B. C., Bassow, S. L., and Bazzaz, F. A.: Net Exchange of $CO_2$ in a Mid-Latitude Forest, Science, 260(5112), 1314–1317, https://doi.org/10.1126/science.260.5112.1314, 1993.

Wohlgemuth, L., Rautio, P., Ahrends, B., Russ, A., Vesterdal, L., Waldner, P., Timmermann, V., Eickenscheidt, N., Fürst, A., Greve, M., Roskams, P., Thimonier, A., Nicolas, M., Kowalska, A., Ingerslev, M., Merilä, P., Benham, S., Iacoban, C., Hoch, G., … Jiskra, M.: Physiological and climate controls on foliar mercury uptake by European tree species, Biogeosciences, 19, 1335–1353, 2022, https://doi.org/10.5194/bg-19-1335-2022, 2021.

Wright, L. P., Zhang, L., and Marsik, F. J.: Overview of mercury dry deposition, litterfall, and throughfall studies, Atmospheric Chemistry and Physics, 16(21), 13399–13416, https://doi.org/10.5194/acp-16-13399-2016, 2016.

Yammine, P., Kfoury, A., El-Khoury, B., Nouali, H., El-Nakat, H., Ledoux, F., Courcot, D., and Aboukaïs, A.: A preliminary evaluation of the inorganic chemical composition of atmospheric tsp in the selaata region, north lebanon, Lebanese Science Journal, 11(1), 18, 2010.

Yanai, R. D., Yang, Y., Wild, A. D., Smith, K. T., and Driscoll, C. T.: New Approaches to Understand Mercury in Trees: Radial and Longitudinal Patterns of Mercury in Tree Rings and Genetic Control of Mercury in Maple Sap, Water, Air, and Soil Pollution, 231(5), 248, https://doi.org/10.1007/s11270-020-04601-2, 2020.

Yang, Y., Yanai, R. D., Driscoll, C. T., Montesdeoca, M., and Smith, K. T.: Concentrations and content of mercury in bark, wood, and leaves in hardwoods and conifers in four forested sites in the northeastern USA, PLOS ONE, 13(4), e0196293, https://doi.org/10.1371/journal.pone.0196293, 2018.

Yazbeck, E. B., Rizk, G. A., Hassoun, G., El-Khoury, R., and Geagea, L.: Ecological characterization of ancient olive trees in Lebanon- Bshaaleh area and their age estimation, 11(2 Ver. 1), 35–44, 2018.

Zhao, X., and Wang, D.: Mercury in some chemical fertilizers and the effect of calcium superphosphate on mercury uptake by corn seedlings (Zea mays L.), Journal of Environmental Sciences, 22(8), 1184–1188, https://doi.org/10.1016/S1001-0742(09)60236-9, 2010

Zhou, J., Obrist, D., Dastoor, A., Jiskra, M., and Ryjkov, A.: Vegetation uptake of mercury and impacts on global cycling, Nature Reviews Earth & Environment, 2(4), 269–284, https://doi.org/10.1038/s43017-021-00146-y, 2021.

Zhou, J., Wang, Z., and Zhang, X.: Deposition and Fate of Mercury in Litterfall, Litter, and Soil in Coniferous and Broad-Leaved Forests, Journal of Geophysical Research: Biogeosciences, 123(8), 2590–2603, https://doi.org/10.1029/2018JG004415, 2018.

In process of publishing to Tree physiology journal

## Chapter III: Annual and seasonal variation of C,N,S,O,H stable isotopes in olives groves of Lebanon

Nagham Tabaja[1,2,3], Lamis Chalak[2], François Fourel [4], Clément Piel[5], Joana Sauze[5], Ihab Jomaa [6], Ilham Bentaleb [1]
[1] ISEM, Université de Montpellier, CNRS, IRD, Montpellier, France
[2] Faculté d'Agronomie, Département Production Végétale, Université Libanaise, Dekwaneh, Liban
[3] Plateforme d0e Recherche et d'Analyses en Sciences de l'Environnement (PRASE), Ecole Doctorale de Sciences et Technologie, Université Libanaise, Hadath, Liban
[4] UMR CNRS 5023 LEHNA, Université Claude Bernard Lyon 1, Villeubanne, France
[5] Ecotron Européen de Montpellier (UAR 3248), Université de Montpellier, Centre National de la Recherche Scientifique 11 (CNRS), Campus Baillarguet, Montferrier-sur-Lez, France
[6] Département d'irrigation et d'agrométéorologie, Institut de recherche agronomique libanais (IRAL), P.O. box 287, Zahle, Liban

*Correspondence to*: Ilham Bentaleb (Email: ilham.bentaleb@umontpellier.fr, Tel: +33 0 638 615 769)

## Abstract

Our study is focused in the Eastern Mediterranean in Lebanon. Two olive grove sites are the main interest of our study, Bchaaleh in the North and Kawkaba in the South. The Stable isotopic techniques of carbon, nitrogen, sulfur, hydrogen and oxygen in plant ecology have been growing during the past years, serving as an important nonradioactive and non-destructive technique to study how plants in the present and the past interacted and responded to the biotic and abiotic environment. In order to understand how were our olive trees affected by the climatic changes in the past, first it should be understood how are those trees affected today by the environmental and climatic parameters. This study is the first to investigate all the different isotopic compositions ($\delta^{13}C$,$\delta^{15}N$,$\delta^{34}S$,$\delta D$ and $\delta^{18}O$) in monumental olive trees. First, it tackled how the olive tree foliage, stems, litter and soil different isotopic compositions are varying between one another. Second, how are the foliage isotopic compositions and $\delta D$, $\delta^{18}O$ of precipitation varying annually and seasonally between Bchaaleh and Kawkaba and between each individual studied site. Third, the respond of the foliage to climatic parameters using the different stable isotopic markers as indicators of the climate.

**Keywords:** Olive groves, plant tissues, litter, soil, $\delta^{13}C$, $\delta^{15}N$, $\delta^{34}S$, $\delta D$, $\delta^{18}O$, climatic parameters.

# I. Introduction

The Stable isotopic techniques in plant ecology have been growing during the past years, serving as an important nonradioactive and non-destructive technique to study how plants in the present and the past interacted and responded to the biotic and abiotic environment (Dawson et al., 2002).

Carbon stable isotope known as $\delta^{13}C$ in plant material had been used for ecological, climatological, or biochemical research in plant science, in addition to the evaluation of the plant performance under different environmental conditions (Barbour & Farquhar, 2000; Dawson et al., 2002; J. L. Araus et al., 2003; Barbour, 2007; J. Araus et al., 2013; Gessler et al., 2014; Sanchez-Bragado et al., 2019). It is also normally used to estimate stomatal activity, photosynthetic rates and water use efficiency of $C_3$ plants (Farquhar et al., 1989; Matteo et al., 2010; Cabrera-Bosquet et al., 2009; Rossi et al., 2013). Rossi et al., (2013) investigated irrigated and rainfed olive trees, and showed that irrigated trees has more negative $\delta^{13}C$ values than those that are rainfed. Isotopic results show that the rainfed plants regulate the stomatal activity and limit wood formation during drought seasons (Tognetti et al., 2004, 2005, 2009; Rossi et al., 2013). The long term hydraulic adaptation of plant reduces the stomatal conductance and acclimatize to water stress (Silva & Horwath, 2013; Rossi et al., 2013). The $pCO_2$ in the atmosphere represents the availability of carbon for plant growth on the land (Schubert & Jahren, 2012). The plant tissues show a depletion in $\delta^{13}C$ in relation to the atmosphere due to the preferential of the $^{12}C$ for the fixation as $CO_2$ is converted into sugar in the foliage (Park & Epstein, 1960; Schubert & Jahren, 2012).

The carbon stable isotope natural abundance in plants can be an indicator of the environment temperature, and also an indicator of the changes in $^{13}C/^{12}C$ ratio of the $pCO_2$ (Leavitt & Long, 1983). The plant photosynthesis discriminates against $\delta^{13}C$ when the $pCO_2$ passes through the stomata during the phase of $CO_2$ carboxylation in RuBisCo (Farquhar et al., 1989; Ogaya & Peñuelas, 2008). The $^{13}C$ discrimination decreases with the decrease in intercellular $CO_2$ concentration that is due to the closure of stomata and the water use efficiency (WUE), in which, higher $\delta^{13}C$ is found in drier sites and years (Peñuelas et al., 2000).

The $\delta^{13}C$ of soil organic matter is known to increase by 1-3‰ with the soil depth relative to the litter layer in the forest ecosystem (Wynn et al., 2005; Boström et al., 2007). This increase in the $\delta^{13}C$ in soil can be explained by the decrease in the $\delta^{13}C$ of the $pCO_2$ that started since the $18^{th}$ century due to the burn of fossil fuel and deforestation (Boström et al., 2007; Francey et al., 1999). The increase in $\delta^{13}C$ in soil can also be explained by other factors such as the preferential composition of certain components, variable mobility of dissolved organic carbon with variable isotopic values, kinetic discrimination against $^{13}C$ during respiration and microbes as precursors of stable organic matter (Boström et al., 2007; Ehleringer et al., 2000; Högberg et al., 2005; Tu & Dawson, 2005).

$\delta^{15}N$ has been used for the past decades in order to assess the ecosystem N cycling and its status in addition to defining the species differences (Pardo et al., 2006, 2013). Nitrogen usually has an important role in the biogeochemical cycling within a forest. Species composition has been proven to be a

determinant of the ecosystem nitrogen cycling dynamics (Templer et al., 2007; Pardo et al., 2013), where the species composition can influence the soil C/N, $NO^-_3$ loss in hardwood forests, and nitrification rates (Lovett et al., 2004; Pardo et al., 2013). Plant $\delta^{15}N$ have normally a negative correlation with the soil bulk and rainfall (Heaton, 1987; Amundson et al., 2003; Swap et al., 2004; Hartman & Danin, 2010); but the relation between the $\delta^{15}N$ and rainfall is not straightforward, for when plant fix C directly from the atmosphere, it gets N from the soil or through symbiotic relationship with N-fixing microorganisms. In addition to that, the variability in soil N source, plant metabolism and the activity of soil microorganisms also influence the plant $\delta^{15}N$ values (Högberg, 1997; Hartman & Danin, 2010). The discrimination in $^{15}N$ also happens in some of the ecological processes as such N transfer from mycorrhizal fungi to plants, or the loss of N from the ecosystem that enriches the N in $^{15}N$ like gaseous N losses and the $NO^{3-}$ leaching when the nitrification is not complete. The rain exclusion changes the N use, since a decrease in the water availability causes significant changes in the biochemical cycles of the ecosystem that reduce nutrient availability and soil nitrogen content (Peñuelas et al., 2000; Hartman & Danin, 2010). The foliar or whole plant $\delta^{15}N$ data is complicated due to the existence of many sources of nitrogen in the soil and a possibility of variable discrimination against $^{15}N$ during the identification of each source (Cernusak et al., 2016).

Sulfur is known to be an important element for plant growth (De Kok, 1990; Trust & Fry, 1992). Normally the total sulfur in plants is the amino acid organic form and sulpholipids, but when there is excess in sulfur the inorganic sulfur can become the main sulfur form (ALLEN & Raven, 1987; Trust & Fry, 1992). $^{32}S$ and $^{34}S$ are the most abundant isotopes that are mostly used for stable isotopes studies (Trust & Fry, 1992). In a study done by Isshi (1953) on laboratory cultures of *Chlorella* and field grown mustard plants, it has shown that there is very little isotopic discrimination during the assimilation of sulphate and plant reduction (Trust & Fry, 1992). Usually plants have values averaging to about 1.5‰ less than the sulphate in the environment (Trust & Fry, 1992). The small discrimination resulting from the uptake of environmental sulfur sources are characteristics of the pathway of sulphate reduction. This pathway is used by plants and the bacteria to meet there biosynthetic sulfur needs and it covers all of the biological synthesis of the sulfur amino acid (Kaplan & Rittenberg, 1964; Rennenberg et al., 1990; Trust & Fry, 1992). Mostly, inorganic sulphate and atmospheric $SO_2$ are major sulfur sources for the plants, but some studies indicated that sulphide sulfur from sediments can also be part of the plants under certain circumstances (Howarth & Teal, 1979; Trust & Fry, 1992). Sulfur is absorbed by plants as water soluble $SO_4^{2-}$ from soil through the root and also as atmospheric sulfur through the stomata (Krouse, 1977; Kawamura et al., 2006). The $\delta^{34}S$ values in the plants reflect the absorbed sulfur which helps identifying the sulfur source (Krouse, 1991; Kawamura et al., 2006).

Water cycle in plants starts with precipitation hitting the foliage and other plant surfaces before reaching the soil. Some of that water evaporates from the plant surface, and the remaining water goes to the soil and down to the plant roots. The plant uses the water for its own metabolism. This water travels upwards

through vascular tubes and evaporates through the stomata on the foliage back into the atmosphere (Sheil, 2018). This water cycle can be described by the isotopic cycle of hydrogen and oxygen isotopic composition. The hydrogen and oxygen isotopic ratios in precipitation are related through the well-known global meteoric water line or GWML (Gat et al., 2001; Marshall et al., 2007) which can be affected by local meteorological conditions such as temperature and relative humidity (Hervé-Fernández et al., 2016) giving rise to local meteoric water lines (LMWL). The δD and $\delta^{18}O$ of the rainwater vary in relation to altitude, temperature, latitude, amount of precipitation falling and distance from the coast (Munksgaard et al., 2012; Cernusak et al., 2016). Any precipitation event mixes with the soil pre-existing water pool, hence there is a variation in $\delta^{18}O$ and δD from one rainfall to another (Munksgaard et al., 2012, 2015; Cernusak et al., 2016). Evaporation is another well-known factor affecting the soil water isotopic composition (Cernusak et al., 2016) leading to an enrichment in $\delta^{18}O$ and δD in comparison to deeper soil (Allison et al., 1983). The stable isotopes of deuterium (δD) and oxygen ($\delta^{18}O$) of extracted water of plant tissue are usually used to identify and quantify the plant water sources (Barbeta et al., 2019; Amin et al., 2021) and according to Barbera et al., (2018) are reflecting the isotopic signature of soil water which is not directly the rain-water. It is often assumed that there is no hydrogen isotopic fractionation during soil water absorption through the plant roots up to the twigs, although some new studies show that isotopic fractionation can take place due to various environmental conditions (Amin et al., 2021) . Since $\delta^{18}O$ of foliage is influenced by climatic (i.e., temperature and relative humidity) and geographical factors (i.e., altitude) and there is no isotopic fractionation during water uptake, $\delta^{18}O$ in foliage water represents the geographical origin of plants even with the evapotranspiration, while δD is also influenced by kinetic isotopic fractionation during different biosynthesis pathways (i.e., photosynthesis, amino acid synthesis) and exchange of isotopes with biomolecules (Schmidt et al., 2003; Khatri et al., 2021). Studying the drivers causing the leaf water $\delta^{18}O$ and δD variations, Cernusak et al., (2022) observed that leaf water $\delta^{18}O$ but not the δD was significantly correlated to relative humidity, the latter being strongly correlated to $\delta^{18}O$ of atmospheric vapor, while xylem water δD was a much stronger driver of variation in leaf water δD than was the case for xylem water $\delta^{18}O$ as a driver of variation in leaf water $\delta^{18}O$. In perspectives of paleoclimate reconstructions, plant bulk organic matter and organic compound specific (ie. cellulose, lipids) $\delta^{18}O$ and δD are recognized as good climate drivers assuming that $\delta^{18}O$ and δD reflect the isotopic signature of the water source though affected by isotopic fractionation during processes such as evapotranspiration between foliage water and water source (Khatri et al., 2021). In the foliage, evapotranspiration is responsible for isotopic fractionation giving usually enriched δD and $\delta^{18}O$ isotopic ratios (Barbour, 2007; Barbour & Farquhar, 2000; Zhang et al., 2010; Sanchez-Bragado et al., 2019). $\delta^{18}O$ and δD of bulk organic material (ie; leaf, stems, tree ring wood) or specific compounds represent the isotopic compositions of O and H elements present in an ensemble of molecules produced through complex reactions during plant physiological activities (ie. Photosynthesis, photorespiration, transpiration, biomolecules

synthesis…). $\delta^{18}O$ and δD reflect the isotopic signature of source water. Both hydrogen and oxygen atoms, entering in the composition of the organic molecules during photosynthetic activity, will reflect foliage water isotopic signature and part of those atoms exchange with water during the synthesis of compounds (ie. sucrose cellulose) in foliage, stems or roots (Yakir, 1992; Roden et al. 2000). Sucrose is produced during photosynthesis in foliage, and then it is transported through the phloem via a translocation process to the different tissues such as roots, stems and vegetation organs in order to provide the carbon and energy needed for the growth.

The Mediterranean environment is characterized by a dry summer and low precipitation, high temperature, high water vapor pressure deficit and high irradiance (Mitrakos, 1980; Pereira & Chaves, 1995; Hartman & Danin, 2010). The rain exclusion is considered a main factor in the Mediterranean environment. With low photosynthetic rates during the summer due to the stomatal control of transpiration water loss (Llusia` & Pen uelas, 2000; Hartman & Danin, 2010). Due to the decrease in stomatal conductance which is higher than that in the photosynthetic rates increases the WUE (Hartman & Danin, 2010). In the Mediterranean conditions, hydraulic function maintenance under drought stress is important for survival (Fonti & Jansen, 2012). The characterization of the Eastern Mediterranean climate is known to have a strong seasonal rainfall pattern where rain is mainly falling in winter season (Goldreich, 2003; Hartman & Danin, 2010).

Olive tree (*Olea europea* L.), a $C_3$ plant, is an evergreen commonly cultivated tree in the Mediterranean countries that is known for its resilience to drought and the importance of olives and olive oil production (Chalak et al., 2015). In Lebanon, ancient olive trees (of about 1400 years old according to Yazbeck et al., 2018) continue to grow along new plantations witnessing the long history of these trees in the country (Chalak et al. 2015). By understanding the present of those ancient trees, we can understand better the past climate through the tree rings and have a more thorough understanding of how the wood anatomy structure and the hydraulic process adapt and change in those trees (Rossi et al., 2013). Olive trees are not yet extensively studied for the different stable isotopes, which aids in understanding the seasonality of stable isotopes, pathway of water and the plant water source (Beyer et al., 2016; Barbeta et al., 2019; Amin et al., 2021).

In this study, we focus on monumental olive trees growing at two different altitudes in Lebanon with the aim of understanding how the olive tree foliage, stems, litter and soil different isotopic compositions are varying between one another. Second, how are the foliage isotopic compositions and δD, $\delta^{18}O$ of precipitation varying annually and seasonally between Bchaaleh and Kawkaba and between each individual studied site. Third, the respond of the foliage to climatic parameters using the different stable isotopic markers as indicators of the climate. Also, since $\delta^{13}C$, $\delta^{15}N$, $\delta^{34}S$,δD and $\delta^{18}O$ cellulose are good indicator of environment and climate, we make the hypothesis that the bulk dry matter of the plant tissues can be good candidate for less time consuming and cost-effective analysis giving the similar and reliable information related to foliage mainly, stems, litter and soil compared to other methods.

## II. Materials and Methods

### II.1 Study sites and climatic conditions

Two groves were selected for this study at different altitudes. The first grove is situated in Batroun district, North of Lebanon, Bchaaleh village (BC) (Latitude 34°12'06''N, Longitude 35º49'23''E, Altitude 1300 ma.s.l.; Figure 1). The olive trees are growing rainfed in a sandy loam texture soil of sand, silt and clay percentages are 52.8%, 38.7% and 10.7% respectively (Yazbeck et al., 2018). Olive trees are growing rainfed in a sandy loam texture soil of grain size analysis of sand, silt and clay percentages are 52.8 %, 38.7 % and 10.7 % respectively (Tabaja et al., 2022). They are maintained by the municipality for the last four decades as an endowment property. Precipitation average ranges between 229 and 392 mm in winter and between zero and less than 2 mm/season in summer, while average temperature is between 4 and 8 °C in winter and between 20 and 23 °C in summer and average relative humidity of 63% (data extracted from LARI climatic data) (Figure S1) (Tabaja et al., 2022).

The second site is located in the South of Lebanon, Kawkaba village (KW) (Latitude 33°23'856''N, Longitude 35°38'588''E, Altitude 672 m a.s.l.; Figure 1). Kawkaba olive is also rainfed as indicated by Kawkaba municipality, in a clay loam soil with 6% sand, 28% silt and 66% clay. Precipitation average ranges between 215 and 374 mm in winter and almost zero mm in summer, while the average temperature is between 7 and 11 °C in winter and 21 and 27 °C in summer and a 61% of relative humidity (data extracted from LARI climatic data) (Figure S1). $CO_2$ data used in this study are from NOAA Global Monitoring Laboratory (https://gml.noaa.gov/webdata/ccgg/trends/co2/co2_trend_gl.txt ).

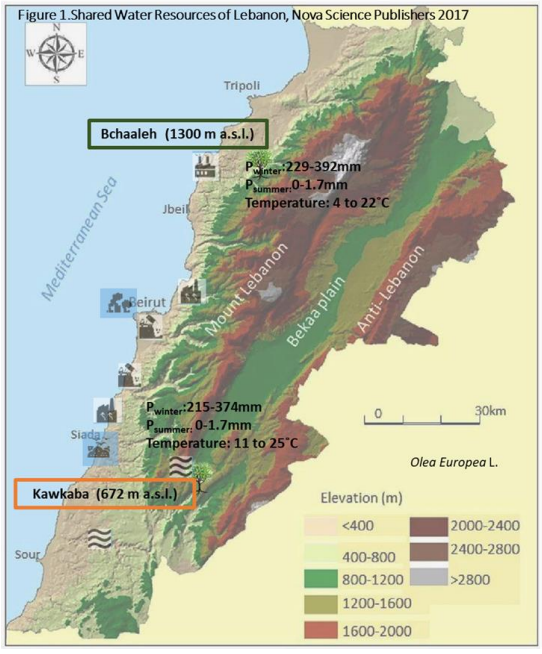


**Figure 6** Site location of the two selected studied sites (modified after Shared Water Resources of Lebanon, Nova Science Publishers, 2017).

## II.2 Field sampling

**Olive trees**

Four main olive trees were sampled in each of the two groves for carbon, nitrogen, sulfur, hydrogen and oxygen isotopic analysis. In Bchaaleh, two trees are taken from the upper terrace (BCO1-Tree 1, BCO4-Tree 4) and two others in a 1.5 m lower terrace (BCO9-Tree 9, BCO12-Tree 12). In Kawkaba, four trees were selected from the same terrace (KWO1-Tree1, KWO2-Tree 2, KWO-Tree 3, and KWO4-Tree 4).

**Foliage, stems, soil and litter**

During the experiment that lasted 16 months, foliage (103 samples) and stems (103 samples) were collected from the trees, for each of those sampled olive trees, sun-exposed and shaded foliage and stems with no evidence of pathogens were collected randomly from the upper, middle, and lower canopy sides of the olive on monthly basis using a manual pruner. While litter (18 samples) and soil (45 samples) were sampled directly under the trees. The Litter and soil surface were collected from the surface area of the olive groves and stored in separate paper bags every quarter of a year. In addition, a manual bucket auger was used for sampling soil reaching a maximum depth of 60 cm. In both sites, the soil cores were divided into soil surface (0-1 cm), 0-30 cm depth, and 30-60 cm depth. The studied samples range from February 2019 till September 2020.

**Rainwater**

A rainwater collector was installed underground in both studied sites (Bchaaleh and Kawkaba) to collect rainwater during rainy seasons that range between November and May for the three-year study 2019-2021 (22 samples). The rain collector was filled with paraffin to separate the water from any other material inside the collector and during the sampling. Duplicates for oxygen and hydrogen samples were collected in a 5 ml bottle each that was then sealed and stored at 4°C temperature.

## II.3 Sample preparation and analytical method

Collected samples of foliage and stems were rinsed with distilled water and oven-dried for 48 hours at a temperature of 40°C. Foliage, stems and litter were grinded using an electrical stainless grinding machine with no heating system for 5-10 minutes, while soil samples were manually grinded using a natural agate grinder. Afterward, the grinded samples were sieved using an inox stainless-steel of 125-micron sieve mesh aiding in collecting homogeneous powders for analysis. An HCL treatment (0.5 M HCl for 12 hours and three thorough deionized water rinsing before drying at 50°C for 24 to 48 hours) was implemented on the soil samples analyzed for carbon isotopes to remove the carbonates present in the samples. Around 2 mg of bulk powders of foliage, stems, litter and soil material were weighed into tin capsules and measured for the carbon, nitrogen, hydrogen and oxygen stable isotope ratios. While for sulfur isotopic analysis a 12mg for the soil and 5 mg for the foliage, stem and litter was weighed,

capsuled and analyzed using Flash Elemental Analyser connected to Isoprime 100 isotopic mass spectrometer (IRMS) ( Fourel et al. 2014; Fourel et al. 2019).

In this article, a conventional delta notation was used, where the isotopic composition of a material relative to that of a standard on a per mil deviation basis is given by $\delta = [(R_{sample})/(R_{standard}) -1 ]* 1000$, where $\delta$ is the isotopic ration of $\delta^{15}N$, $\delta^{13}C$, $\delta^{34}S$, $\delta D$ and $\delta^{18}O$ and R is the ratio of heavy *vs.* light isotope forms. Four standards were used for $\delta^{15}N$ and $\delta^{13}C$ (B2157-2, ASP-3, B2203-2 and IAEA N2-2) giving values expressed in ‰ versus the VPDB. Using also four international Standard for sulfur (IAEA SO5, IAEA S4, IAEA S2 and B2203), and four international Standard for $\delta D$ and $\delta^{18}O$ (B2203, B2205, IAEA 601 and IAEA CH7) giving a precision for $\delta D$ better than ±0.73‰ and ±0.10 ‰ for $\delta^{18}O$. Monthly rainwater collected samples were analyzed at ECOTRON using A Picarro L2140i laser spectrometer as well as Delta V Plus IRMS to access $\delta D$ values of liquid water (OSU-OREME).

### II.4 Statistical analysis

R 4.1.0 program was used for the statistical analysis; Shapiro test is used to check for the data normality distribution. To check the significant difference between the two studied sites and the annual significant difference and seasonal difference for each site individually for C,N,S,H and O isotopic composition, the t-test is used for normally distributed data, while Wilcoxon test is used for the not normally distributed data. The ggplot is used to plot the foliage seasonal variation in Bchaaleh and Kawkaa for year 2019 and 2020 for the isotopic compositions. While for the effect of climatic parameters on the different isotopic compositions of foliage, a Kendall correlation test and correlation plot are used.

## III. Results

### III.1 Plant tissues, soil and litter C,N,S,H,O isotopic compositions in Bchaaleh and Kawkaba

The $\delta^{13}C$, $\delta^{15}N$, $\delta^{34}S$, $\delta D$ and $\delta^{18}O$ of foliage, stems, litter and soils measured for year 2019-2020 at both Bchaaleh and Kawkaba sites are presented on Table S1. Bchaaleh foliage, stems, soil surface and 0-30 cm $\delta^{13}C$ mean values (-26.6 ± 0.7 ‰, -25.7 ± 0.9 ‰, -22.9 ± 7.2 ‰ and -22.9 ± 6.2 ‰ respectively) compared to those of Kawkaba (-28.1 ± 1.2 ‰, -26.7 ± 0.6 ‰, -26.6 ± 1.2 ‰ and -26.0 ± 1.0 ‰ respectively) (Figure 2 a,b) are significantly higher (p-values = $2.7711e^{-13}$, $2.655e^{-10}$, 0.03 and 0.003 respectively for foliage, stems, soil surface and 0-30 cm). While the average $\delta^{13}C$ in litter in Bchaaleh (-26.4 ± 0.7 ‰) and Kawkaba (-26.9 ± 0.6 ‰) showed no significant difference between the two sites (p-values = 0.1) (Figure 2 a,b).

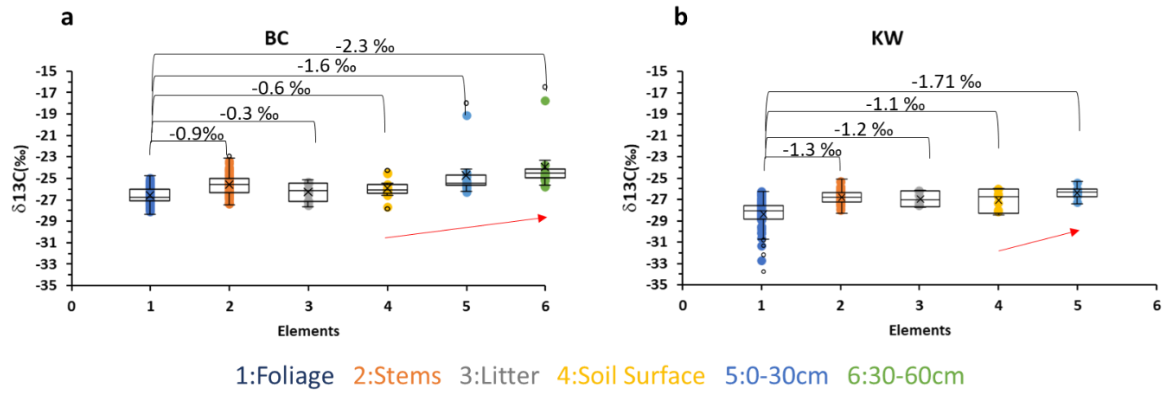


**Figure 7** Mean average of $\delta^{13}C$ for 2019-2020 of olive trees for foliage, stems, litter, soil surface, soil 0-30 cm and 30-60 cm in **(a)** Bchaaleh and **(b)** Kawkaba.

Bchaaleh foliage $\delta^{15}N$ mean values (2.4 ± 1.0 ‰) compared to those of Kawkaba (0.2 ± 1.2 ‰) are significantly higher (p-value: $2.2e^{-16}$) while Bchaaleh stems $\delta^{15}N$ mean values (1.5 ± 3.4 ‰) compared to those of Kawkaba (5.4 ± 2.8 ‰) are significantly lower (p-value: $4.778e^{-08}$) (Figure 3 a,b). Regarding Bchaaleh, the litter average $\delta^{15}N$ (1.2 ± 1.5 ‰) is lower than that of Kawkaba (2.1 ± 1.0 ‰) though not significantly different (p-value: 0.1). No significant differences are observed between Bchaaleh (3.4 ± 1.2 ‰) and Kawkaba (3.2 ± 0.7 ‰) mean $\delta^{15}N$ of soil surface (p-value: 0.6) and between Bchaaleh (1.9 ± 3.4 ‰) and Kawkaba (3.5 ± 1.5 ‰) mean $\delta^{15}N$ of soil 0-30cm (p-value: 0.5) (Figure 3 a,b). The C/N ratios of foliage, stems, litter and soil surface in Bchaaleh (23.8 ± 7.7 ‰, 67.0 ± 17.9 ‰, 24.7 ± 2.1 ‰ and 8.0 ± 5.5 ‰ respectively) and Kawkaba (28.4 ± 2.7 ‰, 76.2 ± 16.5 ‰, 28.4 ± 1.6 ‰ and 14.8 ± 9.5 ‰ respectively) showed significant differences with p-values of 0.0017, $4.445e^{-05}$, 0.001 and 0.03 respectively for foliage, stems, litter and soil surface (Figure 4 a,b). In general, the soil 0-30 cm mean C/N ratios of both Bchaaleh (8.6 ± 7.1 ‰ respectively) and Kawkaba (7.6 ± 2.0 ‰ respectively) sites showed no significant differences with p-values = 0.5 (Figure 4 a,b).

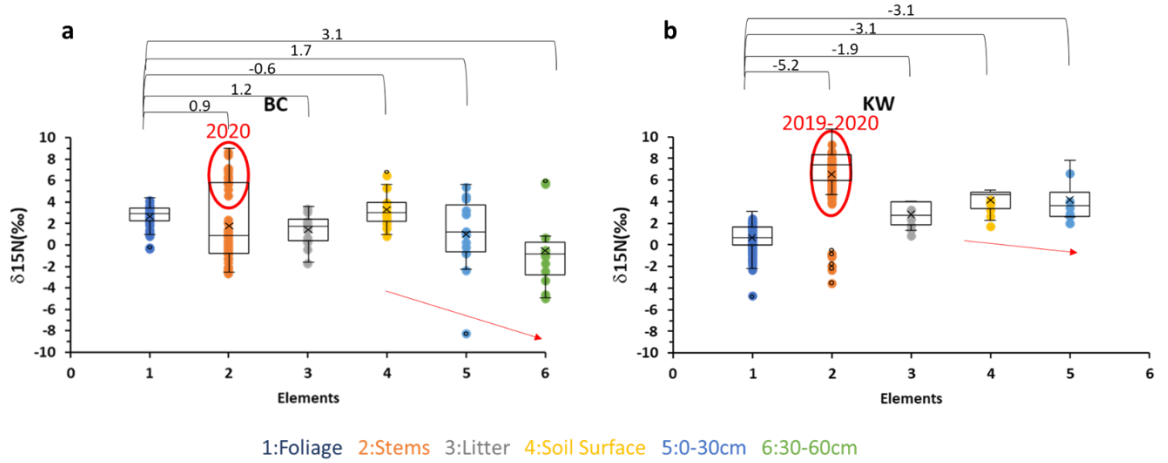


**Figure 8** Mean average of δ15N for 2019-2020 of olive trees for foliage, stems, litter, soil surface, soil 0-30 cm and 30-60 cm in **(a)** Bchaaleh and **(b)** Kawkaba.

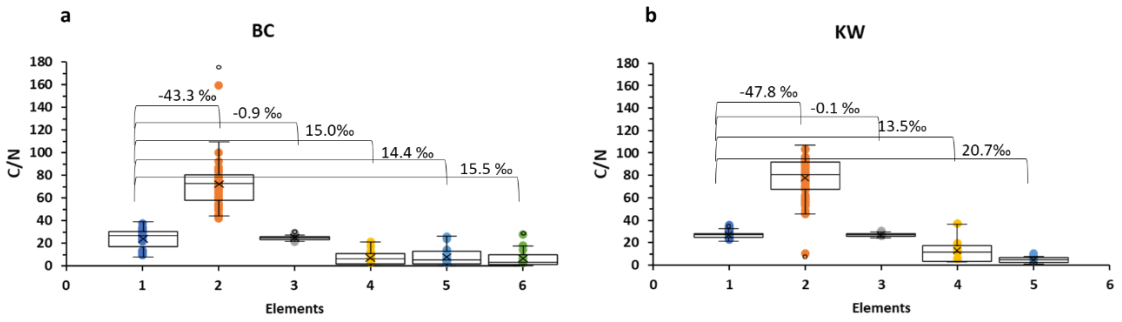


**Figure 9** Mean average of C/N ratio for 2019-2020 of olive trees for foliage, stems, litter, soil surface, soil 0-30 cm and 30-60 cm in **(a)** Bchaaleh and **(b)** Kawkaba.

Bchaaleh foliage $\delta^{34}S$ mean value (6.2 ± 5.7 ‰) compared to that of Kawkaba (9.9 ± 2.4 ‰) is significantly different (p-value = $2.2e^{-16}$), while Bchaaleh (11.3 ± 3.7 ‰) and Kawkaba (11.4 ± 1.6 ‰) stems $\delta^{34}S$ mean values are similar (p-value = 0.6) (Figure 5 a,b). Regarding Bchaaleh, the litter average $\delta^{34}S$ (8.2 ± 3.9 ‰) is slightly higher compared to that of Kawkaba (7.3 ± 0.5 ‰) though not significantly different (p-value = 0.4). On the other hand, significant differences are observed between Bchaaleh (19.9 ± 5.1 ‰) and Kawkaba (10.6 ± 2.0 ‰) mean $\delta^{34}S$ of soil surface (p-value = $1.183e^{-05}$) and between Bchaaleh (23.2 ± 3.8 ‰) and Kawkaba (12.6 ± 2.3 ‰) mean $\delta^{15}N$ of soil 0-30cm (p-value = $3.652e^{-05}$) (Figure 5 a,b).

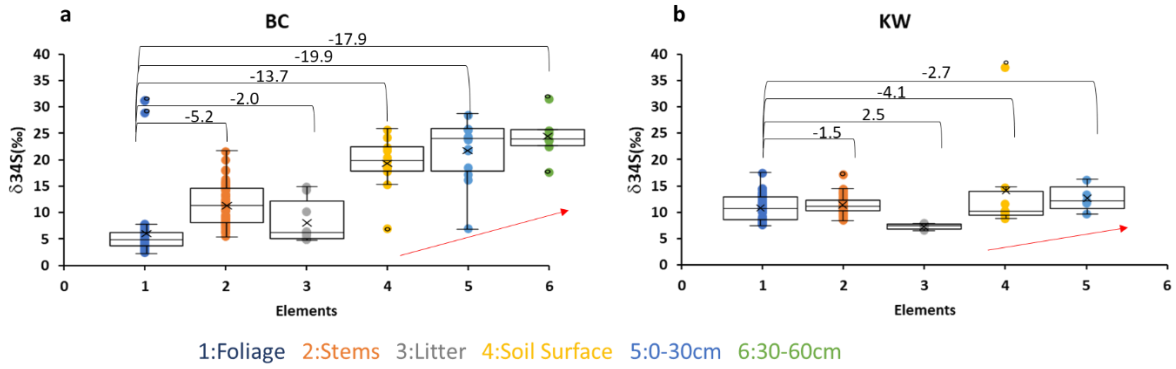


**Figure 10** Mean average of $\delta^{34}S$ ratio for 2019-2020 of olive trees for foliage, stems, litter, soil surface, soil 0-30 cm and 30-60 cm in **(a)** Bchaaleh and **(b)** Kawkaba.

Foliage means δD and $\delta^{18}O$ values in Bchaaleh (-79.7 ± 3.6 ‰ and 26.1 ± 3.3 ‰ respectively) and Kawkaba (-74.8 ± 4.9 ‰ and 31.2 ± 1.6 ‰) are significantly different (p-value = $1.34e^{-06}$ and 0.02 respectively) while stems mean δD and $\delta^{18}O$ values of Bchaaleh (-69.2 ± 5.9 ‰ and 28.0 ± 7.7 ‰, respectively) and Kawkaba (-68.4 ± 4.2 ‰ and 25.3 ± 1.1 ‰, respectively) are not significantly different (p-value > 0.6) (Figure 5 a,b). The litter in Bchaaleh shows the most depleted mean δD and $\delta^{18}O$ values (-91.0 ± 8.2 ‰, 22.8 ± 1.1 ‰). At Kawkaba, litter δD and $\delta^{18}O$ values are -78.6 ‰ and 23.0 ‰ respectively. No significant difference is registered for δD and $\delta^{18}O$ between the litter of Bchaaleh and

Kawkaba (p-value = 0.7 and 1) (Figure 5 a,b). Mean δD and $\delta^{18}O$ values of the soil surface in Bchaaleh (-81.2 ± 8.9 ‰ and 23.5 ± 2.9 ‰ respectively) and Kawkaba (-67.6 ± 3.5 ‰ and 16.5 ± 1.7 ‰ respectively) are significantly different (p-value = $4.435e^{-05}$ and $4.644e^{-07}$). The mean δD values of soil 0-30cm in Bchaaleh (-76.4 ± 17.8 ‰) and Kawkaba (-77.9 ± 5.3 ‰) are not significantly different (p-value = 0.09). While a significant difference (p-value < 0.05) is observed between mean $\delta^{18}O$ values of the soil 0-30cm of Bchaaleh (23.5 ± 2.4 ‰) and Kawkaba (17.2 ± 2.8 ‰) (Figure 5 a,b).

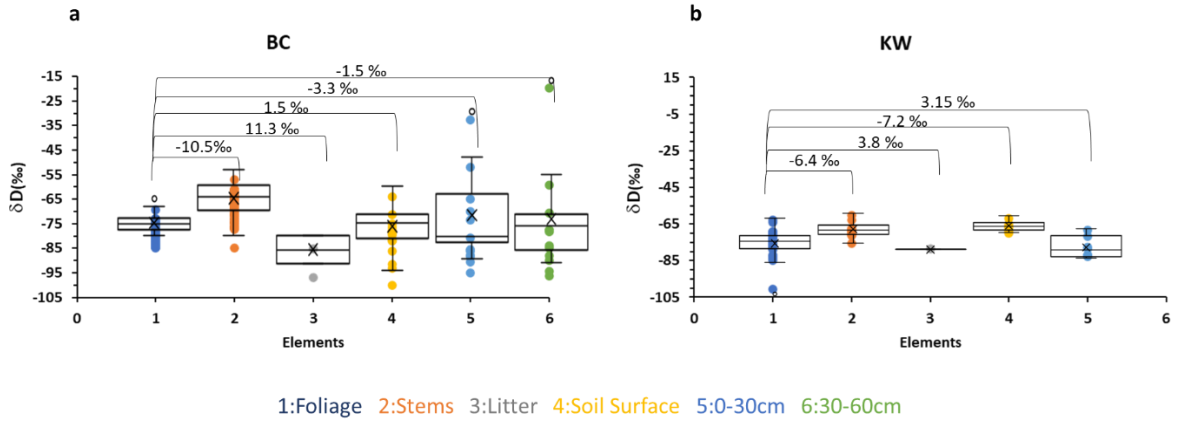


**Figure 11** Mean average of δD ratio for 2019-2020 of olive trees for foliage, stems, litter, soil surface, soil 0-30 cm and 30-60 cm in **(a)** Bchaaleh and **(b)** Kawkaba.

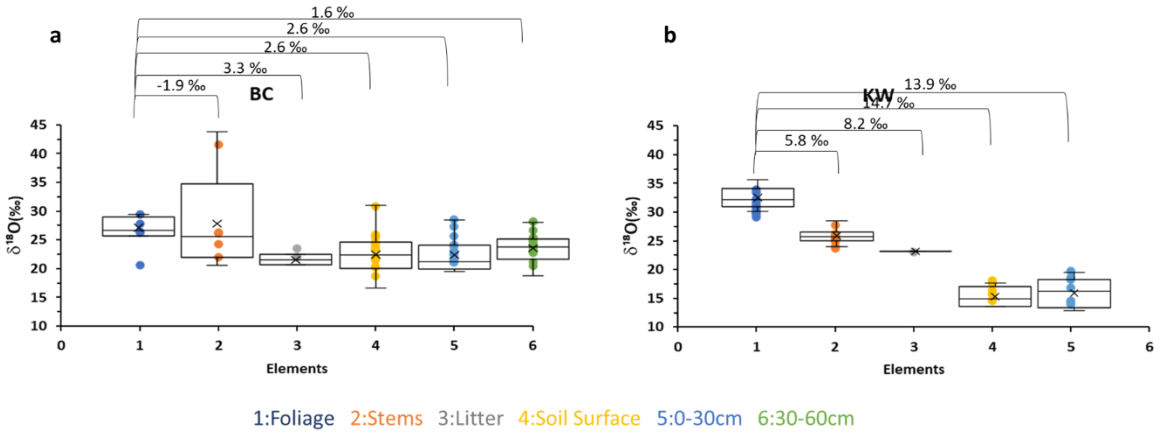


**Figure 12** Mean average of $\delta^{18}O$ ratio for 2019-2020 of olive trees for foliage, stems, litter, soil surface, soil 0-30 cm and 30-60 cm in **(a)** Bchaaleh and **(b)** Kawkaba.

### III.2 Annual variation of C,N,S,H isotopic composition for foliage and $\delta^{18}O$, δD of precipitation in Bchaaleh and Kawkaba .

Bchaaleh and Kawkaba mean annual $\delta^{13}C$ foliage values shows a significant difference between years 2019 and 2020 (p-value = 0.0003 and 0.05 respectively) with more enriched values in 2019 (-26.4 ± 0.8 ‰ and -27.8 ± 1.0 ‰ respectively) than 2020 (-27.0 ± 0.5 ‰ and -28.4 ± 1.3 ‰ respectively) (Figure 8). In 2019, Bchaaleh spring $\delta^{13}C$ mean value (-26.8 ± 0.6 ‰) is the most depleted among all seasons,

and significantly different in comparison to summer and fall (-25.9 ± 0.8 ‰ and -26.2 ± 0.7 ‰ respectively; p-value< 0.05), unlike the winter, summer and fall that register no seasonal significant difference (p-value> 0.3) (Table 1). The seasonal pattern observed in 2019 is not confirmed in 2020, showing the most depleted values in summer (-27.1 ± 0.4 ‰) and highest in spring (-26.7 ± 0.4 ‰) (Figure 8). Though no significant difference is reported between seasons (p-value > 0.3) (Table 1). In Kawkaba, foliage highest mean $\delta^{13}C$ value in 2019 is registered in fall (-27.4 ± 1.1 ‰) and is statistically significantly different from spring and summer (p-value = 0.007) (Table 1). Noting that winter (-28.1 ± 1.7 ‰) is the most depleted although not significantly different compared to all the other seasons (Table 1). Interestingly, summer 2020 $\delta^{13}C$ foliage values are highly variable as 2019 and the mean $\delta^{13}C$ value is the most depleted (-28.8 ± 1.7 ‰) compared to the other seasons (Figure 8), but not statistically significantly different (p-value > 0.06; Table 1).

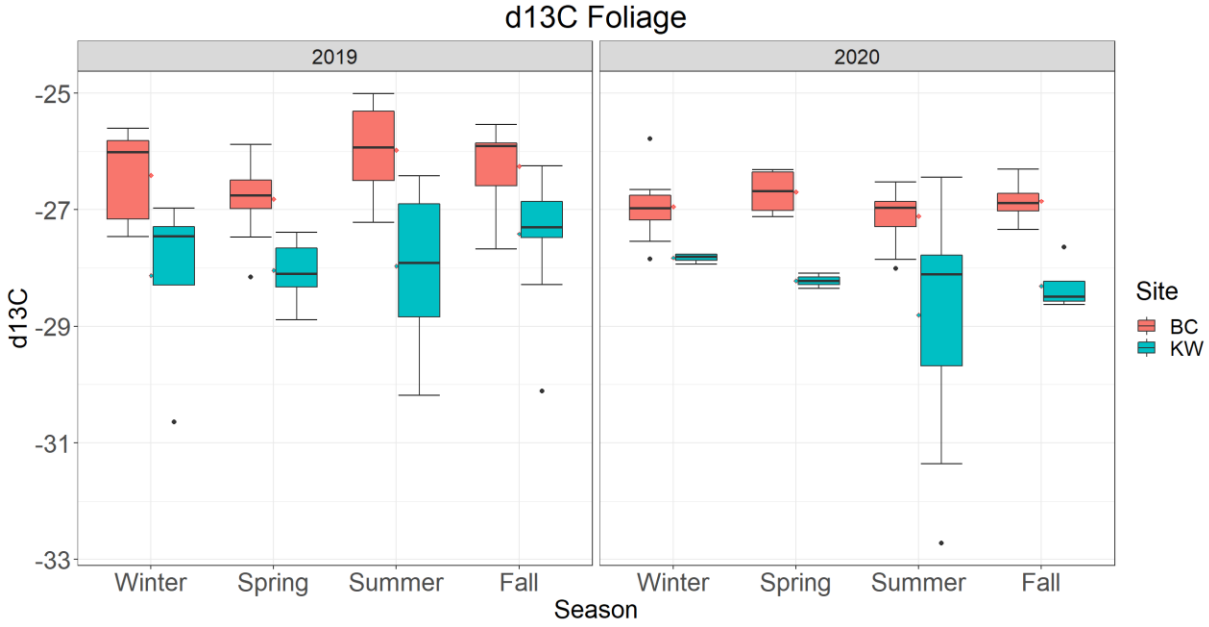


**Figure 13** Foliage $\delta^{13}C$ for 2019 vs. 2020 of olive trees in Bchaaleh and Kawkaba.

**Table 4** Foliage $\delta^{13}C$ for 2019 *vs.* 2020 significant difference between seasons in Bchaaleh and Kawkaba.

| δ¹³C Foliage | BC Winter 2019 | BC Spring 2019 | BC Summer 2019 | BC Fall 2019 | BC Spring 2020 | BC Summer 2020 | BC Fall 2020 |
|---|---|---|---|---|---|---|---|
| BC Winter 2019 | | 0.4 | 0.4 | 0.7 | | | |
| BC Spring 2019 | | | **0.007** | **0.09** | | | |
| BC Summer 2019 | | | | 0.4 | | | |
| BC Winter 2020 | | | | | 0.4 | 0.5 | 0.7 |
| BC Spring 2020 | | | | | | 0.1 | 0.6 |
| BC Summer 2020 | | | | | | | 0.3 |
| BC Fall 2020 | | | | | | | |

| δ¹³C Foliage | KW Winter 2019 | KW Spring 2019 | KW Summer 2019 | KW Fall 2019 | KW Spring 2020 | KW Summer 2020 | KW Fall 2020 |
|---|---|---|---|---|---|---|---|
| KW Winter 2019 | | 0.3 | 0.9 | 0.3 | | | |
| KW Spring 2019 | | | 0.9 | **0.007** | | | |
| KW Summer 2019 | | | | 0.007 | | | |
| KW Winter 2020 | | | | | 0.5 | 0.06 | 0.07 |
| KW Spring 2020 | | | | | | 0.2 | 0.6 |
| KW Summer 2020 | | | | | | | 0.3 |
| KW Fall 2020 | | | | | | | |

Foliage $\delta^{15}N$ values in Bchaaleh and Kawkaba (Figure 9) show no significant variations (p-value = 0.5 and 0.6 respectively) between the studied periods 2019 (2.5 ± 1.1 ‰ and 0.3 ± 1.0 ‰ respectively) and 2020 (2.4 ± 0.9 ‰ and 0.07 ± 1.5 ‰ respectively). For Bchaaleh, no seasonal differences for both years 2019 and 2020 are observed (p-value > 0.3), while Kawkaba registered a statistically significant seasonal variation in 2019 between spring and summer (p-value = 0.0005) and spring and fall (p-value = 0.01) unlike 2020 (p-value > 0.3; Table 2). Despite the lack of statistically significant seasonal differences in 2020, we notice on figure 9 that both years 2019 and 2020 recorded the most depleted $\delta^{15}N$ values in spring (-0.6 ± 0.8 ‰ and -0.4 ± 1.9 ‰ respectively) and the most enriched in summer 2019 and fall 2020 (0.8 ± 0.9 ‰ and 0.4 ± 0.7 ‰ respectively) (Figure 9).

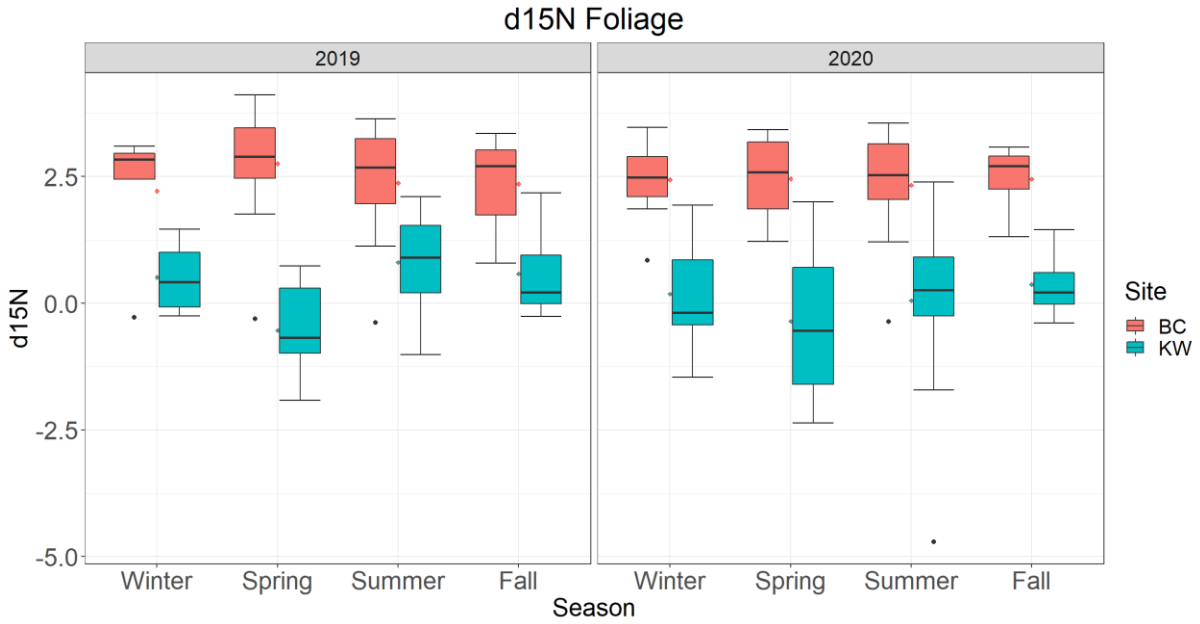


**Figure 14** Foliage $\delta^{15}N$ for 2019 *vs.* 2020 of olive trees in Bchaaleh and Kawkaba.

**Table 5** Foliage $\delta^{15}N$ for 2019 *vs.* 2020 significant difference between seasons in Bchaaleh and Kawkaba.

| $\delta^{15}N$ Foliage | BC Winter 2019 | BC Spring 2019 | BC Summer 2019 | BC Fall 2019 | BC Spring 2020 | BC Summer 2020 | BC Fall 2020 |
|---|---|---|---|---|---|---|---|
| BC Winter 2019 | | 0.5 | 0.9 | 0.9 | | | |
| BC Spring 2019 | | | 0.4 | 0.4 | | | |
| BC Summer 2019 | | | | 0.96 | | | |
| BC Winter 2020 | | | | | 0.97 | 0.8 | 0.98 |
| BC Spring 2020 | | | | | | 0.8 | 0.99 |
| BC Summer 2020 | | | | | | | 0.8 |
| BC Fall 2020 | | | | | | | |
| | | | | | | | |
| $\delta^{15}N$ Foliage | KW Winter 2019 | KW Spring 2019 | KW Summer 2019 | KW Fall 2019 | KW Spring 2020 | KW Summer 2020 | KW Fall 2020 |
| KW Winter 2019 | | 0.08 | 0.5 | 0.5 | | | |
| KW Spring 2019 | | | **0.0005** | **0.01** | | | |
| KW Summer 2019 | | | | 0.4 | | | |
| KW Winter 2020 | | | | | 0.6 | 0.8 | 0.7 |
| KW Spring 2020 | | | | | | 0.7 | 0.4 |
| KW Summer 2020 | | | | | | | 0.6 |
| KW Fall 2020 | | | | | | | |

Bchaaleh foliage $\delta^{34}S$ annual mean value recorded a significant difference (p-value = 0.002) between 2019 (7.7 ± 7.4 ‰) and 2020 (4.4 ± 1.3 ‰) (Figure 10). A seasonal significant difference (p-value > 0.02) was registered in 2019 between winter (4.6 ± 1.5 ‰) and spring (13.5 ± 11.7 ‰) and spring and fall (4.9 ± 1.2 ‰, Table 3). While 2020 recorded no significant difference (p-value > 0.08; Table 3). Winter 2019 and 2020 seasons registered the lowest mean $\delta^{34}S$ values, while the highest $\delta^{34}S$ values occur in spring in 2019 (13.5 ± 11.7 ‰) and in summer in 2020 (4.8 ± 1.4 ‰) (Figure 10). In Kawkaba, the foliage means annual $\delta^{34}S$ value recorded no statistically significant difference (p-value = 0.5) between 2019 (9.9 ± 2.4 ‰) and 2020 (9.8 ± 2.4 ‰) (Figure 10). In 2019, significant statistical seasonal differences (p-value <0.05) are observed between the spring (7.7 ± 0.2 ‰) and fall (10.7 ± 2.8 ‰) and spring and summer (9.4 ± 2.0 ‰) mean $\delta^{34}S$ values (Figure 10, Table 3). While in 2020, no evidence of mean seasonal $\delta^{34}S$ differences (p-value > 0.2) is reported (Table 3). However, summer mean $\delta^{34}S$ (10.3 ± 2.9 ‰) registered the highest value and spring (9.2 ±1.9 ‰) the most depleted value (Figure 10).

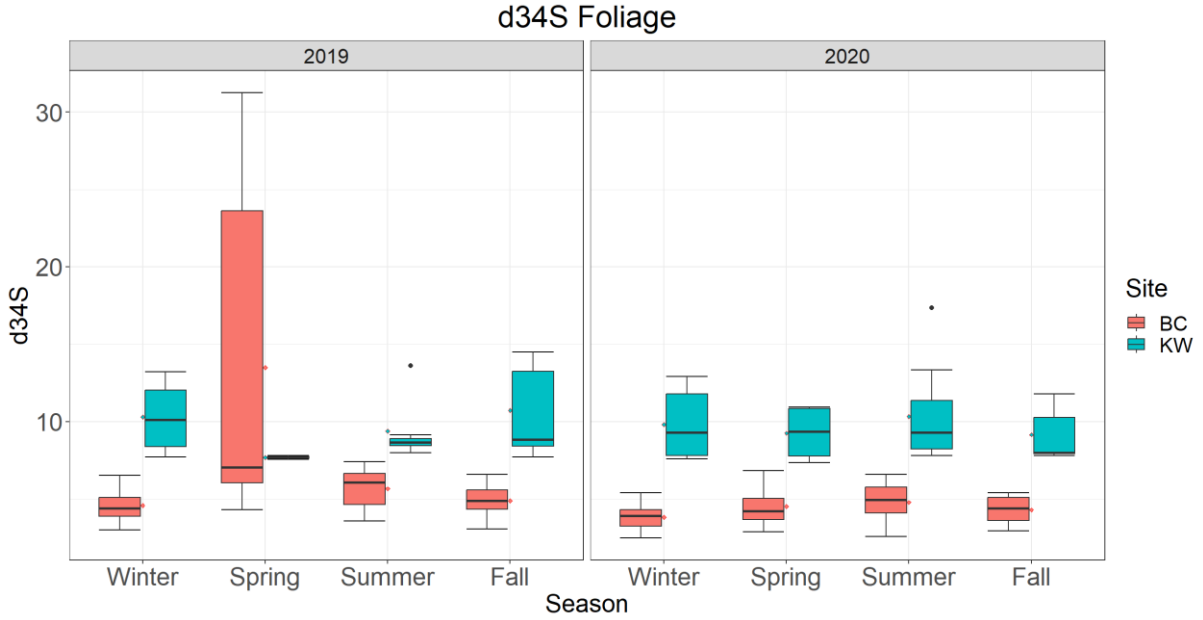


**Figure 15** Foliage $\delta^{34}S$ for 2019 *vs.* 2020 of olive trees in Bchaaleh and Kawkaba.

**Table 6** Foliage $\delta^{34}S$ for 2019 *vs.* 2020 significant difference between seasons in Bchaaleh and Kawkaba.

| $\delta^{34}S$ Foliage | BC Winter 2019 | BC Spring 2019 | BC Summer 2019 | BC Fall 2019 | BC Spring 2020 | BC Summer 2020 | BC Fall 2020 |
|---|---|---|---|---|---|---|---|
| BC Winter 2019 | | 0.05 | 0.2 | 0.7 | | | |
| BC Spring 2019 | | | 0.1 | 0.02 | | | |
| BC Summer 2019 | | | | 0.2 | | | |
| BC Winter 2020 | | | | | 0.5 | 0.09 | 0.5 |
| BC Spring 2020 | | | | | | 0.8 | 0.8 |
| BC Summer 2020 | | | | | | | 0.5 |
| BC Fall 2020 | | | | | | | |
| | | | | | | | |
| $\delta^{34}S$ Foliage | KW Winter 2019 | KW Spring 2019 | KW Summer 2019 | KW Fall 2019 | KW Spring 2020 | KW Summer 2020 | KW Fall 2020 |
| KW Winter 2019 | | 0.1 | 0.8 | 0.7 | | | |
| KW Spring 2019 | | | 0.03 | 0.005 | | | |
| KW Summer 2019 | | | | 0.5 | | | |
| KW Winter 2020 | | | | | 0.7 | 0.5 | 0.6 |
| KW Spring 2020 | | | | | | 0.5 | 0.9 |
| KW Summer 2020 | | | | | | | 0.3 |
| KW Fall 2020 | | | | | | | |

Bchaaleh and Kawkaba foliage δD mean annual values recorded no significant differences (p-value = 0.4 and 0.5 respectively) between 2019 (-80.0 ± 3.3 ‰ and -75.3 ± 5.6 ‰ respectively) and 2020 (-79.2 ± 4.0 ‰ and -74.1 ± 3.4 ‰ respectively) (Figure 11). In Bchaaleh, the foliage δD mean value registered no seasonal significant statistical difference in 2019 (p-value > 0.1) while a difference is observed in 2020 between winter and summer (p-value = 0.03) and winter and fall season (p-value = 0.02) (Table 4). Noting also that winter 2019 and 2020 have the highest seasonal mean δD value (-76.6 ± 4.5 ‰ and -75.7 ± 3.7 ‰ respectively), while summer 2019 and fall 2020 recorded the lowest δD mean values (-81.4 ± 3.0 ‰ and -82.9 ± 2.1 ‰ respectively) (Figure 11).

In Kawkaba, year 2019 registered significant seasonal differences between spring and winter (p-value = 0.05) and spring and fall (P-value = 0.003; Table 4) while year 2020 showing a seasonal difference between winter and spring (p-value = $6.592e^{-05}$; Table 4), winter and summer (p-value = 0.003) and spring and summer (p-value == 0.01). Interestingly, Kawkaba has also shown that winter 2019 and 2020 have the highest mean δ D value (-68.6 ± 6.6 ‰ and -69.7 ± 0.5 ‰ respectively), while spring 2019 and 2020 (-78.8 ± 4.8 ‰ and -78.2 ± 0.007 ‰ respectively) registered the most depleted values (Figure 11).

The same seasonal variation study was performed for the stem values for $\delta^{13}C$, $\delta^{15}N$, $\delta^{34}S$ and δD (Table SI 1). The main trends observed on foliage are mostly also found on stems. For Bchaaleh and Kawkaba, an offset between foliage and stems with an average of 1 ± 0.2 ‰ for $\delta^{13}C$, 1 ± 0.3 ‰ for $\delta^{15}N$, 3 ± 1 ‰ for $\delta^{34}S$, and an average offset of 8 ± 8 ‰ for δD between foliage and stems is observed.

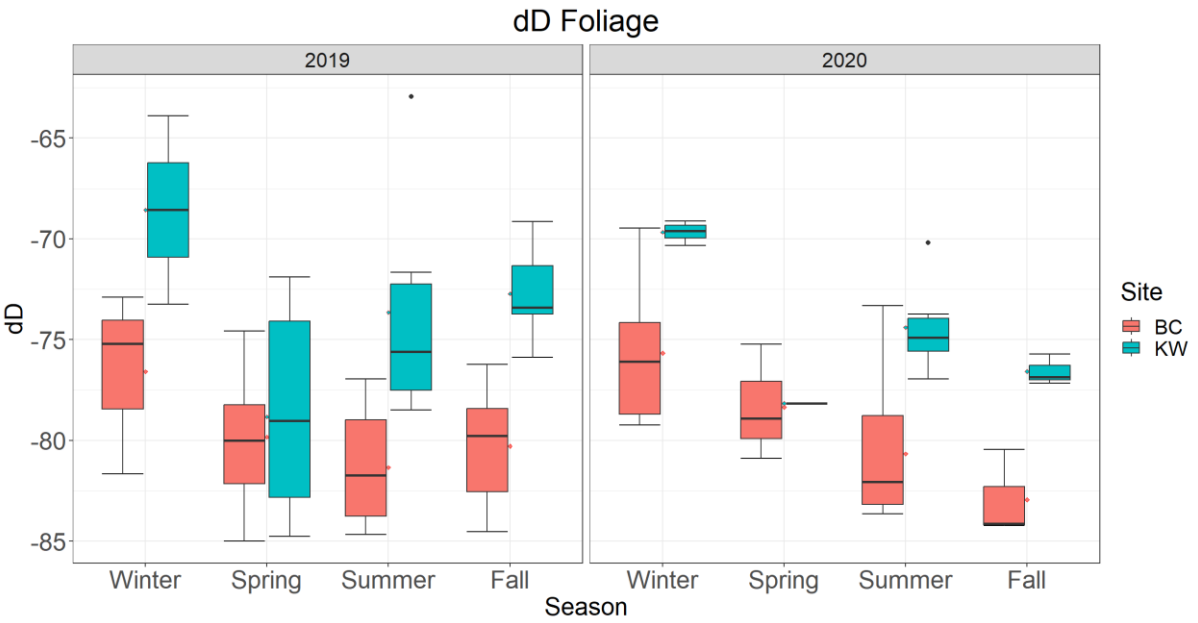


**Figure 16** Foliage δD for 2019 *vs.* 2020 of olive trees in Bchaaleh and Kawkaba.

**Table 7** Foliage δD for 2019 *vs.* 2020 significant difference between seasons in Bchaaleh and Kawkaba.

| δD Foliage | BC Winter 2019 | BC Spring 2019 | BC Summer 2019 | BC Fall 2019 | BC Spring 2020 | BC Summer 2020 | BC Fall 2020 |
|---|---|---|---|---|---|---|---|
| BC Winter 2019 | | 0.3 | 0.2 | 0.3 | | | |
| BC Spring 2019 | | | 0.3 | 0.8 | | | |
| BC Summer 2019 | | | | 0.5 | | | |
| BC Winter 2020 | | | | | 0.3 | **0.03** | **0.02** |
| BC Spring 2020 | | | | | | 0.3 | 0.2 |
| BC Summer 2020 | | | | | | | 0.2 |
| BC Fall 2020 | | | | | | | |
| | | | | | | | |
| δD Foliage | KW Winter 2019 | KW Spring 2019 | KW Summer 2019 | KW Fall 2019 | KW Spring 2020 | KW Summer 2020 | KW Fall 2020 |
| KW Winter 2019 | | **0.05** | 0.4 | 0.3 | | | |
| KW Spring 2019 | | | 0.1 | **0.003** | | | |
| KW Summer 2019 | | | | 0.7 | | | |
| KW Winter 2020 | | | | | **$6.592e^{-05}$** | **0.003** | 0.0004 |
| KW Spring 2020 | | | | | | **0.01** | 0.07 |
| KW Summer 2020 | | | | | | | 0.08 |
| KW Fall 2020 | | | | | | | |

For the studied period lasting from March 2019 until April 2021, the most depleted $\delta D_P$ (-54.8 ‰ and -71.6 ‰ respectively in Bchaaleh and -41. 3‰ and -54.8 ‰ respectively in Kawkaba) and $\delta^{18}O_P$ (9.9 ‰ and -11.44 ‰ in Bchaaleh and -8.0 ‰ and -9.3 ‰ in Kawkaba) values in Bchaaleh and Kawkaba occurred in January 2020 and 2021(Figure 12), concomitantly with the highest precipitation (> 350 mm), relative humidity (> 80 %) and low air temperatures (< 5 °C).

The highest $\delta D_P$ values in Bchaaleh are registered during the months of September and December 2019 (-12.6 ‰), February 2020 (-30.1 ‰) and April 2021 (-17.1 ‰). While for $\delta^{18}O_P$, September and December 2019 (-4.0 ‰), April 2020 (-6.4 ‰) and April 2021 (-4.5 ‰). Kawkaba registered the highest $\delta D_P$ values during the months of December 2019 (-3.16 ‰), March 2020 (-21.6 ‰) and April 2021 (-11.5 ‰). While for $\delta^{18}O_P$, December 2019 (-2.5 ‰), March 2020 (-5.2 ‰) and April 2021 (-4.1 ‰)

(Figure 12), along with the lower precipitation (< 225 mm), relative humidity (< 75 %) and low air temperature (> 5 °C).

The mean average values of both $\delta D_P$ ($\delta D$ of precipitation) and $\delta^{18}O_P$ ($\delta^{18}O$ of precipitation) for Bchaaleh (-35.7 ± 17.1 ‰ *vs.* V-SMOW and -7.14 ± 2.2 ‰ *vs.* V-SMOW respectively) and Kawkaba (-27.7 ± 15.4 ‰ *vs.* V-SMOW and -6.2 ± 2.0 ‰ *vs.* V-SMOW respectively) are not significantly different (p-value = 0.3 and p-value = 0.4 respectively). On figure 13, the local water meteoric lines show a d-excess value varying between 17.9 ‰ at Kawkaba and 18.4 ‰ at Bchaaleh. Joining the two data set we obtained for North and South Lebanon a LMWL as follows: $\delta D = 7.58 * \delta^{18}O_p + 18{,}17$ ($R^2 = 0.98$).

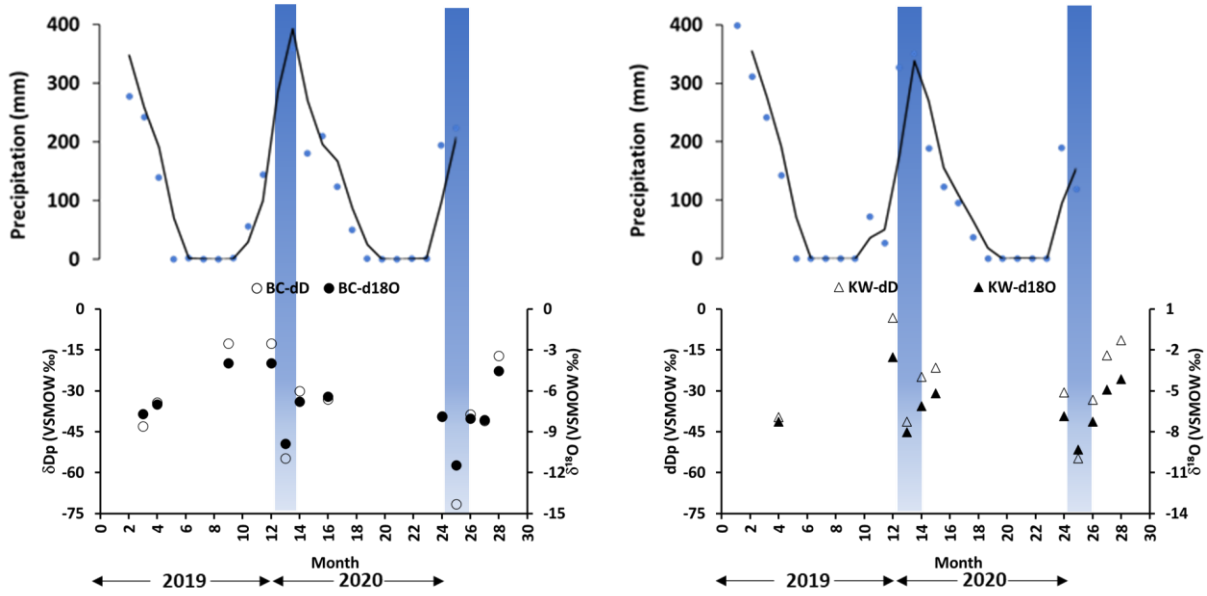


**Figure 17** Precipitation δD and $\delta^{18}O$ for 2019-2021 for the olive groves in Bchaaleh and Kawkaba.

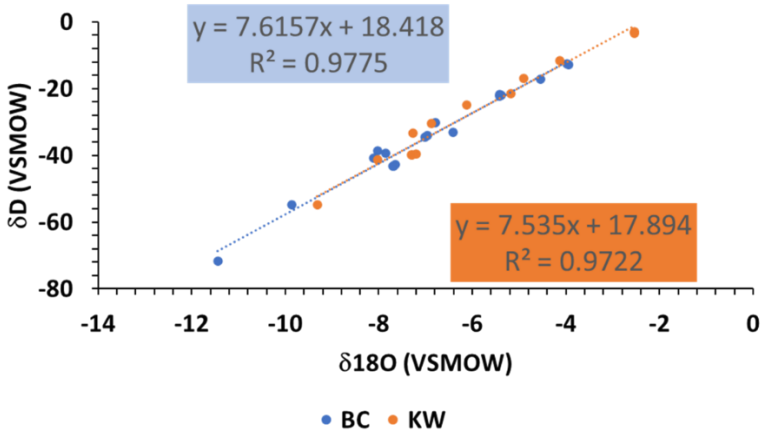


**Figure 18** Local meteoric water lines in two sites of Lebanon Bchaaleh (BC) and Kawkaba (KW): relationship between δD and $\delta^{18}O$ of precipitation.

### III.3 Bchaaleh and Kawkaba foliage C,N,S,H isotopic composition in relation to climatic parameters ( temperature, precipitation, relative humidity and pCO2)

In Bchaaleh and Kawkaba**,** $\delta^{13}C$ of foliage registered no significant correlation with air temperature (r = 0.05, p-value = 0.6 and r = -0.06, p-value = 0.5 respectively), precipitation (r = -0.07, p-value = 0.4 and r = 0.1, p-value = 0.4 respectively) and relative humidity (r = -0.07, p-value = 0.4 and r = 0.05, p-value = 0.5 respectively). While $pCO_2$ registered at both sites, Bchaaleh and Kawkaba a low but significantly negative correlations with $pCO_2$ are observed (r = -0.2, p-value = 0.04 and r = -0.2, p-value = 0.01 respectively; Figure 14).

Bchaaleh and Kawkaba $\delta^{15}N$ of foliage and air temperature (Correlation = -0.04, p-value = 0.6 and r = 0.1, P-value = 0.1 respectively), precipitation (Correlation = 0.05, P-value = 0.6 and r = -0.2, P-value = 0.03 respectively), relative humidity (Correlation = 0.04, p-value = 0.6 and r = -0.1, p-value = 0.2 respectively) and $pCO_2$ (Correlation = 0.01, P-value = 0.9 and r = -0.1, p-value = 0.2 respectively) mostly registered no significant correlation, except in Kawkaba $\delta^{15}N$ of foliage and precipitation that showed a low negative significant correlation (Figure 14).

Bchaaleh and Kawkaba $\delta^{34}S$ of foliage showed no significant correlation with air temperature (r = 0.05, p-value = 0.5 and r = 0.05, p-value = 0.5 respectively), precipitation (r = -0.1, p-value = 0.3 and r = -0.04, p-value = 0.7 respectively), relative humidity (r = -0.05, p-value = 0.6 and r = 0.05, p-value = 0.6 respectively) and $pCO_2$ (r = -0.05, p-value = 0.5 and r = -0.1 and p-value = 0.1; Figure 14).

Bchaaleh δD of foliage showed a negative moderate significant correlation with air temperature (r = -0.4, p-value < 0.05), and a positive moderate significant correlation with precipitation (r = 0.3, p-value < 0.05) and relative humidity (Correlation = 0.3, P-value < 0.05). While a positive low significant correlation was registered between δD of foliage and $pCO_2$ (r = 0.2, P-value = 0.03; Figure 14a). While Kawkaba δD of foliage recorded no significant correlation with any of the climatic parameters, air temperature (r = -0.1, p-value = 0.3), precipitation (r = 0.05, p-value = 0.7), relative humidity (r = -0.006, p-value = 0.9) $pCO_2$ (r = 0.001, P-value = 0.9; Figure 14b).

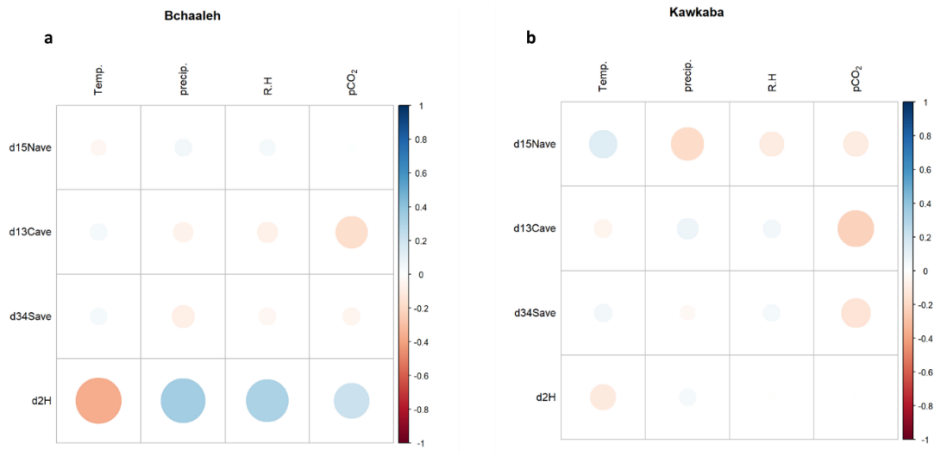


**Figure 19** Correlation between $\delta^{13}C$, $\delta^{15}N$, $\delta^{34}S$ and δD of foliage and climatic parameters in **(a)** Bchaaleh and **(b)** Kawkaba.

# IV. Discussion

## IV.1 Comparative C,N,S,H,O isotopic composition difference between plant tissues, soil and litter in Bchaaleh and Kawkaba

A strong positive correlation between the $\delta^{13}C$ of foliage and stems was recorded in Bchaaleh and Kawkaba ($r=0.53$, p-value = $4.437e^{-10}$; Figure 2) as also seen in different species (ie. Beech, Peuke et al., 2006). An intercept equivalent to a carbon isotopic fractionation of 0.9 and 1.3 ‰ between foliage and stems (Table 1; Figure 2) is observed for Bchaaleh and Kawkaba respectively. The higher isotopic composition in the stems likely results from different organic compound composition and sugar export from foliage to stems (Hobbie & Werner, 2004; Damesin & Lelarge, 2003; Peuke et al., 2006).

Litter $\delta^{13}C$ in Bchaaleh showed a small and insignificant enrichment (-0.3 ‰) compared to the foliage (p-value = 0.32; Figure 2) suggesting that the organic carbon of the litter layer dominated by the shedded foliage preserves the isotopic signature of the foliage as observed by Badeck et al., (2005). In Kawkaba, a higher and significant difference is registered between litter and foliage $\delta^{13}C$ (-1.2 ‰, p-value < 0.05) (Figure 2) that can be explained by the lower altitude in Kawkaba and characterized by slightly higher temperature/lower precipitation which leads to a faster decomposition of litter into the soil layers (Marian et al., 2017). The more depleted $\delta^{13}C$ of plant tissues, soil and litter measured at Bchaaleh is likely due to its higher altitudinal position (1300 m.a.s.l) compared to Kawkaba (672 m.a.s.l).

In Bchaaleh olive groves, the $\delta^{13}C$ increase from the litter ( -26.36 ± 0.75 ‰) to the soil layers (soil surface: -26.05 ± 0.82 ‰, 0-30 cm: -25.00 ± 1.91 ‰, and 30-60 cm: -24.33 ± 2.13 ‰) (Figure 2a). In Kawkaba, the litter $\delta^{13}C$ is -26.88 ± 0.62 ‰ while the soil surface and 0-30 cm layer registered values of -26.96 ± 0.88 ‰ and -26.37 ± 0.57 ‰ respectively. As we go deeper into soil depth the $\delta^{13}C$ values are more enriched (Figure 2b). This is mainly due to the biological activity decrease with the increasing soil depth and in parallel with the root biomass decrease with an increase in root depth (Högberg et al., 2005; Boström et al., 2007, Kaler et al., 2018). This is proven by different evidences, first the disappearance of plant biomarkers during the decomposition of plant material and microbially derived markers appear. Second, production of mycorrhizal hyphae in the soil substantial (Ekblad et al., 1995; Gleixner et al., 1999, 2002; Wallander et al., 2003; Gleixner, 2005; Boström et al., 2007). Also, the production of mycelia down to a depth of 30cm. These Mycelia were most probably mycorrhizal, this is supported by the similarity between $\delta^{13}C$ of mycelia and the mycorrhizal fungi on a study done by Boström et al., (2007).

Foliage and stems $\delta^{15}N$ in Bchaaleh and Kawkaba showed no significant correlation ($r= -0.10$, p-value = 0.25). The decrease observed in Bchaaleh for the $\delta^{15}N$ from foliage (2.44 ± 1.06 ‰) to stems (1.56 ± 3.38 ‰) registered a difference of 0.9 ‰ (Figure 3a). While for Kawkaba, $\delta^{15}N$ increased from foliage (0.21 ± 1.24 ‰) to stems (5.45 ± 2.78 ‰) with -5.2 ‰ difference (Figure 3b). The more depleted values in the foliage of Kawkaba can be explained by the low availability of nitrogen which makes them depend on the mycorrhizal fungi for nitrogen acquisition than those having high nitrogen availability

such as Bchaaleh. Thus, plants obtaining more nitrogen through mycorrhizal fungi is usually more depleted in $\delta^{15}N$ (E. A. Hobbie & Colpaert, 2003; Neff et al., 2003). In Bchaaleh, the more enriched $\delta^{15}N$ values in foliage in comparison to stems can also be related probably to the foliage use of the nutrients available in the stems in order to cover their nutrition limitation (Heineman et al., 2016; Tang et al., 2017).

In Bchaaleh, $\delta^{15}N$ of litter (1.21 ± 0.17) recorded a more depleted value in comparison to soil surface (3.05 ± 1.49 ‰) (Figure 3a). Litter is integrated in to the soil in the form of organic matter, microbial transformed organic matter or as dissolved organic compounds (Klotzbücher et al., 2016; Zheng et al., 2021). With large mass loss of the litter there is large fraction of nitrogen (Asada et al., 2005), usually meaning higher values in soil than in litter. While as we go deeper in to the soil layers, more depleted values are recorded in 0-30 cm and 30-60 cm (0.79 ± 3.45 ‰ and -0.70 ± 3.29 ‰ respectively; Figure 3a) which is due to a downward transport process and the soil organic matter transformation (Baumgartner et al., 2021). Adding to that, the leaching and microbial assimilation of depleted $NO_3^-$ as we go in to lower soil depth causes more depleted $\delta^{15}N$ values at lower soil depth than those of more intermediate depth (Craine et al., 2015; Baumgartner et al., 2021). In Kawkaba, litter registered the most depleted $\delta^{15}N$ values in comparison to soil surface and 0-30 cm (2.12 ± 0.98 ‰, 3.32 ± 0.89 ‰ and 3.34 ± 1.62 ‰ respectively; Figure 3b). $\delta^{15}N$ usually shows an enrichment trend with the increase in soil depth that is related to aging and the turnover of organic matter (Trumbore, 2009; Lorenz et al., 2020). The enrichment of the $\delta^{15}N$ in the soil depth is determined as the difference between the highest enrichment of the $\delta^{15}N$ in the mineral soil and the litter, and the $\delta^{15}N$ development in the soil depth is due to the nitrogen cycling processes that are related to the soil organic matter turnover (Emmett et al., 1998; Lorenz et al., 2020). In addition to that, the type and degree of the mycorrhizal associations, N losses after ammonification, enzymatic hydrolysis, denitrification and nitrification, atmospheric deposition and the soil N mixing through bioturbation, all contribute to the $\delta^{15}N$ enrichment in the soil profile (Lorenz et al., 2020). Altitudinal effect has also an effect on the $\delta^{15}N$ in the soil, where with higher elevation such as that in Bchaaleh, more depleted values are registered (Baumgartner et al., 2021). The higher C/N ratio in Kawkaba indicates a higher efficient nutrition use than that in Bchaaleh (Zhang et al., 2019).

Foliage $\delta^{34}S$ in Bchaaleh and Kawkaba are significantly different (p-value of $2.2e^{-16}$), while the $\delta^{34}S$ of stems had no significant difference between the two studied sites (p-value = 0.61). A higher $\delta^{34}S$ in foliage and stems was registered in Kawkaba, indicating a higher deposit of sulfur in Kawkaba than in Bchaaleh. Foliage and stems $\delta^{34}S$ in both Bchaaleh and Kawkaba showed no correlation (r= -0.035, p-value = 0.71), but we can see an increase from foliage to stems in both studied sites, registering a difference of -5.2 ‰ in Bchaaleh and -1.5 ‰ in Kawkaba (Figure 4). The higher $\delta^{34}S$ in the stems in both sites is mainly due to the main transfer of sulfate from the roots to the shoots through the phloem and xylem (Gigolashvili & Kopriva, 2014).

The pattern of increased $\delta^{34}S$ values in deeper depth, is due to the mineralization of the soil organic matter. Since the organic matter moves downwards as they decay, thus the old proportion of sulfur is higher in deeper soil in comparison to the soil surface (Zhang et al., 1998; Novák et al., 2003). Geologically, Lebanon consists mainly of limestones of Cretaceous origin and Jurassic limestones in some areas. While in the North basaltic rocks may appear (Faour, 2004). This may also affect the sulfur content in soil and thus affect the isotopic sulfur in foliage. It is indicated that $\delta^{34}S$ values of soil from moderately stressed sites ranges between 7 to 12‰ (Winner & Bewley, 1978; Case & Krouse, 1980), while the values in both our studied sites show higher values ranging between 7 and 38 ‰ indicating that the soil is loaded with sulfur.

Foliage means δD and $\delta^{18}O$ values in Bchaaleh (-79.7 ± 3.6 ‰ and 26.1 ± 3.3 ‰ respectively) and Kawkaba (-74.8 ± 4.9 ‰ and 31.2 ± 1.6 ‰) are significantly different (p-value = $1.34e^{-06}$ and 0.02 respectively) while stems mean δD and $\delta^{18}O$ values of Bchaaleh (-69.2 ± 5.9 ‰ and 28.0 ± 7.7 ‰, respectively) and Kawkaba (-68.4 ± 4.2 ‰ and 25.3 ± 1.1 ‰, respectively) are not significantly different (p-value > 0.6) (Figure 5 a,b). The litter in Bchaaleh shows the most depleted mean δD and $\delta^{18}O$ values (-91.0 ± 8.2 ‰, 22.8 ± 1.1 ‰). At Kawkaba, litter δD and $\delta^{18}O$ values are -78.6 ‰ and 23.0 ‰ respectively. No significant difference is registered for δD and $\delta^{18}O$ between the litter of Bchaaleh and Kawkaba (p-value = 0.7 and 1) (Figure 5 a,b). Mean δD and $\delta^{18}O$ values of the soil surface in Bchaaleh (-81.2 ± 8.9 ‰ and 23.5 ± 2.9 ‰ respectively) and Kawkaba (-67.6 ± 3.5 ‰ and 16.5 ± 1.7 ‰ respectively) are significantly different (p-value = $4.435e^{-05}$ and $4.644e^{-07}$). The mean δD values of soil 0-30cm in Bchaaleh (-76.4 ± 17.8 ‰) and Kawkaba (-77.9 ± 5.3 ‰) are not significantly different (p-value = 0.09). While a significant difference (p-value < 0.05) is observed between mean $\delta^{18}O$ values of the soil 0-30cm of Bchaaleh (23.5 ± 2.4 ‰) and Kawkaba (17.2 ± 2.8 ‰) (Figure 5 a,b).

Bchaaleh foliage δD had more depleted values than in Kawkaba (Figure 5). This can be explained by the altitudinal effect (Gat et al., 2001; Singh, 2017; J. Liu et al., 2021) that was also observed by Liu et al., (2021), where values decreased significantly with increase of altitude as seen in Bchaaleh (1300 m.a.s.l). As seen previously, the $\delta D_p$ (-34.1 ± 15.0 ‰) at Bchaaleh is more depleted than that at Kawkaba (-27.7 ± 15.8 ‰) due to various processes and one among them is the lower air temperatures at higher altitude. The δD of stems in Bchaaleh and Kawkaba show more enriched values in comparison to foliage (Figure 5). Since our stems are a mixture of young and mature samples, Thus the more enriched values in stems can be due to the gas exchange ($CO_2$ and $H_2O$) that mainly occur in young stems that are still green (Comstock & Ehleringer, 1992; Dawson & Ehleringer, 1993).

Bchaaleh litter δD had more depleted values than soil surface δD, soil 0-30cm and 30-60cm (Figure 5a). The more depleted values in the litter can be due to the input of rainwater and foliage δD to the litter layer. While the more enriched values in the soil can be caused by the litter layer that is preventing or decreasing the rainwater passage in to the soil which would influence the infiltration process affecting the soil properties from soil surface to 60 cm depth (Han et al., 2019). Another factor that can cause the

more enriched δD in soil in comparison to litter is the evapotranspiration and the root absorption of water. Kawkaba soil surface registered more enriched values than 0-30 cm soil layer (Figure 5b). As per Han et al. (2019), in forest lands the δD of soil layers up usually increases with depth and then decreases followed by another increase. This can also be seen in Bchaaleh and Kawkaba as we move from the soil surface into more depth.

Noting that we have a limited data for foliage $\delta^{18}O$ in the both studied sites (February till May 2019), the $\delta^{18}O$ of foliage in Kawkaba registered higher values than those registered in Bchaaleh (Figure 6) with a significant difference between the studied sites (p-value = 0.001). The more depleted values recorded in Bchaaleh is mainly related to the higher altitude (1300 m.a.s.l) (J. Liu et al., 2021) than that of Kawkaba (672 m.a.s.l). While for the $\delta^{18}O$ of stems, Bchaaleh recorded higher values than Kawkaba (Figure 6) but with no significant difference (p-value = 0.6). There is no significant difference between foliage and stems in Bchaaleh and Kawkaba since there is no fractionation during the transport of water from the roots to the stems through the xylem and that the water can diffuse to the phloem (Han et al., 2019; Amin et al., 2021).

A slight increase of $\delta^{18}O$ is observed from Litter $\delta^{18}O$ in Bchaaleh into soil surface, 0-30 cm and 30-60 cm. The same trend was observed in Kawkaba, where there was a slight and insignificant increase from soil surface to 0-30 cm (Figure 6). The surface soil water mixing that occurs during plant water uptake (Han et al., 2019), in addition to the soil water evaporation at a soil surface layer up to 50 cm, causing an enrichment in $\delta^{18}O$ (Han et al., 2019; Pingyuan et al., 2010).

### IV.2 Adaptability mechanism registered through annual and seasonal variability of C,N,S,H isotopic composition of foliage

The more depleted values of 2020 registered in Bchaaleh and Kawkaba $\delta^{13}C$ of foliage in comparison to year 2019 (Figure 8) can be due the decrease of wind speed and solar radiation from year 2019 to 2020 over time that can cause an increase in the stomatal conductance which can induce stomatal opening leading to a decrease in leaf surface water stress, in addition to an increase in the ratio of substomatal to atmospheric $CO_2$ ($c_i/c_a$) that regulates the stomata, and thus a decrease in the $\delta^{13}C$ of foliage (Cernusak & Marshall, 2001; Betson et al., 2007). Another factor that can cause more depleted foliage values in 2020 might be the lower chlorophyll and photosystem activity in addition to a higher Rubisco activity in the younger foliage collected in 2020 in comparison to the more mature foliage from the previous year (Gielen et al., 2000; Jach & Ceulemans, 2000). Normally, the most depleted $\delta^{13}C$ values in foliage are usually during rainy seasons (Winter) and the most enriched is during dry seasons which is summer in our case. In Bchaaleh, summer 2019 (-26.0 ± 0.8 ‰) registered the most enriched $\delta^{13}C$ values in foliage, while summer 2020 (-27.1 ± 0.5 ‰) registered the most depleted values among all the other seasons. While in Kawkaba, summer of 2019 and 2020 both registered the most depleted values in comparison to the other seasons (Figure 8). This observed depleted values of $\delta^{13}C$ in foliage

during most of the summer seasons in Bchaaleh and Kawkaba may be explained by the $CO_2$ leakage increase from the bundle sheath cells when faced by water stress (Buchmann et al., 1996; Saliendra et al., 1996; Yoneyama et al., 2010).

Both Bchaaleh and Kawkaba had a more depleted $\delta^{15}N$ values in foliage for year 2020 in comparison to 2019 but with no significant difference (p-value = 0.5 and p-value = 0.7 respectively; Figure 8) as also seen in a study done by Driscoll et al. (2021). In Bchaaleh, $\delta^{15}N$ of foliage during the summer season of 2019 and 2020 had depleted values (2.4 ± 1.2 ‰ and 2.3 ± 1.1 ‰ respectively) that where close to the winter season values of 2019 and 2020 (2.2 ± 1.4 ‰ and 2.4 ± 0.9 ‰ respectively) with no significant different between summer and winter seasons for both years (p-value = 0.9). While the $\delta^{15}N$ of foliage in Kawkaba, the summer of 2019 (0.8 ± 0.9 ‰) registered slightly more enriched values in comparison to winter 2019 (0.5 ± 0.8 ‰) with no significant difference (p-value = 0.4). Summer 2020 (0.05 ± 1.9 ‰) registered a slightly more depleted values than winter 2020 (0.18 ± 1.15 ‰; Figure 9) with no significant difference (p-value = 0.76). Hobbie & Colpaert, (2003) in his study on pine trees, showed that with the increase of mycorrhizal colonization, a more depleted $\delta^{15}N$ values in the needles is observed in comparison to the nitrogen source. Noting that olive trees roots are occupied by arbuscular mycorrhizal fungi (AMF) (Barbaro & González Basso, 2022), the depleted values in summer in both Bchaaleh and Kawkaba might be in association with AMF. Normally roots have higher $\delta^{15}N$ than foliage, suggesting that the AMF transfers lighter N to the foliage (E. A. Hobbie & Colpaert, 2003; Tatsumi et al., 2021). The mycorrhizal fungi provides N content to the plant as N limitation and drought stress increases (Hobbie & Hobbie, 2006; Begum et al., 2019).

The higher and significant foliage $\delta^{34}S$ annual mean value for Bchaaleh and Kawkaba registered in 2019 (Figure 10) can be an indication of a higher sulfur stress in the olive tree than in 2020 (Trust & Fry, 1992). Another explanation can be that in 2019, the foliage which is considered a sink organ, is receiving more enriched $\delta^{34}S$ from the proteins (Tcherkez & Tea, 2013) than that in 2020. The highest values of foliage $\delta^{34}S$ in Bchaaleh spring 2019 and Kawkaba fall 2019 (Figure 10), can be due to the lowest organic matter content and lower sulfide concentrations (Oakes & Connolly, 2004) available during those season.

Foliage δD seasonal variability in Bchaaleh and Kawkaba (Figure 11) is affected by the water source such as soil water and leaf water transpiration, in addition biochemical factors. The leaf water enrichment through leaf surface transpiration is affected by wind, photosynthetically active light, leaf water transpiration, in addition to biochemical factors such as soil nutrients, topography, sunlight and rainfall (Hartsough et al., 2008; J. Liu et al., 2021). Most probably due to drought stress, there is a water soil uptake to the foliage leading a depletion in foliage δD (Y. Li et al., 2022) in Bchaaleh and Kawkaba in 2019 and 2020 (Figure 11). In addition to the depleted δD of available cellulose, lipid or starch in foliage (Sanchez-Bragado et al., 2019). The more enriched foliage δD values registered in winter season for both sites (Figure 11) are mainly related to the lower temperature showing a more enriched leaf

water, caused by an increase in fractionation between the liquid and vapor phases during leaf lipid biosynthesis (Y. Zhou et al., 2011).

### IV.3.1 Effect of climatic parameters on the isotopic composition of C,N,H in foliage

Kawkaba and Bchaaleh $\delta^{13}C$ of foliage displayed a negative low correlation with $pCO_2$ (Figure 14) confirming the effect of the atmospheric $CO_2$ on $\delta^{13}C$. The $CO_2$ is considered the ultimate source of the plant carbon, meaning that $pCO_2$ has control over the $^{13}C$ amount in plant tissues (Schubert & Jahren, 2012). In $C_3$ plants, $\delta^{13}C$ discrimination occurs during $CO_2$ diffusion from the air to the intercellular air space through the boundary layer and stomata, and the carboxylation reaction by Rubisco (Farquhar et al., 1982; Sanchez-Bragado et al., 2019). The changes in $\delta^{13}C$ composition are assumed to be related to change in the water use efficiency due to the variation in water availability (Chapin, 1980; Ogaya & Peñuelas, 2008). Drought stress is a major determinant for carbon isotopes fractionation in $C_3$ plants (Swap et al., 2004; Hartman & Danin, 2010), leading to an increasing $\delta^{13}C$ due to the low stomatal conductance driven $CO_2$ diffusion (Condon, 2004; Sanchez-Bragado et al., 2019).

Although the results for foliage $\delta^{15}N$ in Bchaaleh showed no correlation with any of the climatic parameters (Figure 14a). The increase in $pCO_2$ has an effect on plant growth and functions such as the decrease in photosynthetic rate, increase in $CO_2$ assimilation rate and seedling growth, decrease in stomatal density and nitrogen content in foliage and an increase in water-use efficiency (Greer et al., 1995; Royer, 2001; Fitter & Hay, 2002; Gagen et al., 2011; Schubert & Jahren, 2011, 2012). In Bchaaleh, $\delta^{15}N$ values in dry and wet season plants were identical, showing that there is a year around stability in the $\delta^{15}N$ values of $C_3$ plants. For Kawkaba foliage, $\delta^{15}N$ showed a low negative significant correlation with precipitation ($r = -0.2$, p-value = 0.03; Figure 14b) as also shown in other studies such as Houlton et al., (2007). The warmer environment at lower altitudes such as Kawkaba, have a slightly lower precipitation, this reinforces the nitrobacteria and ammonifier activities in soil accelerating the soil mineralization/nitrification ratio, thus increasing NO flux in the soil (Aranibar et al., 2004; Liu & Wang, 2010) which results in an increase in foliage $\delta^{15}N$.

Foliage $\delta^{34}S$ and climatic parameters in Bchaaleh and Kawkaba, showed no significant correlation, thus no conclusions can be drawn (Figure 14).

Bchaaleh δD of foliage and the climatic parameters showed a significant correlation (Figure 14a). Normally, increase in relative humidity and decrease in temperature affect the δD of foliage enrichment caused by evapotranspiration (Cooper et al., 1991; Collins et al., 2013; Niedermeyer et al., 2016; J. Liu et al., 2021). The positive significant correlation between δD of foliage and precipitation is also in consistence with Liu et al., (2021) that showed that the water source such as precipitation and soil water is recorded in leaf water. $pCO_2$ effect on δD of foliage can be related to $CO_2$ stomatal conductance sensitivity and its effect on the evaporative δD enrichment of leaf water (Cernusak et al., 2016; Cormier

et al., 2018). Thus, the more enriched Bchaaleh δD of foliage at higher $pCO_2$ can be explained by the stomatal conductance reduction and transpiration. While for Kawkaba, no conclusions can be drawn between the δD of foliage and the climatic parameters since no significant correlation was recorded (Figure 14b).

### IV.3.2 δD and $\delta^{18}O$ precipitation and δD foliage variation

Most groundwater and precipitation samples plot close to the global meteoric water line (GMWL) defined by the relationship between the stable isotopic ratios of hydrogen (δD) and oxygen ($\delta^{18}O$) of the precipitation following the equation $\delta^{2}H=8*\delta^{18}O+10$ (Craig, 1961). The isotopic ratios we obtained in precipitation of Bchaaleh and Kawkaba (Figure 13) are closer to the Lebanon LMWL equation ($\delta D = 7.13*\delta^{18}O + 15.98$) described in Saad et al., (2005). Adding the data collected from the Global Network of Isotopes in Precipitation (GNIP) in Lebanon and the Near East region to ours, we obtained a LMWL for the Levant sub-region ($\delta D = 7.57*\delta^{18}O + 18.48$) very similar to that obtained at Bchaaleh (Figure 15). The shift we observe between the GMWL and the later defined LMWL (Figure 15) suggests important processes (e.g. rock-water interaction, evaporation, mixing with seawater) leading to the observed shift.

The precipitation is depleted in both δ D and $\delta^{18}O$ during wet seasons and more enriched as we move to dry seasons affected by the temperature (Dansgaard, 1964). In Bchaaleh, we have some snowy seasons, when the precipitation is in snow form the compensation is not direct since it is stored before going through the soil (Aouad et al., 2004).

Our data alines on the local water meteoric water line equation defining our values for both sites are adjacent to the LMWL and in parallel and upper to the GMWL (Figure 15). The offset from LMWL describes the influence of evaporation on water and indicates evaporation enrichment.

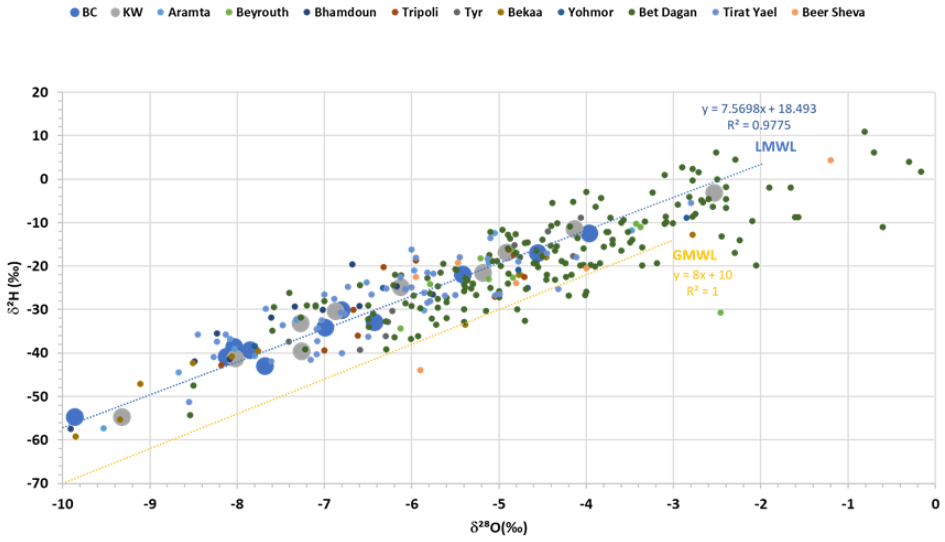


**Figure 20** Relation between δD and $\delta^{18}O$ for precipitation in BC and KW and other sites in Lebanon and neighbouring countries (GNIP).

Figure 16 shows the pattern of d-excess values of precipitation we measured in Bchaaleh and Kawkaba during the period of the study. At Bchaaleh, d-excess is slightly higher than in Kawkaba. In both sites, d-excess is progressively lower from winter to the end of the spring end. Our values range from about 16.9 to 25.5 ‰ with an annual mean value of 20.9 ± 2.5 ‰ in agreement with the well-known uniquely high eastern Mediterranean d-excess values (~20‰) relative to the global average (~10‰) (see Bershaw, 2018; Gat & Carmi, 1970). In both sites, the seasonal variation of the d-excess is related to the evaporation taking place over the Mediterranean Sea (Saad et al., 2000; Aouad et al., 2004; Koeniger & Margane, 2008).

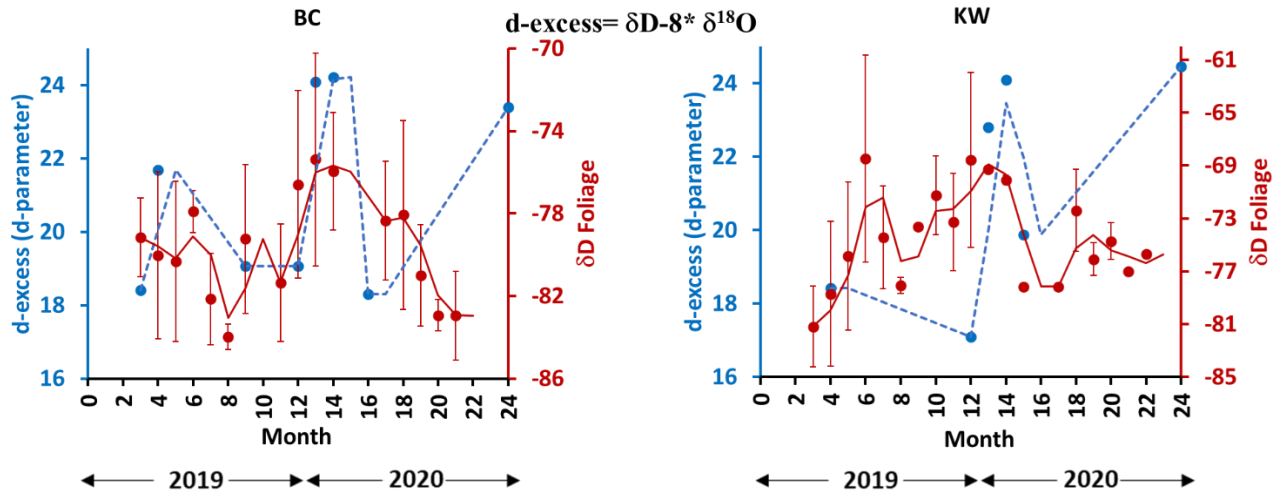


**Figure 21** δD of foliage and d-excess of rainwater in Bchaaleh and Kawkaba.

## V. Conclusion

In Lebanon, the monumental olive trees plant tissues, litter and soil different isotopic composition are studied at two different altitudes in Bchaaleh and Kawkaba. $\delta^{13}C$ in both sites showed a correlation between foliage and stems, unlike $\delta^{15}N$ and $\delta^{34}S$ of foliage and stems that had no correlation. An altitudinal effect is registered for most of the isotopic compositions ($\delta^{13}C$, $\delta^{15}N$, δD and $\delta^{18}O$) of plant tissues, litter and soil. While $\delta^{34}S$ showed a geological effect on the above ground and underground elements. The year 2020 in Bchaaleh and Kawkaba showed more depleted values in the studied isotopic compositions of foliage. While a slight seasonality is shown for the $\delta^{13}C$ and $\delta^{15}N$ of foliage, and a higher seasonality for the foliage δD. In Bchaaleh and Kawkaba, the climatic parameters varied in their significant correlation with the isotopic compositions of the foliage. $pCO_2$ showed a negative correlation with $\delta^{13}C$ of foliage, precipitation showed a negative significant correlation with $\delta^{15}N$, $\delta^{34}S$ showed no significant correlation with any of the climatic parameters, while foliage δD in Bchaaleh showed a significant correlation with all the climatic parameters unlike Kawkaba. These outcomes can mainly indicate that the studied olive trees in Lebanon are tolerant all year long to all the changes in the climatic parameters without being drastically affected. In addition to that we can see that the stems and foliage

$\delta^{13}C$ and $\delta D$ has a good correlation where there is a transport of the isotopic composition from the soil to the foliage through the wood and stems and vice versa. This may confirm that stems can help us understand the wood of monumental olive trees, and indicates that wood cores can hopefully be a good indicator for the past climatic data through isotopic studies. We have also shown in this study that bulk organic material of foliage, stems, litter and soil can be a reliable and cheaper technique to retrieve data on the seasonality and isotopic composition of foliage.

**Acknowledgements:** The authors would like to acknowledge the National Council for Scientific Research of Lebanon (CNRS-L) and Montpellier University for granting a doctoral fellowship to Nagham Tabaja. The authors would also like to thank the Franco-Lebanese Hubert Curien Partnership (PHC-CEDRE) project 44559PL for the funding provided. The authors would also like to thank ISEM at Montpellier University and PRASE at the Lebanese University led by Dr Fouad Haj Hassan for their support of the laboratory work. We also acknowledge Mr R. Geagea, Bchaaleh mayor, and Ms. Mira, Kawkaba mayor deputy, for the support kindly provided during this study.

## Supplementary Information

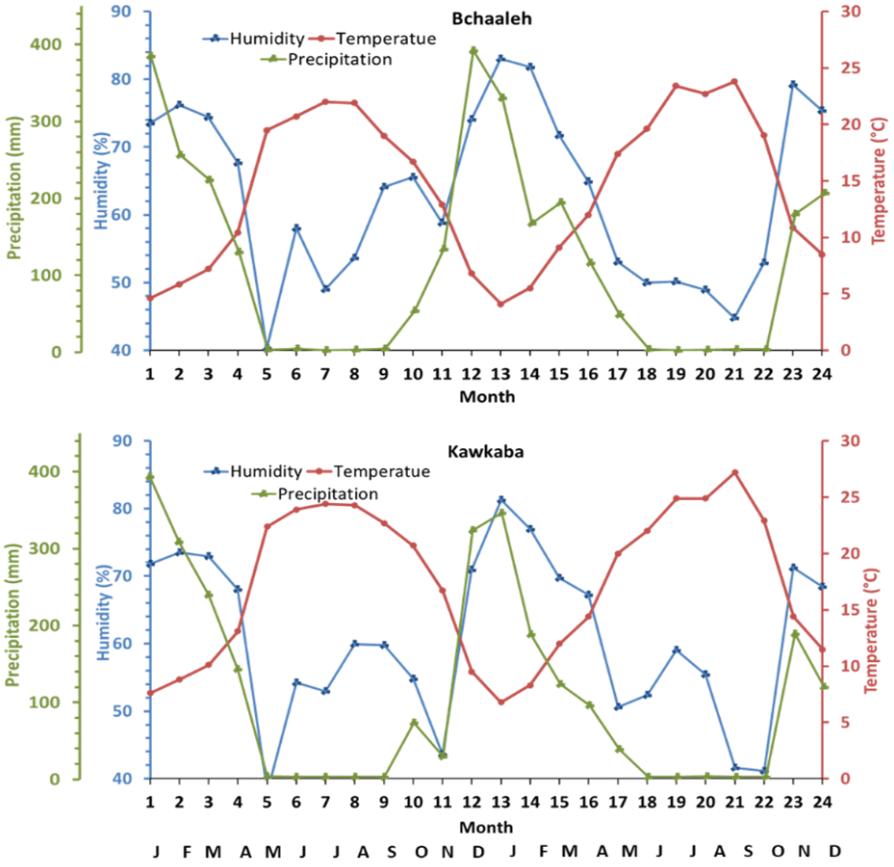


**Figure SI 1** Climatic data of Precipitation, Temperature and Humidity collected from the meteostations installed by LARI for 2018 and 2020 in Bchaaleh and Kawkaba.

**Table SI 1** Monthly $\delta^{13}C$, $\delta^{15}N$, $\delta^{34}S$,$\delta D$ and $\delta^{18}O$ of foliage, stems, litter and different soil depths in Bchaaleh and Kawkaba over the years of 2019 and 2020.

## References


A. Hobbie, E., & Werner, R. A. (2004). Intramolecular, compound-specific, and bulk carbon isotope patterns in C3 and C4 plants: A review and synthesis. *New Phytologist*, *161*(2), 371–385.

ALLEN, S., & Raven, J. A. (1987). Intracellular pH regulation in Ricinus communis grown with ammonium or nitrate as N source: The role of long distance transport. *Journal of Experimental Botany*, *38*(4), 580–596.

Allison, G. B., Barnes, C. J., & Hughes, M. W. (1983). The distribution of deuterium and 18O in dry soils 2. Experimental. *Journal of Hydrology*, *64*(1), 377–397. https://doi.org/10.1016/0022-1694(83)90078-1

Amin, A., Zuecco, G., Marchina, C., Engel, M., Penna, D., McDonnell, J. J., & Borga, M. (2021a). *A simple glasshouse experiment to test the isotopic fractionation in olive trees* [Other]. pico. https://doi.org/10.5194/egusphere-egu21-9300

Amin, A., Zuecco, G., Marchina, C., Engel, M., Penna, D., McDonnell, J. J., & Borga, M. (2021b). No evidence of isotopic fractionation in olive trees ( *Olea europaea* ): A stable isotope tracing experiment. *Hydrological Sciences Journal*, *66*(16), 2415–2430. https://doi.org/10.1080/02626667.2021.1987440

Amundson, R., Austin, A. T., Schuur, E. a. G., Yoo, K., Matzek, V., Kendall, C., Uebersax, A., Brenner, D., & Baisden, W. T. (2003). Global patterns of the isotopic composition of soil and plant nitrogen. *Global Biogeochemical Cycles*, *17*(1). https://doi.org/10.1029/2002GB001903

Aouad, A., Travi, Y., Blavoux, B., Job, J.-O., & Najem, W. (2004). Etude isotopique de la pluie et de la neige sur le Mont Liban: Premiers résultats / Isotope study of snow and rain on Mount Lebanon: preliminary results. *Hydrological Sciences Journal*, *49*(3), 6. https://doi.org/10.1623/hysj.49.3.429.54341

Aranibar, J. N., Otter, L., Macko, S. A., Feral, C. J. W., Epstein, H. E., Dowty, P. R., Eckardt, F., Shugart, H. H., & Swap, R. J. (2004). Nitrogen cycling in the soil–plant system along a precipitation gradient in the Kalahari sands. *Global Change Biology*, *10*(3), 359–373. https://doi.org/10.1111/j.1365-2486.2003.00698.x

Araus, J., Cabrera-Bosquet, L., Serret, M., Bort, J., & Nieto-Taladriz, M. (2013). Comparative performance of δ13C, δ18O and δ15N for phenotyping durum wheat adaptation to a dryland environment. *Functional Plant Biology*, *40*, 595–608. https://doi.org/10.1071/fp12254

Araus, J. L., Villegas, D., Aparicio, N., del Moral, L. F. G., El Hani, S., Rharrabti, Y., Ferrio, J. P., & Royo, C. (2003). Environmental Factors Determining Carbon Isotope Discrimination and

Yield in Durum Wheat under Mediterranean Conditions. *Crop Science*, *43*(1), 170–180. https://doi.org/10.2135/cropsci2003.1700

Asada, T., Warner, B., & Aravena, R. (2005). Effects of the early stage of decomposition on change in carbon and nitrogen isotopes in *Sphagnum* litter. *Journal of Plant Interactions*, *1*(4), 229–237. https://doi.org/10.1080/17429140601056766

Badeck, F.-W., Tcherkez, G., Nogués, S., Piel, C., & Ghashghaie, J. (2005). Post-photosynthetic fractionation of stable carbon isotopes between plant organs—A widespread phenomenon. *Rapid Communications in Mass Spectrometry*, *19*(11), 1381–1391. https://doi.org/10.1002/rcm.1912

Barbaro, G. D., & González Basso, V. (2022). Arbuscular vesicular mycorrhizae in olive tree (Olea europaea L.). *Journal of Applied Biotechnology & Bioengineering*, *9*(4), 98–99. https://doi.org/10.15406/jabb.2022.09.00293

Barbeta, A., Jones, S. P., Clavé, L., Wingate, L., Gimeno, T. E., Fréjaville, B., Wohl, S., & Ogée, J. (2019). *Unexplained hydrogen isotope offsets complicate the identificationand quantification of tree water sources in a riparian forest* [Preprint]. Ecohydrology/Theory development. https://doi.org/10.5194/hess-2018-631

Barbour, M. M. (2007). *Review: Stable oxygen isotope composition of plant tissue: a review*.

Barbour, M. M., & Farquhar, G. D. (2000). Relative humidity- and ABA-induced variation in carbon and oxygen isotope ratios of cotton leaves. *Plant, Cell & Environment*, *23*(5), 473–485. https://doi.org/10.1046/j.1365-3040.2000.00575.x

Baumgartner, S., Bauters, M., Barthel, M., Drake, T. W., Ntaboba, L. C., Bazirake, B. M., Six, J., Boeckx, P., & Van Oost, K. (2021). Stable isotope signatures of soil nitrogen on an environmental–geomorphic gradient within the Congo Basin. *SOIL*, *7*(1), 83–94. https://doi.org/10.5194/soil-7-83-2021

Begum, N., Qin, C., Ahanger, M. A., Raza, S., Khan, M. I., Ashraf, M., Ahmed, N., & Zhang, L. (2019). Role of Arbuscular Mycorrhizal Fungi in Plant Growth Regulation: Implications in Abiotic Stress Tolerance. *Frontiers in Plant Science*, *10*. https://www.frontiersin.org/articles/10.3389/fpls.2019.01068

Bershaw, J. (2018). Controls on Deuterium Excess across Asia. *Geosciences*, *8*(7), 257. https://doi.org/10.3390/geosciences8070257

Betson, N. R., Johannisson, C., Löfvenius, M. O., Grip, H., Granström, A., & Högberg, P. (2007). Variation in the δ13C of foliage of Pinus sylvestris L. in relation to climate and additions of nitrogen: Analysis of a 32-year chronology. *Global Change Biology*, *13*(11), 2317–2328. https://doi.org/10.1111/j.1365-2486.2007.01431.x

Beyer, M., Koeniger, P., Gaj, M., Hamutoko, J. T., Wanke, H., & Himmelsbach, T. (2016). A deuterium-based labeling technique for the investigation of rooting depths, water uptake

dynamics and unsaturated zone water transport in semiarid environments. *Journal of Hydrology*, *533*, 627–643. https://doi.org/10.1016/j.jhydrol.2015.12.037

Boström, B., Comstedt, D., & Ekblad, A. (2007). Isotope fractionation and 13C enrichment in soil profiles during the decomposition of soil organic matter. *Oecologia*, *153*(1), 89–98. https://doi.org/10.1007/s00442-007-0700-8

Buchmann, N., Brooks, J. R., Rapp, K. D., & Ehleringer, J. R. (1996). *Carbon isotope composition of C4 grasses is influenced by light and water supply—BUCHMANN - 1996—Plant, Cell & Environment—Wiley Online Library*. https://onlinelibrary.wiley.com/doi/10.1111/j.1365-3040.1996.tb00331.x

Cabrera-Bosquet, L., Sánchez, C., & Araus, J. L. (2009). How yield relates to ash content, Δ13C and Δ18O in maize grown under different water regimes. *Annals of Botany*, *104*(6), 1207–1216. https://doi.org/10.1093/aob/mcp229

Case, J. W., & Krouse, H. R. (1980). Variations in sulphur content and stable sulphur isotope composition of vegetation near a SO2 source at Fox Creek, Alberta, Canada. *Oecologia*, *44*(2), 248–257. https://doi.org/10.1007/BF00572687

Cernusak, L. A., Barbour, M. M., Arndt, S. K., Cheesman, A. W., English, N. B., Feild, T. S., Helliker, B. R., Holloway-Phillips, M. M., Holtum, J. A. M., Kahmen, A., McInerney, F. A., Munksgaard, N. C., Simonin, K. A., Song, X., Stuart-Williams, H., West, J. B., & Farquhar, G. D. (2016). Stable isotopes in leaf water of terrestrial plants. *Plant, Cell & Environment*, *39*(5), 1087–1102. https://doi.org/10.1111/pce.12703

Cernusak, L. A., & Marshall, J. D. (2001). *(13) (PDF) Responses of foliar 13C, gas exchange and leaf morphology to reduced hydraulic conductivity in Pinus monticola branches*. https://www.researchgate.net/publication/11750716_Responses_of_foliar_13C_gas_exchange_and_leaf_morphology_to_reduced_hydraulic_conductivity_in_Pinus_monticola_branches

Chalak, L., Haouane, H., Essalouh, L., Santoni, S., Besnard, G., & Khadari, B. (2015). Extent of the genetic diversity in Lebanese olive (Olea europaea L.) trees: A mixture of an ancient germplasm with recently introduced varieties. *Genetic Resources and Crop Evolution*, *62*, 621–633. https://doi.org/10.1007/s10722-014-0187-1

Chapin, F. S. (1980). The Mineral Nutrition of Wild Plants. *Annual Review of Ecology and Systematics*, *11*, 233–260.

Collins, J. A., Schefuß, E., Mulitza, S., Prange, M., Werner, M., Tharammal, T., Paul, A., & Wefer, G. (2013). Estimating the hydrogen isotopic composition of past precipitation using leaf-waxes from western Africa. *Quaternary Science Reviews*, *65*, 88–101. https://doi.org/10.1016/j.quascirev.2013.01.007

Comstock, J. P., & Ehleringer, J. R. (1992). Correlating genetic variation in carbon isotopic composition with complex climatic gradients. *Proceedings of the National Academy of Sciences*, *89*(16), 7747–7751.

Condon, A. G. (2004). Breeding for high water-use efficiency. *Journal of Experimental Botany*, *55*(407), 2447–2460. https://doi.org/10.1093/jxb/erh277

Cooper, L. W., Denir, M. J., & Keeley, J. E. (1991). *The relationship between stable oxygen and hydrogen isotope ratios of water in astomatal plants*. *3*.

Cormier, M.-A., Werner, R. A., Sauer, P. E., Gröcke, D. R., Leuenberger, M. C., Wieloch, T., Schleucher, J., & Kahmen, A. (2018). 2H-fractionations during the biosynthesis of carbohydrates and lipids imprint a metabolic signal on the δ2H values of plant organic compounds. *The New Phytologist*, *218*(2), 479–491.

Craig, H. (1953). The geochemistry of the stable carbon isotopes. *Geochimica et Cosmochimica Acta*, *3*(2–3), 53–92. https://doi.org/10.1016/0016-7037(53)90001-5

Craig, H. (1961). Isotopic variations in meteoric waters. *Science*, *133*(3465), 1702–1703.

Craine, J. M., Brookshire, E. N. J., Cramer, M. D., Hasselquist, N. J., Koba, K., Marin-Spiotta, E., & Wang, L. (2015). Ecological interpretations of nitrogen isotope ratios of terrestrial plants and soils. *Plant and Soil*, *396*(1–2), 1–26. https://doi.org/10.1007/s11104-015-2542-1

Damesin, C., & Lelarge, C. (2003). Carbon isotope composition of current-year shoots from Fagus sylvatica in relation to growth, respiration and use of reserves. *Plant, Cell & Environment*, *26*(2), 207–219. https://doi.org/10.1046/j.1365-3040.2003.00951.x

Dansgaard, W. (1964). Stable isotopes in precipitation. *Tellus*, *16*(4), 436–468. https://doi.org/10.1111/j.2153-3490.1964.tb00181.x

Dawson, T. E., & Ehleringer, J. R. (1993). Isotopic enrichment of water in the "woody" tissues of plants: Implications for plant water source, water uptake, and other studies which use the stable isotopic composition of cellulose. *Geochimica et Cosmochimica Acta*, *57*(14), 3487–3492. https://doi.org/10.1016/0016-7037(93)90554-A

Dawson, T. E., Mambelli, S., Plamboeck, A. H., Templer, P. H., & Tu, K. P. (2002). Stable Isotopes in Plant Ecology. *Annual Review of Ecology and Systematics*, *33*(1), 507–559. https://doi.org/10.1146/annurev.ecolsys.33.020602.095451

De Kok, L. J. (1990). SULFUR METABOL18M IN PLANTS EXPOSED TO ATMOSPHERIC SULFUR. *Higher Plonts*, 111.

Driscoll, A. W., Kannenberg, S. A., & Ehleringer, J. R. (2021). Long-term nitrogen isotope dynamics in Encelia farinosa reflect plant demographics and climate. *New Phytologist*, *232*(3), 1226–1237. https://doi.org/10.1111/nph.17668

Ehleringer, J. R., Buchmann, N., & Flanagan, L. B. (2000). Carbon Isotope Ratios in Belowground Carbon Cycle Processes. *Ecological Applications*, *10*(2), 412–422. https://doi.org/10.1890/1051-0761(2000)010[0412:CIRIBC]2.0.CO;2

Ekblad, A., Wallander, H., Carlsson, R., & Huss-Danell, K. (1995). Fungal biomass in roots and extramatrical mycelium in relation to macronutrients and plant biomass of ectomycorrhizal

Pinus sylvestris and Alnus incana. *New Phytologist*, *131*(4), 443–451. https://doi.org/10.1111/j.1469-8137.1995.tb03081.x

Emmett, B. A., Kjønaas, O. J., Gundersen, P., Koopmans, C., Tietema, A., & Sleep, D. (1998). Natural abundance of 15N in forests across a nitrogen deposition gradient. *Forest Ecology and Management*, *101*(1–3), 9–18.

Farquhar, G. D., Ehleringer, J. R., & Hubick, K. T. (1989). Carbon Isotope Discrimination and Photosynthesis. *Annual Review of Plant Physiology and Plant Molecular Biology*, *40*(1), 503–537. https://doi.org/10.1146/annurev.pp.40.060189.002443

Farquhar, G. D., O'Leary, M. H., & Berry, J. A. (1982). On the relationship between carbon isotope discrimination and the intercellular carbon dioxide concentration in leaves. *Functional Plant Biology*, *9*(2), 121–137.

Fitter, A. H., & Hay, R. K. M. (2002). Toxicity. *Environmental Physiology of Plants. 3rd Ed. Academic Press. San Diego*, 241–284.

Fonti, P., & Jansen, S. (2012). Xylem plasticity in response to climate. *The New Phytologist*, *195*(4), 734–736.

Francey, R. J., Allison, C. E., Etheridge, D. M., Trudinger, C. M., Enting, I. G., Leuenberger, M., Langenfelds, R. L., Michel, E., & Steele, L. P. (1999). A 1000-year high precision record of δ13C in atmospheric CO2. *Tellus B*, *51*(2), 170–193. https://doi.org/10.1034/j.1600-0889.1999.t01-1-00005.x

Gagen, M., Finsinger, W., Wagner-Cremer, F., Mccarroll, D., Loader, N. J., Robertson, I., Jalkanen, R., Young, G., & Kirchhefer, A. (2011). Evidence of changing intrinsic water-use efficiency under rising atmospheric CO2 concentrations in Boreal Fennoscandia from subfossil leaves and tree ring δ13C ratios. *Global Change Biology*, *17*(2), 1064–1072. https://doi.org/10.1111/j.1365-2486.2010.02273.x

Gat, J., & Carmi, I. (1970). Evolution of the Isotopic Composition of Atmospheric Waters in the Mediterranean Sea Area. *Journal of Geophysical Research*, *75*, 3039–3048. https://doi.org/10.1029/JC075i015p03039

Gat, J., Mook, W. G., & Meijer, H.A.J. (2001). Willem G. Mook et Harro A .J.Meijer Centre Isotope Research, Groningen, The Netherlands. *2001*, *2*, 73.

Gessler, A., Ferrio, J. P., Hommel, R., Treydte, K., Werner, R. A., & Monson, R. K. (2014). Stable isotopes in tree rings: Towards a mechanistic understanding of isotope fractionation and mixing processes from the leaves to the wood. *Tree Physiology*, *34*(8), 796–818. https://doi.org/10.1093/treephys/tpu040

Ghaleb Faour. (2004). *FOREST FIRE FIGHTING IN LEBANON USING REMOTE SENSING AND GIS*. https://doi.org/10.13140/RG.2.2.28371.78884

Gielen, B., Jach, M. E., & Ceulemans, R. (2000). Effects of Season, Needle Age, and Elevated Atmospheric CO2 on Chlorophyll Fluorescence Parameters and Needle Nitrogen

Concentration in Scots Pine (Pinus sylvestris). *Photosynthetica*, *38*(1), 13–21. https://doi.org/10.1023/A:1026727404895

Gigolashvili, T., & Kopriva, S. (2014). Transporters in plant sulfur metabolism. *Frontiers in Plant Science*, *5*. https://www.frontiersin.org/articles/10.3389/fpls.2014.00442

Gleixner, G. (2005). Stable isotope composition of soil organic matter. In *Stable isotopes and biosphere-atmosphere interactions-Processes and biological* (pp. 29–46). Elsevier.

Gleixner, G., Bol, R., & Balesdent, J. (1999). Molecular insight into soil carbon turnover. *Rapid Communications in Mass Spectrometry*, *13*(13), 1278–1283. https://doi.org/10.1002/(SICI)1097-0231(19990715)13:13<1278::AID-RCM649>3.0.CO;2-N

Gleixner, G., Poirier, N., Bol, R., & Balesdent, J. (2002). Molecular dynamics of organic matter in a cultivated soil. *Organic Geochemistry*, *33*(3), 357–366. https://doi.org/10.1016/S0146-6380(01)00166-8

Goldreich, Y. (2003). The History of Climate and Meteorological Observations and Research in Israel. In *The Climate of Israel* (pp. 3–11). Springer.

Greer, D. H., Laing, W. A., & Campbell, B. D. (1995). Photosynthetic responses of thirteen pasture species to elevated CO2 and temperature. *Functional Plant Biology*, *22*(5), 713–722.

Han, J.-J., Duan, X., Zhao, Y.-Y., & Li, M. (2019). Characteristics of Stable Hydrogen and Oxygen Isotopes of Soil Moisture under Different Land Use in Dry Hot Valley of Yuanmou. *Open Chemistry*, *17*(1), 105–115. https://doi.org/10.1515/chem-2019-0014

Hartman, G., & Danin, A. (2010). Isotopic values of plants in relation to water availability in the Eastern Mediterranean region. *Oecologia*, *162*(4), 837–852. https://doi.org/10.1007/s00442-009-1514-7

Hartsough, P., Poulson, S. R., Biondi, F., & Estrada, I. G. (2008). Stable Isotope Characterization of the Ecohydrological Cycle at a Tropical Treeline Site. *Arctic, Antarctic, and Alpine Research*, *40*(2), 343–354. https://doi.org/10.1657/1523-0430(06-117)[HARTSOUGH]2.0.CO;2

Heaton, T. H. E. (1987). The 15N/14N ratios of plants in South Africa and Namibia: Relationship to climate and coastal/saline environments. *Oecologia*, *74*(2), 236–246. https://doi.org/10.1007/BF00379365

Heineman, K. D., Turner, B. L., & Dalling, J. W. (2016). Variation in wood nutrients along a tropical soil fertility gradient. *New Phytologist*, *211*(2), 440–454. https://doi.org/10.1111/nph.13904

Hervé-Fernández, P., Oyarzún, C., Brumbt, C., Huygens, D., Bodé, S., Verhoest, N. E. C., & Boeckx, P. (2016). Assessing the “two water worlds” hypothesis and water sources for native and exotic evergreen species in south-central Chile: Ecohydrological Assesment. *Hydrological Processes*. https://doi.org/10.1002/hyp.10984

Hobbie, E. A., & Colpaert, J. V. (2003). Nitrogen Availability and Colonization by Mycorrhizal Fungi Correlate with Nitrogen Isotope Patterns in Plants. *The New Phytologist*, *157*(1), 115–126.

Hobbie, J. E., & Hobbie, E. A. (2006). 15N IN SYMBIOTIC FUNGI AND PLANTS ESTIMATES NITROGEN AND CARBON FLUX RATES IN ARCTIC TUNDRA. *Ecology*, *87*(4), 816.

Högberg, P. (1997). Tansley review no. 95 15N natural abundance in soil–plant systems. *The New Phytologist*, *137*(2), 179–203.

Högberg, P., Ekblad, A., Nordgren, A., Plamboeck, A. H., Ohlsson, A., Bhupinderpal-Singh, S., & Högberg, M. (2005). *Factors determining the 13C abundance of soil-respired CO2 in boreal forests*.

Howarth, R. W., & Teal, J. M. (1979). Sulfate reduction in a New England salt marsh1. *Limnology and Oceanography*, *24*(6), 999–1013. https://doi.org/10.4319/lo.1979.24.6.0999

*Improved online hydrogen isotope analysis of halite aqueous inclusions—Fourel—2019—Journal of Mass Spectrometry—Wiley Online Library*. (n.d.). Retrieved March 22, 2022, from https://analyticalsciencejournals.onlinelibrary.wiley.com/doi/full/10.1002/jms.4323?casa_token=Phj2vZWKJvMAAAAA%3ARK8X6LHmOYalaZx3lFczODfNNA9XSuFBGlGSyEqRrEZL9_UnGKYmNyZspw9qX4uIxB4lDhw2vH40rkA

Jach, M. E., & Ceulemans, R. (2000). Effects of season, needle age and elevated atmospheric CO2 on photosynthesis in Scots pine (Pinus sylvestris). *Tree Physiology*, *20*(3), 145–157. https://doi.org/10.1093/treephys/20.3.145

Kaplan, I. R., & Rittenberg, S. C. (1964). Microbiological Fractionation of Sulphur Isotopes. *Journal of General Microbiology*, *34*(2), 195–212. https://doi.org/10.1099/00221287-34-2-195

Kawamura, H., Matsuoka, N., Momoshima, N., Koike, M., & Takashima, Y. (2006). Isotopic Evidence in Tree Rings for Historical Changes in Atmospheric Sulfur Sources. *Environmental Science & Technology*, *40*(18), 5750–5754. https://doi.org/10.1021/es060321w

Khatri, P. K., Larcher, R., Camin, F., Ziller, L., Tonon, A., Nardin, T., & Bontempo, L. (2021). Stable Isotope Ratios of Herbs and Spices Commonly Used as Herbal Infusions in the Italian Market. *ACS Omega*, *6*(18), 11925–11934. https://doi.org/10.1021/acsomega.1c00274

Klotzbücher, T., Kalbitz, K., Cerli, C., Hernes, P. J., & Kaiser, K. (2016). Gone or just out of sight? The apparent disappearance of aromatic litter components in soils. *SOIL*, *2*(3), 325–335. https://doi.org/10.5194/soil-2-325-2016

Koeniger, P., & Margane, A. (n.d.). *Stable Isotope Investigations in the Jeita Spring Catchment*. 56.

Krouse, H. R. (1977). Sulphur isotope abundance elucidate uptake of atmospheric sulphur emissions by vegetation. *Nature*, *265*(5589), 45–46. https://doi.org/10.1038/265045a0

Krouse, H. R. (1991). Stable isotopes: Natural and anthropogenic sulfur in the environment. *SCOPE*.

Leavitt, S. W., & Long, A. (1983). An atmospheric $^{13}C/^{12}C$ reconstruction generated through removal of climate effects from tree-ring $^{13}C/^{12}C$ measurements. *Tellus B*, *35B*(2), 92–102. https://doi.org/10.1111/j.1600-0889.1983.tb00013.x

Li, Y., Shi, F., Li, X., Wu, H., Zhao, S., Wu, X., & Huang, Y. (2022). *Divergent roles of deep soil water uptake in seasonal tree growth under natural drought events in North China | Elsevier Enhanced Reader*. https://doi.org/10.1016/j.agrformet.2022.109102

Liu, J., Wu, H., Zhang, H., Peng, G., Jiang, C., Zhao, Y., & Hu, J. (2021). *Controls of seasonality and altitude on generation of leaf water isotopes* [Preprint]. Ecohydrology/Instruments and observation techniques. https://doi.org/10.5194/hess-2021-289

Liu, X.-Z., & Wang, G. (2010). Measurements of nitrogen isotope composition of plants and surface soils along the altitudinal transect of the eastern slope of Mount Gongga in southwest China. *Rapid Communications in Mass Spectrometry : RCM*, *24*, 3063–3071. https://doi.org/10.1002/rcm.4735

Llusia`, J., & Pen uelas, J. (2000). Seasonal patterns of terpene content and emission from seven Mediterranean woody species in field conditions. *American Journal of Botany*, *87*(1), 133–140. https://doi.org/10.2307/2656691

Lorenz, M., Derrien, D., Zeller, B., Udelhoven, T., Werner, W., & Thiele-Bruhn, S. (2020). The linkage of 13C and 15N soil depth gradients with C:N and O:C stoichiometry reveals tree species effects on organic matter turnover in soil. *Biogeochemistry*, *151*(2–3), 203–220. https://doi.org/10.1007/s10533-020-00721-3

Lovett, G. M., Weathers, K. C., Arthur, M. A., & Schultz, J. C. (2004). Nitrogen cycling in a northern hardwood forest: Do species matter? *Biogeochemistry*, *67*(3), 289–308. https://doi.org/10.1023/B:BIOG.0000015786.65466.f5

Marian, F., Sandmann, D., Krashevska, V., Maraun, M., & Scheu, S. (2017). Leaf and root litter decomposition is discontinued at high altitude tropical montane rainforests contributing to carbon sequestration. *Ecology and Evolution*, *7*(16), 6432–6443. https://doi.org/10.1002/ece3.3189

Marshall, J. D., Brooks, J. R., & Lajtha, K. (2007). Sources of Variation in the Stable Isotopic Composition of Plants. In R. Michener & K. Lajtha (Eds.), *Stable Isotopes in Ecology and Environmental Science* (pp. 22–60). Blackwell Publishing Ltd. https://doi.org/10.1002/9780470691854.ch2

Matteo, G., Angelis, P., Brugnoli, E., Cherubini, P., & Scarascia-Mugnozza, G. (2010). Tree-ring Δ13C reveals the impact of past forest management on water-use efficiency in a Mediterranean oak coppice in Tuscany (Italy). *Annals of Forest Science*, *67*(5), 510–510. https://doi.org/10.1051/forest/2010012

Mitrakos, K. (1980). *A theory for Mediterranean plant life*.

Munksgaard, N. C., Wurster, C. M., Bass, A., & Bird, M. I. (2012). Extreme short-term stable isotope variability revealed by continuous rainwater analysis. *Hydrological Processes*, *26*(23), 3630–3634. https://doi.org/10.1002/hyp.9505

Munksgaard, N. C., Zwart, C., Kurita, N., Bass, A., Nott, J., & Bird, M. I. (2015). Stable Isotope Anatomy of Tropical Cyclone Ita, North-Eastern Australia, April 2014. *PLOS ONE*, *10*(3), e0119728. https://doi.org/10.1371/journal.pone.0119728

Neff, J. C., Chapin III, F. S., & Vitousek, P. M. (2003). Breaks in the cycle: Dissolved organic nitrogen in terrestrial ecosystems. *Frontiers in Ecology and the Environment*, *1*(4), 205–211. https://doi.org/10.1890/1540-9295(2003)001[0205:BITCDO]2.0.CO;2

Niedermeyer, E. M., Forrest, M., Beckmann, B., Sessions, A. L., Mulch, A., & Schefuß, E. (2016). The stable hydrogen isotopic composition of sedimentary plant waxes as quantitative proxy for rainfall in the West African Sahel. *Geochimica et Cosmochimica Acta*, *184*, 55–70. https://doi.org/10.1016/j.gca.2016.03.034

Novák, M., Buzek, F., Harrison, A. F., Přechová, E., Jačková, I., & Fottová, D. (2003). Similarity between C, N and S stable isotope profiles in European spruce forest soils: Implications for the use of δ34S as a tracer. *Applied Geochemistry*, *18*(5), 765.

Oakes, J., & Connolly, R. (2004). Causes of sulfur isotope variability in the seagrass, Zostera capricorni. *Journal of Experimental Marine Biology and Ecology*, *302*. https://doi.org/10.1016/j.jembe.2003.10.011

Ogaya, R., & Peñuelas, J. (2008). Changes in leaf δ13C and δ15N for three Mediterranean tree species in relation to soil water availability. *Acta Oecologica*, *34*(3), 331–338. https://doi.org/10.1016/j.actao.2008.06.005

Pardo, L. H., Semaoune, P., Schaberg, P. G., Eagar, C., & Sebilo, M. (2013). Patterns in δ15N in roots, stems, and leaves of sugar maple and American beech seedlings, saplings, and mature trees. *Biogeochemistry*, *112*(1–3), 275–291. https://doi.org/10.1007/s10533-012-9724-1

Pardo, L. H., Templer, P. H., Goodale, C. L., Duke, S., Groffman, P. M., Adams, M. B., Boeckx, P., Boggs, J., Campbell, J., Colman, B., Compton, J., Emmett, B., Gundersen, P., Kjønaas, J., Lovett, G., Mack, M., Magill, A., Mbila, M., Mitchell, M. J., … Wessel, W. (2006). Regional Assessment of N Saturation using Foliar and Root $$\varvec {\delta}^{\bf 15}{\bf N}$$. *Biogeochemistry*, *80*(2), 143–171. https://doi.org/10.1007/s10533-006-9015-9

Park, R., & Epstein, S. (1960). CARBON ISOTOPE FRACTIONATION DURING PHOTOSYNTHESIS. *Geochim. et Cosmochim. Acta, Vol: 21*. https://doi.org/10.1016/S0016-7037(60)80006-3

Peñuelas, J., Filella, I., Lloret, F., Piñol, J., & Siscart, D. (2000). Effects of a severe drought on water and nitrogen use by Quercus ilex and Phyllyrea latifolia. *Biologia Plantarum*, *43*(1), 47–53.

Pereira, J. S., & Chaves, M. M. (1995). Plant responses to drought under climate change in Mediterranean-type ecosystems. In *Global change and Mediterranean-type ecosystems* (pp. 140–160). Springer.

Peuke, A. D., Gessler, A., & Rennenberg, H. (2006). The effect of drought on C and N stable isotopes in different fractions of leaves, stems and roots of sensitive and tolerant beech ecotypes.

*Plant, Cell and Environment*, *29*(5), 823–835. https://doi.org/10.1111/j.1365-3040.2005.01452.x

Pingyuan, W., Liu, W., & Li, J.-T. (2010). Water use strategy of Ficus tinctoria in tropical rainforest region of Xishuangbanna, South-western China. *Chinese Journal of Applied Ecology*, *21*, 836–842.

Rennenberg, H., Brunold, C., Rijksuniversiteit Groningen, & Rijksuniversiteit (Eds.). (1990). *Sulfur nutrition and sulfur assimilation in higher plants: Fundamental, environmental and agricultural aspects ; proceedings of a workshop organized by the Department of Plant Physiology, University of Groningen ... Haren, 28 - 31 March 1989*. SPB Adacemic Publ.

Rossi, L., Sebastiani, L., Tognetti, R., d'Andria, R., Morelli, G., & Cherubini, P. (2013). Tree-ring wood anatomy and stable isotopes show structural and functional adjustments in olive trees under different water availability. *Plant and Soil*, *372*(1–2), 567–579. https://doi.org/10.1007/s11104-013-1759-0

Royer, D. L. (2001). Stomatal density and stomatal index as indicators of paleoatmospheric CO2 concentration. *Review of Palaeobotany and Palynology*, *114*(1–2), 1–28. https://doi.org/10.1016/S0034-6667(00)00074-9

Saad, Z., Slim, K., Ghaddar, A., Nasreddine, M., & Kattan, Z. (2000). Chemical composition of rain water in Lebanon. *Journal Européen d'hydrologie*, *31*(2), 223–238. https://doi.org/10.1051/water/20003102223

Saliendra, N., Meinzer, F., Perry, M., & Thom, M. (1996). Associations between partitioning of carboxylase activity and bundle sheath leakiness to CO2, carbon isotope discrimination, photosynthesis, and growth in sugarcane. *Journal of Experimental Botany*, *47*. https://doi.org/10.1093/jxb/47.7.907

Sanchez-Bragado, R., Serret, M. D., Marimon, R. M., Bort, J., & Araus, J. L. (2019). The Hydrogen Isotope Composition $\delta^{2}$ H Reflects Plant Performance. *Plant Physiology*, *180*(2), 793–812. https://doi.org/10.1104/pp.19.00238

Schmidt, H.-L., Werner, R. A., & Eisenreich, W. (2003). Systematics of 2H patterns in natural compounds and its importance for the elucidation of biosynthetic pathways. *Phytochemistry Reviews*, *2*(1–2), 61–85. https://doi.org/10.1023/B:PHYT.0000004185.92648.ae

Scholl, M. A., Giambelluca, T. W., Gingerich, S. B., Nullet, M. A., & Loope, L. L. (2007). Cloud water in windward and leeward mountain forests: The stable isotope signature of orographic cloud water: ISOTOPE SIGNATURE OF CLOUD WATER. *Water Resources Research*, *43*(12). https://doi.org/10.1029/2007WR006011

Schubert, B. A., & Jahren, A. H. (2011). Fertilization trajectory of the root crop Raphanus sativus across atmospheric pCO2 estimates of the next 300 years. *Agriculture, Ecosystems & Environment*, *140*(1–2), 174–181. https://doi.org/10.1016/j.agee.2010.11.024

Schubert, B. A., & Jahren, A. H. (2012). The effect of atmospheric CO2 concentration on carbon isotope fractionation in C3 land plants. *Geochimica et Cosmochimica Acta*, *96*, 29–43. https://doi.org/10.1016/j.gca.2012.08.003

Sheil, D. (2018). Forests, atmospheric water and an uncertain future: The new biology of the global water cycle. *Forest Ecosystems*, *5*(1), 19. https://doi.org/10.1186/s40663-018-0138-y

Silva, L. C. R., & Horwath, W. R. (2013). Explaining Global Increases in Water Use Efficiency: Why Have We Overestimated Responses to Rising Atmospheric CO2 in Natural Forest Ecosystems? *PLoS ONE*, *8*(1), e53089. https://doi.org/10.1371/journal.pone.0053089

Singh, B. P. (2017). Original isotopic composition of water in precipitation by different methods. *Applied Water Science*, *7*(6), 3385–3390. https://doi.org/10.1007/s13201-016-0500-6

Swap, R. J., Aranibar, J. N., Dowty, P. R., Gilhooly III, W. P., & Macko, S. A. (2004). Natural abundance of 13C and 15N in C3 and C4 vegetation of southern Africa: Patterns and implications. *Global Change Biology*, *10*(3), 350–358. https://doi.org/10.1111/j.1365-2486.2003.00702.x

Tabaja, N., Amouroux, D., Chalak, L., Fourel, F., Tessier, E., Jomaa, I., El Riachy, M., & Bentaleb, I. (2022). Seasonal variation of mercury concentration of ancient olive groves of Lebanon. *EGUsphere*, *2022*, 1–25. https://doi.org/10.5194/egusphere-2022-174

Tang, Z., Xu, W., Zhou, G., Bai, Y., Li, J., Tang, X., Chen, D., Liu, Q., Ma, W., Xiong, G., He, N., Guo, Y., Guo, Q., Zhu, J., Han, W., Hu, H., Fang, J., & Xie, Z. (2017). *Patterns of plant carbon, nitrogen, and phosphorus concentration in relation to productivity in China's terrestrial ecosystems*. https://doi.org/10.1073/pnas.1700295114

Tatsumi, C., Hyodo, F., Taniguchi, T., Shi, W., Koba, K., Fukushima, K., Du, S., Yamanaka, N., Templer, P., & Tateno, R. (2021). Arbuscular Mycorrhizal Community in Roots and Nitrogen Uptake Patterns of Understory Trees Beneath Ectomycorrhizal and Non-ectomycorrhizal Overstory Trees. *Frontiers in Plant Science*, *11*. https://www.frontiersin.org/articles/10.3389/fpls.2020.583585

Tcherkez, G., & Tea, I. (2013). 32S/34S isotope fractionation in plant sulphur metabolism. *New Phytologist*, *200*(1), 44–53. https://doi.org/10.1111/nph.12314

Templer, P. H., Arthur, M. A., Lovett, G. M., & Weathers, K. C. (2007). Plant and soil natural abundance δ 15N: Indicators of relative rates of nitrogen cycling in temperate forest ecosystems. *Oecologia*, *153*(2), 399–406. https://doi.org/10.1007/s00442-007-0746-7

*The water cycle (article) | Ecology | Khan Academy*. (n.d.). Retrieved March 21, 2022, from https://www.khanacademy.org/science/biology/ecology/biogeochemical-cycles/a/the-water-cycle

Tognetti, R., d'Andria, R., Morelli, G., & Alvino, A. (2005). The effect of deficit irrigation on seasonal variations of plant water use in Olea europaea L. *Plant and Soil*, *273*(1–2), 139–155. https://doi.org/10.1007/s11104-004-7244-z

Tognetti, R., d'Andria, R., Morelli, G., Calandrelli, D., & Fragnito, F. (2004). Irrigation effects on daily and seasonal variations of trunk sap flow and leaf water relations in olive trees. *Plant and Soil*, *263*(1), 249–264. https://doi.org/10.1023/B:PLSO.0000047738.96931.91

Tognetti, R., Giovannelli, A., Lavini, A., Morelli, G., Fragnito, F., & d'Andria, R. (2009). Assessing environmental controls over conductances through the soil–plant–atmosphere continuum in an experimental olive tree plantation of southern Italy. *Agricultural and Forest Meteorology*, *149*(8), 1229–1243. https://doi.org/10.1016/j.agrformet.2009.02.008

Trumbore, S. (2009). Radiocarbon and soil carbon dynamics. *Annual Review of Earth and Planetary Sciences*, *37*(1), 47–66.

Trust, B. A., & Fry, B. (1992). Stable sulphur isotopes in plants: A review. *Plant, Cell and Environment*, *15*(9), 1105–1110. https://doi.org/10.1111/j.1365-3040.1992.tb01661.x

Tu, K., & Dawson, T. (2005). Partitioning ecosystem respiration using stable carbon isotope analyses of CO2. *Flanagan, LB, Ehleringer, JR, and Pataki, DE, Physiological Ecology, Elsevier Academic Press, London, UK*, 125–153.

Wallander, H., Nilsson, L. O., Hagerberg, D., & Rosengren, U. (2003). Direct estimates of C:N ratios of ectomycorrhizal mycelia collected from Norway spruce forest soils. *Soil Biology and Biochemistry*, *35*(7), 997–999. https://doi.org/10.1016/S0038-0717(03)00121-4

Winner, W. E., & Bewley, J. D. (1978). Contrasts between bryophyte and vascular plant synecological responses in an SO2-stressed white spruce association in central Alberta. *Oecologia*, *33*(3), 311–325. https://doi.org/10.1007/BF00348116

Wynn, J. G., Bird, M. I., & Wong, V. N. L. (2005). Rayleigh distillation and the depth profile of 13C/12C ratios of soil organic carbon from soils of disparate texture in Iron Range National Park, Far North Queensland, Australia. *Geochimica et Cosmochimica Acta*, *69*(8), 1961–1973. https://doi.org/10.1016/j.gca.2004.09.003

Yazbeck, E. B., Rizk, G. A., Hassoun, G., El-Khoury, R., & Geagea, L. (2018). *Ecological characterization of ancient olive trees in Lebanon- Bshaaleh area and their age estimation*. *11*(2 Ver. 1), 35–44.

Yoneyama, T., Okada, H., & Ando, S. (2010). Seasonal variations in natural $^{13}$C abundances in $C_3$ and $C_4$ plants collected in Thailand and the Philippines. *Soil Science and Plant Nutrition*, *56*(3), 422–426. https://doi.org/10.1111/j.1747-0765.2010.00477.x

Z. Houlton, B., M. Sigman, D., A. G. Schuur, E., & Hedin, L. (2007). *A climate-driven switch in plant nitrogen acquisition within tropical forest communities*. https://doi.org/10.1073/pnas.0609935104

Zhang, J., He, N., Liu, C., Xu, L., Chen, Z., Li, Y., Wang, R., Yu, G., Sun, W., Xiao, C., & Reich, P. (2019). Variation and evolution of C:N ratio among different organs enable plants to adapt to N-limited environments. *Global Change Biology*, *26*. https://doi.org/10.1111/gcb.14973

Zhang, S., Wen, X., Wang, J., Yu, G., & Sun, X. (2010). The use of stable isotopes to partition evapotranspiration fluxes into evaporation and transpiration. *Acta Ecologica Sinica, 30*(4), 201–209. https://doi.org/10.1016/j.chnaes.2010.06.003

Zhang, Y., Mitchell, M. J., Christ, M., Likens, G. E., & Krouse, H. R. (1998). Stable sulfur isotopic biogeochemistry of the Hubbard Brook Experimental Forest, New Hampshire. *Biogeochemistry*, *41*(3), 259–275. https://doi.org/10.1023/A:1005992430776

Zheng, Y., Hu, Z., Pan, X., Chen, X., Derrien, D., Hu, F., Liu, M., & Hättenschwiler, S. (2021). Carbon and nitrogen transfer from litter to soil is higher in slow than rapid decomposing plant litter: A synthesis of stable isotope studies. *Soil Biology and Biochemistry*, *156*, 108196. https://doi.org/10.1016/j.soilbio.2021.108196

Zhou, Y., Grice, K., Chikaraishi, Y., Stuart-Williams, H., Farquhar, G. D., & Ohkouchi, N. (2011). Temperature effect on leaf water deuterium enrichment and isotopic fractionation during leaf lipid biosynthesis: Results from controlled growth of C3 and C4 land plants. *Phytochemistry*, *72*(2–3), 207.

## Chapter IV: Disentangling the monumental olive tree rings at the Eastern Mediterranean using different techniques of dendrology.


### Abstract

The monumental olive trees had been an important cultural heritage in the Eastern Mediterranean. The identification of annual rings and reconstructing the environmental and climatic changes in olive trees is not an easy task. That is why in this study we used multiple approaches to detect the annual tree rings in two olive groves in Bchaaleh (North Lebanon) and Kawkaba (South Lebanon). Such approaches are dendrochronology, densitometry, X-ray tomography, radiocarbon dating and carbon isotopic composition of tree rings ($\delta^{13}C$). The X-ray tomography and radiocarbon dating proved to be complementary techniques to detect the tree rings and the age of those centennial olive trees. While $\delta^{13}C$ of tree rings shows the difference between the climatic parameters in the past and the present.



**Keywords:** Monumental olive trees, Dendrochronology, Densitometry, X-ray tomography, Radiocarbon dating, $\delta^{13}C$

## I. Introduction

Olive tree (*Olea europaea* L.) is undoubtedly the most iconic species of the Mediterranean basin. It is characterized by remarkable longevity and strong resistance to drought and fires, mainly due to different forms of anatomical and physiological adaptation, so much that it can survive and provide a certain production even in rainfed conditions (Schicchi et al., 2021). On top of that, the olive tree has a significant ecological, economic and cultural value (Carrión et al., 2010; Zohary et al., 2012). The olive tree is exploited at least since the Mesolithic (Kaniewski et al., 2012) and is cultivated for the production of oil at least since the Bronze Age (Caracuta, 2020). The olive tree has accompanied the emergence of Early Mediterranean civilizations and has a wide distribution in all countries neighboring the Mediterranean basin (Besnard et al., 2013). According to Zohary & Hopf, 2000, the olive tree was one of the first fruit plants to be domesticated within the Mediterranean countries, perhaps as early as the 5th millennium BC (Ehrlich et al., 2017). Therefore, the contemporary olive varieties would be the result of an ancient selection process (Guerci, 2005; Chalak et al., 2015) established by Syrian, Lebanese and Palestinian farmers and probably also those from the vast area extending from the Southern Caucasus to the Iranian highlands, starting from the wild olive tree, widespread in that time period to today cultivars rich in oil and without thorns (Castiglioni & Maniscalco, 2008; Besnard et al., 2018).

Numerous monumental olive trees are still standing across the Mediterranean landscape which is characterized with a dry and hot summer and a wet and cold winter, where the trees need to tolerate both environmental conditions (Ehrlich et al., 2017). These trees are known to have large foot and trunk circumference (Schicchi et al., 2021). Many monumental olive trees have been studied in the Mediterranean region for their age and climatic resilience. They are known for their adaptation to extreme conditions, growing in rocky and arid soil, surviving under drought conditions and also strong winds (Yazbeck et al., 2018). They are known for their un-existing pith that rots with time, irregular and not easily detected tree rings. It is possible that new trunks are created around the main base of the tree (Lavee, 1996) and with time a breakage can take place in the bark due to physical pressure. A tissue bridge can be formed with time which forms a "continuous cambium ring (Ehrlich et al., 2017).

Determining the precise age of olive trees is a complicated procedure, especially when it comes to olive trees in the Mediterranean region due to asymmetric cambial growth. The use of olive tree rings for dating is very challenging since the trees do not always form distinct annual growth rings and may produce extra intra-annual density fluctuation during changes in temperature or drought period creating false rings due to their ability of forming wood after being "affected by an induced stress of radial growth" which is a problematic by itself for identifying the annual rings (Cherubini and Lev-Yadun, 2014; Ehrlich et al., 2017). A more advanced study that used isotopic analysis in addition to the X-ray tomography which provides a three-dimensional imaging of a wood core with a non-destruction effect and radiocarbon dating, showed a good outcome in revealing the age of olive tree upon using these three different methods combined. In addition, the results showed that there could exist an intra-annual

fluctuation pattern of $\delta^{13}C$ for tree species in response to environmental stresses (Van den Bulcke et al., 2014; Ehrlich et al., 2021).

Lebanon, a small country at the Eastern Mediterranean shore, is home to several monumental olive trees, testifying to the ancient history of olive growth in this part of the world. These trees are found alone, or in mixture with young trees, growing mostly in calcareous soils, along the coast and up to 1300 m a.s.l. where the temperature could drop for few days below 0°C (Chalak et al., 2015). Some of these monumental olive trees are believed by elderly villagers to be more than 7000 years old. Certain municipalities have recently undertaken actions for the preservation of this patrimony in certain localities. In Lebanon, ancient olive trees have not been studied extensively for their age. Yazbeck et al. (2018) conducted tree's age estimation using the growth rate method approximating the olive tree age to be around 1400 years.

The significance of this study is it being the first study in Lebanon of a set of wood cores taken from the interior of the monumental olive trees from two different sites (North and South) at different altitudes. This allowed the collection of a big data set of the available interior of the olive tree in order to study the age and the possible climatic changes, using dendrochronology, densitometry, X-ray tomography, radiocarbon dating ($^{14}C$) and isotopic analysis ($\delta^{13}C$).

## II. Materials and Methods

### II.1 Study area and sampling procedure

Monumental olive trees were sampled from two ancient olive groves located in Lebanon. The first grove is situated in Bchaaleh (BC), North Lebanon (1300 m a.s.l.), while the second grove is located in the village of Kawkaba (KW), South Lebanon (672 m a.s.l.) (Figure 1a,b,c).

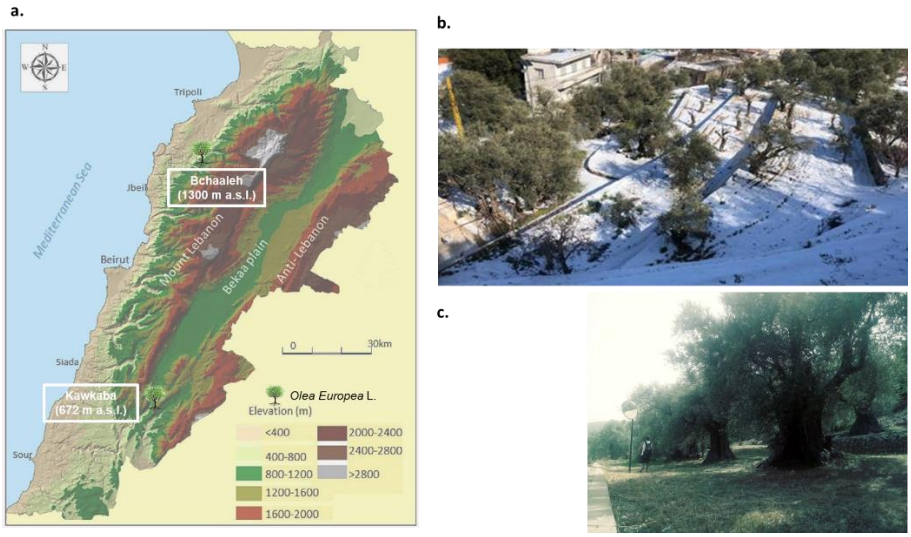


**Figure 22 (a)** Site locations of the two selected focus areas (modified after Shared Water Resources of Lebanon, Nova Science Publishers 2017). (**b)** Bchaaleh site, **(c)** Kawkaba site.

The climatic data, precipitation and temperature from Bchaaleh and Kawkaba were collected from the meteorological stations installed by the Lebanese Agricultural Research Institute (LARI).

In Bchaaleh, precipitation average ranged between 229 and 392 mm/year in winter and between zero and less than 2 mm/year in summer, while the average temperature was between 4 and 8 °C in winter and between 20 and 23 °C in summer (data extracted from LARI climatic data).

In Kawkaba, average precipitation ranged between 215 and 374 mm/year in winter and dropped to almost zero mm in summer, while the average temperature was between 7 and 11 °C in winter and between 21 and 27 °C in summer (data extracted from LARI climatic data).

Olive tree's wood coring was conducted in March-May 2019. A coring strategy was designed using an electric drill (Bosh GSB28VE2LI with a mesh of 22 cm length and 0.7cm width), based on the accessibility through the tree and the visual investigation of the wood anatomy and potential core depth from the inner to the outer side of the tree. For each ancient tree, six cores were collected, with three main cores and three duplicates located above or below the first collected wood core. The samples were taken from the inside of trees that were empty from the pith and accessible (Figure SI 1a) or from the bark towards the pith for ancient trees that were inaccessible from the pith, noting that those trees were also empty from the inside (Figure SI 1b). For considered medium young trees, three cores were collected from the bark towards the pith that was believed to still be available, these cores were taken from three different sides of the tree, in a way that the cores cover the whole surrounding of the trees (Figure SI 1c). For the few considered very young trees, one core was retrieved from the bark to the other end of the bark, covering the whole dimension of the tree (Figure SI 1d). A total of 216 cores (107 cores from Bchaaleh and 109 wood cores from Kawkaba) were collected from 41 trees of which 32 are monumental olive trees, six are young to medium trees and three are young trees (Table SI 1). It is important to note that the extracted wood cores were found divided into different parts per core upon sampling, and that the number of broken parts varied between 3 to 14 pieces (Table SI 1).

In parallel to monumental trees, young olive trees of 20-100 years old (tree age according to the owners), growing in young plantations next to the ancient groves, were also considered in both Bchaaleh and Kawkaba sites in order to use them for calibration and comparison with the monumental trees ring formation.

## II.2 Sampling design

### II.2.1 Classical approach

#### Dendrochronology

Using a wood base to support the wood core, a sanding machine (Seheppach bsm 2000) and three sand papers (300, 600, 1000 nm) were used to get a good visual ring detection. A set of three cores (BCO4.1, BCOY3.3 and BCOY2.2) (Table SI 1) from the Bchaaleh site was selected for the trial of this method, including two young and one monumental olive core of lengths ranging between 18 and 20cm.

After the sample preparation, the wood cores are identified under a microscope in order to have a better visual identification for the detection and manual counting of the tree rings. For the two young wood cores, the bark was identified as the last year before sampling, which in this study is 2018. Afterwards,

a scan of the wood core was done using Coorecorder followed by TSAP-win and COFECHA for tree ring reading, where it is possible to digitally select the tree rings for counting and width measurement between the different identified rings and identify the years for each ring.

**Micro-Densitometry**

This method requires first treatment of the samples for microdensitometer analysis. This is the most time-consuming step and destructive for the wood cores where the cores are cut with a double-bladed saw to a thickness of 1.4 mm to be scanned. A total of two olive cores were analyzed, one from Bchaaleh (BCO2.2D) and the other from Kawkaba (KWO1.2) with a length of 7 cm and 14.4 cm respectively (Table SI 1).

This method is used for density profiling of the tree wood cores (De Mil et al., 2016) and for detecting intra-annual density fluctuation (Gonzalez-Benecke et al., 2015; De Mil et al., 2016). It can be used for cross dating (Polge, 1966, 1970; Allen et al., 2012; Drew et al.,2013) cores (De Mil et al., 2016) were ring width is matched and anomalies detected to be able to match every ring to a calendar year (Fritts, 1976; De Mil et al., 2016). Noting that with density profiles, cross-dating can be improved (De Mil et al., 2016).

### II.2.2 New-approach

**X-ray computed tomography**

In total, 33 wood cores out of 216 cores of length range between 9 and 22 cm and width of 0.7 cm were selected. They were selected from 12 monumental olive trees, two medium trees and two young trees from Bchaaleh. In addition to 8 monumental trees, two considered medium trees and one young tree in Kawkaba.

The cores were first placed on a 2 cm sample holder suitable for a 12 µm resolution and then a dental glue is used to connect the different parts of wood (Table SI 1).

The samples were placed in the EasyTom 150 kV machine core (ISEM plateform), between an X-ray source and a detector on a rotating platform (Figure 2a) and the protocol would be selected and settings calibrated for the scan. X-rays are emitted and the number of X-ray reaching the detector is collected for a short while resulting into the production of a radiographic image. Then the platform is rotated through a small angle (average of 0.75 ˚), and the process is repeated for many times (few hundred times to reach a total rotation of 360˚). One part of one wood core can take up to two hours to produce around 800 images.

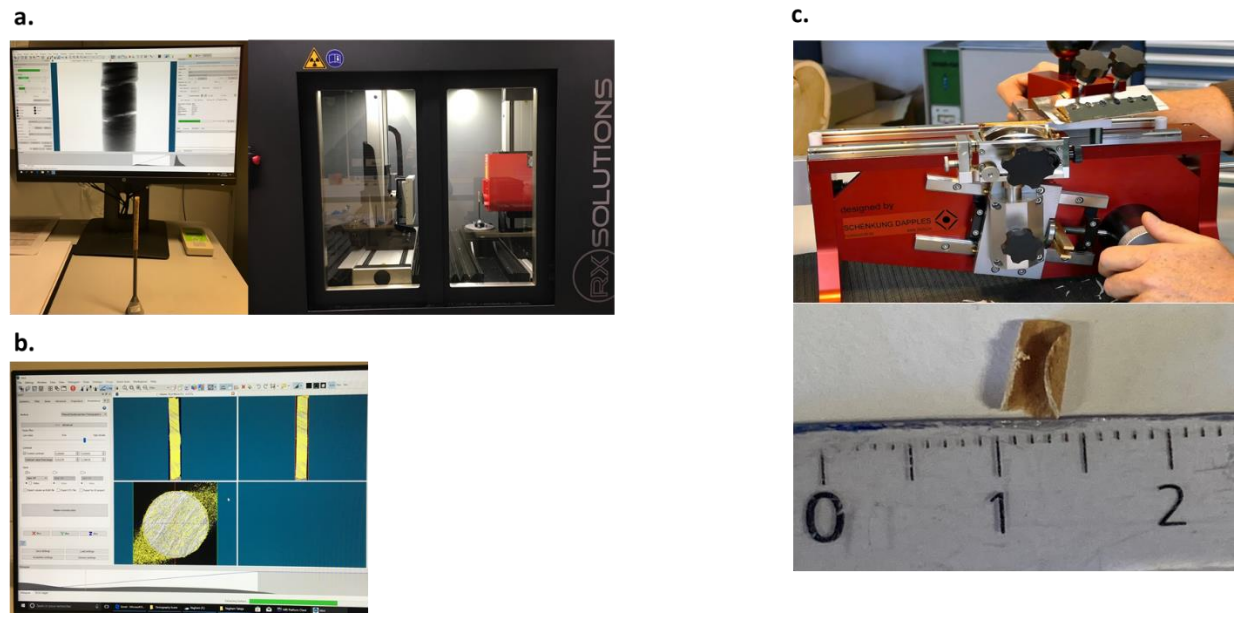


**Figure 23 (a)** X-ray tomography, **(b)** Xact program, **(c)** microtone.

After scanning the 33 wood cores, Xact program is used to fix the resolution of the wood cores (Figure 2b). The third step was using FIJI program on a total of 23 samples (10 from Kawkaba, and 13 from Bchaaleh) in order to reconstruct and connect the different parts of the wood cores and detect the tree rings, in addition to measuring the ring width. To do so, it is first needed to rotate the wood core imaging in 360° to get the highest possible resolution of the wood part where the maximum number of tree rings is possible to detect and visualize. In a second step, algorithms are used to transform the radiographies into virtual slices.

### II.2.3 Radiocarbon dating

A first set of 36 wood samples (18 from Bchaaleh and 18 from Kawkaba) using a manual blade to collect five to 10 mg of wood at the base of the wood cores in march 2019. These samples were cut from the assumed to be the oldest side of the wood core that was mainly collected from the inside of the tree. In 2020 and 2021, using the X-ray tomography microstructure reconstructions of our cores made it possible to select very precise positions on the wood cores at the ring level resolution. A new set of 92 samples (54 samples from Bchaaleh and 38 samples from Kawkaba) of two to six mg of wood was weighed and prepared using a driller by selecting different points from the wood core according to the visualization done using the tomography in order to select the samples for dating. In 2022, a set of seven samples from Bchaaleh were prepared using the microtone with high resolution of 20 µm (Figure 2c). A total of 135 wood samples (Table SI 1) were sent to the Carbon 14 Measurement Laboratory (LMC14-ARTEMIS) to be dated using the accelerator mass spectrometry. An OxCal v 4.4 was used to calibrate the radiocarbon dates using the IntCal20 (for pre-bomb) or Bomb 13 NH2 (for post-bomb)

calibration curves. A last set was sent in June 2022 constituting of 19 new samples prepared using a 20 µm resolution microtone machine.

### II.2.4 Stable carbon and deuterium isotopic ratios of bulk wood samples $\delta^{13}C_{BW}$)

After the X-ray tomography and $^{14}C$ step, $\delta^{13}C$ samples were selected. Since $\delta^{13}C$ preparation and analysis is time consuming, a decision had to be made regarding the sample selection. The selected samples were BCO9.1 (Part one and two) and BCO4.4 (Part one and four) from Bchaaleh site (Table SI 1). These samples were selected due to the clarity of the tree rings in the wood cores, and the available age retrieved using radiocarbon dates. A part with a recent age was selected in order to compare the C14 records with the modern condition such as the temperature, precipitation and $pCO_2$. Another part was selected according to a C14 date of an old period.

The selected part from BCO4.4 was sliced with an 11 µm resolution and due to a time-consuming process, the resolution was reduced to 20 µm (Each ring is cut in around 4 pieces). Each slice (weighing between 5 and 10 mg on average) is transferred in a cleaned vial. Between 2 to 3 mg of each wood sample are transferred into a tin capsule for $\delta^{13}C$ and $\delta D$ analysis using an elemental analyser (FlashEA1112- Thermo Scientific) coupled to an Isoprime 100 isotopic mass spectrometer. The precision of the analysis was 0.51‰. A conventional delta notation was used, where the isotopic composition of a material relative to that of a standard on a per mil deviation basis is given by $\delta$ = [(R sample)/(Rstandard) -1 ]* 1000, where $\delta$ is the isotopic ratio $\delta^{13}C$ and R is the molar ration of heavy to light isotope forms. Three international Standard for $\delta^{13}C$ were used (ASP3, B2215 and IAEA CH6) giving values expressed in ‰ versus the VPDB.

More than 700 samples have been prepared and sent for analysis, however the results of the three mentioned parts from two wood cores are presented here only.

## III. Results

### III.1 Dendrochronology and densitometry

For dendrochronology, a trial was done on three olive wood cores including two assumed to be young wood cores (BCOY2.2-Length:19.8 cm, BCOY3.3, Length: 19 cm) and one monumental wood core (BCO4.1-Length: 19.5 cm) from Bchaaleh (Figure 3a). With the microscope, it was not only difficult to clearly identify the true and false tree rings, but also to clearly point out all the available rings. Afterwards, the Coorecorder was used for tree ring reading. Using this more advanced dendrological technique still did not give the needed information in order to have a good identification and counting for the tree rings. The trial done on the three olive wood cores using dendrochronology showed irregularity of the tree rings and difficulty in detecting the rings visually using the classical methods even in a full young tree with an existing pith.

A total of two olive cores were selected for densitometry method, one from Bchaaleh (BCO2.2D wood core) and the other from Kawkaba (KWO1.2 wood core), with a 7 cm and 14.4 cm respectively**.** In

sample BCO2.2D and KWO1.2 a total of 44 and 118 tree rings respectively were detected. The detected rings were not completely accurate due to the difficulty in identifying the tree rings and realizing the true or false tree rings using the density of the rings (Figure 3b).

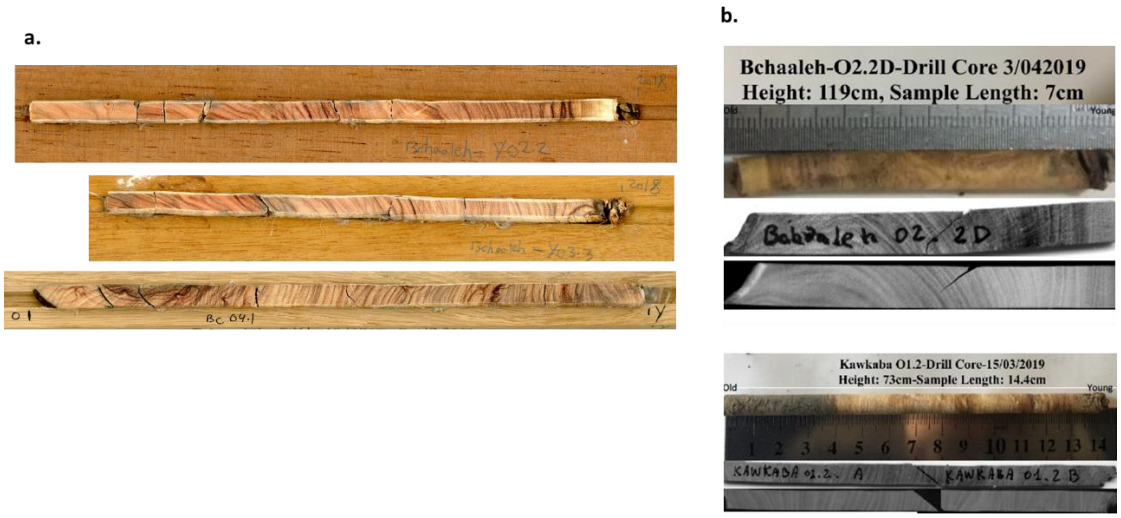


**Figure 24 (a)** Sanded samples prepared for dendrochronology from Bchaaleh, **(b)** samples done using densitometry from Bchaaleh and Kawkaba.

### III.2 X-ray tomography

Each tree ring represents one year and constitutes of two layers. The first is a light-colored layer (Early wood) which forms in the spring and early summer, and is usually thicker since the tree is growing. The second layer is a dark colored layer (Late wood) which forms in late summer and fall, it is thinner since the tree growth is slower (Figure 4a). The tree rings and ring width are identified and measured using the early and late wood, were these two layers constituted one tree ring.

It is worth noting that some tree rings are unclear even after using the X-ray tomography technique. Other wood cores are partially clear and some shows full clarity. Some wood parts seem continuous to other parts of the wood core (Figure 4a) and the analysis of the tree rings show a full path from the bark to the pith. In other cases, even when we cross from the bark to the pith in medium to young trees, it seems that the different wood parts are not always connected (Figure 4b).

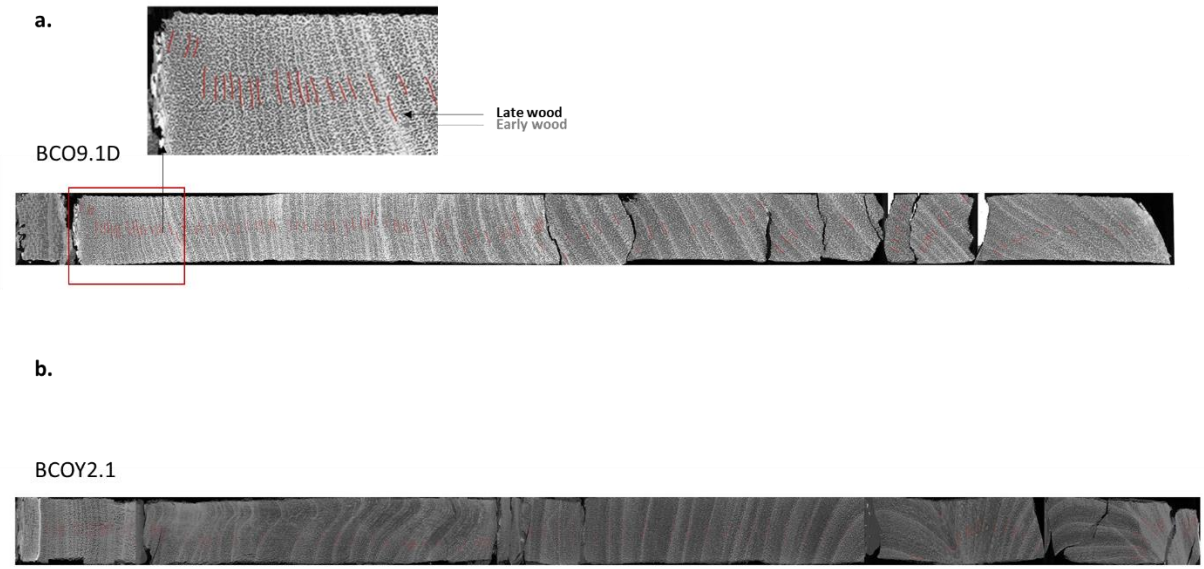


**Figure 25** Wood cores prepared using X-ray tomography **(a)** BCO9.1D, **(b)** BCOY2.1 from Bchaaleh.

## Tree Rings

As an example of young trees of Bchaaleh, BCOY4 registered different number of tree rings for the different seven parts of the wood core (Figure 5a, Table SI 1). This sample was taken from the bark into the pith with no cavity in the tree. The starting date at the bark is assumed to be 2019, with the tomography it was possible to hypothesize that the center of the tree can be identified in such a core and that the first three parts of the wood core are connected. Based on the visualization detected from the X-ray tomography and the rings identification using the early and late wood, the age of BCOY4 is expected to date back to the year 1994 with 28 tree rings.

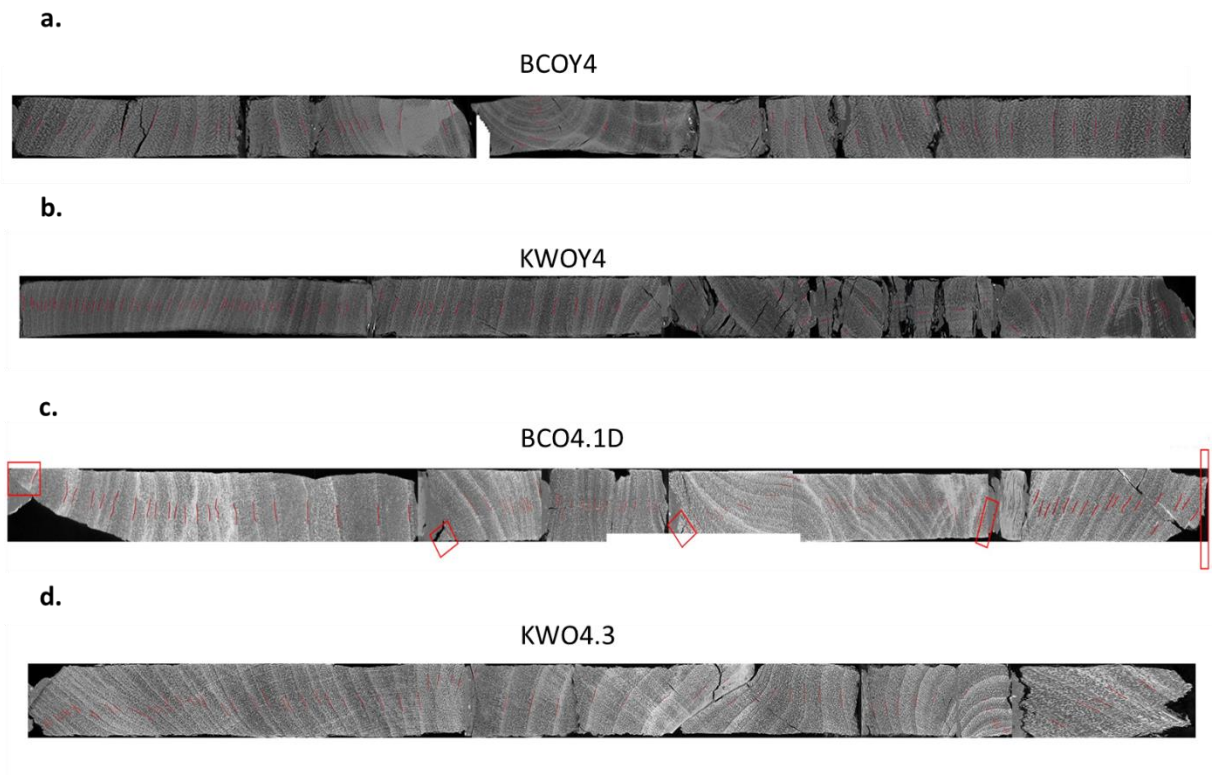


**Figure 26** X-ray tomography samples for ring counting **(a)** BCOY4, **(b)** KWOY4, **(c)** BCO4.1D, **(d)** KWO4.3.

In Kawkaba, the same hypothesis can be made, were for example, KWOY4 has six separated parts, of which the core was taken from the Bark (2019) till the pith. The X-ray tomography showed that the first two parts of the wood core are hypothesized to be continues to one another, with 47 rings in part one and 16 rings in part two of the wood core, dating back to year 1956. However, it was difficult to identify tree rings of the other parts of the core since the rings are of different directions and formation, and as such it was assumed that a new trunk has developed within this young tree, thus creating a new age range (Figure 5b).

Another example providing a different hypothesis is BCO4.1D, a monumental tree from Bchaaleh, where the wood core is divided into five parts (Figure 5c, Table SI 1). Through the tomography, it was hypothesized that different parts of the wood core are related to a different branch or new developed trunk of the same tree. In this case it was possible to identify the tree rings and have a counting per wood part, however it was not possible to determine the age of the core by only using the X-ray tomography technique. This core has five different parts with different tree ring directions per part, showing 22 rings, 10 rings, 14 rings, 30 rings, and 17 rings per part respectively (Figure 5c).

As an example, for a monumental olive tree from Kawkaba, KWO4.3 of five different parts, shows disconnected parts with different tree ring direction and formation. This confirmed the hypothesis that different parts in this monumental tree in Kawkaba is a combination of different trunks entangled in the same tree (Figure 5d).

**Tree rings width**

The tree rings width for BCOY4 from a considered young tree in Bchaaleh, were measured separately for each part of the full wood core. Part one of the wood core had an average of 2.18 mm between two rings, while part two registered an average ring width of 2.44 mm, part three had an average of 1.49 mm, part four registered an average of 4.07 mm, the fifth part indicated an average ring width of 1.83 mm, the sixth part had an average width of 1.80 mm and the final part has an average of 1.95 mm (Table SI 2). For Kawkaba, KWOY4 wood core from a considered young tree had six identified parts with 1.06 mm average ring width for part one, 2.40 mm for part two, 2.48 mm registered for part three, 1.95 mm regarding part four, 2.34 mm and 1.95 mm respectively for part five and six (Table SI 2).

A monumental olive tree in Bchaaleh (BCO4.1D) on the other hand had five parts, with the first part having an average ring width of 2.09 mm, part two registering an average of 1.22 mm, part three having an average of 0.87 mm, part four with an average tree ring of 0.90 mm and the fifth part with an average of 1.24 mm (Table SI 2). The monumental olive tree in Kawkaba (KWO4.3) had five different parts, part one with an average ring width of 0.94 mm, 2.52 mm for part two, 1.93 mm was registered for part three, 0.94 mm and 1.42 mm for parts four and five respectively (Table SI 2).

### III.3 Radiocarbon dating

After all of the above-mentioned steps, final results were retrieved in order to partially select samples for radiocarbon dating ($^{14}C$). As mentioned in the material and methods, different sampling has been selected and dated using the $^{14}C$ technique, and the data is summarized in Table SI 3.

The 135 $^{14}C$ samples were mainly from the beginning of each part of the wood core and/or the end of the same piece, assuming that by dating those points the ring counting between those two ages can be confirmed. All dates have been calibrated using IntCal20, which gave the calibrated ages. These ages show that 36% range between the age of 1801 and 1900 AD, 25% are between 1701 and 1800, while the rest of the ages varied between less than 1600 or more than 1900 AD (Figure SI 2, 3).

For example, the uncalibrated $^{14}C$ from a considered young tree in Bchaaleh (BCOY4) from part one, ring one (Figure 6a) revealed a date of 35± 30 BP, while the third dated part where it was radiocarbon dated at the end of the selected part (Ring 10) revealed a post bomb date of 109.56 ± 0.29 MC. Part four was dated in two different points, revealing a date for ring one of 108.93 ± 0.28 MC and ring eight of 108.71 ±0.28 MC. Part five was radiocarbon dated at ring 1 with a post bomb date of 108.21 ± 0.28 MC, part six had two dates, for ring one the date retrieved was post bomb of 106.89 ± 0.31 MC and ring seven was 103.83 ± 0.31 MC. The last seventh part was dated at the last ring (Ring 12), and revealed a date of 100.30 ± 0.29 MC (Figure 6a).

KWOY4 is an example of one of the young wood cores selected from Kawkaba. It is divided into six disconnected parts (Figure 6b). Part one was dated at Ring one (Beginning of the part) and Ring 47 (End of the part) dating back to 445± 30 BP and 147.16 ±0.33 MC respectively. The second part is 4.1 cm long with no dated rings. Part three (2 cm) was dated at ring three and gave a result of 101.96±0.27

MC. The fourth part of 1 cm was dated at the ring that was assumed or detected visually to be the center, dating back to 130±30 BP. Part five (1.8cm) and part six of 2.7 cm were both not dated (Figure 6b).

BCO4.1D a monumental tree from Bchaaleh that was radiocarbon dated at various points, showed the following results (Figure 6c). For part one, ring one date was 865 ± 30 BP. Ring one from part two had a date of 1025 ± 30 BP, while part four had two dated points, ring one with a date of 940 ± 30 BP and the end of the same part (Ring 30) with a date of 315 ± 30 BP. The last part had one date at the end of the piece (Ring 17) with a date of 440 ± 30 BP.

The monumental olive tree KWO4.3 in Kawkaba, was sampled at ring one of part one dating back to 1030 ± 30 BP (Figure 6d). Part two, ring one registered a date of 85 ± 30 BP, while the fourth part was dated at the last ring (Ring 15) giving a date of 175 ± 30 BP, and the last part (Part five) was dated at the end of the core with a date back to 235 ± 30 BP.

Wood core KWO16.2D from a monumental olive tree in Kawkaba gave the oldest age during the second collected batch for $^{14}C$, were Ring one of part one was dated back to a very old age of 7440 ± 40 BP (Figure 6e). Another set of samples were collected to confirm this age, where two more samples of the same core part were selected directly after Ring one. This batch came back with dates of 115 ± 30 BP and 65 ± 30 BP respectively. Another batch was sampled using the microtone to have a higher resolution giving dates of 165, 135 and 335 ± 40 BP (Table SI 2).

A set of 19 samples were selected even more precisely in order to improve the precision of the dating using the microtome of resolution 20 µm from BCO4.4, BC9.1D and KWOY4.

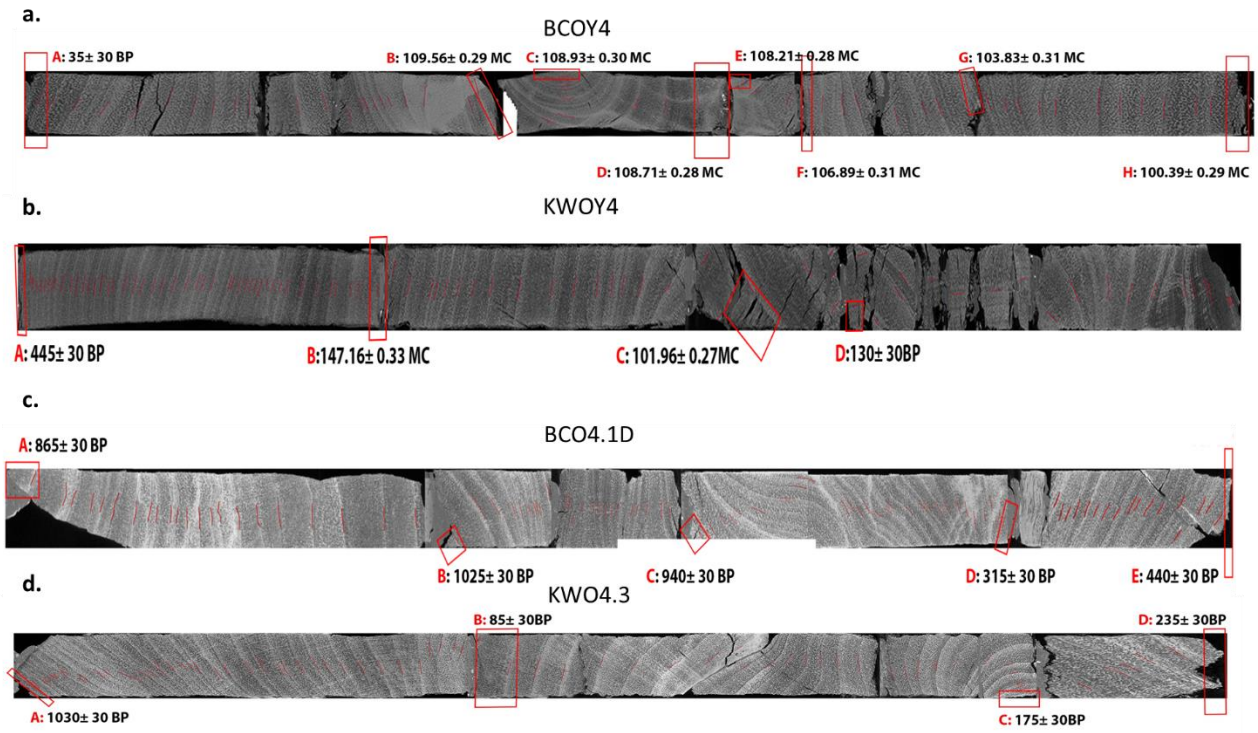


**Figure 27** Uncalibrated radiocarbon dates of the X-ray tomography wood cores from Bchaaleh and Kawkaba.

### III.4 $\delta^{13}C$ analysis

The available results of $\delta^{13}C$ bulk wood are related to the Bchaaleh monumental olive trees collected samples from BCO4.4 (Part one and four) and BCO9.1D (Part one and two) and corresponds to 300 analysis. The available results showed that the values range between -25.60 and -23.96 ± 0.37‰ for BCO4.4 part one and -26.41 and -23.17 ± 0.4 ‰ for part four. For BCO9.1, part one ranged between -26.11 and -25.07 ± 0.38 ‰ and -22.88 and -25.91 ± 0.66 ‰ for BCO9.1D part two. It is observed that there is no $\delta^{13}C_{BW}$ variation within the ring width (Figure 7).

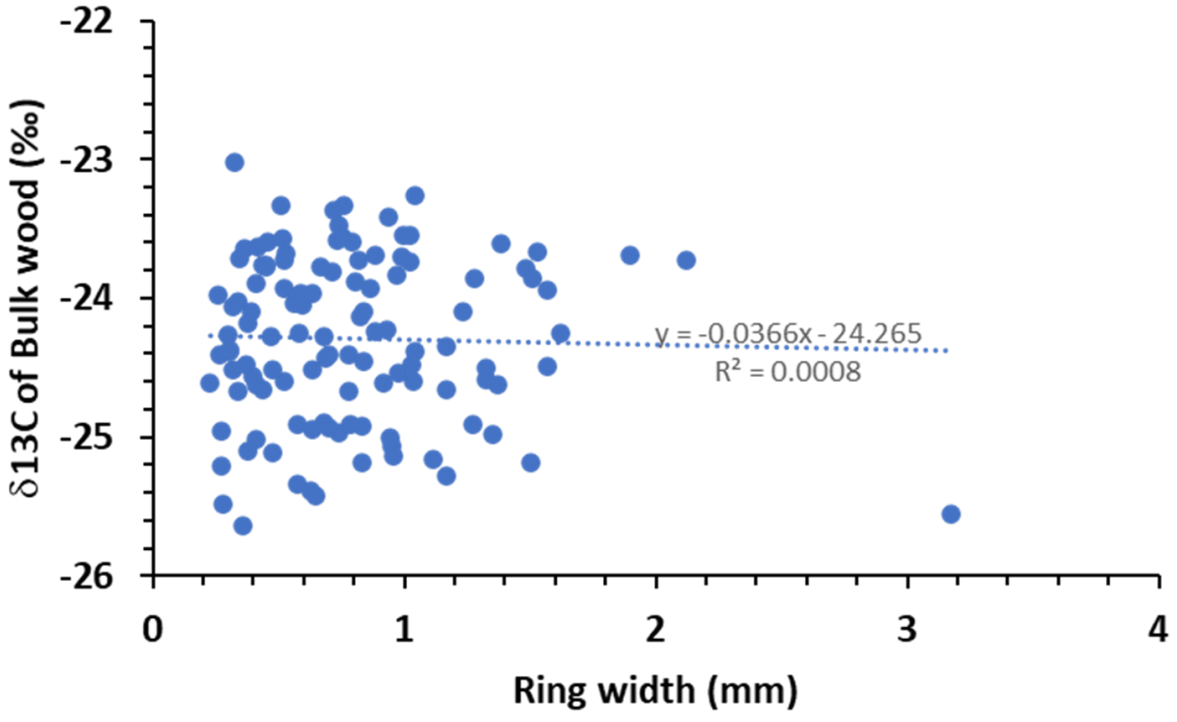


**Figure 28** Correlation between ring width and $\delta^{13}C$ of the sampled wood cores.

In a second step, due to Suess effect (declining $\delta^{13}C$ of atmospheric $CO_2$ since the beginning of the industrial period over the last 200 years; Francey et al., 1999; Sidorova et al., 2008), the average $\delta^{13}C$

was corrected. Figure 8 presents the corrected and uncorrected raw data, where a rise can be observed in the values of $\delta^{13}C$ after correction.

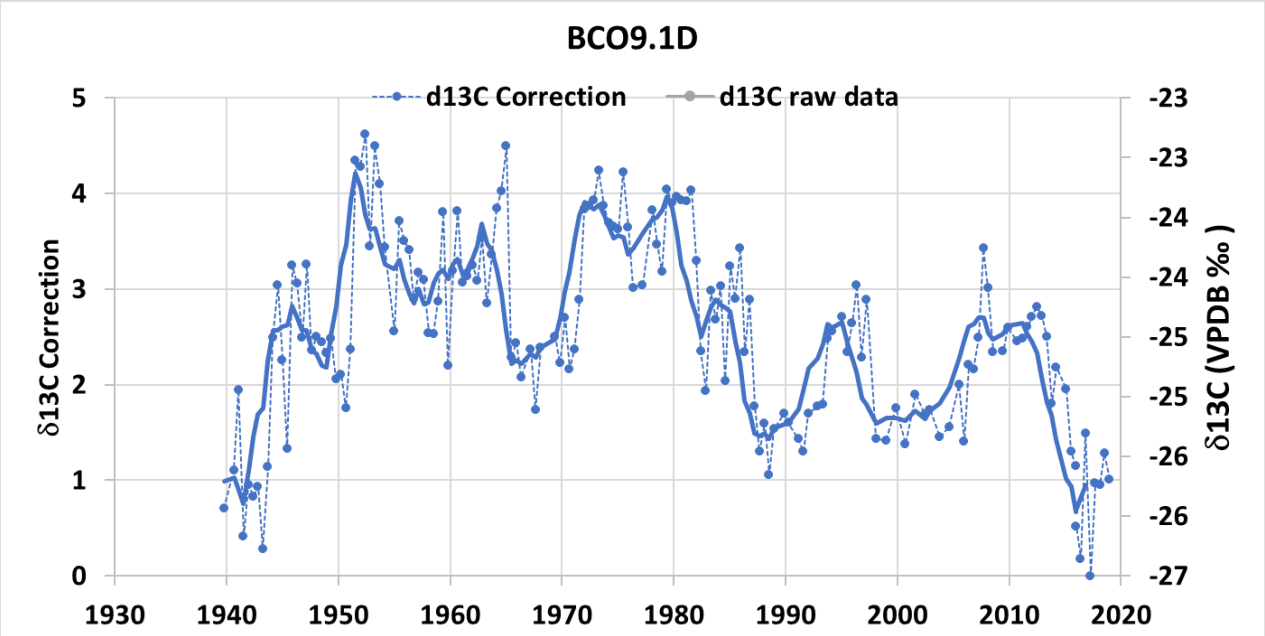


**Figure 29** The raw and corrected $\delta^{13}C$ series for wood. The series was corrected using $\delta^{13}C$ of atmospheric $CO_2$.

# IV. Discussion

## IV.1 The different methodologies used for tree ring identification

Olive wood is not usually dated using dendrochronology or densitometry techniques due to the difficulty in identifying the annual tree rings. In this study, existing ancient olive trees and young trees were used in order to identify the annual rings in the olive wood and create a data set that can be used as a chronological reference of other olive trees around the world, by combining X-ray tomography, $^{14}C$ and carbon stable isotopes.

The study has shown that tree rings in the ancient and young olive trees can be identified. Each ring represents one year of growth identified through early and late wood. The ring boundaries are detected when there is an increase in density (white streaks) while the intra-annual density fluctuation (IAFDs) is found as white narrow streaks between thicker areas of increased density which are identified as rings. These, have thinner and uncontentious rings (Ehrlich et al., 2021). In order to detect these tree rings, different methodologies and techniques were used to assist this objective. However, it is more difficult to identify annual tree rings in olive trees using the more classical technique of dendrochronology or even densitometry. X-ray tomography proved to be the most effective on olive wood cores. Tomography helped identify the tree rings and helped in determining a counting for the number of rings per part, specifying the direction of the rings per wood part and understanding the connection or disconnection of the different wood parts through the ring identification and formation (Figure 5).

## IV.2 Tree rings identification and radiocarbon dating

Olive trees shows from a young age the possibility of creating and deviating into more branches within the tree even with a full available interior wood (Lavee, 1996; Ehrlich et al., 2017), and this was seen in the considered young trees that also showed old ages using $^{14}C$ in comparison to their circumference and formation (Figure 6a,b). After X-ray tomography and $^{14}C$, wood cores in some cases showed that the orientation of the growth ring differs and does not follow the main assumption that the inner is the oldest in some cases and this can be attributed to the fact that there can be more than one branch and pith within the same tree.

### IV.2.1 Young olive trees

BCOY4, a wood core from a considered young tree from Bchaaleh, constitutes of seven parts (Figure 6a). The first part is 2.7 cm long with 10 identified rings. Ring one was dated and although it was expected to give a young age of 2018-2019, it turned out to be much older (35 ± 30 BP). As such, this refutes the previous assumption, disconnecting this part from any part that comes afterwards. Part three (1.8 cm) with 10 identified tree rings gave a date of 109.56 ± 0.29 MC (1957.62 - 2001.8 AD) at Ring 10. With this date, it was possible to count back this part at Ring one to 1967 – 2011.8 AD confirming that this part of the wood core is a young branch. Part four of 2.7 cm with 8 rings was dated at Ring one and Ring 8 and gave a $^{14}C$ of 108.93 ± 0.30 MC and 108.71 ± 0.28 MC respectively. This outcome assumes that both dated parts have the same date although eight rings separate them, making the possible assumption that two branches of the same age is formed in the fourth part (Figure 6a).

KWOY4 is an example of one of the young wood cores selected from Kawkaba. It is divided into six parts (Figure 6b). Piece one has a length of 5.6 cm with 47 detectable rings. This part was dated at Ring one (Beginning of the part) and Ring 47 (End of the part) dating back to 445 ± 30 BP and 147.16 ± 0.33 MC respectively, indicating two different trunks in this first part unlike expectations shown using the X-ray tomography. Were it would be assumed that Ring one would be at year 2019 and date back till Ring 47 to year 1972. This confirms the second assumption that within the same part, a new trunk formation is created within the same tree. The second part is 4.1 cm long with 16 rings and no dated parts, but according to the tree rings formation and direction it seems to be a continuity of the previous part. Part three (2 cm) has seven identified rings, and was dated at ring three and gave a result of 101.96 ± 0.27 MC, this part formation is complex which makes it difficult to count any rings to date back this part. The fourth part of 1 cm and three rings was dated at the ring that was assumed or detected visually to be the center, dating back to 130 ± 30 BP, which gave a more recent age than that of part one (Ring one). An assumption can be made that this part is a formation of a new branch on its own. Part five (1.8 cm) had two rings that seemed to have a very different ring direction and was not dated. The last part of 2.7 cm length and 12 rings seems to be disconnected from the previous parts and was also not dated (Figure 6b).

In such case of both young wood cores, more dates are needed to confirm any assumption. However, it definitely confirms that the use of both methods, the X-ray tomography and $^{14}C$ complement each other especially in olive trees.

### IV.2.2 Monumental olive trees

A set of monumental olive trees were selected from Bchaaleh for both X-ray tomography $^{14}C$. Wood core BCO4.4 is constituted of five disconnected parts. The first part of 1.2cm was dated at the beginning of the core part which resulted in a date of 900 ± 30 BP having 14 identified rings with tilted direction (Figure 9a). The second part of 3.3 cm, this part seems to be connected to part one, were visually it can be assumed that ring 13 and 14 in piece one is the same first and second ring in piece two. Ring five in piece two was radiocarbon dated and it gave a date of 405 ± 30 BP, which denies the visual assumption of the continuity of the rings of part one to the second part (Figure 9a). In part two, 33 rings were identified where the last identified ring was dated, giving a radiocarbon date of 425 ± 30 BP. Part three of 3.1cm length had a total of 30 visually identified rings. This part is assumed to be a continuity of the second part, were ring one, two and three are the same rings as part two, ring 31,32 and 33. Part four had 41 identified rings with a length of 6.1 cm, Ring one in this part was radiocarbon dated giving a date of 855 ± 30 BP. The last sampled part of 3.6 cm and 35 identified rings, gave a result for Ring one that was dated back to 375 ± 30BP and ring 35 dated back to 390 ± 30BP. These outcomes result in 15 rings between the two dates unlike the 35 rings count that were visually identified (Figure 6c). This confirms the possibility of identifying false rings or the need for more radiocarbon analysis to confirm the outcome.

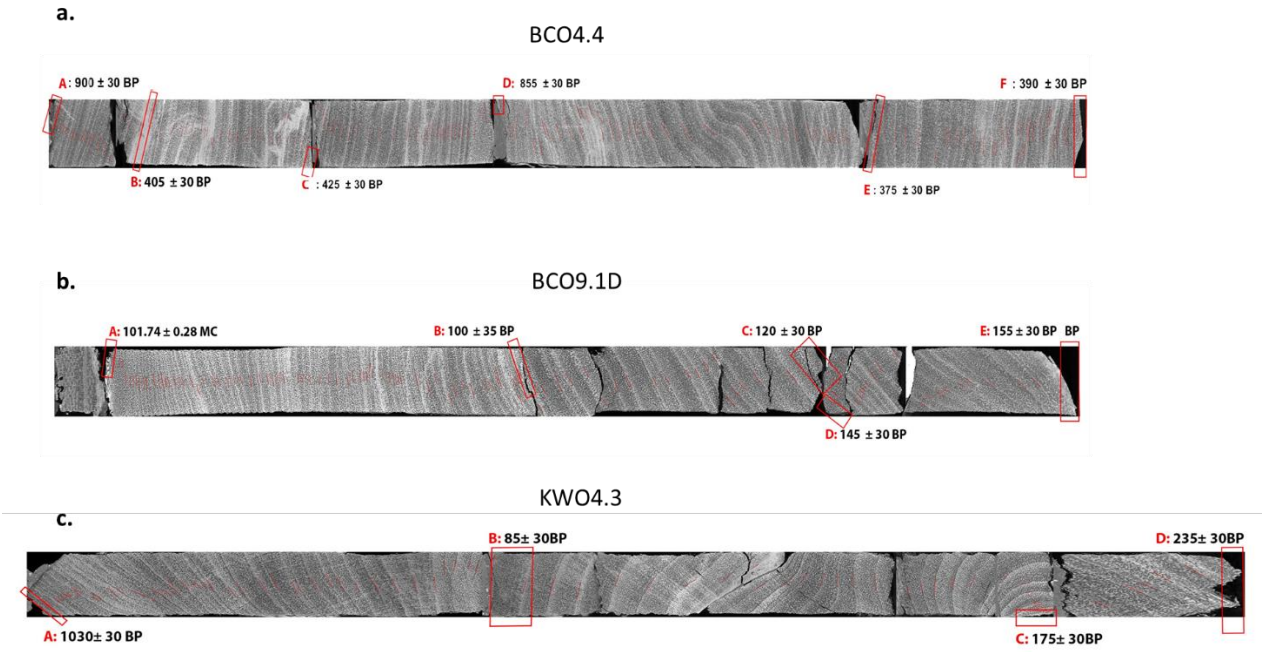


**Figure 30** Set of wood cores radiocarbon dated and X-ray tomographed.

Another example of Bchaaleh monumental olive tree was sample BCO9.1D. This core constituted of seven parts (Figure 9b). Part one was of 0.6 cm in length and zero detectable rings. Part two (4.7cm) had 66 identified rings, with two dates, one at the very beginning (Ring one) dating back to 101.74 ± 0.28 MC which is post year 1950. Ring 66 was also dated to 100 ± 35 BP, assuming as per the ring direction and formation that this piece is one continuous trunk. Part three (0.9cm) had five visualized rings and assumed to be connected to part two and was not dated. Part four also seeming to continue part three with the same ring direction with nine rings. Part five of 1.2cm length had five rings, with the fifth ring being dating back to 120 ± 30 BP. Looking at the direction of the rings and the connection with part four, it seems that Ring one and three are a continuity for ring eight and nine in the fourth part. With the date in part two and part five, it seems to be a new trunk with 17 rings in between which is close to the visual ring counting that was observed (16 rings) (Figure 9b). Part six (0.9cm) had 11 rings and was only dated in ring one giving a date of 145 ±3 0 BP disconnecting this part from the other previous parts, leading to the assumption of a new trunk formation. The last part is number seven of 1.9 cm length and nine visually identified rings, dated back to 155 ± 30 BP, and seems to be a continuation of part six, with Ring one and four to be possibly identified as ring 10 and 11 in part six giving a close estimation of rings (10 Rings) with what was visually identified (13 Rings). This wood core was assumed to be old, but with the X-ray tomography and $^{14}C$ it was concluded that it is from a young time range.

A set of centennial trees were also selected from Kawkaba for tomography and detailed $^{14}C$. As an example, we take KWO4.3 of 13 cm total length was considered. This wood core constitutes of five separated parts (Figure 9c). Part one was dated at Ring one, at the beginning of the wood core, giving a date of 1030 ± 30 BP with 41 rings in a 4.9 cm length part. Part two of 1.2 cm and four identified rings had been dated at ring one of this part dating back to 85 ± 30 BP. Part three of the wood core was identified with 12 rings in 3.2 cm with no dating. Part five of 1.8 cm had 15 counted rings with a $^{14}C$ of ring 15 going back to 175 ± 30 BP. The last sixth part of length 1.9 cm had 5 identifiable rings with a dating at the fifth ring of 235 ± 30 BP. Part two, three and four seems to be one trunk with the same ring directions and continuity between the different parts (Figure 9c). 17 rings were counted in between the date of part two and that of part four, which indicates some missing rings between the different parts.

KWO16.2D, a centennial olive tree of 19.9cm total length was tomographed and radiocarbon dated. This wood core is divided into seven parts, part one of 5.6 cm length had 25 identified rings, it was dated extensively (six dates) at the beginning of this part. The first date gave an age of 7440 ± 40 BP. In order to confirm this age, we radiocarbon dated consecutive points after the first dated point but the dates retrieved were very different from the first date (Figure 6e). This indicates the possibility that much more $^{14}C$ needs to be done close to the first dated point to confirm more the age retrieved.

The rings that were identified with X-ray tomography were correlated with the rings confirmed by $^{14}C$. However, it was shown that some rings can be masked and not identified through the tomography images, or microscopic identification, since the expected rings between the $^{14}C$ was not fully met through the X-ray tomography which might lead to misdating olive trees sometimes with many years.
It has been proven through modern living olive branch that the outer wood towards the bark can be off by decades form the expected date, which means that the outer wood towards the bark that is supposed to represent the last year of growth may be very old due to the fact that olive wood can grow in one area of the branch and at the same time continue to grow in another different branch (Ehrlich et al., 2017). Based on this observation, the same issue was considered and observed in ancient olive wood cores through the X-ray tomography and confirmed by the $^{14}C$ that showed a gap of years in comparison to the number of rings between the different dates. This should confirm and emphasize on the difficulty of visually detecting the oldest tree just depending on the size and circumference of a tree and the need of big set of wood samples from different positions of the monumental trees considering the complex architecture of the unseen interior of the tangled branches within a single tree. Additionally, a very high-resolution $^{14}C$ of the wood cores is required to detect the age range and not miss the investigation of the highest possible existing wood age.
In the dating model, the range of ages of the radiocarbon dated wood cores were shown (Figure 9). The ages range between 800 and 2001 AD in Bchaaleh and back to 6000 BC to 2001 AD in Kawkaba after calibration using IntCal20.

### IV.3 $\delta^{13}C$ and ring width

Thanks to tree ring width, $^{14}C$, and X-ray tomography, we have been able to reconstruct a preliminary chronological frame for the last 60 years. We show that very thin sliced wood core allow the reconstruction of high resolution $\delta^{13}C$ which is a good indicator of water stress (Ehleringer & Cooper, 1988). $\delta^{13}C_{BW}$ is higher when temperature is higher (Figure 10). This is usually detected in $C_3$ plants (Liu et al., 2017) such as the olive tree. In water limited conditions such as in this case, that can be usually attributed to the soil moisture that is impacted by the temperature (Liu et al., 2017).

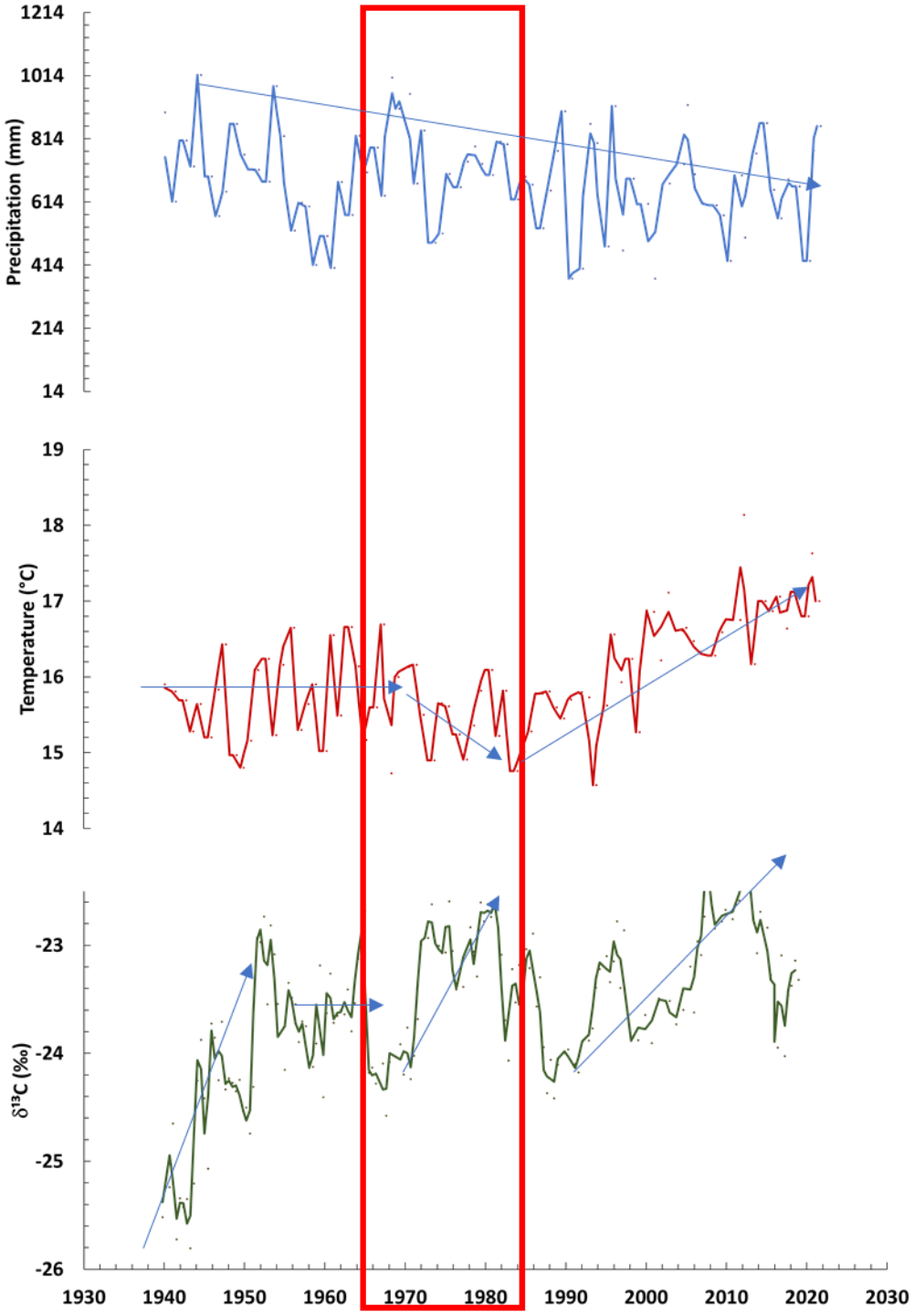


**Figure 31** $\delta^{13}C$ in relation to temperature and precipitation. The red rectangle indicates the year range of the cold annual seasons for temperature.

A good covariation between $\delta^{13}C$ and tree ring width of Bchaaleh is identified (Figure 11). This must be more thoroughly studied since we were more expecting the opposite indeed when tree ring growth increase a decrease of $\delta^{13}C$ resulting from Photosynthetic activity (Fichtler et al., 2010). However, the late and early wood width would have been better indicator of $\delta^{13}C$.

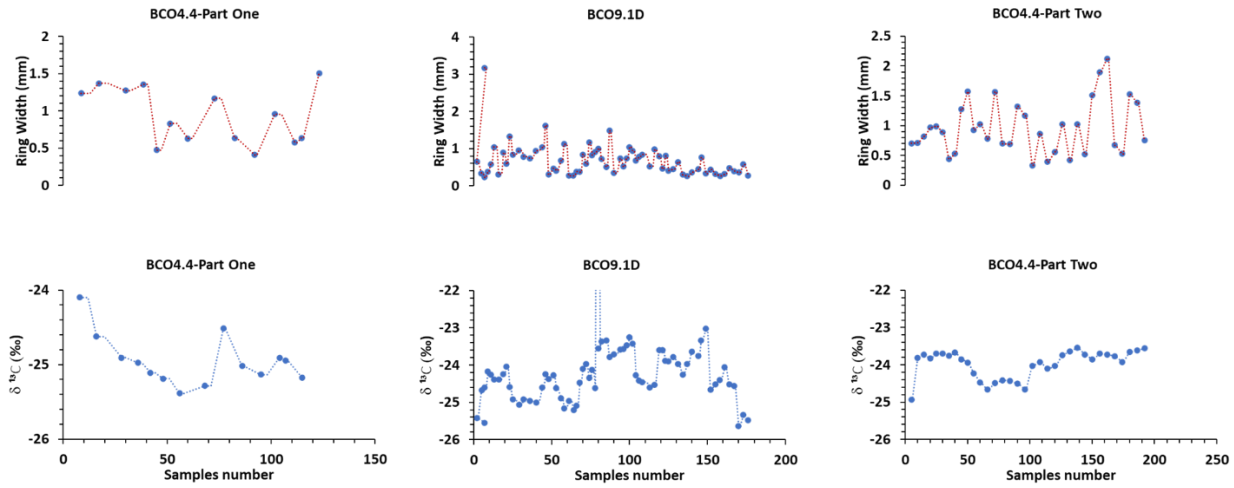


**Fig. 32** Covariation of $\delta^{13}C$ and Ring width of wood cores.

During the period from 1960 to early 1980 temperatures were low compared to the period from 1980 onwards. The annual spring temperature rose by 1.23°C while the summer and autumn warmed by 1.5 (ie. 1.23°C respectively (El-Kadi, n.d.). In this study, a cooler time range between 1970 and 1980 can be observed, which might have been reflected by the $\delta^{13}C$ in the olive wood tree rings (Figure 10), $\delta^{13}C$ increasing with a decrease in temperature.

The rings identified by X-ray tomography were not always correlated with the dates of the rings confirmed by $^{14}C$ due to the lack of high-resolution dates to confirm this relation. Nonetheless, $\delta^{13}C$ and $^{14}C$ in some cores with the ring width confirmed the radiocarbon dated rings, noting that some rings along the wood core are masked when checking with the tomography scans and that was evident by $^{14}C$ and $\delta^{13}C$. Wood is a complex material chemically, it consists of cellulose, lignin, resin and other extractives. So, it is considered difficult to use bulk wood in isotopic analysis (Taylor et al., 2008), but the $\delta^{13}C$ in bulk wood and in cellulose showed very similar trends of offset between 1.45 and 2‰ (Sidorova et al., 2008). Thus, bulk wood can be a good indicator of the interannual variability of $\delta^{13}C$. It is also known the $\delta^{13}C$ of wood is usually less negative than in foliage that is the source of photosynthate (Cernusak & Ubierna, 2022). The variation in $\delta^{13}C$ of foliage exported and the transport of sugar through phloem can affect the $\delta^{13}C$ of the cellulose of the tree rings (Gessler & Ferrio, 2022), thus the link between leaf processes and wood $\delta^{13}C$.

The $\delta^{13}C$ of wood tree rings in the Middle age showed higher $\delta^{13}C$ values than those in the modern days. Even in the modern days, the past registered higher $\delta^{13}C$ values in comparison to the present values of 2020.

The mean values of $\delta^{13}C$ of foliage in olive trees registered an average of -26.63 ± 0.72 ‰ in Bchaaleh. The stems registered an average of -25.75 ± 0.93 ‰ which indicates that the wood samples $\delta^{13}C$ are close to the stems registered values.

## V. Conclusion

The use of X-ray tomography helps the identification of a great number of annual rings in the sampled cores, which assists in selecting the $^{14}C$ samples and asses the different dates in relation to the ring numbers and orientation. The application of the XrRay tomography in the case of very complex tree ring as known for the olive trees proved to be a very successful and a step forward in identifying the annual growth rings (early and late wood). This technic was a main key for understanding the structures of the wood pieces (different branches) and for the selection of the $^{14}C$ samples. Hence these two techniques (X-ray tomography and radiocarbon) combined together allowed to improve our knowledge on olive trees age in Lebanon. The preliminary $\delta^{13}C$ results of this work show a variability at an interannual scale. These results seem to confirm the potential of reconstructing paleoenvironment and paleoclimate with the tree ring stable isotopes of the olive wood cores though more analysis of $\delta^{13}C$ is still awaiting. We obtained a minimum oldest age of 7,400 years BP from the existing wood sampled from the trunk of one of the monumental olive trees in Kawkaba and around 1800 years for Bchaaleh. These ages should be further confirmed with more extensive wood cores, $^{14}C$ and tomography.

**Acknowledgements:** The authors would like to acknowledge the National Council for Scientific Research of Lebanon (CNRS-L) and Montpellier University for granting a doctoral fellowship to Nagham Tabaja. The authors would also like to thank the Franco-Lebanese Hubert Curien Partnership (PHC-CEDRE) project 44559PL for the funding provided. The authors would also like to thank ISEM at Montpellier University and PRASE at the Lebanese University led by Dr Fouad Haj Hassan for their support of the laboratory work. We acknowledge the MRI platform member of the national infrastructure France-BioImaging supported by the French National Research Agency (ANR-10-INBS-04, «Investments for the future»), the labex CEMEB (ANR-10-LABX-0004) and NUMEV (ANR-10-LABX-0020). We also acknowledge ARTEMIS (Pascal Dumoulin), Mr R. Geagea, Bchaaleh mayor, and Ms M Merhi, Kawkaba mayor deputy, for the support kindly provided during this study.

## References

Besnard, G., Khadari, B., Navascues, M., Fernandez-Mazuecos, M., Bakkali, A. E., Arrigo, N., Baali-Cherif, D., de Caraffa, V. B.-B., Santoni, S., Vargas, P., & Savolainen, V. (2013). The complex history of the olive tree: From Late Quaternary diversification of Mediterranean lineages to primary domestication in the northern Levant. *Proceedings of the Royal Society B: Biological Sciences*, *280*(1756), 20122833–20122833.

Besnard, G., Terral, J.-F., & Cornille, A. (2018). On the origins and domestication of the olive: A review and perspectives. *Annals of Botany*, *121*(3), 385–403. https://doi.org/10.1093/aob/mcx145

Caracuta, V. (2020). Olive growing in Puglia (southeastern Italy): A review of the evidence from the Mesolithic to the Middle Ages. *Vegetation History and Archaeobotany*, *29*(5), 595–620. https://doi.org/10.1007/s00334-019-00765-y

Carrión, Y., Ntinou, M., & Badal, E. (2010). Olea europaea L. in the North Mediterranean Basin during the Pleniglacial and the Early–Middle Holocene. *Quaternary Science Reviews*, *29*(7–8), 952–968. https://doi.org/10.1016/j.quascirev.2009.12.015

Castiglioni, E., & Maniscalco, L. (2008). *Il santuario dei Palici. Un centro di culto nella Valle del Margi*.

Cernusak, L. A., & Ubierna, N. (2022). Carbon Isotope Effects in Relation to CO2 Assimilation by Tree Canopies. *Series Editors*, 291.

Chalak, L., Haouane, H., Essalouh, L., Santoni, S., Besnard, G., & Khadari, B. (2015). Extent of the genetic diversity in Lebanese olive (Olea europaea L.) trees: A mixture of an ancient germplasm with recently introduced varieties. *Genetic Resources and Crop Evolution*, *62*, 621–633. https://doi.org/10.1007/s10722-014-0187-1

Cherubini, P., & Lev-Yadun, S. (2014). The olive tree-ring problematic dating. *Antiquity*, *88*, 290–291. https://doi.org/10.1017/S0003598X00050420

De Mil, T., Vannoppen, A., Beeckman, H., Van Acker, J., & Van den Bulcke, J. (2016). A field-to-desktop toolchain for X-ray CT densitometry enables tree ring analysis. *Annals of Botany*, *117*(7), 1187–1196. https://doi.org/10.1093/aob/mcw063

Ehleringer, J. R., & Cooper, T. A. (1988). Correlations between carbon isotope ratio and microhabitat in desert plants. *Oecologia*, *76*(4), 562–566. https://doi.org/10.1007/BF00397870

Ehrlich, Y., Regev, L., & Boaretto, E. (2021). Discovery of annual growth in a modern olive branch based on carbon isotopes and implications for the Bronze Age volcanic eruption of Santorini. *Scientific Reports*, *11*(1), 704. https://doi.org/10.1038/s41598-020-79024-4

Ehrlich, Y., Regev, L., Kerem, Z., & Boaretto, E. (2017). Radiocarbon Dating of an Olive Tree Cross-Section: New Insights on Growth Patterns and Implications for Age Estimation of Olive Trees. *Frontiers in Plant Science*, *08*, 1918. https://doi.org/10.3389/fpls.2017.01918

El-Kadi, A. K. A. (n.d.). *Lebanon Temperature and the Global Warming During the 20th Century*. 10.

Fichtler, E., Helle, G., & Worbes, M. (2010). Stable-carbon isotope time series from tropical tree rings indicate a precipitation signal. *Tree-Ring Research*, *66*(1), 35–49.

Francey, R. J., Allison, C. E., Etheridge, D. M., Trudinger, C. M., Enting, I. G., Leuenberger, M., Langenfelds, R. L., Michel, E., & Steele, L. P. (1999). A 1000-year high precision record of δ13C in atmospheric CO2. *Tellus B*, *51*(2), 170–193. https://doi.org/10.1034/j.1600-0889.1999.t01-1-00005.x

Gessler, A., & Ferrio, J. P. (2022). Postphotosynthetic Fractionation in Leaves, Phloem and Stem. *Series Editors*, 381.

Guerci, A. (2005). *L'olivo tra empirismo e scienza*. 5.

Kaniewski, D., Van Campo, E., Boiy, T., Terral, J.-F., Khadari, B., & Besnard, G. (2012). Primary domestication and early uses of the emblematic olive tree: Palaeobotanical, historical and molecular evidence from the Middle East. *Biological Reviews*, *87*(4), 885–899. https://doi.org/10.1111/j.1469-185X.2012.00229.x

Lavee, S. (1996). Biology and physiology of the olive tree. *World Olive Encyclopedia. International Olive Council*, 61–110.

Liu, X., Zhang, Y., Li, Z., Feng, T., Su, Q., & Song, Y. (2017). Carbon isotopes of C3 herbs correlate with temperature on removing the influence of precipitation across a temperature transect in the agro-pastoral ecotone of northern China. *Ecology and Evolution*, *7*(24), 10582–10591. https://doi.org/10.1002/ece3.3548

Schicchi, R., Speciale, C., Amato, F., Bazan, G., Di Noto, G., Marino, P., Ricciardo, P., & Geraci, A. (2021). The Monumental Olive Trees as Biocultural Heritage of Mediterranean Landscapes: The Case Study of Sicily. *Sustainability*, *13*(12), 6767. https://doi.org/10.3390/su13126767

Sidorova, O. V., Siegwolf, R. T. W., Saurer, M., Naurzbaev, M. M., & Vaganov, E. A. (2008). Isotopic composition (δ13C, δ18O) in wood and cellulose of Siberian larch trees for early Medieval and recent periods. *Journal of Geophysical Research: Biogeosciences*, *113*(G2). https://doi.org/10.1029/2007JG000473

Taylor, A. M., Renée Brooks, J., Lachenbruch, B., Morrell, J. J., & Voelker, S. (2008). Correlation of carbon isotope ratios in the cellulose and wood extractives of Douglas-fir. *Dendrochronologia*, *26*(2), 125–131. https://doi.org/10.1016/j.dendro.2007.05.005

Yazbeck, E. B., Rizk, G. A., Hassoun, G., El-Khoury, R., & Geagea, L. (2018). *Ecological characterization of ancient olive trees in Lebanon- Bshaaleh area and their age estimation*. *11*(2 Ver. 1), 35–44.

Zohary, D., & Hopf, M. (2000). Domestication of plants in the Old World: The origin and spread of cultivated plants in West Asia, Europe and the Nile Valley. *Domestication of Plants in the Old World: The Origin and Spread of Cultivated Plants in West Asia, Europe and the Nile Valley.*, *Ed.3*. https://www.cabdirect.org/cabdirect/abstract/20013014838

Zohary, D., Hopf, M., & Weiss, E. (2012). *Domestication of Plants in the Old World: The origin and spread of domesticated plants in Southwest Asia, Europe, and the Mediterranean Basin* (4th ed.). Oxford University Press. https://doi.org/10.1093/acprof:osobl/9780199549061.001.0001

## Supplementary Information

**a.**

BCO1

BCO2

BCO3

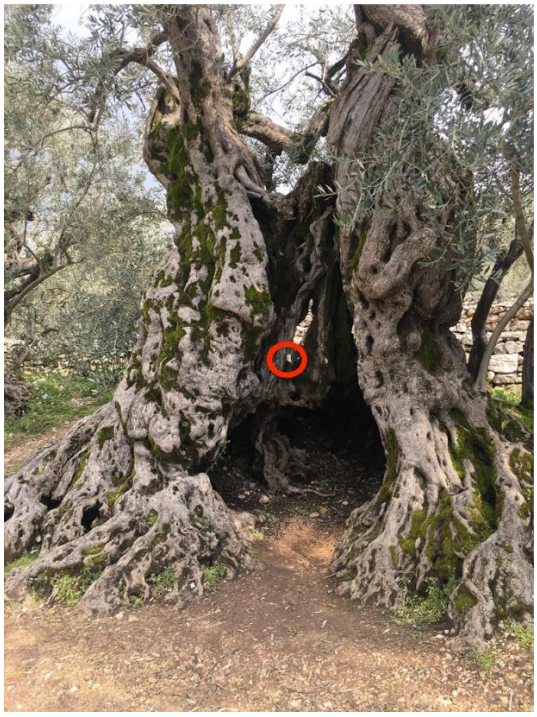

BCO4


Bchaaleh-Drill Core-16/03/2019
O4.1-Height: 124cm-Sample LengthL 19.5cm

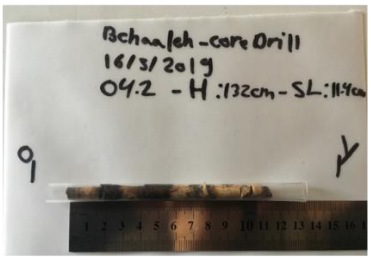
Bchaaleh-core Drill
16/3/2019
04.2 - H:132cm - SL:11.9cm

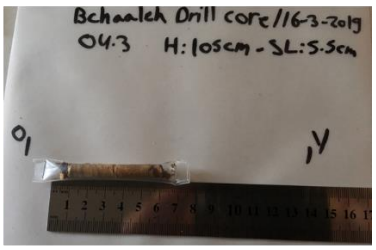
Bchaaleh Drill core/16-3-2019
04.3 H:105cm - SL:5.5cm

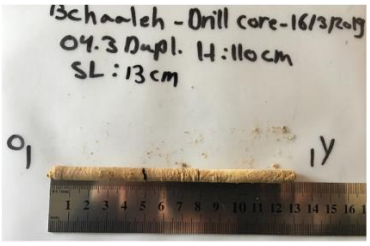
Bchaaleh - Drill core-16/3/2019
04.3 Dupl. H:110cm
SL:13cm

BCO5

BCO6

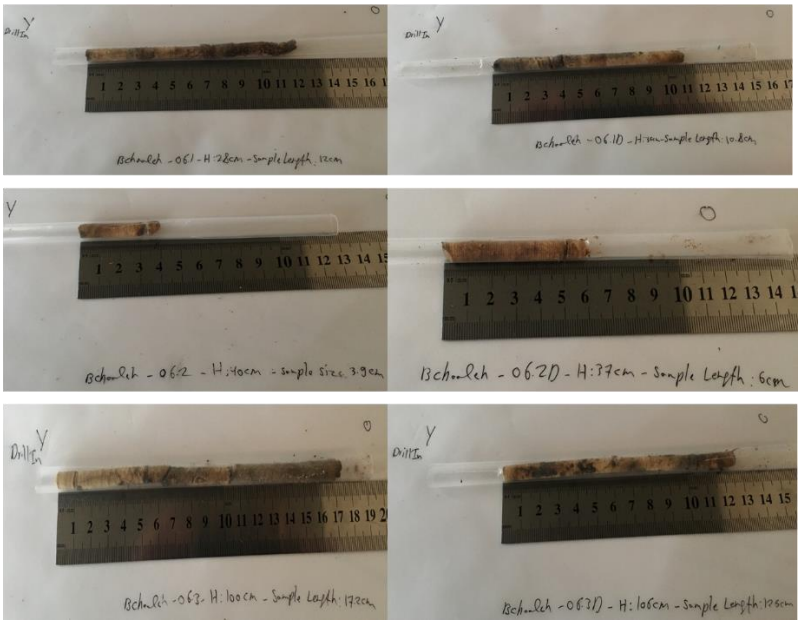

BCO7

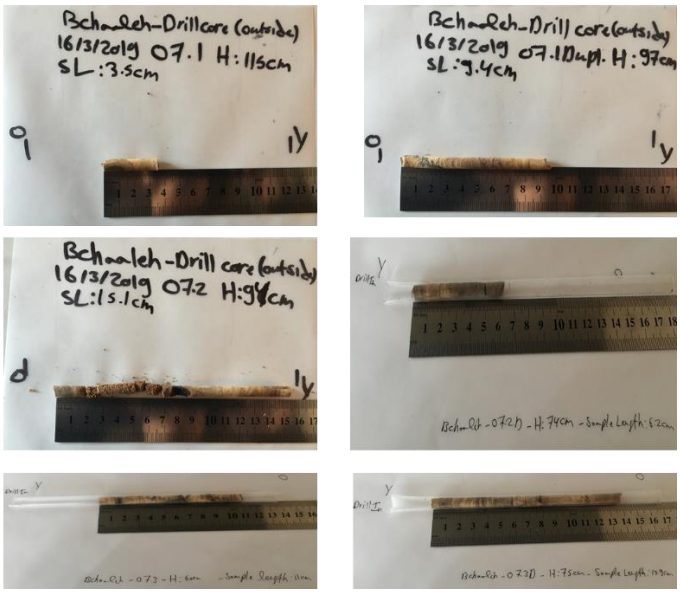
Bchaaleh-Drillcore (outside)
16/3/2019 07.1 H:115cm
SL:3.5cm
Bchaaleh-Drill core(outside)
16/3/2019 07.1Dupl. H:97cm
SL:9.4cm
Bchaaleh-Drill core(outside)
16/3/2019 07.2 H:94cm
SL:15.1cm

BCO10

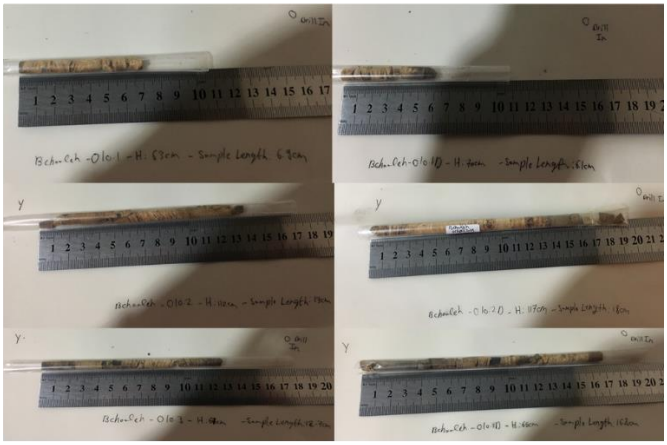

BCO14

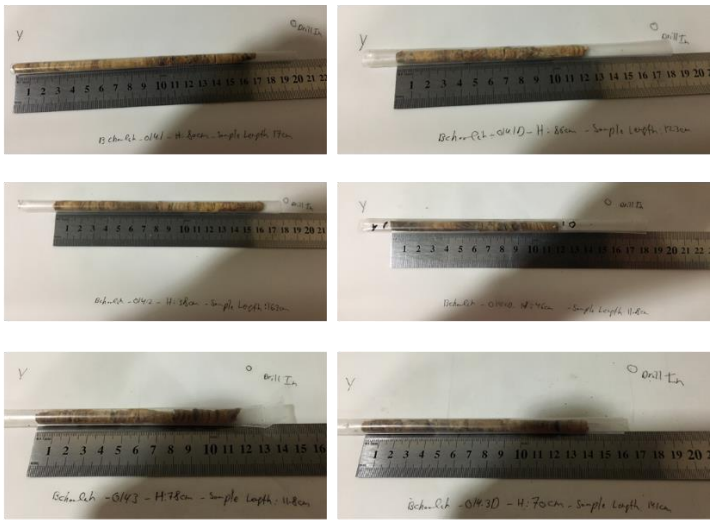

BCO15

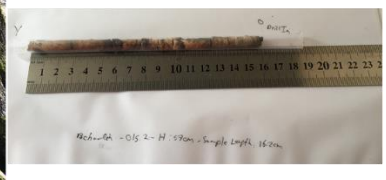

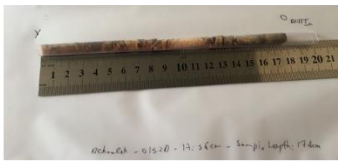

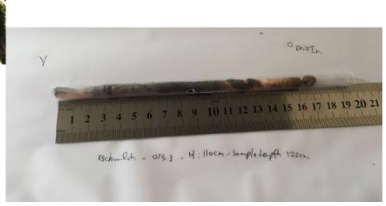

BCO16

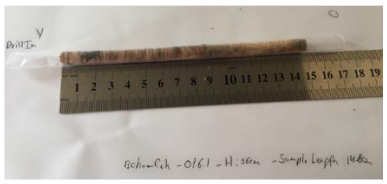

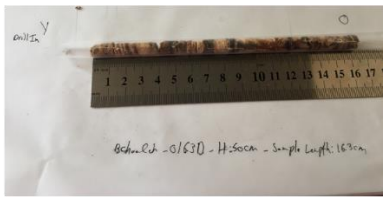

KWO1

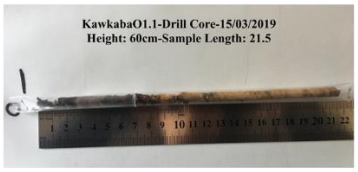
KawkabaO1.1-Drill Core-15/03/2019
Height: 60cm-Sample Length: 21.5


KawkabaO1.1D-Drill Core-30/04/2019
Height: 55cm-Sample Length: 15.8cm


Kawkaba O1.2-Drill Core-15/03/2019
Height: 73cm-Sample Length: 14.4cm


Kawkaba O1.2D-Drill Core-15/03/2019
Height: 72cm-Sample Length: 10.6cm


Kawkaba O1.3-Drill Core-30/04/2019
Height: 103cm-Sample Length: 12.9cm


Kawkaba O1.3D-Drill Core-30/04/2019
Height: 100cm-Sample Length: 14cm

KWO2


Kawkaba O2 trial-Drill Core-15/03/2019
Height: 100cm-Sample Length: 2.3cm


Kawkaba O2.1-Drill Core-15/03/2019
Height: 100cm-Sample Length: 6.5cm

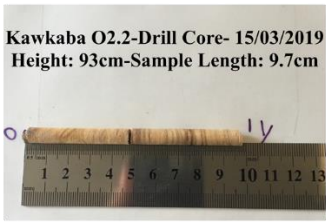
Kawkaba O2.2-Drill Core- 15/03/2019
Height: 93cm-Sample Length: 9.7cm


Kawkaba O2.2D-Drill Core-15/03/2019
Height: 103cm-Sample Length: 12.8cm


Kawkaba O2.3-Drill Core-15/03/2019
Height: 130cm-Sample Length: 10.9cm


Kawkaba-O2.3D-Drill Core-30/04/2019
Height:135-Sample Length:3.5cm


Kawkaba-O2.4D-Drill Core-30/04/2019
Height:125 cm-Sample Length:13cm

KWO3


Kawkaba-O3.1-Drill Core-30/04/2019
Height:90cm-Sample Length:17.3cm


Kawkaba-O3.1D-Drill Core-30/04/2019
Height:80cm-Sample Length:17.4cm


Kawkaba-O3.2-Drill Core-30/04/2019
Height:102cm-Sample Length:16.3cm


Kawkaba-O3.2D-Drill Core-30/04/2019
Height:98cm-Sample Length:13.1cm

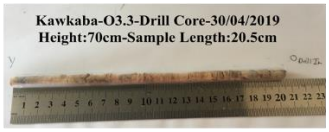
Kawkaba-O3.3-Drill Core-30/04/2019
Height:70cm-Sample Length:20.5cm


Kawkaba-O3.3D-Drill Core-30/04/2019
Height:69cm-Sample Length:6.8cm

KWO4

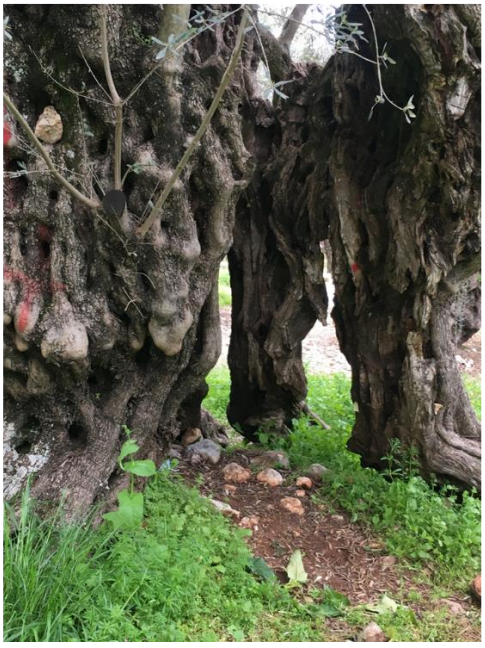


Kawkaba-O4.1-Drill Core-16/03/2019
Height:60cm-Sample Length:17.3cm


Kawkaba-O4.1D-Drill Core-15/03/2019
Height:55cm-Sample Length:5.6cm


Kawkaba-O4.2-Drill Core-16/03/2019
Height:40cm-Sample Length:16.2cm


Kawkaba-O4.2D-Drill Core-16/03/2019
Height:37cm-Sample Length:11.7cm


Kawkaba-O4.3-Drill Core-07/05/2019
Height:114cm-Sample Length:13.1cm


Kawkaba-O4.3D-Drill Core-07/05/2019
Height:110cm-Sample Length:8.5cm

KWO5


Kawkaba-O5.1-Drill Core-07/05/2019
Height:143cm-Sample Length:13.7cm


Kawkaba-O5.1D-Drill Core-07/05/2019
Height: 135cm-Sample Length: 9.5cm


Kawkaba-O5.2-Drill Core-07/05/2019
Height: 131cm-Sample Length: 14.4cm


Kawkaba-O5.2D-Drill Core-07/05/2019
Height: 127cm-Sample Length: 17.7cm


Kawkaba-O5.3-Drill Core-07/05/2019
Height: 108cm-Sample Length: 16.5cm


Kawkaba-O5.3D-Drill Core-07/05/2019
Height: 98cm-Sample Length: 16cm

KWO6

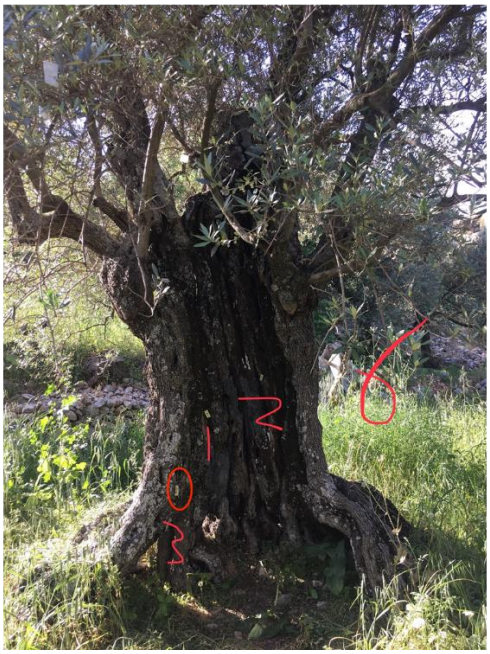


Kawkaba-O6.1-Drill Core-07/05/2019
Height: 110cm-Sample Length: 11.7cm


Kawkaba-O6.1D-Drill Core-07/05/2019
Height: 98cm-Sample Length: 16.2cm


Kawkaba-O6.2-Drill Core-07/05/2019
Height: 130cm-Sample Length: 9.2cm

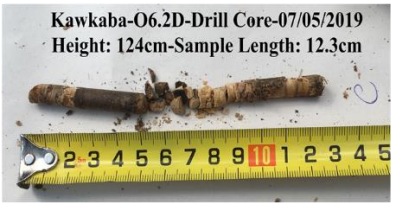
Kawkaba-O6.2D-Drill Core-07/05/2019
Height: 124cm-Sample Length: 12.3cm


Kawkaba-O6.3-Drill Core-07/05/2019
Height: 76cm-Sample Length: 12.5cm


Kawkaba-O6.3D-Drill Core-07/05/2019
Height: 70cm- Sample Length: 15.7cm

KWO7


Kawkaba-O7.1-Drill Core-30/04/2019
Height: 57cm-Sample Length: 16.1cm


Kawkaba-O7.1D-Drill Core-30/04/2019
Height: 63cm-Sample Length: 16.4cm


Kawkaba-O7.2-Drill Core-30/04/2019
Height: 105cm-Sample Length: 11cm


Kawkaba-O7.2D-Drill Core-30/04/2019
Height: 100cm-Sample Length: 8.2cm


Kawkaba-O7.3-Drill Core-30/04/2019
Height: 130cm-Sample Length: 10.6cm


Kawkaba-O7.3D-Drill Core-30/04/2019
Height: 127cm-Sample Length: 18.2cm

KWO8


Kawkaba-O8.1-Drill Core-30/04/2019
Height: 114cm-Sample Length: 18.5cm


Kawkaba-O8.1D-Drill Core-30/04/2019
Height: 108cm-Sample Length: 18cm


Kawkaba-O8.2-Drill Core-30/04/2019
Height: 98cm-Sample Length: 20.3cm


Kawkaba-O8.2D-Drill Core-30/04/2019
Height: 90cm-Sample Length:18cm


Kawkaba-O8.3-Drill Core-30/04/2019
Height: 103cm-Sample Length: 12cm


Kawkaba-O8.3D-Drill Core-30/04/2019
Height: 95cm-Sample Length: 13.6cm

KWO12


12


Kawkaba-O12.1-Drill Core-7/05/2019
Height: 24cm-Sample Length: 17.3cm


Kawkaba-O12.1D-Drill Core-7/05/2019
Height: 30cm-Sample Length: 14.3cm


Kawkaba- O12.2D -Drill Core-7/05/2019
Height: 115cm-Sample Length: 13.1cm


Kawkaba-O12.3-Drill Core-7/05/2019
Height: 130cm-Sample Length: 12.3cm


Kawkaba-O12.3D-Drill Core-7/05/2019
Height: 140cm-Sample Length: 10.5cm
O12.3D


Kawkaba-O12.4-Drill Core-7/05/2019
Height: 120cm-Sample Length: 10cm

KWO13


13


Kawkaba-O13.1-Drill Core-7/05/2019
Height: 126cm-Sample Length: 13.5cm


Kawkaba-O13.1D-Drill Core-7/05/2019
Height: 122cm-Sample Length: 14.8cm


Kawkaba-O13.2-Drill Core-7/05/2019
Height: 138cm-Sample Length: 6cm


Kawkaba-O13.2D-Drill Core-7/05/2019
Height:135cm-Sample Length: 9cm
Y
O


Kawkaba-O13.3-Drill Core-7/05/2019
Height:138cm-Sample Length: 19cm


Kawkaba-O13.3D-Drill Core-7/05/2019
Height:129cm-Sample Length: 13.3cm

KWO14







KWO16






**b.**

BCO8

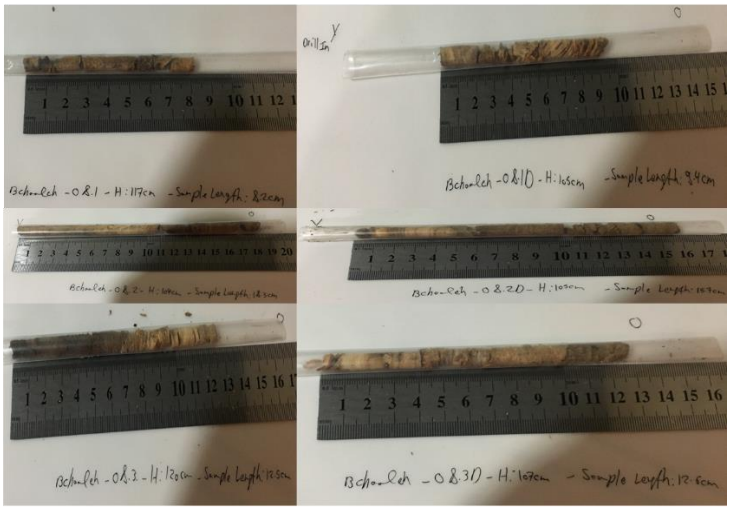

BCO9

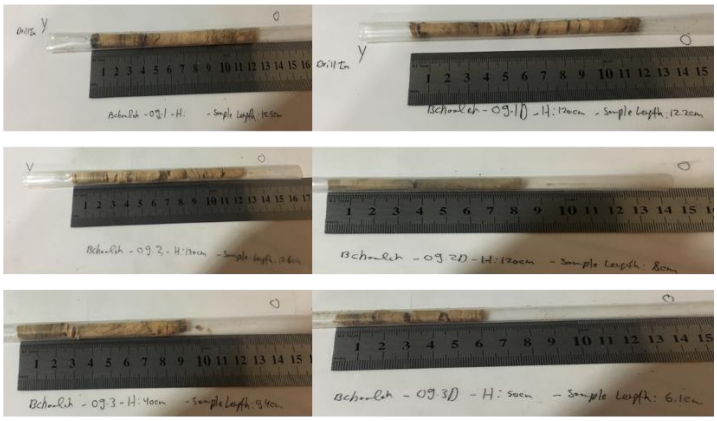

BCO11

BCO12

BCO13


13

KWO15

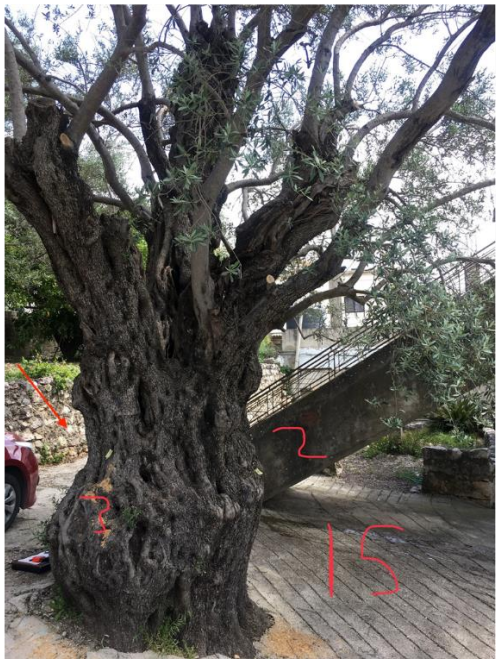
2
15


Kawkaba-O15.1-Drill Core- 07/05/2019
Height: 115cm-Sample Length: 7.4cm


Kawkaba-O15.1D-Drill Core- 07/05/2019
Height: 108cm-Sample Length: 16.3cm


Kawkaba-O15.2-Drill Core-07/05/2019
Height: 111cm- Sample Length: 17.4cm


Kawkaba-O15.2D-Drill Core-07/05/2019
Height:106cm- Sample Length: 18.8cm


Kawkaba-O15.3-Drill Core-07/05/2019
Height: 104cm-Sample Length: 17.5cm


Kawkaba-O15.3D-Drill Core-07/05/2019
Height: 105cm-Sample Length: 17.8cm

KWO17


Kawkaba-O17.2-Drill Core-07/05/2019
Height: 103cm-Sample Length: 11cm


Kawkaba-O17.3D-Drill Core-07/05/2019
Height: 106cm-Sample Length: 10.6cm

KWO18


Kawkaba-O18.2-Drill Core-12/05/2019
Height: 95cm-Sample Length: 21cm

KWO19







**c.**

BCOY1

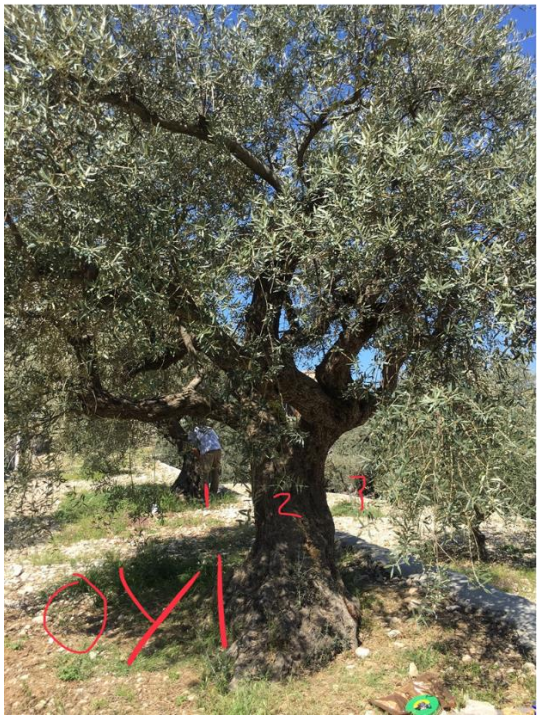


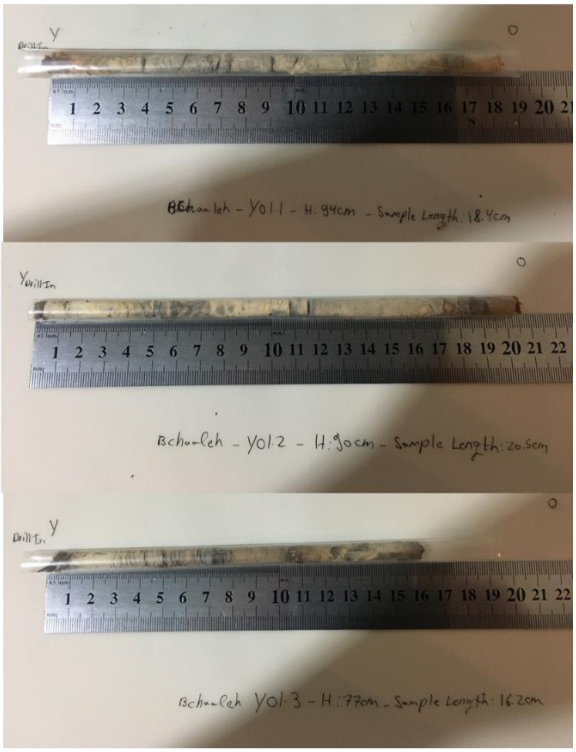

BCOY2


BCOY2

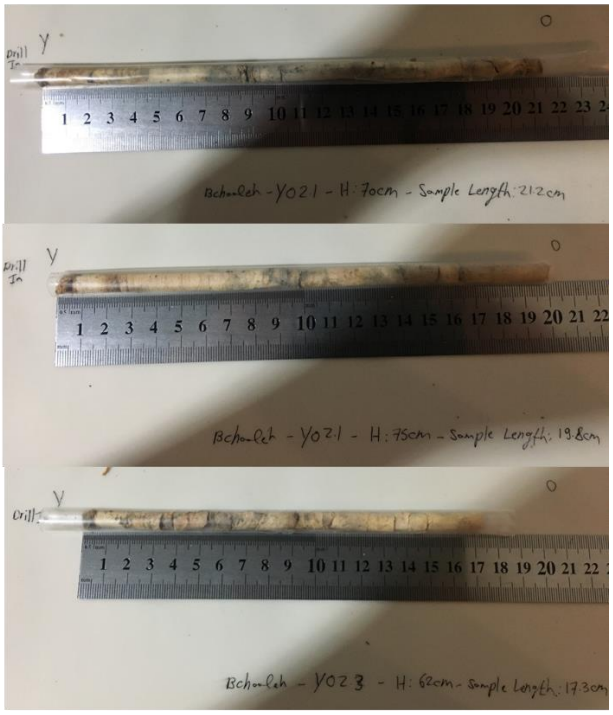
Bchoufch - Y021 - H: 70cm - Sample Length: 21.2cm
Bchoufch - Y021 - H: 75cm - Sample Length: 19.8cm
Bchoufch - Y023 - H: 82cm - Sample Length: 17.3cm

BCOY3

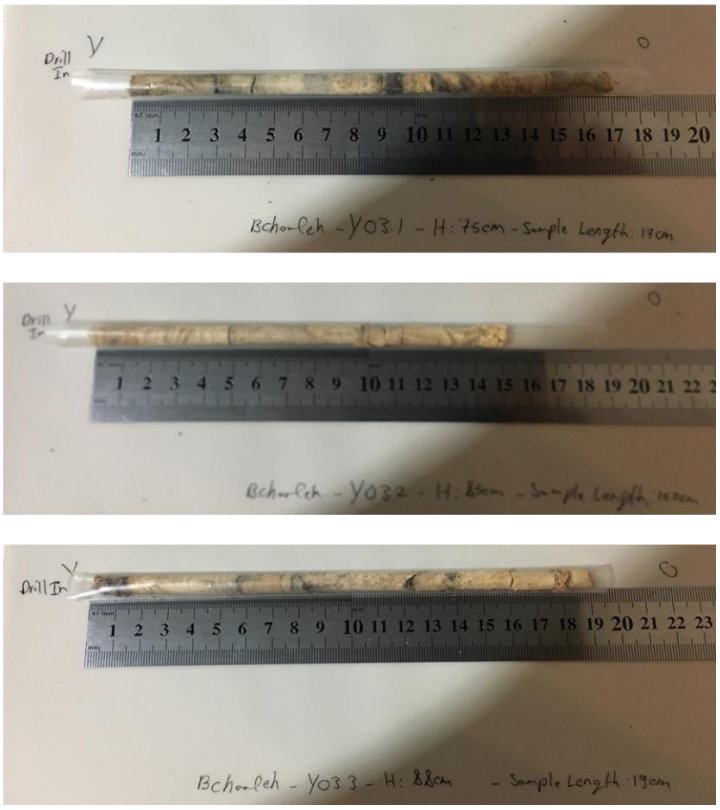
Bchoufch - Y031 - H: 75cm - Sample Length: 17cm
Bchoufch - Y032 - H: 85cm - Sample Length: 15.2cm
Bchoufch - Y033 - H: 88cm - Sample Length: 19cm

KWOY1


1
2
3
OY1


Kawkaba-YO1.1-Drill Core-12/05/2019
Height: 75cm-Sample Length: 9.5cm
O
Y


Kawkaba-YO1.2-Drill Core-12/05/2019
Height: 68cm-Sample Length: 20cm


Kawkaba-YO1.3-Drill Core-12/05/2019
Height: 42cm-Sample Length: 16.5cm

KWOY2


3
1
2
OY2


Kawkaba-YO2.1-Drill Core-12/05/2019
Height: 55cm-Sample Length: 19cm


Kawkaba-YO2.2-Drill Core-12/05/2019
Height: 62cm-Sample Length: 915cm


Kawkaba-YO2.3-Drill Core-12/05/2019
Height: 82cm-Sample Length:20cm

KWOY3


Y3
1
2


Kawkaba-YO3.1-Drill Core-12/05/2019
Height: 70cm-Sample Length 14.9cm
Y
O


Kawkaba-YO3.2-Drill Core-12/05/2019
Height: 70cm-Sample Length:20cm

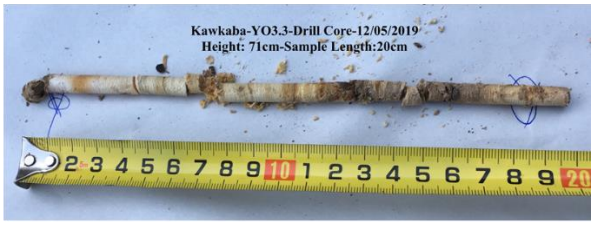
Kawkaba-YO3.3-Drill Core-12/05/2019
Height: 71cm-Sample Length:20cm

**d.**

BCO4


Bchaaleh-BCOY4-Drill Core-05/012021-Height: 20cm-Sample Length:16cm-
Y-Bark
O-Center-Bark

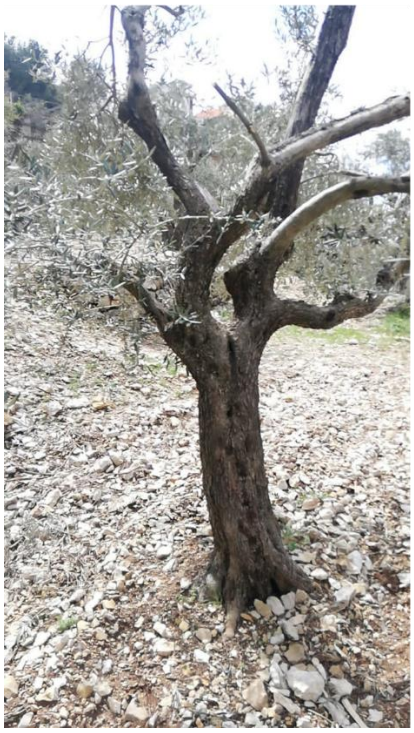

BCOY5

KWOY4

**Figure SI 5** Sampled olive trees and extracted wood cores from Bchaaleh and Kawkaba **(a)** accessible monumental olive trees from the inside (towards the pith) towards the outside (bark), **(b)** accessible monumental olive trees from the bark towards the pith, **(c)** medium young olive trees, **(d)** young olive trees.

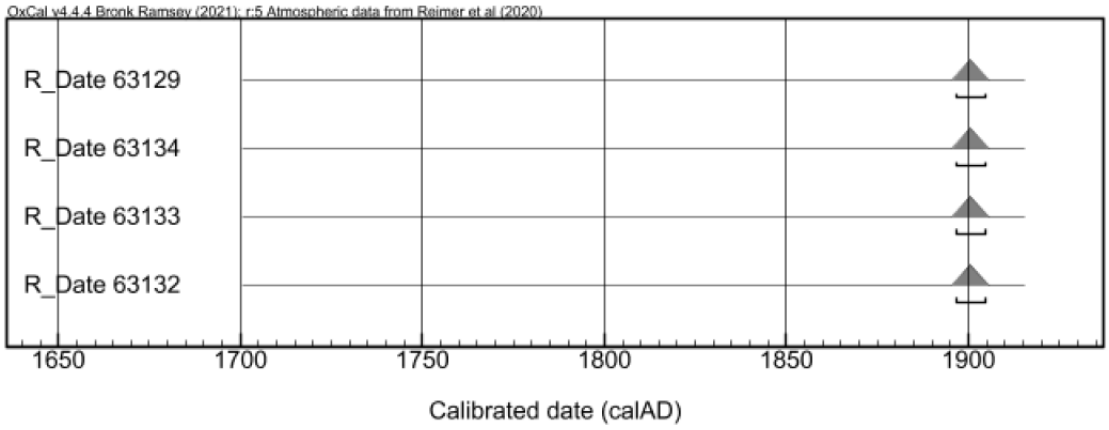
OxCal v4.4.4 Bronk Ramsey (2021); r:5 Atmospheric data from Reimer et al (2020)
R_Date 63129
R_Date 63134
R_Date 63133
R_Date 63132
1650
1700
1750
1800
1850
1900
Calibrated date (calAD)

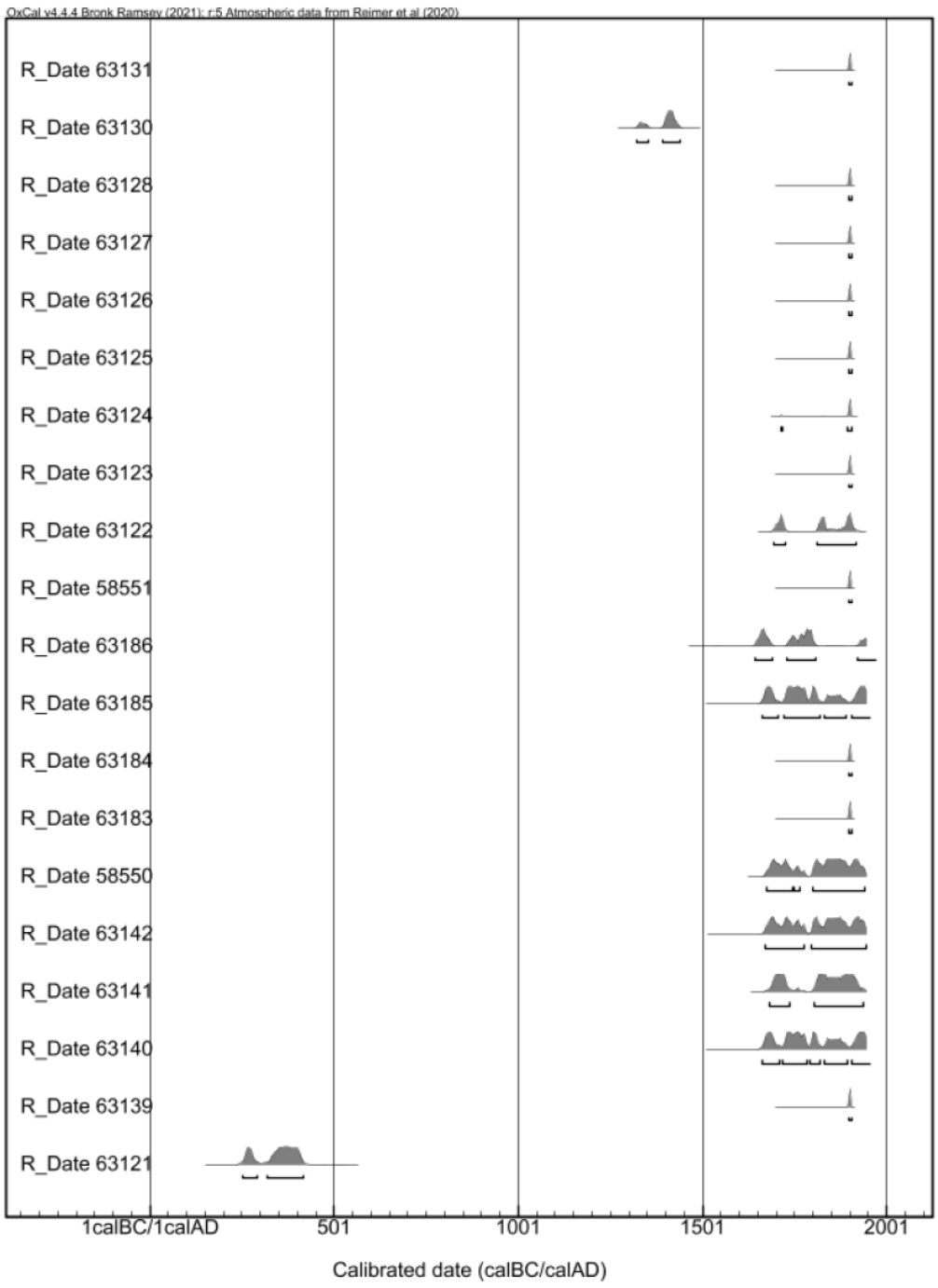
OxCal v4.4.4 Bronk Ramsey (2021); r:5 Atmospheric data from Reimer et al (2020)
R_Date 63131
R_Date 63130
R_Date 63128
R_Date 63127
R_Date 63126
R_Date 63125
R_Date 63124
R_Date 63123
R_Date 63122
R_Date 58551
R_Date 63186
R_Date 63185
R_Date 63184
R_Date 63183
R_Date 58550
R_Date 63142
R_Date 63141
R_Date 63140
R_Date 63139
R_Date 63121
1calBC/1calAD
501
1001
1501
2001
Calibrated date (calBC/calAD)

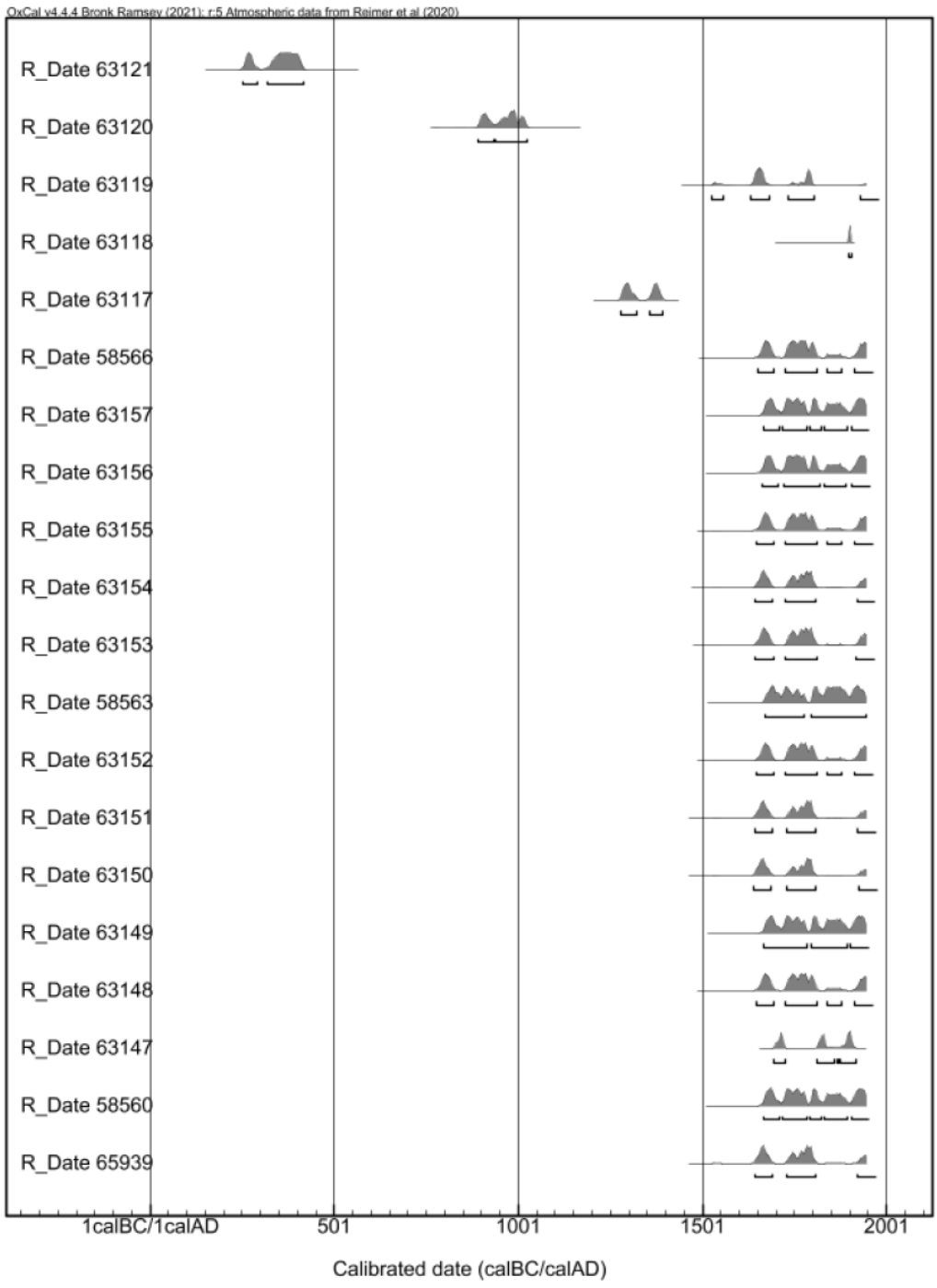
OxCal v4.4.4 Bronk Ramsey (2021); r:5 Atmospheric data from Reimer et al (2020)
R_Date 63121
R_Date 63120
R_Date 63119
R_Date 63118
R_Date 63117
R_Date 58566
R_Date 63157
R_Date 63156
R_Date 63155
R_Date 63154
R_Date 63153
R_Date 58563
R_Date 63152
R_Date 63151
R_Date 63150
R_Date 63149
R_Date 63148
R_Date 63147
R_Date 58560
R_Date 65939
1calBC/1calAD
501
1001
1501
2001
Calibrated date (calBC/calAD)

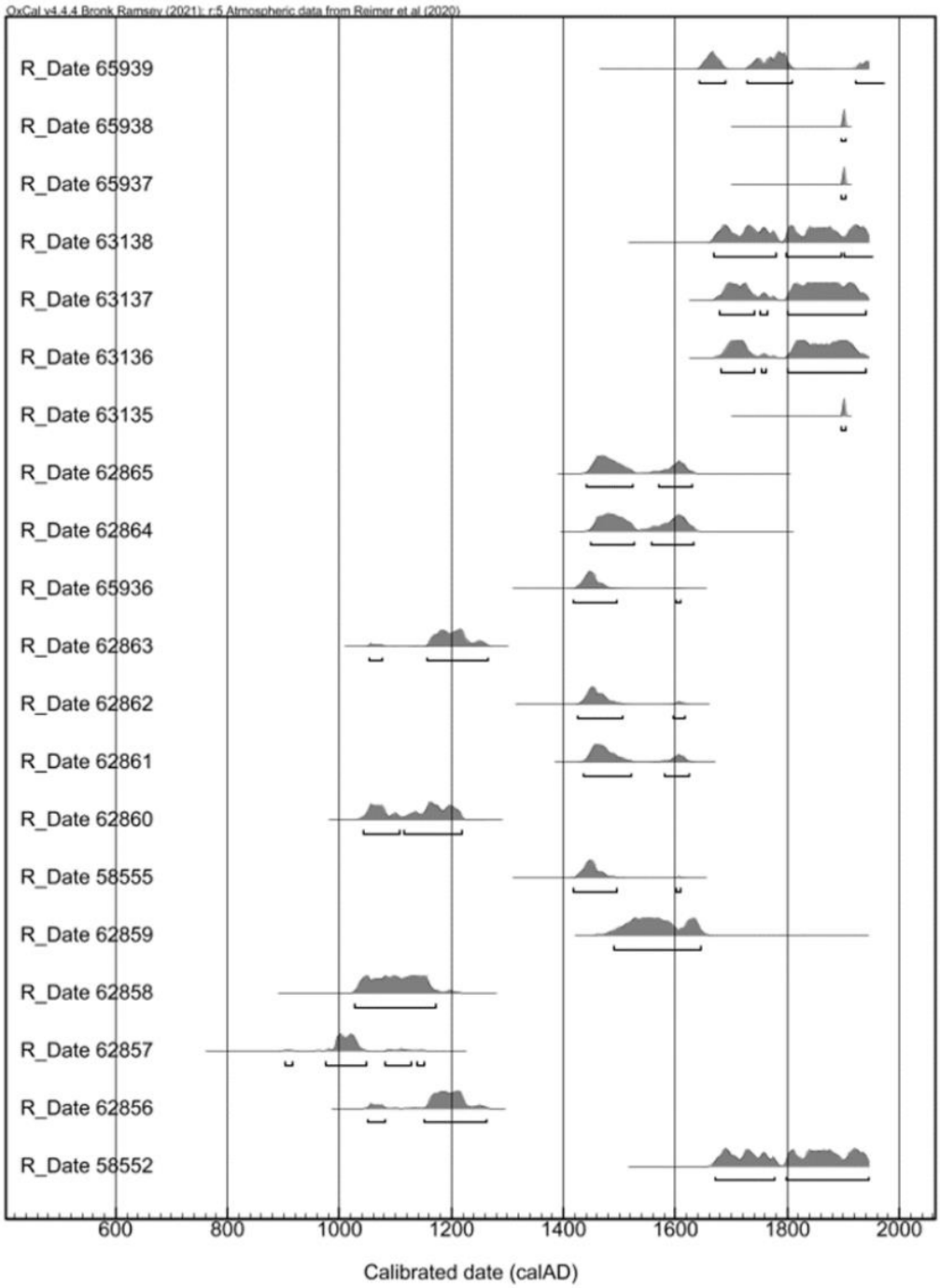


**Figure SI 6** Modeling dating outcomes for the olive wood cores from Bchaaleh.

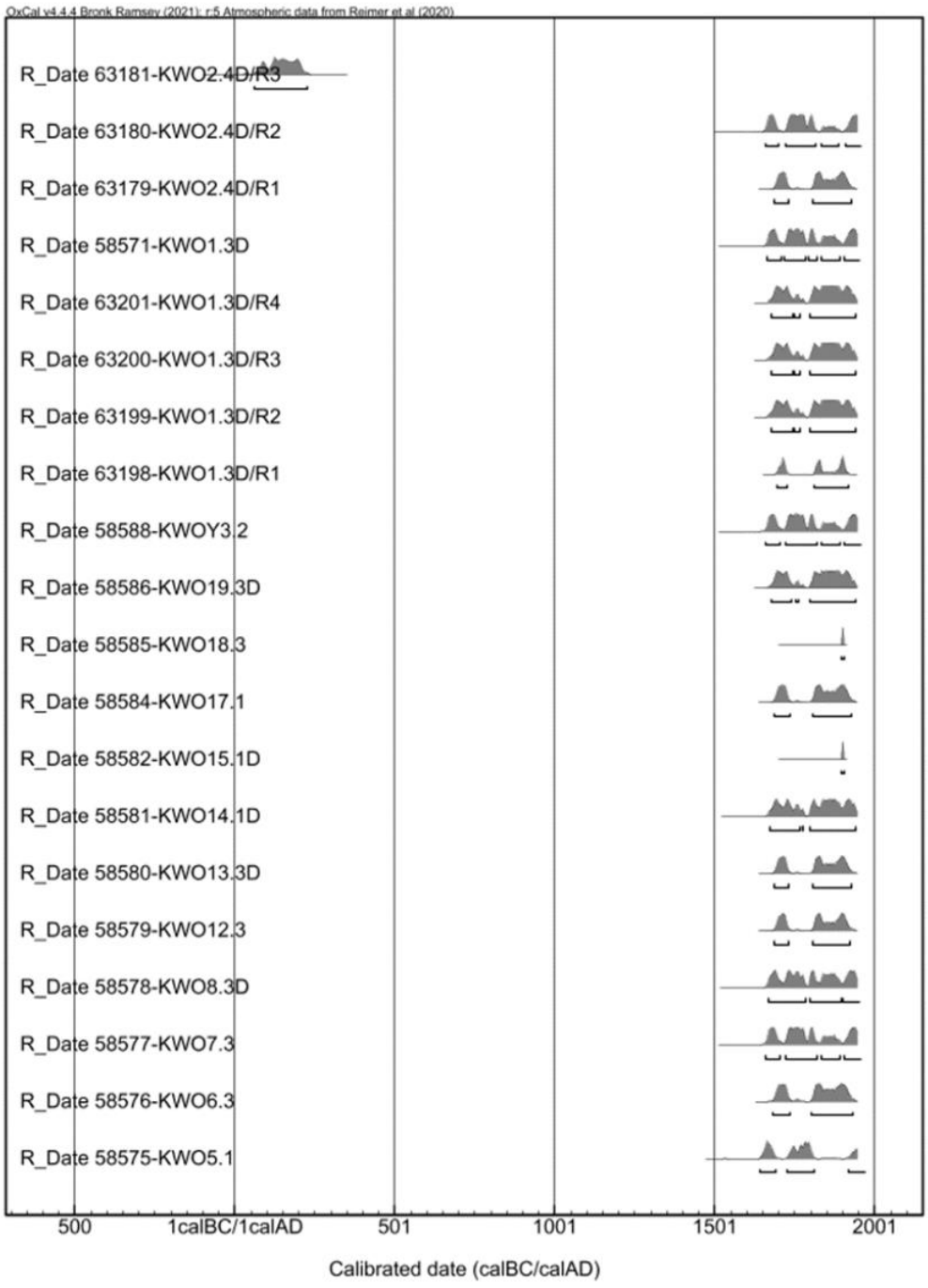
OxCal v4.4.4 Bronk Ramsey (2021); r:5 Atmospheric data from Reimer et al (2020)
R_Date 63181-KWO2.4D/R3
R_Date 63180-KWO2.4D/R2
R_Date 63179-KWO2.4D/R1
R_Date 58571-KWO1.3D
R_Date 63201-KWO1.3D/R4
R_Date 63200-KWO1.3D/R3
R_Date 63199-KWO1.3D/R2
R_Date 63198-KWO1.3D/R1
R_Date 58588-KWOY3.2
R_Date 58586-KWO19.3D
R_Date 58585-KWO18.3
R_Date 58584-KWO17.1
R_Date 58582-KWO15.1D
R_Date 58581-KWO14.1D
R_Date 58580-KWO13.3D
R_Date 58579-KWO12.3
R_Date 58578-KWO8.3D
R_Date 58577-KWO7.3
R_Date 58576-KWO6.3
R_Date 58575-KWO5.1
500
1calBC/1calAD
501
1001
1501
2001
Calibrated date (calBC/calAD)

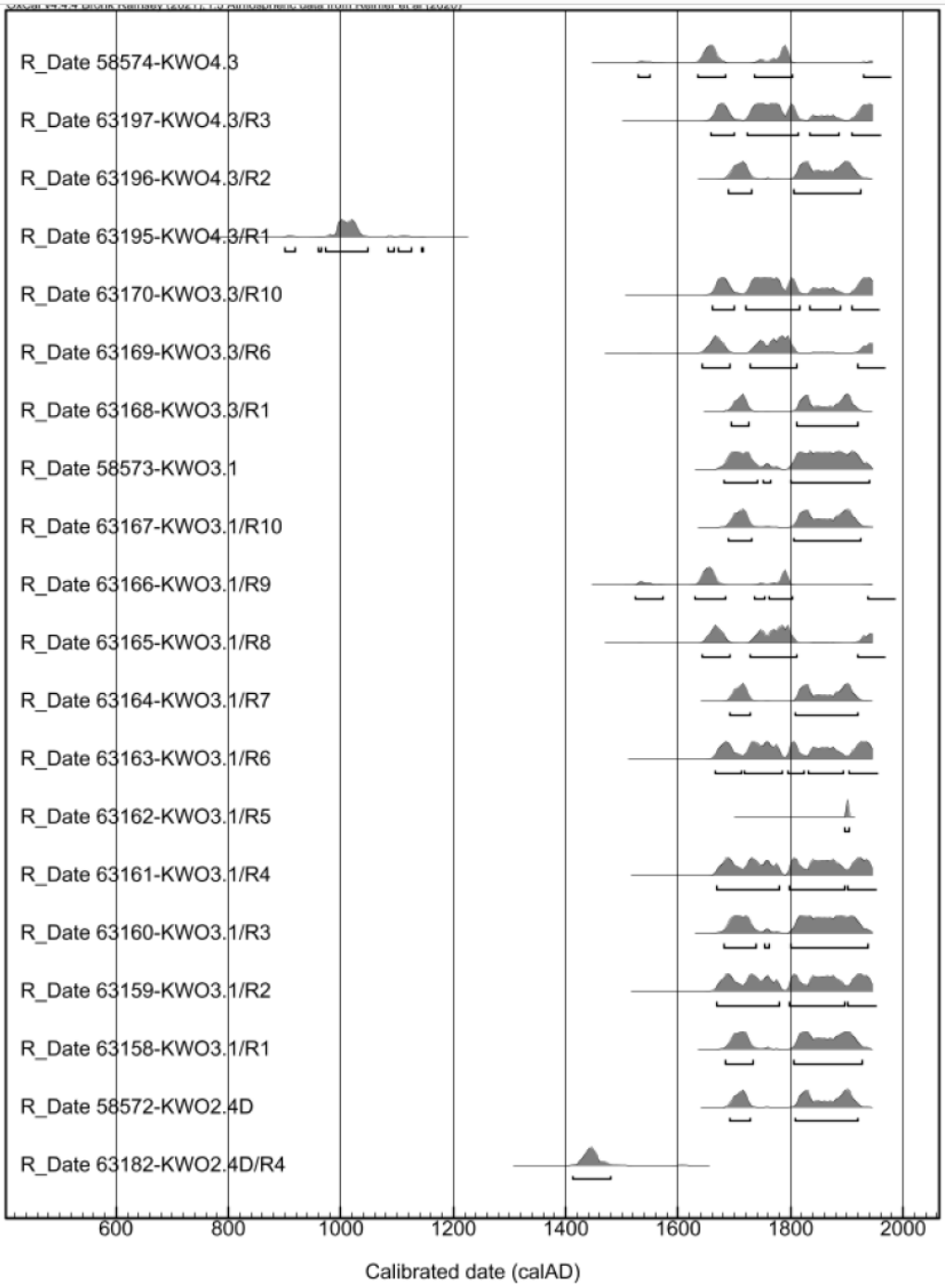
R_Date 58574-KWO4.3
R_Date 63197-KWO4.3/R3
R_Date 63196-KWO4.3/R2
R_Date 63195-KWO4.3/R1
R_Date 63170-KWO3.3/R10
R_Date 63169-KWO3.3/R6
R_Date 63168-KWO3.3/R1
R_Date 58573-KWO3.1
R_Date 63167-KWO3.1/R10
R_Date 63166-KWO3.1/R9
R_Date 63165-KWO3.1/R8
R_Date 63164-KWO3.1/R7
R_Date 63163-KWO3.1/R6
R_Date 63162-KWO3.1/R5
R_Date 63161-KWO3.1/R4
R_Date 63160-KWO3.1/R3
R_Date 63159-KWO3.1/R2
R_Date 63158-KWO3.1/R1
R_Date 58572-KWO2.4D
R_Date 63182-KWO2.4D/R4
600
800
1000
1200
1400
1600
1800
2000
Calibrated date (calAD)

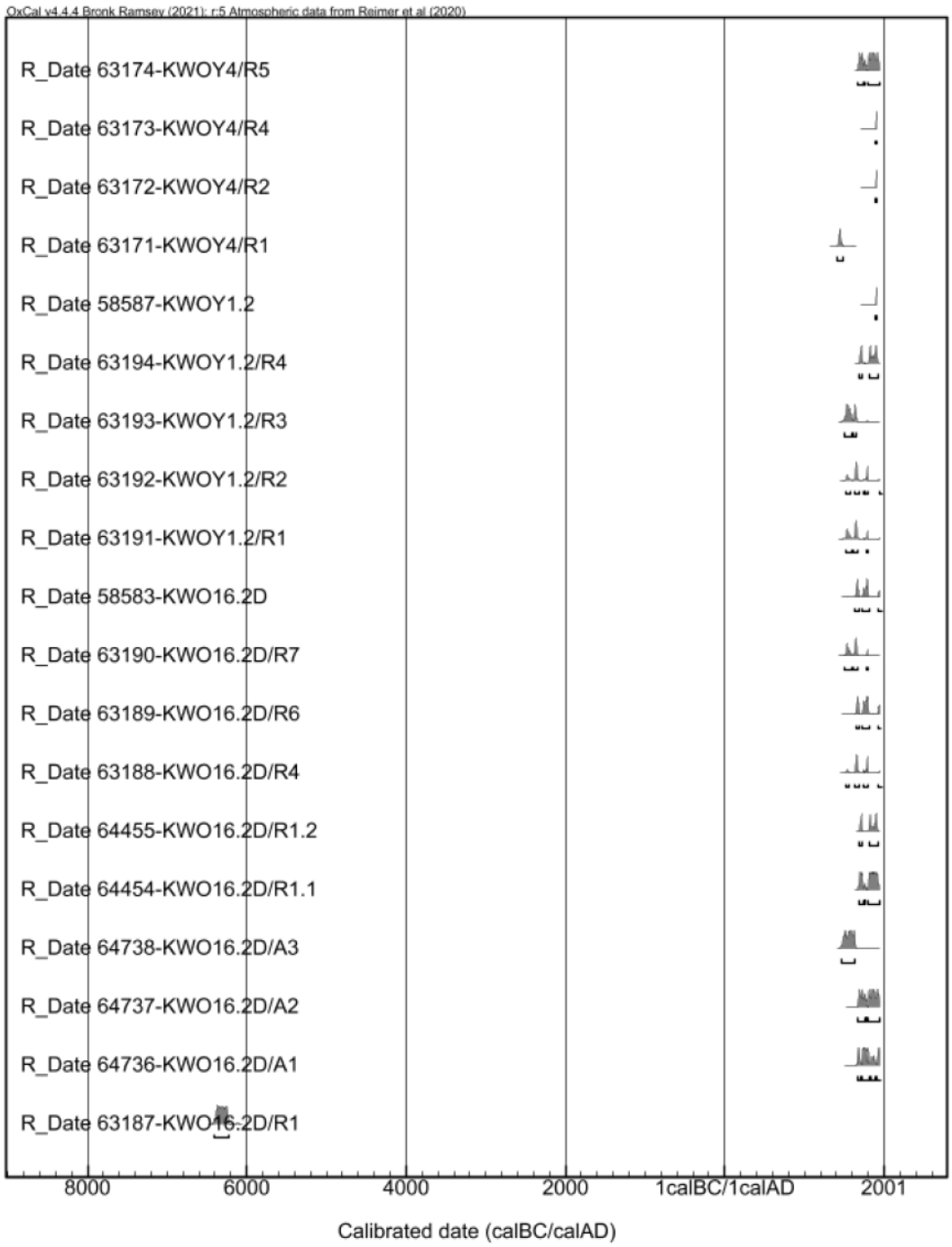


**Figure SI 7** Modeling dating outcomes for the olive wood cores from Kawkaba.

**Table SI 4** Wood core samples analyzed using $\delta^{13}C$, radiocarbon dating, densitometry and X ray tomography (X) indicates the analysis done to the mentioned sample.

| Site | Bchaaleh | Olive | Altitude:1300 m.a.s.l | | | | | | |
|---|---|---|---|---|---|---|---|---|---|
| Tree no. | Core reference no. | Height of | Length of Core | Number of parts | Date of collection | d13C | C14 | X Ray Densitometry | X-Ray Tomography |
| Tree 1 | O1.1 | 60 | 10.2 | 3 | 3/04/2019 | | | | |
| | O1.1D | 64 | 12.1 | 3 | 3/04/2019 | | X | | X |
| | O1.2 | 70 | 15.6 | 2 | 3/04/2019 | | | | |
| | O1.2D | 64 | 17.3 | 5 | 3/04/2019 | | | | X |
| | O1.3 | 56 | 7.9 | 4 | 3/04/2019 | | | | |
| | O1.3D | 72 | 9.5 | | 3/04/2019 | | | | |
| | | | | | | | | | |
| Tree 2 | O2.1 | 147 | 9.6 | 2 | 3/04/2019 | | | | |
| | O2.1D | 143 | 11.2 | 5 | 3/04/2019 | | X | | |
| | O2.2 | 127 | 11.8 | 1 | 3/04/2019 | | | | |
| | O2.2D | 119 | 7 | 2 | 3/04/2019 | | | X | |
| | O2.3 | 73 | 15.8 | 6 | 3/04/2019 | | | | X |
| | O2.4 | 133 | 6.8 | 2 | 3/04/2019 | | | | |
| | | | | | | | | | |
| Tree 3 | O3.1 | 55 | 7.1 | 3 | 3/04/2019 | | | | |
| | O3.1D | 57 | 11.3 | 3 | 3/04/2019 | | X | | |
| | O3.2 | 140 | 8.4 | 6 | 3/04/2019 | | | | |
| | O3.2D | 143 | 12 | 8 | 3/04/2019 | | | | |
| | O3.3 | 141 | 18 | 4 | 3/04/2019 | | | | X |
| | O3.3D | 148 | 13.7 | 3 | 3/04/2019 | | | | |
| | | | | | | | | | |
| Tree 4 | O4.1 | 124 | 19.5 | 5 | 16/03/2019 | | | | |
| | O4.1D | 132 | 14.9 | 5 | 3/04/2019 | | X | | X |
| | O4.2 | 132 | 11.4 | 5 | 16/03/2019 | | | | |
| | O4.3 | 105 | 5.5 | 3 | 16/03/2019 | | | | |
| | O4.3D | 110 | 13 | 3 | 16/03/2019 | | | | |
| | O4.4 | 124 | 17.3 | 5 | 3/04/2019 | X | X | | X |
| | | | | | | | | | |
| Tree 5 | O5.1 | 40 | 7.7 | 2 | 3/04/2019 | | | | |
| | O5.1D | 47 | 6.3 | 2 | 3/04/2019 | | | | |
| | O5.2 | 90 | 7.9 | 3 | 3/04/2019 | | | | |
| | O5.2D | 95 | 9.4 | 2 | 3/04/2019 | | | | |
| | O5.3 | 24 | 8.8 | 3 | 3/04/2019 | | X | | |
| | O5.3D | 43 | 10.3 | 3 | 3/04/2019 | | | | X |
| | | | | | | | | | |

| | | | | | | | | | |
|---|---|---|---|---|---|---|---|---|---|
| Tree 6 | O6.1 | 28 | 12 | 3 | 4/04/2019 | | X | | |
| | O6.1D | 35 | 10.8 | 3 | 4/04/2019 | | | | |
| | O6.2 | 40 | 3.9 | 2 | 4/04/2019 | | | | |
| | O6.2D | 37 | 6 | 2 | 4/04/2019 | | | | |
| | O6.3 | 100 | 17.2 | 4 | 4/04/2019 | | | | |
| | O6.3D | 106 | 12.5 | 4 | 4/04/2019 | | | | X |
| | | | | | | | | | |
| Tree 7 | O7.1 | 115 | 3.5 | 1 | 16/03/2019 | | | | |
| | O7.1D | 97 | 9.4 | 1 | 16/03/2019 | | | | |
| | O7.2 | 94 | 15.1 | 5 | 16/03/2019 | | X | | |
| | O7.2D | 74 | 6.2 | 2 | 4/04/2019 | | | | |
| | O7.3 | 60 | 11 | 4 | 4/04/2019 | | | | |
| | O7.3D | 75 | 13.9 | 4 | 4/04/2019 | | | | X |
| | | | | | | | | | |
| Tree 8 | O8.1 | 117 | 8.2 | 7 | 4/04/2019 | | | | |
| | O8.1D | 105 | 9.4 | 4 | 4/04/2019 | | | | |
| | O8.2 | 104 | 18.3 | 4 | 4/04/2019 | | | | |
| | O8.2D | 105 | 15.7 | 6 | 4/04/2019 | | X | | |
| | O8.3 | 120 | 12.5 | 8 | 4/04/2019 | | | | |
| | O8.3D | 107 | 12.6 | 7 | 4/04/2019 | | | | |
| | | | | | | | | | |
| Tree 9 | O9.1 | | 12.5 | 5 | 4/04/2019 | | | | |
| | O9.1D | 120 | 11.7 | 7 | 4/04/2019 | X | X | | X |
| | O9.2 | 130 | 12.6 | 10 | 4/04/2019 | | | | |
| | O9.2D | 120 | 8 | 2 | 4/04/2019 | | | | |
| | O9.3 | 40 | 9.4 | 4 | 4/04/2019 | | | | |
| | O9.3D | 50 | 6.1 | 4 | 4/04/2019 | | | | |
| | | | | | | | | | |
| Tree 10 | O10.1 | 63 | 6.9 | 6 | 26/04/2019 | | | | |
| | O10.1D | 70 | 6.1 | 6 | 26/04/2019 | | | | |
| | O10.2 | 112 | 13 | 4 | 26/04/2019 | | X | | |
| | O10.2D | 117 | 18 | 7 | 26/04/2019 | | | | |
| | O10.3 | 67 | 12.7 | 5 | 26/04/2019 | | | | |
| | O10.3D | 65 | 16.8 | 12 | 26/04/2019 | | | | |
| | | | | | | | | | |

| | | | | | | | | | |
|---|---|---|---|---|---|---|---|---|---|
| **Tree 11** | O11.1 | 105 | 17.8 | 7 | 26/04/2019 | | | | |
| | O11.1D | 110 | 18 | 4 | 26/04/2019 | | | | |
| | O11.2 | 175 | 16 | 8 | 26/04/2019 | | | | |
| | O11.2D | 180 | 16.3 | 5 | 26/04/2019 | | **X** | | **X** |
| | O11.3 | 150 | 12.6 | 6 | 26/04/2019 | | | | |
| | O11.3D | 130 | 10.5 | 2 | 26/04/2019 | | | | |
| | | | | | | | | | |
| **Tree 12** | O12.1 | 35 | 11 | 6 | 26/04/2019 | | | | |
| | O12.1D | 30 | 9.8 | 11 | 26/04/2019 | | | | |
| | O12.2 | 50 | 17.1 | 6 | 26/04/2019 | | | | |
| | O12.2D | 45 | 10 | 3 | 26/04/2019 | | | | |
| | O12.3 | 130 | 17.9 | 4 | 26/04/2019 | | | | |
| | O12.3D | 122 | 16.5 | 7 | 26/04/2019 | | **X** | | **X** |
| | | | | | | | | | |
| **Tree 13** | O13.1 | 60 | 15.1 | 5 | 26/04/2019 | | | | |
| | O13.1D | 56 | 10.2 | 5 | 26/04/2019 | | | | |
| | O13.2 | 55 | 9.2 | 4 | 26/04/2019 | | | | |
| | O13.2D | 40 | 16.8 | 4 | 26/04/2019 | | | | |
| | O13.3 | 145 | 13.5 | 5 | 26/04/2019 | | **X** | | |
| | O13.3D | 140 | 12.3 | 6 | 26/04/2019 | | | | |
| | | | | | | | | | |
| **Tree 14** | O14.1 | 80 | 17 | 5 | 26/04/2019 | | | | |
| | O14.1D | 86 | 12.3 | 3 | 26/04/2019 | | | | |
| | O14.2 | 38 | 16.3 | 8 | 26/04/2019 | | **X** | | |
| | O14.2D | 46 | 11.8 | 4 | 26/04/2019 | | | | |
| | O14.3 | 78 | 11.8 | 9 | 29/04/2019 | | | | |
| | O14.3D | 70 | 14.1 | 7 | 29/04/2019 | | | | |
| | | | | | | | | | |
| **Tree 15** | O15.1 | 53 | 13.2 | 6 | 29/04/2019 | | | | |
| | O15.1D | 55 | 10.5 | 4 | 29/04/2019 | | | | |
| | O15.2 | 57 | 16.2 | 6 | 29/04/2019 | | | | |
| | O15.2D | 56 | 18.3 | 5 | 29/04/2019 | | **X** | | **X** |
| | O15.3 | 110 | 17.2 | 6 | 29/04/2019 | | | | |
| | O15.3D | 97 | 15.2 | 3 | 29/04/2019 | | | | |
| | | | | | | | | | |

| | | | | | | | | | |
|---|---|---|---|---|---|---|---|---|---|
| Tree 3 | O3.1 | 90 | 17.7 | 7 | 30/04/2019 | | X | | X |
| | O3.1D | 80 | 17.4 | 2 | 30/04/2019 | | | | |
| | O3.2 | 102 | 16.3 | 5 | 30/04/2019 | | | | |
| | O3.2D | 98 | 13.1 | 10 | 30/04/2019 | | | | |
| | O3.3 | 70 | 21.2 | 8 | 30/04/2019 | | X | | X |
| | O3.3D | 69 | 6.8 | 4 | 30/04/2019 | | | | |
| | | | | | | | | | |
| Tree 4 | O4.1 | 60 | 17.3 | 1 | 15/03/2019 | | | | X |
| | O4.1D | 55 | 5.6 | 1 | 15/03/2019 | | | | |
| | O4.2 | 40 | 16.2 | 5 | 15/03/2019 | | | | |
| | O4.2D | 37 | 11.7 | 2 | 15/03/2019 | | | | |
| | O4.3 | 114 | 13 | 5 | 7/05/2019 | | X | | X |
| | O4.3D | 110 | 8.5 | 4 | 7/05/2019 | | | | |
| | | | | | | | | | |
| Tree 5 | O5.1 | 143 | 13.7 | 10 | 7/05/2019 | | X | | |
| | O5.1D | 135 | 9.5 | 2 | 7/05/2019 | | | | |
| | O5.2 | 131 | 13.8 | 8 | 7/05/2019 | | | | |
| | O5.2D | 127 | 18.6 | 8 | 7/05/2019 | | | | |
| | O5.3 | 108 | 16.5 | 8 | 7/05/2019 | | | | X |
| | O5.3D | 98 | 15.7 | 11 | 7/05/2019 | | | | |
| | | | | | | | | | |
| Tree 6 | O6.1 | 110 | 11.7 | 9 | 7/05/2019 | | | | |
| | O6.1D | 98 | 16.2 | 8 | 7/05/2019 | | | | |
| | O6.2 | 130 | 8.5 | 7 | 7/05/2019 | | | | |
| | O6.2D | 124 | 11.6 | 8 | 7/05/2019 | | | | |
| | O6.3 | 76 | 12.5 | 5 | 7/05/2019 | | X | | |
| | O6.3D | 70 | 15.7 | 9 | 7/05/2019 | | | | |
| | | | | | | | | | |
| Tree 7 | O7.1 | 57 | 16.1 | 10 | 30/04/2019 | | | | |
| | O7.1D | 63 | 16.9 | 6 | 30/04/2019 | | | | |
| | O7.2 | 105 | 11.5 | 10 | 30/04/2019 | | | | |
| | O7.2D | 100 | 5.5 | 10 | 30/04/2019 | | | | |
| | O7.3 | 130 | 10.6 | 5 | 30/04/2019 | | X | | |
| | O7.3D | 127 | 18.2 | 8 | 30/04/2019 | | | | |
| | | | | | | | | | |
| Tree 8 | O8.1 | 114 | 19.5 | 6 | 30/04/2019 | | | | |
| | O8.1D | 108 | 18 | 12 | 30/04/2019 | | | | |
| | O8.2 | 98 | 20.3 | 6 | 30/04/2019 | | | | |
| | O8.2D | 90 | 18 | 19 | 30/04/2019 | | | | |
| | O8.3 | 103 | 12 | 4 | 30/04/2019 | | | | |
| | O8.3D | 95 | 13.6 | 15 | 30/04/2019 | | X | | |
| | | | | | | | | | |
| Tree 12 | O12.1 | 24 | 17.3 | 8 | 7/05/2019 | | | | |
| | O12.1D | 30 | 15.2 | 9 | 7/05/2019 | | | | |
| | O12.2 | 120 | 4 | | 7/05/2019 | | | | |
| | O12.2D | 140 | 8.8 | 3 | 7/05/2019 | | | | |
| | O12.3 | 130 | 12.3 | 10 | 7/05/2019 | | X | | |
| | O12.3D | 115 | 13.5 | 3 | 7/05/2019 | | | | |
| | O12.4 | 120 | 10 | 5 | 7/05/2019 | | | | |
| | | | | | | | | | |

| | | | | | | | | | |
|---|---|---|---|---|---|---|---|---|---|
| Tree 16 | O16.1 | 57 | 17.9 | 7 | 29/04/2019 | | | | |
| | O16.1D | 56 | 14.8 | 3 | 29/04/2019 | | | | |
| | O16.2 | 125 | 16.5 | 5 | 29/04/2019 | | X | | X |
| | O16.2D | 130 | 13 | 4 | 29/04/2019 | | | | |
| | O16.3 | 55 | 15.4 | 8 | 29/04/2019 | | | | |
| | O16.3D | 50 | 16.3 | 8 | 29/04/2019 | | | | |
| | | | | | | | | | |
| Tree 1 | YO1.1 | 94 | 18.4 | 9 | 4/05/2019 | | | | |
| | YO1.2 | 90 | 20.4 | 5 | 4/05/2019 | | X | | X |
| | YO1.3 | 77 | 14.8 | 5 | 4/05/2019 | | X | | X |
| | | | | | | | | | |
| Tree 2 | YO2.1 | 70 | 21 | 6 | 4/05/2019 | | X | | X |
| | YO2.2 | 75 | 19.8 | 6 | 4/05/2019 | | | | |
| | YO2.3 | 62 | 17.3 | 13 | 4/05/2019 | | | | |
| | | | | | | | | | |
| Tree 3 | YO3.1 | 75 | 17 | 7 | 4/05/2019 | | | | |
| | YO3.2 | 85 | 15.2 | 4 | 4/05/2019 | | | | |
| | YO3.3 | 88 | 19 | 7 | 4/05/2019 | | | | |
| | | | | | | | | | |
| Tree 4 | BCOY4 | 100 | 16 | 7 | 20/09/2020 | | X | | X |
| | | | | | | | | | |
| Tree 5 | BCOY5 | 100 | 15.8 | 10 | 20/09/2020 | | X | | X |
| **Site** | **Kawkaba** | **Olive** | **Altitude: 672 m.a.s.l** | | | | | | |
| **Tree no.** | **Core reference no.** | **Height of** | **Length of Core** | | **Date of collection** | | **C14** | **Xray Densitometry** | **X-Ray Tomography** |
| Tree 1 | O1.1 | 60 | 21.5 | 4 | 15/03/2019 | | | | |
| | O1.1D | 55 | 15.8 | 3 | 30/04/2019 | | | | |
| | O1.2 | 73 | 14.4 | 1 | 15/03/2019 | | | X | |
| | O1.2D | 72 | 10.6 | 1 | 15/03/2019 | | | | |
| | O1.3 | 103 | 12.9 | 4 | 30/04/2019 | | | | |
| | O1.3D | 100 | 13.6 | 4 | 30/04/2019 | | X | | X |
| | | | | | | | | | |
| Tree 2 | O2-Trial | 100 | 2.3 | 1 | 15/03/2019 | | | | |
| | O2.1 | 100 | 6.5 | 3 | 15/03/2019 | | | | |
| | O2.2 | 93 | 9.7 | 2 | 15/03/2019 | | | | |
| | O2.2D | 103 | 12.8 | 1 | 15/03/2019 | | | | |
| | O2.3 | 130 | 10.9 | 12 | 15/03/2019 | | | | |
| | O2.3D | 135 | 3.5 | 2 | 30/04/2019 | | | | |
| | O2.4 | 130 | 18 | 5 | 30/04/2019 | | | | X |
| | O2.4D | 125 | 12.7 | 4 | 30/04/2019 | | X | | |
| | | | | | | | | | |

| | | | | | | | | | |
|---|---|---|---|---|---|---|---|---|---|
| **Tree 13** | O13.1 | 126 | 14.7 | 5 | 7/05/2019 | | | | |
| | O13.1D | 122 | 14.8 | 5 | 7/05/2019 | | | | |
| | O13.2 | 138 | 5.9 | 4 | 7/05/2019 | | | | |
| | O13.2D | 135 | 9.2 | 8 | 7/05/2019 | | | | |
| | O13.3 | 138 | 19 | 13 | 7/05/2019 | | | | |
| | O13.3D | 129 | 13.3 | 10 | 7/05/2019 | | X | | |
| | | | | | | | | | |
| **Tree 14** | O14.1 | 70 | 17.5 | 4 | 7/05/2019 | | | | |
| | O14.1D | 74 | 12.3 | 5 | 7/05/2019 | | X | | |
| | O14.2 | 108 | 19.7 | 13 | 7/05/2019 | | | | |
| | O14.2D | 101 | 15.3 | 14 | 7/05/2019 | | | | |
| | O14.3 | 122 | 10.5 | 2 | 7/05/2019 | | | | |
| | O14.3D | 118 | 9.5 | 3 | 7/05/2019 | | | | |
| | | | | | | | | | |
| **Tree 15** | O15.1 | 115 | 7.4 | 4 | 7/05/2019 | | | | |
| | O15.1D | 108 | 14.5 | 5 | 7/05/2019 | | X | | X |
| | O15.2 | 111 | 17.4 | 5 | 7/05/2019 | | | | |
| | O15.2D | 106 | 19 | 2 | 7/05/2019 | | | | |
| | O15.3 | 108 | 17.5 | 4 | 7/05/2019 | | | | |
| | O15.3D | 105 | 16.8 | 5 | 7/05/2019 | | | | |
| | | | | | | | | | |
| **Tree 16** | O16.1 | 50 | 16.7 | 12 | 12/05/2019 | | | | |
| | O16.1D | 47 | 18 | 10 | 12/05/2019 | | | | |
| | O16.2 | 70 | 16.5 | 6 | 12/05/2019 | | | | |
| | O16.2D | 63 | 19.9 | 7 | 12/05/2019 | | X | | X |
| | O16.3 | 87 | 18 | 5 | 12/05/2019 | | | | |
| | O16.3D | 91 | 14.3 | 10 | 12/05/2019 | | | | |
| | | | | | | | | | |
| **Tree 17** | O17.1 | 83 | 20.5 | 13 | 12/05/2019 | | X | | |
| | O17.1D | 84 | 15 | 6 | 12/05/2019 | | | | |
| | O17.2 | 103 | 10.5 | 6 | 12/05/2019 | | | | |
| | O17.2D | 95 | 20 | 3 | 12/05/2019 | | | | |
| | O17.3 | 112 | 18.3 | 5 | 12/05/2019 | | | | |
| | O17.3D | 106 | 10.6 | 2 | 12/05/2019 | | | | |
| | | | | | | | | | |
| **Tree 18** | O18.1 | 85 | 20 | 8 | 12/05/2019 | | | | |
| | O18.1D | 78 | 13.9 | 7 | 12/05/2019 | | | | |
| | O18.2 | 95 | 21 | 6 | 12/05/2019 | | | | |
| | O18.2D | 88 | 20 | 4 | 12/05/2019 | | | | |
| | O18.3 | 60 | 20 | 14 | 12/05/2019 | | X | | X |
| | O18.3D | 54 | 19 | 9 | 12/05/2019 | | | | |
| | | | | | | | | | |
| **Tree 19** | O19.1 | 67 | 15.8 | 4 | 12/05/2019 | | | | |
| | O19.1D | 68 | 20 | 12 | 12/05/2019 | | | | |
| | O19.2 | 80 | 19.5 | 3 | 12/05/2019 | | | | |
| | O19.2D | 73 | 20 | 6 | 12/05/2019 | | | | |
| | O19.3 | 58 | 20.6 | 7 | 12/05/2019 | | | | |
| | O19.3D | 50 | 21 | 9 | 12/05/2019 | | X | | |
| | | | | | | | | | |

| | | | | | | | | | |
|---|---|---|---|---|---|---|---|---|---|
| **Tree 1** | YO1.1 | 75 | 9.5 | 5 | 12/05/2019 | | | | |
| | YO1.2 | 68 | 18.9 | 8 | 12/05/2019 | | X | | X |
| | YO1.3 | 42 | 17.5 | 10 | 12/05/2019 | | | | |
| | | | | | | | | | |
| **Tree 2** | YO2.1 | 55 | 15.8 | 11 | 12/05/2019 | | | | X |
| | YO2.2 | 62 | 12.4 | 9 | 12/05/2019 | | | | |
| | YO2.3 | 82 | 18.2 | 12 | 12/05/2019 | | | | X |
| | | | | | | | | | |
| **Tree 3** | YO3.1 | 70 | 14.9 | 14 | 12/05/2019 | | | | |
| | YO3.2 | 70 | 20 | 9 | 12/05/2019 | | X | | |
| | YO3.3 | 71 | 19.5 | 8 | 12/05/2019 | | | | |
| | | | | | | | | | |
| **Tree 4** | YO4 | 100 | 12.9 | 6 | 15/09/2020 | | X | | X |

**Table SI 5** Ring width and calibrated dating of tomographed and radiocarbon dated wood cores.

**Table SI 6** Radiocarbon dated wood samples with celebrated dates using Oxcal.

| N° Sack | Tree number | Référence échantillon | Nature | mg C | Delta C13 | pMC | Err pMC | Age BP | Err âge BP | FC14 | FC14 Error | Unmodelled BC/AD | from | to | BC/AD | % | mu | sigma | median |
|---|---|---|---|---|---|---|---|---|---|---|---|---|---|---|---|---|---|---|---|
| 58553 | BC-2 | BC-O2.1D | Wood | 1.02 | -22.7 | 97.67358 | 0.23417 | 190 | 30 | 1.0434014 | 0.0026193 | R_Date 5553 | 1649 | AD | AD | 95.4 | 1778 | 86 | 1768 |
| 58554 | BC-3 | BC-O3.1D | Wood | 1.24 | -31.2 | 104.24014 | 0.26193 | Postérieur à 1950 | | 1.0434014 | 0.0026193 | R_Date(1.0434,0.0026193) | 1956 | 2009 | AD | 95.4 | 1974 | 25 | 1956 |
| 58556 | BC-5 | BC-O5.3 | Wood | 1.13 | -23.5 | 110.54415 | 0.28607 | Postérieur à 1950 | | 1.1054415 | 0.0028607 | R_Date(1.10544,0.0028607) | 1957 | 1999 | AD | 95.4 | 1996 | 8 | 1997 |
| 58557 | BC-6 | BC-O6.1 | Wood | 0.79 | -21.8 | 112.65179 | 0.26113 | Postérieur à 1950 | | 1.1265179 | 0.0026113 | R_Date(1.12652,0.0026113) | 1958 | 1996 | AD | 95.4 | 1992 | 9 | 1995 |
| 58558 | BC-7 | BC-O7.2 | Wood | 1.24 | -24.3 | 98.4447 | 0.24461 | 125 | 30 | | | R_Date 5558 | 1675 | 1942 | AD | 95.4 | 1818 | 79 | 1837 |
| 58559 | BC-8 | BC-O8.2D | Wood | 1.2 | -20.6 | 97.8298 | 0.23539 | 175 | 30 | | | R_Date 5559 | 1638 | ... | AD | 95.4 | 1790 | 87 | 1772 |
| 58561 | BC-10 | BC-O10.2 | Wood | 1.19 | -21.7 | 97.31251 | 0.24159 | 220 | 30 | | | R_Date 5561 | 1639 | ... | AD | 95.4 | 1742 | 83 | 1753 |
| 58562 | BC-11 | BC-O11.2D | Wood | 1.19 | -23.1 | 97.51344 | 0.25221 | 200 | 30 | | | R_Date 5562 | 1643 | ... | AD | 95.4 | 1768 | 84 | 1766 |
| 58564 | BC-13 | BC-13.3 | Wood | 1.08 | -20.9 | 97.98157 | 0.233 | 165 | 30 | | | R_Date 5564 | 1661 | ... | AD | 95.4 | 1797 | 86 | 1777 |
| 58565 | BC-14 | BC-O14.2 | Wood | 1.25 | -24 | 97.76115 | 0.25199 | 180 | 30 | | | R_Date 5565 | 1655 | ... | AD | 95.4 | 1786 | 86 | 1770 |
| 58567 | BC-16 | BC-O16.2 | Wood | 1.26 | -24 | 97.40366 | 0.24517 | 210 | 30 | | | R_Date 5567 | 1642 | ... | AD | 95.4 | 1756 | 83 | 1763 |
| 63202 | BC1 | BC01.1DR1 | Wood | 1.25 | -28.7 | 98.69 | 0.28 | 105 | 30 | | | R_Date 63202 | 1683 | 1936 | AD | 95.4 | 1821 | 77 | 1839 |
| 63203 | | BC01.1DR2 | Wood | 1.10 | -26.2 | 93.92 | 0.29 | 505 | 30 | | | R_Date 63203 | 1396 | 1450 | AD | 95.4 | 1420 | 20 | 1423 |
| 63204 | | BC01.1DR3 | Wood | 1.02 | -26.1 | 95.65 | 0.28 | 360 | 30 | | | R_Date 63204 | 1456 | 1635 | AD | 95.4 | 1545 | 55 | 1547 |
| 58552 | | BC-01.1D | Wood | 0.51 | -35.9 | 98.30 | 0.31 | 140 | 30 | | | R_Date 58552 | 1672 | 1944 | AD | 95.4 | 1812 | 82 | 1823 |
| 62856 | BC4-1 | BC04.1DR1 | Wood | 1.26 | -22.8 | 89.79223 | 0.27025 | 865 | 30 | | | R_Date 62856 | 1050 | 1262 | AD | 95.4 | 1183 | 46 | 1190 |
| 62857 | | BC04.1DR2 | Wood | 1.04 | -26.4 | 113.60566 | 0.28259 | 1025 | 30 | | | R_Date 62857 | 902 | 1150 | AD | 95.4 | 1020 | 39 | 1015 |
| 62858 | | BC04.1DR3 | Wood | 1.14 | -25.5 | 88.95605 | 0.24344 | 940 | 30 | | | R_Date 62858 | 1028 | 1172 | AD | 95.4 | 1102 | 42 | 1102 |
| 62859 | | BC04.1DR4 | Wood | 1.24 | -22.5 | 96.14363 | 0.25426 | 315 | 30 | | | R_Date 62859 | 1490 | 1646 | AD | 95.4 | 1566 | 46 | 1562 |
| 58555 | | BC-04.1D | Wood | 1.08 | -22.6 | 94.69142 | 0.2363 | 440 | 30 | | | R_Date 58555 | 1419 | 1610 | AD | 95.4 | 1455 | 31 | 1449 |
| 62860 | BC4-4 | BC04.4R1 | Wood | 1.13 | -26.5 | 89.38553 | 0.25719 | 900 | 30 | | | R_Date 62860 | 1042 | 1219 | AD | 95.4 | 1134 | 55 | 1150 |
| 62861 | | BC04.4R2 | Wood | 0.59 | -25.5 | 95.07877 | 0.26203 | 405 | 30 | | | R_Date 62861 | 1436 | 1624 | AD | 95.4 | 1498 | 56 | 1475 |
| 62862 | | BC04.4R3 | Wood | 1.1 | -19.7 | 94.86504 | 0.26028 | 425 | 30 | | | R_Date 62862 | 1425 | 1618 | AD | 95.4 | 1472 | 44 | 1458 |
| 62863 | | BC04.4R4 | Wood | 1.18 | -24.2 | 89.92708 | 0.25479 | 855 | 30 | | | R_Date 62863 | 1053 | 1264 | AD | 95.4 | 1194 | 41 | 1198 |
| 63916 | | BC04.4114 | Wood | 1.22 | -23 | 94.6596 | 0.27845 | 440 | 30 | | | R_Date 63916 | 1419 | 1610 | AD | 95.4 | 1455 | 31 | 1449 |
| 62864 | | BC04.4R5 | Wood | 1.22 | -24.5 | 95.45974 | 0.26568 | 375 | 30 | | | R_Date 62864 | 1450 | 1632 | AD | 95.4 | 1533 | 38 | 1512 |
| 62865 | | BC04.4R6 | Wood | 1 | -24.9 | 95.25196 | 0.26308 | 390 | 30 | | | R_Date 62865 | 1442 | 1631 | AD | 95.4 | 1517 | 39 | 1492 |
| 63135 | BC9 | BC09.1DR1 | Wood | 0.93 | -24.70 | 101.74244 | 0.27581 | Postérieur à 1950 | 35 | 1.01742 | 0.0027581 | R_F14C(1.01742,0.0027581) | 1955 | 1956 | AD | 95.4 | 1955 | 0 | 1955 |
| 63136 | | BC09.1DR2 | Wood | 0.28 | -25.50 | 98.75543 | 0.40781 | 100 | 30 | | | R_Date 63136 | 1681 | 1940 | AD | 95.4 | 1820 | 78 | 1837 |
| 63137 | | BC09.1DR3 | Wood | 1.01 | -26.10 | 98.53669 | 0.27642 | 120 | 30 | | | R_Date 63137 | 1679 | 1941 | AD | 95.4 | 1819 | 79 | 1838 |
| 63138 | | BC09.1DR4 | Wood | 0.95 | -22.50 | 98.18766 | 0.28187 | 145 | 30 | | | R_Date 63138 | 1669 | ... | AD | 95.4 | 1809 | 83 | 1813 |
| 65937 | | BC09.1D/52A | Wood | 1.28 | -22.5 | 124.76201 | 0.269 | Postérieur à 1950 | | 1.2476201 | 0.00269 | R_F14C(1.24762,0.00269) | 1959 | 1983 | AD | 95.4 | 1978 | 8 | 1982 |
| 65938 | | BC09.1D/91 | Wood | 1.04 | -20.9 | 133.75526 | 0.27585 | Postérieur à 1950 | | 1.3375526 | 0.0027585 | R_F14C(1.33755,0.0027585) | 1962 | 1978 | AD | 95.4 | 1976 | 4 | 1977 |
| 65939 | | BC09.1D/142 | Wood | 1 | -22.7 | 102.64249 | 0.2375 | 210 | 30 | | | R_Date 65939 | 1642 | ... | AD | 95.4 | 1756 | 83 | 1763 |
| 58560 | | BC-09.1D | Wood | 0.94 | -21.2 | 98.09507 | 0.23553 | 155 | 30 | | | R_Date 58560 | 1665 | ... | AD | 95.4 | 1804 | 85 | 1800 |
| 63147 | BC12 | BC012.3DR1 | Wood | 1.11 | -21 | 99.77849 | 0.29473 | 30 | 30 | | | R_Date 63147 | 1695 | 1917 | AD | 95.4 | 1819 | 77 | 1839 |
| 63148 | | BC012.3DR2 | Wood | 1 | -22.7 | 97.63805 | 0.31108 | 190 | 30 | | | R_Date 63148 | 1649 | ... | AD | 95.4 | 1778 | 86 | 1768 |
| 63149 | | BC012.3DR3 | Wood | 0.92 | -24.7 | 98.13195 | 0.30225 | 150 | 30 | | | R_Date 63149 | 1667 | ... | AD | 95.4 | 1807 | 84 | 1806 |
| 63150 | | BC012.3DR4 | Wood | 1.04 | -23 | 97.35088 | 0.27841 | 215 | 30 | | | R_Date 63150 | 1641 | ... | AD | 95.4 | 1749 | 83 | 1760 |
| 63151 | | BC012.3DR5 | Wood | 1.08 | -16.5 | 97.41449 | 0.27081 | 210 | 30 | | | R_Date 63151 | 1642 | ... | AD | 95.4 | 1756 | 83 | 1763 |
| 63152 | | BC012.3DR6 | Wood | 1.02 | -23.9 | 97.64191 | 0.25554 | 190 | 30 | | | R_Date 63152 | 1649 | ... | AD | 95.4 | 1778 | 86 | 1768 |
| 58563 | | BC-012.3D | Wood | 1.25 | -21 | 98.24987 | 0.24072 | 140 | 30 | | | R_Date 58563 | 1672 | 1944 | AD | 95.4 | 1812 | 82 | 1823 |
| 63153 | BC15 | BC015.2DR1 | Wood | 1.03 | -24 | 97.51699 | 0.30066 | 200 | 30 | | | R_Date 63153 | 1643 | ... | AD | 95.4 | 1768 | 84 | 1766 |
| 63154 | | BC015.2DR2 | Wood | 0.92 | -23.1 | 97.45718 | 0.27457 | 205 | 30 | | | R_Date 63154 | 1643 | ... | AD | 95.4 | 1762 | 84 | 1765 |
| 63155 | | BC015.2DR3 | Wood | 0.84 | -25.5 | 97.6588 | 0.28486 | 190 | 30 | | | R_Date 63155 | 1649 | ... | AD | 95.4 | 1778 | 86 | 1768 |
| 63156 | | BC015.2DR4 | Wood | 0.81 | -25.1 | 97.98939 | 0.27342 | 165 | 30 | | | R_Date 63156 | 1661 | ... | AD | 95.4 | 1797 | 86 | 1777 |
| 63157 | | BC015.2DR5 | Wood | 0.79 | -26.4 | 98.08387 | 0.27204 | 155 | 30 | | | R_Date 63157 | 1665 | ... | AD | 95.4 | 1804 | 85 | 1800 |
| 58566 | | BC-015.2D | Wood | 1.32 | -25.6 | 97.7005 | 0.25619 | 185 | 30 | | | R_Date 58566 | 1653 | ... | AD | 95.4 | 1782 | 86 | 1769 |

| | | | | | | | | | | | | | | | | | | | |
|---|---|---|---|---|---|---|---|---|---|---|---|---|---|---|---|---|---|---|---|
| 63117 | BCY1-2 | BCOY1.2/R1 | Wood | 1,04 | -27,10 | 91,97100 | 0,27194 | 670 | 30 | | | R_Date 63117 | 1277 | 1392 | AD | 95.4 | 1332 | 39 | 1316 |
| 63118 | | BCOY1.2/R2 | Wood | 1,19 | -26,10 | 134,86450 | 0,33236 | Postérieur à 1950 | | 1.34865 | 0.0033236 | R_F14C(1.34865,0.0033236) | 1962 | 1978 | AD | 95.4 | 1975 | 4 | 1976 |
| 63119 | | BCOY1.2/R3 | Wood | 1,08 | -24,00 | 97,06300 | 0,26861 | 240 | 30 | | | R_Date 63119 | 1526 | ... | AD | 95.4 | 1699 | 85 | 1663 |
| 63120 | | BCOY1.2/R4 | Wood | 1,04 | -23,40 | 87,40852 | 0,25787 | 1080 | 30 | | | R_Date 63120 | 892 | 1023 | AD | 95.4 | 959 | 40 | 967 |
| 63121 | | BCOY1.2/R5 | Wood | 1,00 | -25,60 | 80,85837 | 0,24445 | 1705 | 30 | | | R_Date 63121 | 252 | 418 | AD | 95.4 | 347 | 49 | 359 |
| 63139 | BCY1-3 | BCY01.3/R1 | Wood | 1,00 | -24,30 | 105,48816 | 0,29764 | Postérieur à 1950 | | 1.05488 | 0.0029764 | R_F14C(1.05488,0.0029764) | 1956 | ... | AD | 95.4 | 1999 | 19 | 2008 |
| 63140 | | BCY01.3/R2 | Wood | 1,02 | -23,80 | 98,01644 | 0,28724 | 160 | 30 | | | R_Date 63140 | 1663 | ... | AD | 95.4 | 1800 | 86 | 1784 |
| 63141 | | BCY01.3/R3 | Wood | 1,11 | -25,40 | 98,72711 | 0,27738 | 105 | 30 | | | R_Date 63141 | 1683 | 1936 | AD | 95.4 | 1821 | 77 | 1839 |
| 63142 | | BCY01.3/R4 | Wood | 1,05 | -27,30 | 98,25816 | 0,28964 | 140 | 30 | | | R_Date 63142 | 1672 | 1944 | AD | 95.4 | 1812 | 82 | 1823 |
| 58550 | | BC-YO1.3 | Wood | 1,27 | -19,9 | 98,38053 | 0,26047 | 130 | 30 | | | R_Date 58550 | 1675 | 1942 | AD | 95.4 | 1816 | 80 | 1835 |
| 63183 | BCY2 | BCOY2.1/R1 | Wood | 1,06 | -15,1 | 111,99 | 0,33 | Postérieur à 1950 | | 1.119918 | 0.0032834 | R_Date(1.11992,0.0032834) | 1957 | 1996 | AD | 95.4 | 1992 | 9 | 1995 |
| 63184 | | BCOY2.1/R6 | Wood | 0,93 | -24,3 | 103,41 | 0,30 | Postérieur à 1950 | | 1.0340713 | 0.0029555 | R_Date(1.03407,0.0029555) | 1955 | 1956 | AD | 95.4 | 1957 | 9.00 | 1956 |
| 63185 | | BCOY2.1/R7 | Wood | 0,96 | -23,0 | 97,98 | 0,28 | 165 | 30 | | | R_Date 63185 | 1661 | ... | AD | 95.4 | 1797 | 86 | 1777 |
| 63186 | | BCOY2.1/R9 | Wood | 0,93 | -20,0 | 97,45 | 0,29 | 210 | 30 | | | R_Date 63186 | 1642 | ... | AD | 95.4 | 1756 | 83 | 1763 |
| 58551 | | BC-YO2.1 | Wood | 0,69 | -30,8 | 121,66 | 0,30 | Postérieur à 1950 | | 1.21662 | 0.0030042 | R_F14C(1.21662,0.0030042) | 1959 | 1985 | AD | 95.4 | 1974 | 12 | 1984 |
| 63122 | BCY4 | BCOY4/R1 | Wood | 1,18 | -25,20 | 99,57617 | 0,27320 | 35 | 30 | | | R_Date 63122 | 1694 | 1917 | AD | 95.4 | 1819 | 77 | 1830 |
| 63123 | | BCOY4/R2 | Wood | 1,07 | -26,70 | 109,55544 | 0,29063 | Postérieur à 1950 | | 1.09555 | 0.00291 | R_F14C(1.09555,0.00291) | 1957 | 2001 | AD | 95.4 | 1996 | 11 | 2000 |
| 63124 | | BCOY4/R3 | Wood | 0,96 | -24,90 | 108,92941 | 0,29876 | Postérieur à 1950 | | 1.08929 | 0.00299 | R_F14C(1.08929,0.00299) | 1957 | 2002 | AD | 95.4 | 1997 | 12 | 2001 |
| 63125 | | BCOY4/R4 | Wood | 1,09 | -27,10 | 108,70719 | 0,28448 | Postérieur à 1950 | | 1.08707 | 0.00284 | R_F14C(1.08707,0.00284) | 1957 | 2002 | AD | 95.4 | 1997 | 12 | 2001 |
| 63126 | | BCOY4/R5 | Wood | 1,11 | -28,70 | 108,21217 | 0,28487 | Postérieur à 1950 | | 1.08212 | 0.00285 | R_F14C(1.08212,0.00285) | 1957 | 2993 | AD | 95.4 | 1998 | 13 | 2002 |
| 63127 | | BCOY4/R6 | Wood | 1,26 | -26,90 | 106,89402 | 0,30877 | Postérieur à 1950 | | 1.0689 | 0.00309 | R_F14C(1.06894,0.00309) | 1957 | 2007 | AD | 95.4 | 2000 | 14 | 2005 |
| 63128 | | BCOY4/R7 | Wood | 1,17 | -19,80 | 103,82826 | 0,30654 | Postérieur à 1950 | | 1.03828 | 0.00307 | R_F14C(1.03828,0.00307) | 1956 | 2009 | AD | 95.4 | 1963 | 18 | 1956 |
| 63129 | | BCOY4/R8 | Wood | 1,14 | -25,30 | 100,39099 | 0,28867 | Postérieur à 1950 | | 1.00391 | 0.00289 | R_F14C(1.00391,0.00289) | 1955 | 1955 | AD | 95.4 | 1955 | 2 | 1955 |
| 63130 | BCY5 | BCYO5/R1 | Wood | 0,97 | -27,20 | 93,56298 | 0,27981 | 535 | 30 | | | R_Date 63130 | 1323 | 1439 | AD | 95.4 | 1396 | 34 | 1409 |
| 63131 | | BCYO5/R3 | Wood | 1,18 | -23,20 | 113,21977 | 0,29766 | Postérieur à 1950 | | 1.1322 | 0.0029766 | R_F14C(1.1322,0.0029766) | 1958 | 1995 | AD | 95.4 | 1991 | 9 | 1993 |
| 63132 | | BCYO5/R6 | Wood | 1,00 | -24,90 | 158,30917 | 0,35414 | Postérieur à 1950 | | 1.58309 | 0.0035414 | R_F14C(1.58309,0.0035414) | 1963 | 1969 | AD | 95.4 | 1968 | 1 | 1968 |
| 63133 | | BCYO5/R7 | Wood | 0,53 | -23,10 | 175,33266 | 0,37610 | Postérieur à 1950 | | 1.75333 | 0.003761 | R_F14C(1.75333,0.003761) | 1963 | 1965 | AD | 95.4 | 1964 | 1 | 1965 |
| 63134 | | BCYO5/R10 | Wood | 1,14 | -24,60 | 115,69214 | 0,31329 | Postérieur à 1950 | | 1.15692 | 0.0031329 | R_F14C(1.15692,0.0031329) | 1958 | 1991 | AD | 95.4 | 1987 | 9 | 1990 |
| 58575 | KW5 | KW-O5.1 | Wood | 1,16 | -22,3 | 97,50147 | 0,22697 | 205 | 30 | | | R_Date 5575 | 1643 | ... | AD | 95.4 | 1762 | 84 | 1765 |
| 58576 | KW6 | KW-O6.3 | Wood | 0,94 | -22,3 | 98,76589 | 0,22979 | 100 | 30 | | | R_Date 5576 | 1683 | 1930 | AD | 95.4 | 1821 | 77 | 1839 |
| 58577 | KW7 | KW-O7.3 | Wood | 1,04 | -23,3 | 97,97643 | 0,23689 | 165 | 30 | | | R_Date 5577 | 1661 | ... | AD | 95.4 | 1797 | 86 | 1777 |
| 58578 | KW8 | KW-O8.3D | Wood | 0,99 | -21,8 | 98,17069 | 0,24218 | 150 | 30 | | | R_Date 5578 | 1667 | ... | AD | 95.4 | 1807 | 84 | 1806 |
| 58579 | KW12 | KW-O12.3 | Wood | 1,21 | -21,7 | 98,97153 | 0,26985 | 85 | 30 | | | R_Date 5579 | 1688 | 1924 | AD | 95.4 | 1821 | 76 | 1836 |
| 58580 | KW13 | KW-O13.3D | Wood | 0,88 | -23,9 | 98,89152 | 0,23472 | 90 | 30 | | | R_Date 5580 | 1687 | 1926 | AD | 95.4 | 1821 | 76 | 1837 |
| 58581 | KW14 | KW-O14.1D | Wood | 1,12 | -20,9 | 98,30358 | 0,23789 | 135 | 30 | | | R_Date 5581 | 1674 | 1943 | AD | 95.4 | 1814 | 81 | 1831 |
| 58582 | KW15 | KW-O15.1D | Wood | 1,08 | -21,4 | 158,80265 | 0,27959 | Postérieur à 1950 | | 1.5880265 | 0.0027959 | R_Date(1.58803,0.0027959) | 1963 | 1969 | AD | 95.4 | 1967 | 2 | 1967 |
| 58584 | KW17 | KW-O17.1 | Wood | 1,07 | -21,5 | 98,81075 | 0,22539 | 95 | 30 | | | R_Date 5584 | 1685 | 1928 | AD | 95.4 | 1821 | 76 | 1838 |
| 58585 | KW18 | KW-O18.3 | Wood | 1,41 | -21,2 | 101,12395 | 0,23342 | Postérieur à 1950 | | 1.0112395 | 0.0023342 | R_Date(1.01124,0.0023342) | 1955 | 1956 | AD | 95.4 | 1955 | 0 | 1955 |
| 58586 | KW19 | KW-O19.3D | Wood | 1,13 | -21,8 | 98,51991 | 0,25162 | 120 | 30 | | | R_Date 5586 | 1679 | 1941 | AD | 95.4 | 1819 | 79 | 1838 |
| 58588 | KWY3 | KW-OY3.2 | Wood | 0,98 | -23 | 97,98271 | 0,22968 | 165 | 30 | | | R_Date 5587 | 1661 | ... | AD | 95.4 | 1797 | 86 | 1777 |
| 63198 | KW1-3 | KWO1.3D/R1 | Wood | 1,07 | -25,2 | 99,50 | 0,29 | 40 | 30 | | | R_Date 63198 | 1694 | 1917 | AD | 95.4 | 1819 | 77 | 1830 |
| 63199 | | KWO1.3D/R2 | Wood | 0,80 | -24,9 | 98,43 | 0,29 | 125 | 30 | | | R_Date 63199 | 1675 | 1942 | AD | 95.4 | 1818 | 79 | 1837 |
| 63200 | | KWO1.3D/R3 | Wood | 0,45 | -25,8 | 98,45 | 0,29 | 125 | 30 | | | R_Date 63200 | 1675 | 1942 | AD | 95.4 | 1818 | 79 | 1837 |
| 63201 | | KWO1.3D/R4 | Wood | 1,04 | -25,4 | 98,47 | 0,28 | 125 | 30 | | | R_Date 63201 | 1675 | 1942 | AD | 95.4 | 1818 | 79 | 1837 |
| 58571 | | KW-O1.3D | Wood | 1,01 | -20,3 | 98,02 | 0,23 | 160 | 30 | | | R_Date 58571 | 1663 | ... | AD | 95.4 | 1800 | 86 | 1784 |
| 63179 | KW2 | KWO2.4D/R1 | Wood | 1,17 | -19,0 | 98,86 | 0,29 | 90 | 30 | | | R_Date 63179 | 1687 | 1926 | AD | 95.4 | 1821 | 76 | 1837 |
| 63180 | | KWO2.4D/R2 | Wood | 1,21 | -15,9 | 97,86 | 0,28 | 175 | 30 | | | R_Date 63180 | 1658 | ... | AD | 95.4 | 1790 | 87 | 1772 |
| 63181 | | KWO2.4D/R3 | Wood | 1,07 | -23,6 | 78,93 | 0,26 | 1900 | 30 | | | R_Date 63181 | 62 | 225 | AD | 95.4 | 145 | 45 | 148 |
| 63182 | | KWO2.4D/R4 | Wood | 1,07 | -16,6 | 94,53 | 0,29 | 450 | 30 | | | R_Date 63182 | 1413 | 1480 | AD | 95.4 | 1447 | 23 | 1445 |
| 58572 | | KW-O2.4D | Wood | 1 | -22 | 99,07334 | 0,23749 | 75 | 30 | | | R_Date 58572 | 1691 | 1920 | AD | 95.4 | 1821 | 76 | 1834 |
| 63158 | KW3-1 | KWO3.1/R1 | Wood | 0,99 | -25,2 | 98,8031 | 0,27626 | 95 | 30 | | | R_Date 63158 | 1685 | 1928 | AD | 95.4 | 1821 | 76 | 1838 |
| 63159 | | KWO3.1/R2 | Wood | 0,99 | -26 | 98,20423 | 0,27644 | 145 | 30 | | | R_Date 63159 | 1669 | ... | AD | 95.4 | 1809 | 83 | 1813 |
| 63160 | | KWO3.1/R3 | Wood | 1,06 | -26,3 | 98,61519 | 0,26819 | 110 | 30 | | | R_Date 63160 | 1682 | 1938 | AD | 95.4 | 1821 | 77 | 1839 |
| 63161 | | KWO3.1/R4 | Wood | 0,69 | -28,2 | 98,23705 | 0,26641 | 145 | 30 | | | R_Date 63161 | 1669 | ... | AD | 95.4 | 1809 | 83 | 1813 |
| 63162 | | KWO3.1/R5 | Wood | 0,98 | -26 | 110,15843 | 0,2806 | Postérieur à 1950 | | 1.10158 | 0.002806 | R_F14C(1.10158,0.002806) | 1957 | 2000 | AD | 95.4 | 1996 | 9 | 1998 |
| 63163 | | KWO3.1/R6 | Wood | 1,19 | -27,1 | 98,08 | 0,2675 | 155 | 30 | | | R_Date 63163 | 1665 | ... | AD | 95.4 | 1804 | 85 | 1800 |
| 63164 | | KWO3.1/R7 | Wood | 1,05 | -26,1 | 99,05647 | 0,2949 | 75 | 30 | | | R_Date 63164 | 1691 | 1920 | AD | 95.4 | 1821 | 76 | 1834 |
| 63165 | | KWO3.1/R8 | Wood | 0,85 | -25,7 | 97,46641 | 0,28482 | 205 | 30 | | | R_Date 63165 | 1643 | ... | AD | 95.4 | 1762 | 84 | 1765 |
| 63166 | | KWO3.1/R9 | Wood | 0,99 | -24 | 97,02087 | 0,28585 | 245 | 30 | | | R_Date 63166 | 1523 | ... | AD | 95.4 | 1685 | 86 | 1659 |
| 63167 | | KWO3.1/R10 | Wood | 0,96 | -27,4 | 98,9557 | 0,30947 | 85 | 30 | | | R_Date 63167 | 1688 | 1924 | AD | 95.4 | 1821 | 76 | 1836 |
| 58573 | | KW-O3.1 | Wood | 0,72 | -26,9 | 98,55914 | 0,22699 | 115 | 30 | | | R_Date 58573 | 1680 | 1940 | AD | 95.4 | 1820 | 78 | 1839 |
| 63168 | KW3-3 | KWO3.3/R1 | Wood | 1 | -25,3 | 99,2059 | 0,26657 | 65 | 30 | | | R_Date 63168 | 1693 | 1918 | AD | 95.4 | 1820 | 76 | 1832 |
| 63169 | | KWO3.3/R6 | Wood | 0,98 | -21,9 | 97,49762 | 0,26337 | 205 | 30 | | | R_Date 63169 | 1643 | ... | AD | 95.4 | 1762 | 84 | 1765 |
| 63170 | | KWO3.3/R10 | Wood | 0,92 | -23,2 | 97,92694 | 0,26164 | 170 | 30 | | | R_Date 63170 | 1660 | ... | AD | 95.4 | 1794 | 86 | 1774 |
| 63195 | KW4 | KWO4.3/R1 | Wood | 1,05 | -22,9 | 87,98 | 0,30 | 1030 | 30 | | | R_Date 63195 | 899 | 1147 | AD | 95.4 | 1013 | 37 | 1011 |
| 63196 | | KWO4.3/R2 | Wood | 0,39 | -28,0 | 98,97 | 0,32 | 85 | 30 | | | R_Date 63196 | 1688 | 1924 | AD | 95.4 | 1821 | 76 | 1836 |
| 63197 | | KWO4.3/R3 | Wood | 0,99 | -24,9 | 97,85 | 0,29 | 175 | 30 | | | R_Date 63197 | 1658 | ... | AD | 95.4 | 1790 | 87 | 1772 |
| 58574 | | KW-O4.3 | Wood | 1,06 | -23,2 | 97,133 | 0,2249 | 235 | 30 | | | R_Date 58574 | 1528 | ... | AD | 95.4 | 1712 | 85 | 1670 |

| | | | | | | | | | | | | | | | | | | | |
|---|---|---|---|---|---|---|---|---|---|---|---|---|---|---|---|---|---|---|---|
| 63187 | KW16 | KWO16.2D/R1 | Wood | 1.37 | -26.5 | 39.61 | 0.20 | 7440 | 40 | | | R_Date 63187 | 6405 | 6231 | BC | 95.4 | 6314 | 53 | 6316 |
| 64736 | | KWO16.2D/A1 | Wood | 0.79 | -24.6 | 97.94151 | 0.2609 | 165 | 30 | | | R_Date 64736 | 1661 | ... | | 95.4 | 1797 | 86 | 1777 |
| 64737 | | KWO16.2D/A2 | Wood | 0.81 | -24.5 | 98.33504 | 0.25837 | 135 | 30 | | | R_Date 64737 | 1674 | 1943 | | 95.4 | 1814 | 81 | 1831 |
| 64738 | | KWO16.2D/A3 | Wood | 0.86 | -23.5 | 95.93429 | 0.2462 | 335 | 30 | | | R_Date 64738 | 1475 | 1640 | | 95.4 | 1559 | 48 | 1562 |
| 64454 | | KWO16.2D/R1.1 | Wood | 1.05 | -21.9 | 98.57 | 0.23 | 115 | 30 | | | R_Date 64454 | 1680 | 1940 | AD | 95.4 | 1820 | 78 | 1839 |
| 64455 | | KWO16.2D/R1.2 | Wood | 0.86 | -23.8 | 99.21 | 0.23 | 165 | 30 | | | R_Date 64455 | 1661 | ... | | 95.4 | 1797 | 86 | 1777 |
| 63188 | | KWO16.2D/R4 | Wood | 0.99 | -19.0 | 97.03 | 0.31 | 240 | 30 | | | R_Date 63188 | 1526 | ... | AD | 95.4 | 1699 | 85 | 1663 |
| 63189 | | KWO16.2D/R6 | Wood | 1.15 | -21.7 | 97.45 | 0.29 | 205 | 30 | | | R_Date 63189 | 1643 | ... | AD | 95.4 | 1762 | 84 | 1765 |
| 63190 | | KWO16.2D/R7 | Wood | 0.94 | -24.0 | 96.71 | 0.29 | 270 | 30 | | | R_Date 63190 | 1510 | 1798 | AD | 95.4 | 1612 | 73 | 1633 |
| 58583 | | KW-O16.2D | Wood | 1.12 | -20.9 | 97.36018 | 0.23332 | 215 | 30 | | | R_Date 58583 | 1641 | ... | AD | 95.4 | 1749 | 83 | 1760 |
| 63191 | KWY1 | KWOY1.2/R1 | Wood | 0.92 | -25.2 | 96.75 | 0.29 | 265 | 30 | | | R_Date 63191 | 1513 | 1799 | AD | 95.4 | 1625 | 78 | 1640 |
| 63192 | | KWOY1.2/R2 | Wood | 1.08 | -24.0 | 96.92 | 0.30 | 250 | 30 | | | R_Date 63192 | 1522 | ... | AD | 95.4 | 1670 | 86 | 1654 |
| 63193 | | KWOY1.2/R3 | Wood | 1.14 | -21.6 | 96.40 | 0.31 | 295 | 30 | | | R_Date 63193 | 1495 | 1659 | AD | 95.4 | 1576 | 51 | 1564 |
| 63194 | | KWOY1.2/R4 | Wood | 1.01 | -25.9 | 99.09 | 0.29 | 75 | 30 | | | R_Date 63194 | 1691 | 1920 | AD | 95.4 | 1821 | 76 | 1834 |
| 58587 | | KW-YO1.2 | Wood | 1.25 | -21.9 | 102.24429 | 0.24258 | Postérieur à 1950 | | 1.02244 | 0.0024258 | R_Date(1.02244,0.0024258) | 1955 | 1956 | AD | 95.4 | 1956 | 0 | 1956 |
| 63171 | KWY4 | KWOY4/R1 | Wood | 0.96 | -28.2 | 94.60888 | 0.2635 | 445 | 30 | | | R_Date 63171 | 1416 | 1490 | AD | 95.4 | 1451 | 27 | 1447 |
| 63172 | | KWOY4/R2 | Wood | 0.91 | -21.8 | 147.16247 | 0.33058 | Postérieur à 1950 | | 1.4716247 | 0.002806 | R_F14C(1.4716247,0.002806) | 1962 | 1973 | AD | 95.4 | 1970 | 4 | 1972 |
| 63173 | | KWOY4/R4 | Wood | 0.68 | -26.7 | 101.96258 | 0.26938 | Postérieur à 1950 | | 1.01963 | 0.0026938 | R_F14C(1.01963,0.0026938) | 1955 | 1956 | AD | 95.4 | 1955 | 0 | 1955 |
| 63174 | | KWOY4/R5 | Wood | 0.91 | -23.4 | 98.36943 | 0.26303 | 130 | 30 | | | R_Date 63174 | 1675 | 1942 | AD | 95.5 | 1816 | 80 | 1835 |

# Chapter V. General Discussion and Conclusion

This study is conducted on the olive, most iconic tree in the Mediterranean (Kaniewski et al., 2012; Besnard et al., 2013) and which remains a key component of agriculture today and in the future. Therefore, it is important, not only to preserve this heritage, but also to understand the on-site behavior of the olive tree to the different environmental and climatic changes, based on two timeframes: studying the present to understand the past which will teach us about adaptation of this tree to climatic and anthropogenic shocks.

The combination of the different methodologies in this dissertation, from Hg concentration, isotopic analysis (C, N, S, H, O) to different methods of dendrology studies (radiocarbon, microtomography), was applied on Lebanese monumental olive groves, as a multi-proxy approach to better understand how these trees function and build resilience to different climatic and environmental stresses.

In chapter I, the monumental olive trees subject of the study, and which have survived many climatic and environmental conditions for centuries in Bchaaleh village in North Lebanon, 1300 m a.s.l and in Kawkaba village in South Lebanon, 672 m a.s.l., were presented. Also, the different methods used in this study from the isotopic analyses to the dendrology were described in details. Chapter II assessed the Hg concentration in the monumental olive groves, which are quietly recognized as nonpolluted areas, on a monthly basis over 18 months in 2019-2021. Chapter III investigates how does the olive tree foliage respond to climatic parameters using C,N,S,H and O stable isotopic markers as indicators of the climate, and how the fractionation of the different isotopic compositions are exchanged between foliage, stems, litter and soil. After these chapters focusing on the present, Chapter IV came to examine the past through a set of wood cores taken from the interior of the monumental olive trees to assess the age and the possible climatic changes, using different techniques from dendrochronology, densitometry, X-Ray tomography, radiocarbon dating, and carbon isotopic analysis.

**Hg concentration**

Hg concentration registered higher values in foliage than in stems, with the soil having the highest Hg content among plant tissues and litter. A good covariation was observed between the foliage Hg time series analysis and those of $pCO_2$ and Hg concentration of the atmospheric Northern Hemisphere. Hg concentration seasonality was well detected in the foliage of the olive trees. The late winter-early spring registered the highest Hg concentration for foliage in both groves, while summer and early fall to a less extent recorded the lowest concentrations. This seasonal change is explained by the seasonal tree physiology variations such as the Hg accumulation in leaves after stomatal uptake (Pleijel et al., 2021; Wohlgemuth et al., 2021). We can suggest that during winter-early spring, water is available and photosynthetic activity is not limited, hence both $CO_2$ and Hg diffuse through opened stomata inside the foliage. Evergreen olive foliage at our sites show a decrease in Hg contents from end of March to

late August, with minimum values centered in August suggesting a decline of the plant Hg uptake likely explained by the reduction of the stomatal conductance (Lindberg et al., 2007; Pleijel et al., 2021). This minimal photosynthetic activity occurs during the driest season (0 mm precipitation) and hottest temperatures (above 25°C) at our sites. The significant correlation between our $Hg_{Foliage}$ contents and the atmospheric Hg content and $pCO_2$, despite the one to two months' time lag, suggests that the main source of $Hg_{Foliage}$ is the atmospheric Hg as observed in different species and studies (conifers and hardwood). Hg is absorbed by the foliage, via the open stomata, driven by the interaction of high vegetal activity, temperature, water availability and the processes that control transpiration, which is likely to be seasonal. Hence physiological and climatic processes explain the seasonal Hg accumulation in foliage. This study also highlights the significant differences between $Hg_{soil}$ in Bchaaleh and Kawkaba groves due to differences in soil characteristics.

**$\delta^{13}C$, $\delta^{15}N$, $\delta^{34}S$, $\delta D$, $\delta^{18}O$**

In Lebanon, the monumental olive trees plant tissues, litter and soil different isotopic composition are studied at two different altitudes in Bchaaleh and Kawkaba. $\delta^{13}C$ in both sites showed a correlation between foliage and stems, unlike $\delta^{15}N$ and $\delta^{34}S$ of foliage and stems that had no correlation. An altitudinal effect is registered for most of the isotopic compositions ($\delta^{13}C$, $\delta^{15}N$, $\delta D$ and $\delta^{18}O$) of plant tissues, litter and soil. While $\delta^{34}S$ showed a geological effect on the above ground and underground elements. The year 2020 in Bchaaleh and Kawkaba showed more depleted values in the studied isotopic compositions of foliage which can be due to the decrease of wind speed and solar radiation from year 2019 to 2020 over time that can cause an increase in the stomatal conductance which can induce stomatal opening leading to a decrease in leaf surface water stress, in addition to an increase in the ratio of substomatal to atmospheric $CO_2$ ($c_i/c_a$) that regulates the stomata, and thus a decrease in the $\delta^{13}C$ of foliage (Cernusak & Marshall, 2001; Betson et al., 2007). Another factor that can cause more depleted foliage values in 2020 might be the lower chlorophyll and photosystem activity in addition to a higher Rubisco activity in the younger foliage collected in 2020 in comparison to the more mature foliage from the previous year (Gielen et al., 2000; Jach & Ceulemans, 2000). The depleted values of $\delta^{13}C$ in foliage during most of the summer seasons in Bchaaleh and Kawkaba may be explained by the $CO_2$ leakage increase from the bundle sheath cells when faced by water stress (Buchmann et al., 1996; Saliendra et al., 1996; Yoneyama et al., 2010).

The depleted values of in the $\delta^{15}N$ of foliage during summer in both Bchaaleh and Kawkaba might be in association with AMF (E. A. Hobbie & Colpaert, 2003; Tatsumi et al., 2021). The mycorrhizal fungi provides N content to the plant as N limitation and drought stress increases (Hobbie & Hobbie, 2006; Begum et al., 2019). The higher and significant foliage $\delta^{34}S$ annual mean value for Bchaaleh and Kawkaba registered in 2019 can be an indication of a higher sulfur stress in the olive tree than in 2020 (Trust & Fry, 1992). Another explanation can be that in 2019, the foliage which is considered a sink

organ, is receiving more enriched $\delta^{34}S$ from the proteins (Tcherkez & Tea, 2013) than that in 2020. Noting no important seasonality registered for foliage $\delta^{34}S$ in both studied sites.

While foliage δD seasonal variability in Bchaaleh and Kawkaba is affected by the water source such as soil water and leaf water transpiration, in addition biochemical factors (Hartsough et al., 2008; J. Liu et al., 2021). Most probably due to drought stress, there is a water soil uptake to the foliage leading a depletion in foliage δD (Y. Li et al., 2022) in Bchaaleh and Kawkaba in 2019 and 2020. In addition to the depleted δD of available cellulose, lipid or starch in foliage (Sanchez-Bragado et al., 2019).

While a slight seasonality is shown for the $\delta^{13}C$ and $\delta^{15}N$ of foliage, and a higher seasonality for the foliage δD. In Bchaaleh and Kawkaba, the climatic parameters varied in their significant correlation with the isotopic compositions of the foliage. These outcomes can mainly indicate that the studied olive trees in Lebanon are tolerant all year long to all the changes in the climatic parameters without being drastically affected. In addition to that, we can see that the stems and foliage $\delta^{13}C$ and δD has a good correlation, which may confirm that stems can help us understand the wood of monumental olive trees, and indicates that wood cores can be a good indicator for the past climatic data through isotopic studies. We have also shown in this study that bulk organic material of foliage, stems, litter and soil can be a reliable and cheaper technique to retrieve data on the seasonality and isotopic composition of foliage.

**X-Ray tomography and radiocarbon dating**

Finally, the X-Ray tomography and radiocarbon dating are successful techniques to identify the annual tree rings and date the wood cores in relation to the ring numbers and orientation. This technique resulted in giving us the oldest age of 7400 years from the existing wood sampled from one of the centennial olive trees from Kawkaba, and the age back to 1800 years from Bchaaleh.

Olive wood is not usually dated using dendrochronology or densitometry techniques due to the difficulty in identifying the annual tree rings. In this study, both monumental olive trees and young trees were used in order to identify the annual rings in the olive wood and create a data set that can be used as a chronological reference of other olive trees around the world, by combining X-Ray tomography, radiocarbon dating and carbon stable isotopes.

Tomography helped identify the tree rings and helped in determining a counting for the number of rings per part, specifying the direction of the rings per wood part and understanding the connection or disconnection of the different wood parts through the ring identification and formation

The use of X-Ray tomography was a main key for the selection of the radiocarbon dating samples. These two techniques combined together, proved to be a very successful and a step forward in identifying the annual growth rings (early and late wood). Additionally, they help detect a great number of annual rings in the sampled cores, which assists in selecting the radiocarbon dating samples and thus asses the different dates in relation to the ring numbers and orientation.

Similar studies conducted on olive tree are rare. In Santorini, (Ehrlich et al., 2021) were able to detect a verifed annual growth in a modern olive branch for the frst time, using stable isotope analysis and high-resolution radiocarbon dating, identifying down to the growing season in some years. The verifed growth was largely visible by X-Ray tomography, both in the branch's fresh and charred forms. Authors observed some chronological anomalies in modern olive and thus simulated possible date range scenarios of the volcanic eruption of Santorini. Their findings offer a way to reconcile this longstanding debate towards a mid-sixteenth century BCE date (Ehrlich et al., 2021). In our study, we didn't have high resolution radiocarbon dating as per Ehrlich to be able to compare the $\delta^{13}C$ values of wood samples with the radiocarbon dates to support the assignment of each minimum point of $\delta^{13}C$ values between growth rings. However, a variability at an interannual scale was found. The X-Ray tomography helped in identifying the tree rings with the assistance of the radiocarbon dating, where it was also possible to identify new developed branches within the same tree. This was done through using wood cores extracted from the actual living monumental olive trees. There is a need to further have a high resolution radiocarbon dating to reliably identify annual and even seasonal growth in olive wood.

**Conclusion**

This dissertation is the first research in the Levant region reporting the use of multi-proxies analysis on monumental olive trees to understand the onsite present and past resilience of these trees to climatic and environmental stress in the Lebanese agroclimatic conditions. Major results concluded that the monumental olive trees in Lebanon are tolerant all year long to all the changes in the climatic parameters without being drastically affected. On the other hand, seasonality was registered in foliage Hg concentration, while the low Hg concentration values recorded in both study groves sites confirm the absence of contamination. By understanding how the present registers the isotopic compositions in the plant tissues, we would be able to understand the past through studying the isotopic compositions in the old wood. Wood cores analyses indicated that X-Ray tomography and radiocarbon dating are complementary proxies to date centennial olive trees indicating an age of 7400 BC in Kawkaba, which makes it the oldest age recorded a priori in the Levant region.

By the end of this work, several recommendations could be foreseen as a step forward in order to improve the understanding of present/past situation of monumental olive trees, and how olive trees in general will act in the future vis-à-vis any climatic and environmental changes:

- to continue with the isotopic analysis along a larger time scale in order to confirm the effect of climate on the different isotopic markers.
- to increase the resolution of radiocarbon dating through analyzing a large set of adequate old wood cores in order to determine accurately the age of monumental trees.
- to increase the resolution of $\delta^{13}C$ on bulk wood to allow assessing the relation between the ring width and the $\delta^{13}C$ and understanding the impact of climatic data on tree growth.

In addition to that, the ultimate future perspective of this work is to understand how the monumental olive trees of Lebanon have contributed to the domestication process of the olive trees in the Mediterranean. Thus, it would be important to have studies using archeological sites and carbonized seeds. In addition to including ancient DNA in comparison to other kinds of trees, and collaborating with different countries of the Mediterranean shore to be able to have a good data collection that could be useful for the region.

## References


A. Hobbie, E., & Werner, R. A. (2004). Intramolecular, compound-specific, and bulk carbon isotope patterns in C3 and C4 plants: A review and synthesis. *New Phytologist*, *161*(2), 371–385.

Abou Habib, N., Taleb, M., & Khoury, R. (2015). *ENVIRONMENTAL AND SOCIAL SAFEGUARD STUDIES FOR LAKE QARAOUN POLLUTION PREVENTION PROJECT*. *V1*(E4749).

Alcaras, L. M. A., Rousseaux, M. C., & Searles, P. S. (2016). Responses of several soil and plant indicators to post-harvest regulated deficit irrigation in olive trees and their potential for irrigation scheduling. *Agricultural Water Management*, *171*, 10–20. https://doi.org/10.1016/j.agwat.2016.03.006

ALLEN, S., & Raven, J. A. (1987). Intracellular pH regulation in Ricinus communis grown with ammonium or nitrate as N source: The role of long distance transport. *Journal of Experimental Botany*, *38*(4), 580–596.

Alliance nationale de recherche pour l'environnement, & Nations Unies (Eds.). (2016). *The Mediterranean region under climate change: A scientific update*. IRD éditions.

Allison, G. B., Barnes, C. J., & Hughes, M. W. (1983). The distribution of deuterium and 18O in dry soils 2. Experimental. *Journal of Hydrology*, *64*(1), 377–397. https://doi.org/10.1016/0022-1694(83)90078-1

Alloway, B. J. (1995). *Heavy Metals in Soils*. Springer Science & Business Media.

Al-Zubaidi, A., Yanni, S., & Bashour, I. (2008). Potassium status in some Lebanese soils. *Lebanese Science Journal*, *9*(1), 81–97.

Amin, A., Zuecco, G., Marchina, C., Engel, M., Penna, D., McDonnell, J. J., & Borga, M. (2021a). *A simple glasshouse experiment to test the isotopic fractionation in olive trees* [Other]. pico. https://doi.org/10.5194/egusphere-egu21-9300

Amin, A., Zuecco, G., Marchina, C., Engel, M., Penna, D., McDonnell, J. J., & Borga, M. (2021b). No evidence of isotopic fractionation in olive trees ( *Olea europaea* ): A stable isotope tracing experiment. *Hydrological Sciences Journal*, *66*(16), 2415–2430. https://doi.org/10.1080/02626667.2021.1987440

Amundson, R., Austin, A. T., Schuur, E. a. G., Yoo, K., Matzek, V., Kendall, C., Uebersax, A., Brenner, D., & Baisden, W. T. (2003). Global patterns of the isotopic composition of soil and plant nitrogen. *Global Biogeochemical Cycles*, *17*(1). https://doi.org/10.1029/2002GB001903

Aouad, A., Travi, Y., Blavoux, B., Job, J.-O., & Najem, W. (2004). Etude isotopique de la pluie et de la neige sur le Mont Liban: Premiers résultats / Isotope study of snow and rain on Mount Lebanon: preliminary results. *Hydrological Sciences Journal*, *49*(3), 6. https://doi.org/10.1623/hysj.49.3.429.54341

Aranibar, J. N., Otter, L., Macko, S. A., Feral, C. J. W., Epstein, H. E., Dowty, P. R., Eckardt, F., Shugart, H. H., & Swap, R. J. (2004). Nitrogen cycling in the soil–plant system along a precipitation gradient in the Kalahari sands. *Global Change Biology*, *10*(3), 359–373. https://doi.org/10.1111/j.1365-2486.2003.00698.x

Araus, J., Cabrera-Bosquet, L., Serret, M., Bort, J., & Nieto-Taladriz, M. (2013). Comparative performance of δ13C, δ18O and δ15N for phenotyping durum wheat adaptation to a dryland environment. *Functional Plant Biology*, *40*, 595–608. https://doi.org/10.1071/fp12254

Araus, J. L., Villegas, D., Aparicio, N., del Moral, L. F. G., El Hani, S., Rharrabti, Y., Ferrio, J. P., & Royo, C. (2003). Environmental Factors Determining Carbon Isotope Discrimination and Yield in Durum Wheat under Mediterranean Conditions. *Crop Science*, *43*(1), 170–180. https://doi.org/10.2135/cropsci2003.1700

Arnan, X., Claramunt-López, B., Martinez Vilalta, J., Estorach, M., & Poyatos, R. (2012). The age of monumental olive trees (Olea europaea) in northeastern Spain. *Dendrochronologia*, *30*, 11–14. https://doi.org/10.1016/j.dendro.2011.02.002

Asada, T., Warner, B., & Aravena, R. (2005). Effects of the early stage of decomposition on change in carbon and nitrogen isotopes in *Sphagnum* litter. *Journal of Plant Interactions*, *1*(4), 229–237. https://doi.org/10.1080/17429140601056766

Assad, M. (n.d.). *Transfert des éléments traces métalliques vers les végétaux: Mécanismes et évaluations des risques dans des environnements exposés à des activités anthropiques*. 218.

Baayoun, A., Itani, W., El Helou, J., Halabi, L., Medlej, S., El Malki, M., Moukhadder, A., Aboujaoude, L. K., Kabakian, V., Mounajed, H., Mokalled, T., Shihadeh, A., Lakkis, I., & Saliba, N. A. (2019). Emission inventory of key sources of air pollution in Lebanon. *Atmospheric Environment*, *215*, 116871. https://doi.org/10.1016/j.atmosenv.2019.116871

Badeck, F.-W., Tcherkez, G., Nogués, S., Piel, C., & Ghashghaie, J. (2005). Post-photosynthetic fractionation of stable carbon isotopes between plant organs—A widespread phenomenon. *Rapid Communications in Mass Spectrometry*, *19*(11), 1381–1391. https://doi.org/10.1002/rcm.1912

Badr, R., Holail, H., & Olama, Z. (2014). *WATER QUALITY ASSESSMENT OF HASBANI RIVER IN SOUTH LEBANON: MICROBIOLOGICAL AND CHEMICAL CHARACTERISTICS AND THEIR IMPACT ON THE ECOSYSTEM*. *3*, 16.

Barbaro, G. D., & González Basso, V. (2022). Arbuscular vesicular mycorrhizae in olive tree (Olea europaea L.). *Journal of Applied Biotechnology & Bioengineering*, *9*(4), 98–99. https://doi.org/10.15406/jabb.2022.09.00293

Barber, S. A. (1995). *Soil Nutrient Bioavailability: A Mechanistic Approach*. John Wiley & Sons.

Barbeta, A., Jones, S. P., Clavé, L., Wingate, L., Gimeno, T. E., Fréjaville, B., Wohl, S., & Ogée, J. (2019). *Unexplained hydrogen isotope offsets complicate the identificationand quantification of tree water sources in a riparian forest* [Preprint]. Ecohydrology/Theory development. https://doi.org/10.5194/hess-2018-631

Barbour, M. M. (2007). *Review: Stable oxygen isotope composition of plant tissue: a review*.

Barbour, M. M., & Farquhar, G. D. (2000). Relative humidity- and ABA-induced variation in carbon and oxygen isotope ratios of cotton leaves. *Plant, Cell & Environment*, *23*(5), 473–485. https://doi.org/10.1046/j.1365-3040.2000.00575.x

Bargagli, R. (1995). The elemental composition of vegetation and the possible incidence of soil contamination of samples. *Science of The Total Environment*, *176*(1–3), 121–128. https://doi.org/10.1016/0048-9697(95)04838-3

Barre, J. P. G., Deletraz, G., Sola-Larrañaga, C., Santamaria, J. M., Bérail, S., Donard, O. F. X., & Amouroux, D. (2018). Multi-element isotopic signature (C, N, Pb, Hg) in epiphytic lichens to discriminate atmospheric contamination as a function of land-use characteristics (Pyrénées-Atlantiques, SW France). *Environmental Pollution*, *243*, 961–971. https://doi.org/10.1016/j.envpol.2018.09.003

Basheer-salimia, R., & Ward, J. K. (2014). CLIMATE CHANGE AND ITS EFFECTS ON OLIVE TREE PHYSIOLOGYIN PALESTINE. *Review Of Research*, *3*(7). https://doi.org/10.9780/2249-894X/372014/688

Baumgartner, S., Bauters, M., Barthel, M., Drake, T. W., Ntaboba, L. C., Bazirake, B. M., Six, J., Boeckx, P., & Van Oost, K. (2021). Stable isotope signatures of soil nitrogen on an environmental–geomorphic gradient within the Congo Basin. *SOIL*, *7*(1), 83–94. https://doi.org/10.5194/soil-7-83-2021

Beauford, W., Barber, J., & Barringer, A. R. (1977). Uptake and Distribution of Mercury within Higher Plants. *Physiologia Plantarum*, *39*(4), 261–265. https://doi.org/10.1111/j.1399-3054.1977.tb01880.x

Begum, N., Qin, C., Ahanger, M. A., Raza, S., Khan, M. I., Ashraf, M., Ahmed, N., & Zhang, L. (2019). Role of Arbuscular Mycorrhizal Fungi in Plant Growth Regulation: Implications in Abiotic Stress Tolerance. *Frontiers in Plant Science*, *10*. https://www.frontiersin.org/articles/10.3389/fpls.2019.01068

Bershaw, J. (2018). Controls on Deuterium Excess across Asia. *Geosciences*, *8*(7), 257. https://doi.org/10.3390/geosciences8070257

Besnard, G., Khadari, B., Navascues, M., Fernandez-Mazuecos, M., Bakkali, A. E., Arrigo, N., Baali-Cherif, D., de Caraffa, V. B.-B., Santoni, S., Vargas, P., & Savolainen, V. (2013). The complex history of the olive tree: From Late Quaternary diversification of Mediterranean lineages to primary domestication in the northern Levant. *Proceedings of the Royal Society B: Biological Sciences*, *280*(1756), 20122833–20122833.

Besnard, G., & Rubio de Casas, R. (2016). Single vs multiple independent olive domestications: The jury is (still) out. *New Phytologist*, *209*(2), 466–470. https://doi.org/10.1111/nph.13518

Besnard, G., Terral, J.-F., & Cornille, A. (2018). On the origins and domestication of the olive: A review and perspectives. *Annals of Botany*, *121*(3), 385–403. https://doi.org/10.1093/aob/mcx145

Betson, N. R., Johannisson, C., Löfvenius, M. O., Grip, H., Granström, A., & Högberg, P. (2007). Variation in the δ13C of foliage of Pinus sylvestris L. in relation to climate and additions of nitrogen: Analysis of a 32-year chronology. *Global Change Biology*, *13*(11), 2317–2328. https://doi.org/10.1111/j.1365-2486.2007.01431.x

Beyer, M., Koeniger, P., Gaj, M., Hamutoko, J. T., Wanke, H., & Himmelsbach, T. (2016). A deuterium-based labeling technique for the investigation of rooting depths, water uptake dynamics and unsaturated zone water transport in semiarid environments. *Journal of Hydrology*, *533*, 627–643. https://doi.org/10.1016/j.jhydrol.2015.12.037

Bishop, K. H., Lee, Y.-H., Munthe, J., & Dambrine, E. (1998). Xylem sap as a pathway for total mercury and methylmercury transport from soils to tree canopy in the boreal forest. *Biogeochemistry*, *40*, 101–113.

Bishop, K., Shanley, J. B., Riscassi, A., de Wit, H. A., Eklöf, K., Meng, B., Mitchell, C., Osterwalder, S., Schuster, P. F., Webster, J., & Zhu, W. (2020). Recent advances in understanding and measurement of mercury in the environment: Terrestrial Hg cycling. *Science of The Total Environment*, *721*, 137647. https://doi.org/10.1016/j.scitotenv.2020.137647

Blackwell, B. D., & Driscoll, C. T. (2015). Using foliar and forest floor mercury concentrations to assess spatial patterns of mercury deposition. *Environmental Pollution*, *202*, 126–134. https://doi.org/10.1016/j.envpol.2015.02.036

Boening, D. W. (2000). *Ecological e€ ects, transport, and fate of mercury: A general review*. 17.

Borjac, J., El Joumaa, M., Kawach, R., Youssef, L., & Blake, D. A. (2019). Heavy metals and organic compounds contamination in leachates collected from Deir Kanoun Ras El Ain dump and its adjacent canal in South Lebanon. *Heliyon*, *5*(8), e02212. https://doi.org/10.1016/j.heliyon.2019.e02212

Borjac, J., El Joumaa, M., Youssef, L., Kawach, R., & Blake, D. A. (2020). Quantitative Analysis of Heavy Metals and Organic Compounds in Soil from Deir Kanoun Ras El Ain Dump, Lebanon. *The Scientific World Journal*, *2020*, 1–10. https://doi.org/10.1155/2020/8151676

Boström, B., Comstedt, D., & Ekblad, A. (2007). Isotope fractionation and 13C enrichment in soil profiles during the decomposition of soil organic matter. *Oecologia*, *153*(1), 89–98. https://doi.org/10.1007/s00442-007-0700-8

Briffa, J., Sinagra, E., & Blundell, R. (2020). Heavy metal pollution in the environment and their toxicological effects on humans. *Heliyon*, *6*(9), e04691. https://doi.org/10.1016/j.heliyon.2020.e04691

Buchmann, N., Brooks, J. R., Rapp, K. D., & Ehleringer, J. R. (1996). *Carbon isotope composition of C4 grasses is influenced by light and water supply—BUCHMANN - 1996—Plant, Cell & Environment—Wiley Online Library*. https://onlinelibrary.wiley.com/doi/10.1111/j.1365-3040.1996.tb00331.x

Cabrera-Bosquet, L., Sánchez, C., & Araus, J. L. (2009). How yield relates to ash content, Δ13C and Δ18O in maize grown under different water regimes. *Annals of Botany*, *104*(6), 1207–1216. https://doi.org/10.1093/aob/mcp229

Caracuta, V. (2020). Olive growing in Puglia (southeastern Italy): A review of the evidence from the Mesolithic to the Middle Ages. *Vegetation History and Archaeobotany*, *29*(5), 595–620. https://doi.org/10.1007/s00334-019-00765-y

Carrasco-Gil, S., Estebaranz-Yuberob, M., Medel-Cuestab, D., Millán, R., & Hernández, L. E. (2012). Influence of nitrate fertilization on Hg uptake and oxidative stress parameters in alfalfa plants cultivated in a Hg-polluted soil. *Environmental and Experimental Botany*, *75*. https://doi.org/10.1016/j.envexpbot.2011.08.013

Carrión, Y., Ntinou, M., & Badal, E. (2010). Olea europaea L. in the North Mediterranean Basin during the Pleniglacial and the Early–Middle Holocene. *Quaternary Science Reviews*, *29*(7–8), 952–968. https://doi.org/10.1016/j.quascirev.2009.12.015

Case, J. W., & Krouse, H. R. (1980). Variations in sulphur content and stable sulphur isotope composition of vegetation near a SO2 source at Fox Creek, Alberta, Canada. *Oecologia*, *44*(2), 248–257. https://doi.org/10.1007/BF00572687

Castiglioni, E., & Maniscalco, L. (2008). *Il santuario dei Palici. Un centro di culto nella Valle del Margi*.

Cavallini, A., Natali, L., Durante, M., & Maserti, B. (1999). Mercury uptake, distribution and DNA affinity in durum wheat (Triticum durum Desf.) plants. *Science of The Total Environment*, *243–244*, 119–127. https://doi.org/10.1016/S0048-9697(99)00367-8

Cernusak, L. A., Barbour, M. M., Arndt, S. K., Cheesman, A. W., English, N. B., Feild, T. S., Helliker, B. R., Holloway-Phillips, M. M., Holtum, J. A. M., Kahmen, A., McInerney, F. A., Munksgaard, N. C., Simonin, K. A., Song, X., Stuart-Williams, H., West, J. B., & Farquhar, G. D. (2016). Stable isotopes in leaf water of terrestrial plants. *Plant, Cell & Environment*, *39*(5), 1087–1102. https://doi.org/10.1111/pce.12703

Cernusak, L. A., & Marshall, J. D. (2001). *(13) (PDF) Responses of foliar 13C, gas exchange and leaf morphology to reduced hydraulic conductivity in Pinus monticola branches*. https://www.researchgate.net/publication/11750716_Responses_of_foliar_13C_gas_exchange_and_leaf_morphology_to_reduced_hydraulic_conductivity_in_Pinus_monticola_branches

Cernusak, L. A., & Ubierna, N. (2022). Carbon Isotope Effects in Relation to CO2 Assimilation by Tree Canopies. *Series Editors*, 291.

Chalak, L., Haouane, H., Essalouh, L., Santoni, S., Besnard, G., & Khadari, B. (2015). Extent of the genetic diversity in Lebanese olive (Olea europaea L.) trees: A mixture of an ancient germplasm with recently introduced varieties. *Genetic Resources and Crop Evolution*, *62*, 621–633. https://doi.org/10.1007/s10722-014-0187-1

Chapin, F. S. (1980). The Mineral Nutrition of Wild Plants. *Annual Review of Ecology and Systematics*, *11*, 233–260.

Chen, X., Ji, H., Yang, W., Zhu, B., & Ding, H. (2016). Speciation and distribution of mercury in soils around gold mines located upstream of Miyun Reservoir, Beijing, China. *Journal of Geochemical Exploration*, *163*, 1–9. https://doi.org/10.1016/j.gexplo.2016.01.015

Cherubini, P., & Lev-Yadun, S. (2014). The olive tree-ring problematic dating. *Antiquity*, *88*, 290–291. https://doi.org/10.1017/S0003598X00050420

Clarkson, T. W., & Magos, L. (2006). The Toxicology of Mercury and Its Chemical Compounds. *Critical Reviews in Toxicology*, *36*(8), 609–662. https://doi.org/10.1080/10408440600845619

Collins, J. A., Schefuß, E., Mulitza, S., Prange, M., Werner, M., Tharammal, T., Paul, A., & Wefer, G. (2013). Estimating the hydrogen isotopic composition of past precipitation using leaf-waxes from western Africa. *Quaternary Science Reviews*, *65*, 88–101. https://doi.org/10.1016/j.quascirev.2013.01.007

Comstock, J. P., & Ehleringer, J. R. (1992). Correlating genetic variation in carbon isotopic composition with complex climatic gradients. *Proceedings of the National Academy of Sciences*, *89*(16), 7747–7751.

Condon, A. G. (2004). Breeding for high water-use efficiency. *Journal of Experimental Botany*, *55*(407), 2447–2460. https://doi.org/10.1093/jxb/erh277

Cooper, L. W., Denir, M. J., & Keeley, J. E. (1991). *The relationship between stable oxygen and hydrogen isotope ratios of water in astomatal plants*. *3*.

Cormier, M.-A., Werner, R. A., Sauer, P. E., Gröcke, D. R., Leuenberger, M. C., Wieloch, T., Schleucher, J., & Kahmen, A. (2018). 2H-fractionations during the biosynthesis of carbohydrates and lipids imprint a metabolic signal on the δ2H values of plant organic compounds. *The New Phytologist*, *218*(2), 479–491.

Craig, H. (1953). The geochemistry of the stable carbon isotopes. *Geochimica et Cosmochimica Acta*, *3*(2–3), 53–92. https://doi.org/10.1016/0016-7037(53)90001-5

Craig, H. (1961). Isotopic variations in meteoric waters. *Science*, *133*(3465), 1702–1703.

Craine, J. M., Brookshire, E. N. J., Cramer, M. D., Hasselquist, N. J., Koba, K., Marin-Spiotta, E., & Wang, L. (2015). Ecological interpretations of nitrogen isotope ratios of terrestrial plants and soils. *Plant and Soil*, *396*(1–2), 1–26. https://doi.org/10.1007/s11104-015-2542-1

Damesin, C., & Lelarge, C. (2003). Carbon isotope composition of current-year shoots from Fagus sylvatica in relation to growth, respiration and use of reserves. *Plant, Cell & Environment*, *26*(2), 207–219. https://doi.org/10.1046/j.1365-3040.2003.00951.x

Dansgaard, W. (1964). Stable isotopes in precipitation. *Tellus*, *16*(4), 436–468. https://doi.org/10.1111/j.2153-3490.1964.tb00181.x

Dastoor, A., Angot, H., Bieser, J., Christensen, J. H., Douglas, T. A., Heimbürger-Boavida, L.-E., Jiskra, M., Mason, R. P., McLagan, D. S., Obrist, D., Outridge, P. M., Petrova, M. V., Ryjkov, A., St. Pierre, K. A., Schartup, A. T., Soerensen, A. L., Toyota, K., Travnikov, O., Wilson, S. J., & Zdanowicz, C. (2022). Arctic mercury cycling. *Nature Reviews Earth & Environment*, *3*(4), Article 4. https://doi.org/10.1038/s43017-022-00269-w

Dawson, T. E., & Ehleringer, J. R. (1993). Isotopic enrichment of water in the "woody" tissues of plants: Implications for plant water source, water uptake, and other studies which use the stable isotopic composition of cellulose. *Geochimica et Cosmochimica Acta*, *57*(14), 3487–3492. https://doi.org/10.1016/0016-7037(93)90554-A

Dawson, T. E., Mambelli, S., Plamboeck, A. H., Templer, P. H., & Tu, K. P. (2002). Stable Isotopes in Plant Ecology. *Annual Review of Ecology and Systematics*, *33*(1), 507–559. https://doi.org/10.1146/annurev.ecolsys.33.020602.095451

de Gruchy, M., Deckers, K., & Riehl, S. (2016). A diachronic reconstruction of the Northern Mesopotamian landscape (4th to 2nd millennia BCE) from three separate sources of evidence. *Journal of Archaeological Science: Reports*, *8*, 250–267. https://doi.org/10.1016/j.jasrep.2016.05.047

De Kok, L. J. (1990). SULFUR METABOL18M IN PLANTS EXPOSED TO ATMOSPHERIC SULFUR. *Higher Plonts*, 111.

De Mil, T., Vannoppen, A., Beeckman, H., Van Acker, J., & Van den Bulcke, J. (2016). A field-to-desktop toolchain for X-ray CT densitometry enables tree ring analysis. *Annals of Botany*, *117*(7), 1187–1196. https://doi.org/10.1093/aob/mcw063

Demers, J. D., Blum, J. D., & Zak, D. R. (2013). Mercury isotopes in a forested ecosystem: Implications for air-surface exchange dynamics and the global mercury cycle: MERCURY ISOTOPES IN A FORESTED ECOSYSTEM. *Global Biogeochemical Cycles*, *27*(1), 222–238. https://doi.org/10.1002/gbc.20021

*Dendro manual.pdf*. (n.d.). Retrieved March 13, 2022, from http://uwice.gov.bt/admin_uwice/publications/publication_files/Books-Manuals/2017/Dendro%20manual.pdf

Driscoll, A. W., Kannenberg, S. A., & Ehleringer, J. R. (2021). Long-term nitrogen isotope dynamics in Encelia farinosa reflect plant demographics and climate. *New Phytologist*, *232*(3), 1226–1237. https://doi.org/10.1111/nph.17668

Drobinski, P., Da Silva, N., Bastin, S., Mailler, S., Muller, C., Ahrens, B., Christensen, O., & Lionello, P. (2020). How warmer and drier will the Mediterranean region be at the end of the twenty-first century? *Regional Environmental Change*, *20*. https://doi.org/10.1007/s10113-020-01659-w

Du, S.-H., & Fang, S. C. (1983). Catalase activity of C3 and C4 species and its relationship to mercury vapor uptake. *Environmental and Experimental Botany*, *23*(4), 347–353. https://doi.org/10.1016/0098-8472(83)90009-6

Duval, B., Gredilla, A., Fdez-Ortiz de Vallejuelo, S., Tessier, E., Amouroux, D., & de Diego, A. (2020). A simple determination of trace mercury concentrations in natural waters using dispersive Micro-Solid phase extraction preconcentration based on functionalized graphene nanosheets. *Microchemical Journal*, *154*, 104549. https://doi.org/10.1016/j.microc.2019.104549

Edwards, H., & Vandenabeele, P. (2016). *Analytical Archaeometry: Selected Topics*. Royal Society of Chemistry.

Ehleringer, J. R., Buchmann, N., & Flanagan, L. B. (2000). Carbon Isotope Ratios in Belowground Carbon Cycle Processes. *Ecological Applications*, *10*(2), 412–422. https://doi.org/10.1890/1051-0761(2000)010[0412:CIRIBC]2.0.CO;2

Ehleringer, J. R., & Cooper, T. A. (1988). Correlations between carbon isotope ratio and microhabitat in desert plants. *Oecologia*, *76*(4), 562–566. https://doi.org/10.1007/BF00397870

Ehrlich, Y., Regev, L., & Boaretto, E. (2021). Discovery of annual growth in a modern olive branch based on carbon isotopes and implications for the Bronze Age volcanic eruption of Santorini. *Scientific Reports*, *11*(1), 704. https://doi.org/10.1038/s41598-020-79024-4

Ehrlich, Y., Regev, L., Kerem, Z., & Boaretto, E. (2017). Radiocarbon Dating of an Olive Tree Cross-Section: New Insights on Growth Patterns and Implications for Age Estimation of Olive Trees. *Frontiers in Plant Science*, *08*, 1918. https://doi.org/10.3389/fpls.2017.01918

EJOLT. (2019). *Cimenterie Nationale Factory in Chekaa, Lebanon | EJAtlas*. Environmental Justice Atlas. https://ejatlas.org/conflict/chekaa

Ekblad, A., Wallander, H., Carlsson, R., & Huss-Danell, K. (1995). Fungal biomass in roots and extramatrical mycelium in relation to macronutrients and plant biomass of ectomycorrhizal Pinus sylvestris and Alnus incana. *New Phytologist*, *131*(4), 443–451. https://doi.org/10.1111/j.1469-8137.1995.tb03081.x

El-Kadi, A. K. A. (n.d.). *Lebanon Temperature and the Global Warming During the 20th Century*. 10.

Emmett, B. A., Kjønaas, O. J., Gundersen, P., Koopmans, C., Tietema, A., & Sleep, D. (1998). Natural abundance of 15N in forests across a nitrogen deposition gradient. *Forest Ecology and Management*, *101*(1–3), 9–18.

Ericksen, J. A., Gustin, M. S., Schorran, D. E., Johnson, D. W., Lindberg, S. E., & Coleman, J. S. (2003). Accumulation of atmospheric mercury in forest foliage. *Atmospheric Environment*, *37*(12), 1613–1622. https://doi.org/10.1016/S1352-2310(03)00008-6

Ermolin, M. S., Fedotov, P. S., Malik, N. A., & Karandashev, V. K. (2018). Nanoparticles of volcanic ash as a carrier for toxic elements on the global scale. *Chemosphere*, *200*, 16–22. https://doi.org/10.1016/j.chemosphere.2018.02.089

Evans, J. P. (2009). 21st century climate change in the Middle East. *Climatic Change*, *92*(3–4), 417–432. https://doi.org/10.1007/s10584-008-9438-5

Farquhar, G. D., Ehleringer, J. R., & Hubick, K. T. (1989). Carbon Isotope Discrimination and Photosynthesis. *Annual Review of Plant Physiology and Plant Molecular Biology*, *40*(1), 503–537. https://doi.org/10.1146/annurev.pp.40.060189.002443

Farquhar, G. D., O'Leary, M. H., & Berry, J. A. (1982). On the relationship between carbon isotope discrimination and the intercellular carbon dioxide concentration in leaves. *Functional Plant Biology*, *9*(2), 121–137.

Fichtler, E., Helle, G., & Worbes, M. (2010). Stable-carbon isotope time series from tropical tree rings indicate a precipitation signal. *Tree-Ring Research*, *66*(1), 35–49.

Fitter, A. H., & Hay, R. K. M. (2002). Toxicity. *Environmental Physiology of Plants. 3rd Ed. Academic Press. San Diego*, 241–284.

Fonti, P., & Jansen, S. (2012). Xylem plasticity in response to climate. *The New Phytologist*, *195*(4), 734–736.

Fourel, F., Martineau, F., Seris, M., & Lécuyer, C. (2014). Simultaneous N, C, S stable isotope analyses using a new purge and trap elemental analyzer and an isotope ratio mass spectrometer: New methodology for simultaneous NCS isotopic analyses. *Rapid Communications in Mass Spectrometry*, *28*(23), 2587–2594. https://doi.org/10.1002/rcm.7048

Francey, R. J., Allison, C. E., Etheridge, D. M., Trudinger, C. M., Enting, I. G., Leuenberger, M., Langenfelds, R. L., Michel, E., & Steele, L. P. (1999). A 1000-year high precision record of δ13C in atmospheric CO2. *Tellus B*, *51*(2), 170–193. https://doi.org/10.1034/j.1600-0889.1999.t01-1-00005.x

FREEMAN, M., & CARLSON, R. M. (2005). ESSENTIAL NUTRIENTS. *Olive Production Manual*, *3353*, 75.

Friedli, H. R., Arellano, A. F., Cinnirella, S., & Pirrone, N. (2009). Initial Estimates of Mercury Emissions to the Atmosphere from Global Biomass Burning. *Environmental Science & Technology*, *43*(10), 3507–3513. https://doi.org/10.1021/es802703g

Friedrich, W. L., Kromer, B., Friedrich, M., Heinemeier, J., Pfeiffer, T., & Talamo, S. (2006). Santorini eruption radiocarbon dated to 1627-1600 B.C. *Science (New York, N.Y.)*, *312*(5773), 548. https://doi.org/10.1126/science.1125087

Fuller, D. Q. (2018). Long and attenuated: Comparative trends in the domestication of tree fruits. *Vegetation History and Archaeobotany*, *27*(1), 165–176. https://doi.org/10.1007/s00334-017-0659-2

Gagen, M., Finsinger, W., Wagner-Cremer, F., Mccarroll, D., Loader, N. J., Robertson, I., Jalkanen, R., Young, G., & Kirchhefer, A. (2011). Evidence of changing intrinsic water-use efficiency under rising atmospheric CO2 concentrations in Boreal Fennoscandia from subfossil leaves and tree ring δ13C ratios. *Global Change Biology*, *17*(2), 1064–1072. https://doi.org/10.1111/j.1365-2486.2010.02273.x

Galatali, S., A., N., & Kaya, E. (2021). *Characterization of Olive (Olea Europaea L.) Genetic Resources via PCR-Based Molecular Marker Systems*. *2*, 26–33. https://doi.org/10.24018/ejbio.2021.2.1.146

Galili, E., Langgut, D., Terral, J. F., Barazani, O., Dag, A., Kolska Horwitz, L., Ogloblin Ramirez, I., Rosen, B., Weinstein-Evron, M., Chaim, S., Kremer, E., Lev-Yadun, S., Boaretto, E., Ben-Barak-Zelas, Z., & Fishman, A. (2021). Early production of table olives at a mid-7th millennium BP submerged site off the Carmel coast (Israel). *Scientific Reports*, *11*(1), 2218. https://doi.org/10.1038/s41598-020-80772-6

Gårdfeldt, K., Sommar, J., Ferrara, R., Ceccarini, C., Lanzillotta, E., Munthe, J., Wängberg, I., Lindqvist, O., Pirrone, N., Sprovieri, F., Pesenti, E., & Strömberg, D. (2003). Evasion of mercury from coastal and open waters of the Atlantic Ocean and the Mediterranean Sea. *Atmospheric Environment*, *37*, 73–84. https://doi.org/10.1016/S1352-2310(03)00238-3

Gat, J., & Carmi, I. (1970). Evolution of the Isotopic Composition of Atmospheric Waters in the Mediterranean Sea Area. *Journal of Geophysical Research*, *75*, 3039–3048. https://doi.org/10.1029/JC075i015p03039

Gat, J., Mook, W. G., & Meijer, H.A.J. (2001). Willem G. Mook et Harro A .J.Meijer Centre Isotope Research, Groningen, The Netherlands. *2001*, *2*, 73.

Gérard, J., & Nehmé, C. (2020). Lebanon. *Méditerranée. Revue Géographique Des Pays Méditerranéens / Journal of Mediterranean Geography*, *131*, Article 131. https://journals.openedition.org/mediterranee/11018#

Gessler, A., & Ferrio, J. P. (2022). Postphotosynthetic Fractionation in Leaves, Phloem and Stem. *Series Editors*, 381.

Gessler, A., Ferrio, J. P., Hommel, R., Treydte, K., Werner, R. A., & Monson, R. K. (2014). Stable isotopes in tree rings: Towards a mechanistic understanding of isotope fractionation and mixing processes from the leaves to the wood. *Tree Physiology*, *34*(8), 796–818. https://doi.org/10.1093/treephys/tpu040

Ghaleb Faour. (2004). *FOREST FIRE FIGHTING IN LEBANON USING REMOTE SENSING AND GIS*. https://doi.org/10.13140/RG.2.2.28371.78884

Gibelin, A.-L., & Déqué, M. (2003). Anthropogenic climate change over the Mediterranean region simulated by a global variable resolution model. *Climate Dynamics*, *20*(4), 327–339. https://doi.org/10.1007/s00382-002-0277-1

Gielen, B., Jach, M. E., & Ceulemans, R. (2000). Effects of Season, Needle Age, and Elevated Atmospheric CO2 on Chlorophyll Fluorescence Parameters and Needle Nitrogen Concentration in Scots Pine (Pinus sylvestris). *Photosynthetica*, *38*(1), 13–21. https://doi.org/10.1023/A:1026727404895

Giesler, R., Clemmensen, K. E., Wardle, D. A., Klaminder, J., & Bindler, R. (2017). Boreal Forests Sequester Large Amounts of Mercury over Millennial Time Scales in the Absence of Wildfire. *Environmental Science & Technology*, *51*(5), 2621–2627. https://doi.org/10.1021/acs.est.6b06369

Gigolashvili, T., & Kopriva, S. (2014). Transporters in plant sulfur metabolism. *Frontiers in Plant Science*, *5*. https://www.frontiersin.org/articles/10.3389/fpls.2014.00442

Giorgi, F. (2006). Climate change hot-spots. *Geophysical Research Letters*, *33*(8). https://doi.org/10.1029/2006GL025734

Gleixner, G. (2005). Stable isotope composition of soil organic matter. In *Stable isotopes and biosphere-atmosphere interactions-Processes and biological* (pp. 29–46). Elsevier.

Gleixner, G., Bol, R., & Balesdent, J. (1999). Molecular insight into soil carbon turnover. *Rapid Communications in Mass Spectrometry*, *13*(13), 1278–1283. https://doi.org/10.1002/(SICI)1097-0231(19990715)13:13<1278::AID-RCM649>3.0.CO;2-N

Gleixner, G., Poirier, N., Bol, R., & Balesdent, J. (2002). Molecular dynamics of organic matter in a cultivated soil. *Organic Geochemistry*, *33*(3), 357–366. https://doi.org/10.1016/S0146-6380(01)00166-8

Goldreich, Y. (2003). The History of Climate and Meteorological Observations and Research in Israel. In *The Climate of Israel* (pp. 3–11). Springer.

Gonzàlez-Meler, M. A., Blanc-Betes, E., Flower, C. E., Ward, J. K., & Gomez-Casanovas, N. (2009). Plastic and adaptive responses of plant respiration to changes in atmospheric CO2 concentration. *Physiologia Plantarum*, *137*(4), 473–484. https://doi.org/10.1111/j.1399-3054.2009.01262.x

Greer, D. H., Laing, W. A., & Campbell, B. D. (1995). Photosynthetic responses of thirteen pasture species to elevated CO2 and temperature. *Functional Plant Biology*, *22*(5), 713–722.

Grigal, D. (2003). Mercury Sequestration in Forests and Peatlands: A Review. *Journal of Environmental Quality - J ENVIRON QUAL*, *32*. https://doi.org/10.2134/jeq2003.0393

Guarino, F., Improta, G., Triassi, M., Castiglione, S., & Cicatelli, A. (2021). Air quality biomonitoring through Olea europaea L.: The study case of “Land of pyres.” *Chemosphere*, *282*, 131052. https://doi.org/10.1016/j.chemosphere.2021.131052

Guerci, A. (2005). *L’olivo tra empirismo e scienza*. 5.

Gworek, B., Dmuchowski, W., & Baczewska-Dąbrowska, A. H. (2020). Mercury in the terrestrial environment: A review. *Environmental Sciences Europe*, *32*(1), 128. https://doi.org/10.1186/s12302-020-00401-x

Han, J.-J., Duan, X., Zhao, Y.-Y., & Li, M. (2019). Characteristics of Stable Hydrogen and Oxygen Isotopes of Soil Moisture under Different Land Use in Dry Hot Valley of Yuanmou. *Open Chemistry*, *17*(1), 105–115. https://doi.org/10.1515/chem-2019-0014

Hanson, P. J., Lindberg, S. E., Tabberer, T. A., Owens, J. G., & Kim, K.-H. (1995). Foliar exchange of mercury vapor: Evidence for a compensation point. *Water, Air, & Soil Pollution*, *80*(1–4), 373–382. https://doi.org/10.1007/BF01189687

Hartman, G., & Danin, A. (2010). Isotopic values of plants in relation to water availability in the Eastern Mediterranean region. *Oecologia*, *162*(4), 837–852. https://doi.org/10.1007/s00442-009-1514-7

Hartsough, P., Poulson, S. R., Biondi, F., & Estrada, I. G. (2008). Stable Isotope Characterization of the Ecohydrological Cycle at a Tropical Treeline Site. *Arctic, Antarctic, and Alpine Research*, *40*(2), 343–354. https://doi.org/10.1657/1523-0430(06-117)[HARTSOUGH]2.0.CO;2

Hawkins. (2018). *Show Your Stripes*. https://showyourstripes.info/l/globe

Heaton, T. H. E. (1987). The 15N/14N ratios of plants in South Africa and Namibia: Relationship to climate and coastal/saline environments. *Oecologia*, *74*(2), 236–246. https://doi.org/10.1007/BF00379365

Heineman, K. D., Turner, B. L., & Dalling, J. W. (2016). Variation in wood nutrients along a tropical soil fertility gradient. *New Phytologist*, *211*(2), 440–454. https://doi.org/10.1111/nph.13904

Hervé-Fernández, P., Oyarzún, C., Brumbt, C., Huygens, D., Bodé, S., Verhoest, N. E. C., & Boeckx, P. (2016). Assessing the “two water worlds” hypothesis and water sources for native and exotic evergreen species in south-central Chile: Ecohydrological Assesment. *Hydrological Processes*. https://doi.org/10.1002/hyp.10984

Higueras, P., Amorós, J. A., Esbrí, J. M., García-Navarro, F. J., Pérez de los Reyes, C., & Moreno, G. (2012). Time and space variations in mercury and other trace element contents in olive tree leaves from the Almadén Hg-mining district. *Journal of Geochemical Exploration*, *123*, 143–151. https://doi.org/10.1016/j.gexplo.2012.04.012

Higueras, P. L., Amorós, J. Á., Esbrí, J. M., Pérez-de-los-Reyes, C., López-Berdonces, M. A., & García-Navarro, F. J. (2016a). Mercury transfer from soil to olive trees. A comparison of three different contaminated sites. *Environmental Science and Pollution Research*, *23*(7), 6055–6061. https://doi.org/10.1007/s11356-015-4357-2

Higueras, P. L., Amorós, J. Á., Esbrí, J. M., Pérez-de-los-Reyes, C., López-Berdonces, M. A., & García-Navarro, F. J. (2016b). Mercury transfer from soil to olive trees. A comparison of three different contaminated sites. *Environmental Science and Pollution Research*, *23*(7), 6055–6061. https://doi.org/10.1007/s11356-015-4357-2

Hobbie, E. A., & Colpaert, J. V. (2003). Nitrogen Availability and Colonization by Mycorrhizal Fungi Correlate with Nitrogen Isotope Patterns in Plants. *The New Phytologist*, *157*(1), 115–126.

Hobbie, J. E., & Hobbie, E. A. (2006). 15N IN SYMBIOTIC FUNGI AND PLANTS ESTIMATES NITROGEN AND CARBON FLUX RATES IN ARCTIC TUNDRA. *Ecology*, *87*(4), 816.

Högberg, P. (1997). Tansley review no. 95 15N natural abundance in soil–plant systems. *The New Phytologist*, *137*(2), 179–203.

Högberg, P., Ekblad, A., Nordgren, A., Plamboeck, A. H., Ohlsson, A., Bhupinderpal-Singh, S., & Högberg, M. (2005). *Factors determining the 13C abundance of soil-respired CO2 in boreal forests*.

Howarth, R. W., & Teal, J. M. (1979). Sulfate reduction in a New England salt marsh1. *Limnology and Oceanography*, *24*(6), 999–1013. https://doi.org/10.4319/lo.1979.24.6.0999

*Improved online hydrogen isotope analysis of halite aqueous inclusions—Fourel—2019—Journal of Mass Spectrometry—Wiley Online Library*. (n.d.). Retrieved March 22, 2022, from https://analyticalsciencejournals.onlinelibrary.wiley.com/doi/full/10.1002/jms.4323?casa_token=Phj2vZWKJvMAAAAA%3ARK8X6LHmOYalaZx3lFczODfNNA9XSuFBGlGSyEqRrEZL9_UnGKYmNyZspw9qX4uIxB4lDhw2vH40rkA

IPCC (Ed.). (2007). *Climate change 2007: The physical science basis: contribution of Working Group I to the Fourth Assessment Report of the Intergovernmental Panel on Climate Change*. Cambridge University Press.

IPCC. (2021). *Climate Change 2021: The Physical Science Basis, the Working Group I contribution to the Sixth Assessment Report | NDC Action Project*. https://www.unep.org/ndc/resources/report/climate-change-2021-physical-science-basis-working-group-i-contribution-sixth

Jach, M. E., & Ceulemans, R. (2000). Effects of season, needle age and elevated atmospheric CO2 on photosynthesis in Scots pine (Pinus sylvestris). *Tree Physiology*, *20*(3), 145–157. https://doi.org/10.1093/treephys/20.3.145

Janick, J. (2010). The Origins of Fruits, Fruit Growing, and Fruit Breeding. In J. Janick (Ed.), *Plant Breeding Reviews* (pp. 255–321). John Wiley & Sons, Inc. https://doi.org/10.1002/9780470650301.ch8

Jindrich Petrlik, Kodeih, N., IndyACT, Arnika Association, & IPEN WG. (2013). *Mercury in Fish and Hair Samples from Batroun, Lebanon*. https://doi.org/10.13140/RG.2.2.12052.40327

Jiskra, M., Sonke, J. E., Obrist, D., Bieser, J., Ebinghaus, R., Myhre, C. L., Pfaffhuber, K. A., Wängberg, I., Kyllönen, K., Worthy, D., Martin, L. G., Labuschagne, C., Mkololo, T.,

Ramonet, M., Magand, O., & Dommergue, A. (2018a). A vegetation control on seasonal variations in global atmospheric mercury concentrations. *Nature Geoscience*, *11*(4), 244–250. https://doi.org/10.1038/s41561-018-0078-8

Jiskra, M., Sonke, J. E., Obrist, D., Bieser, J., Ebinghaus, R., Myhre, C. L., Pfaffhuber, K. A., Wängberg, I., Kyllönen, K., Worthy, D., Martin, L. G., Labuschagne, C., Mkololo, T., Ramonet, M., Magand, O., & Dommergue, A. (2018b). A vegetation control on seasonal variations in global atmospheric mercury concentrations. *Nature Geoscience*, *11*(4), 244–250. https://doi.org/10.1038/s41561-018-0078-8

Johnson, & Lindberg. (n.d.). The biogeochemical cycling of Hg in forests: Alternative methods for quantifying total deposition and soil emission. *1995*, *80: 1069–1077*, 9.

Jurdi, M., Korfali, S. I., Karahagopian, Y., & Davies, B. E. (2002). *Evaluation of Water Quality of the Qaraaoun Reservoir, Lebanon: Suitability for Multipurpose Usage*. *77*(11–30), 20.

Kabata-Pendias, A., & Pendias, H. (2000). *Trace elements in soils and plants* (3rd ed). CRC Press.

Kaniewski, D., Van Campo, E., Boiy, T., Terral, J.-F., Khadari, B., & Besnard, G. (2012). Primary domestication and early uses of the emblematic olive tree: Palaeobotanical, historical and molecular evidence from the Middle East. *Biological Reviews*, *87*(4), 885–899. https://doi.org/10.1111/j.1469-185X.2012.00229.x

Kaplan, I. R., & Rittenberg, S. C. (1964). Microbiological Fractionation of Sulphur Isotopes. *Journal of General Microbiology*, *34*(2), 195–212. https://doi.org/10.1099/00221287-34-2-195

Kawamura, H., Matsuoka, N., Momoshima, N., Koike, M., & Takashima, Y. (2006). Isotopic Evidence in Tree Rings for Historical Changes in Atmospheric Sulfur Sources. *Environmental Science & Technology*, *40*(18), 5750–5754. https://doi.org/10.1021/es060321w

Khadari, B., El Bakkali, A., Essalouh, L., Tollon, C., Pinatel, C., & Besnard, G. (2019). Cultivated Olive Diversification at Local and Regional Scales: Evidence From the Genetic Characterization of French Genetic Resources. *Frontiers in Plant Science*, *10*. https://www.frontiersin.org/articles/10.3389/fpls.2019.01593

Khatri, P. K., Larcher, R., Camin, F., Ziller, L., Tonon, A., Nardin, T., & Bontempo, L. (2021). Stable Isotope Ratios of Herbs and Spices Commonly Used as Herbal Infusions in the Italian Market. *ACS Omega*, *6*(18), 11925–11934. https://doi.org/10.1021/acsomega.1c00274

Kitoh, A., Yatagai, A., & Alpert, P. (2008). First super-high-resolution model projection that the ancient “Fertile Crescent” will disappear in this century. *Hydrological Research Letters*, *2*, 1–4. https://doi.org/10.3178/hrl.2.1

Klotzbücher, T., Kalbitz, K., Cerli, C., Hernes, P. J., & Kaiser, K. (2016). Gone or just out of sight? The apparent disappearance of aromatic litter components in soils. *SOIL*, *2*(3), 325–335. https://doi.org/10.5194/soil-2-325-2016

Kobrossi, R., Nuwayhid, I., Sibai, A. M., El-Fadel, M., & Khogali, M. (2002). Respiratory health effects of industrial air pollution on children in North Lebanon. *International Journal of Environmental Health Research*, *12*(3), 205–220. https://doi.org/10.1080/09603/202/000000970

Koeniger, P., & Margane, A. (n.d.). *Stable Isotope Investigations in the Jeita Spring Catchment*. 56.

Kotnik, J., Sprovieri, F., Ogrinc, N., Horvat, M., & Pirrone, N. (2014). Mercury in the Mediterranean, part I: Spatial and temporal trends. *Environmental Science and Pollution Research*, *21*(6), 4063–4080. https://doi.org/10.1007/s11356-013-2378-2

Krouse, H. R. (1977). Sulphur isotope abundance elucidate uptake of atmospheric sulphur emissions by vegetation. *Nature*, *265*(5589), 45–46. https://doi.org/10.1038/265045a0

Krouse, H. R. (1991). Stable isotopes: Natural and anthropogenic sulfur in the environment. *SCOPE*.

Labdaoui, D., Lotmani, B., & Aguedal, H. (2021). Assessment of Metal Pollution on the Cultivation of Olive Trees in the Petrochemical Industrial Zone of Arzew (Algeria). *South Asian Journal of Experimental Biology*, *11*(3), Article 3. https://doi.org/10.38150/sajeb.11(3).p227-233

Lange, M. A. (2018). *The Impacts of Climate Change in the MENA Region and the Water-Energy Nexus* [Preprint]. EARTH SCIENCES. https://doi.org/10.20944/preprints201810.0197.v1

Lavee, S. (1996). Biology and physiology of the olive tree. *World Olive Encyclopedia. International Olive Council*, 61–110.

Leavitt, S. W., & Long, A. (1983). An atmospheric $^{13}C/^{12}C$ reconstruction generated through removal of climate effects from tree-ring $^{13}C/^{12}C$ measurements. *Tellus B*, *35B*(2), 92–102. https://doi.org/10.1111/j.1600-0889.1983.tb00013.x

*Lebanon: Air Pollution | IAMAT*. (2020). https://www.iamat.org/country/lebanon/risk/air-pollution

Lelieveld, J., Hadjinicolaou, P., Kostopoulou, E., Chenoweth, J., El Maayar, M., Giannakopoulos, C., Hannides, C., Lange, M. A., Tanarhte, M., Tyrlis, E., & Xoplaki, E. (2012). Climate change and impacts in the Eastern Mediterranean and the Middle East. *Climatic Change*, *114*(3–4), 667–687. https://doi.org/10.1007/s10584-012-0418-4

Li, D., Fang, K., Li, Y., Chen, D., Liu, X., Dong, Z., Zhou, F., Guo, G., Shi, F., Xu, C., & Li, Y. (2017). Climate, intrinsic water-use efficiency and tree growth over the past 150 years in humid subtropical China. *PLOS ONE*, *12*(2), e0172045. https://doi.org/10.1371/journal.pone.0172045

Li, R., Wu, H., Ding, J., Fu, W., Gan, L., & Li, Y. (2017). Mercury pollution in vegetables, grains and soils from areas surrounding coal-fired power plants. *Scientific Reports*, *7*(1), 46545. https://doi.org/10.1038/srep46545

Li, Y., Shi, F., Li, X., Wu, H., Zhao, S., Wu, X., & Huang, Y. (2022). *Divergent roles of deep soil water uptake in seasonal tree growth under natural drought events in North China | Elsevier Enhanced Reader*. https://doi.org/10.1016/j.agrformet.2022.109102

Lindberg, S., Bullock, R., Ebinghaus, R., Engstrom, D., Feng, X., Fitzgerald, W., Pirrone, N., Prestbo, E., & Seigneur, C. (2007). A Synthesis of Progress and Uncertainties in Attributing the Sources of Mercury in Deposition. *Ambio*, *36*(1), 19–32.

Lindberg, S. E., Jackson, D. R., Huckabee, J. W., Janzen, S. A., Levin, M. J., & Lund, J. R. (1979). Atmospheric Emission and Plant Uptake of Mercury from Agricultural Soils near the Almadén Mercury Mine. *Journal of Environmental Quality*, *8*(4), 572–578. https://doi.org/10.2134/jeq1979.00472425000800040026x

Liphschitz, N., Gophna, R., Hartman, M., & Biger, G. (1991). The beginning of olive (olea europaea) cultivation in the old world: A reassessment. *Journal of Archaeological Science*, *18*(4), 441–453. https://doi.org/10.1016/0305-4403(91)90037-P

Liu, J., Wu, H., Zhang, H., Peng, G., Jiang, C., Zhao, Y., & Hu, J. (2021). *Controls of seasonality and altitude on generation of leaf water isotopes* [Preprint]. Ecohydrology/Instruments and observation techniques. https://doi.org/10.5194/hess-2021-289

Liu, X., Zhang, Y., Li, Z., Feng, T., Su, Q., & Song, Y. (2017). Carbon isotopes of C3 herbs correlate with temperature on removing the influence of precipitation across a temperature transect in the agro-pastoral ecotone of northern China. *Ecology and Evolution*, *7*(24), 10582–10591. https://doi.org/10.1002/ece3.3548

Liu, X.-Z., & Wang, G. (2010). Measurements of nitrogen isotope composition of plants and surface soils along the altitudinal transect of the eastern slope of Mount Gongga in southwest China. *Rapid Communications in Mass Spectrometry : RCM*, *24*, 3063–3071. https://doi.org/10.1002/rcm.4735

Llusia`, J., & Pen uelas, J. (2000). Seasonal patterns of terpene content and emission from seven Mediterranean woody species in field conditions. *American Journal of Botany*, *87*(1), 133–140. https://doi.org/10.2307/2656691

*LMC14*. (n.d.). Retrieved March 13, 2022, from https://lmc14.lsce.ipsl.fr/echantillons.html

Lodenius, M., Tulisalo, E., & Soltanpour-Gargari, A. (2003). Exchange of mercury between atmosphere and vegetation under contaminated conditions. *Science of The Total Environment*, *304*(1–3), 169–174. https://doi.org/10.1016/S0048-9697(02)00566-1

Lorenz, M., Derrien, D., Zeller, B., Udelhoven, T., Werner, W., & Thiele-Bruhn, S. (2020). The linkage of 13C and 15N soil depth gradients with C:N and O:C stoichiometry reveals tree species effects on organic matter turnover in soil. *Biogeochemistry*, *151*(2–3), 203–220. https://doi.org/10.1007/s10533-020-00721-3

Lovett, G. M., Weathers, K. C., Arthur, M. A., & Schultz, J. C. (2004). Nitrogen cycling in a northern hardwood forest: Do species matter? *Biogeochemistry*, *67*(3), 289–308. https://doi.org/10.1023/B:BIOG.0000015786.65466.f5

Luo, Y., Duan, L., Driscoll, C. T., Xu, G., Shao, M., Taylor, M., Wang, S., & Hao, J. (2016). Foliage/atmosphere exchange of mercury in a subtropical coniferous forest in south China.

*Journal of Geophysical Research: Biogeosciences*, *121*(7), 2006–2016. https://doi.org/10.1002/2016JG003388

Maillard, F., Girardclos, O., Assad, M., Zappelini, C., Pérez Mena, J. M., Yung, L., Guyeux, C., Chrétien, S., Bigham, G., Cosio, C., & Chalot, M. (2016). Dendrochemical assessment of mercury releases from a pond and dredged-sediment landfill impacted by a chlor-alkali plant. *Environmental Research*, *148*, 122–126. https://doi.org/10.1016/j.envres.2016.03.034

Maldonado, N. G., López, M. J., Caudullo, G., & de Rigo, D. (n.d.). *Olea europaea in Europe: Distribution, habitat, usage and threats*. 2.

Marian, F., Sandmann, D., Krashevska, V., Maraun, M., & Scheu, S. (2017). Leaf and root litter decomposition is discontinued at high altitude tropical montane rainforests contributing to carbon sequestration. *Ecology and Evolution*, *7*(16), 6432–6443. https://doi.org/10.1002/ece3.3189

Marshall, J. D., Brooks, J. R., & Lajtha, K. (2007). Sources of Variation in the Stable Isotopic Composition of Plants. In R. Michener & K. Lajtha (Eds.), *Stable Isotopes in Ecology and Environmental Science* (pp. 22–60). Blackwell Publishing Ltd. https://doi.org/10.1002/9780470691854.ch2

Matteo, G., Angelis, P., Brugnoli, E., Cherubini, P., & Scarascia-Mugnozza, G. (2010). Tree-ring Δ13C reveals the impact of past forest management on water-use efficiency in a Mediterranean oak coppice in Tuscany (Italy). *Annals of Forest Science*, *67*(5), 510–510. https://doi.org/10.1051/forest/2010012

McLagan, D. S., Biester, H., Navrátil, T., Kraemer, S. M., & Schwab, L. (2022). *Internal tree cycling and atmospheric archiving of mercury: Examination with concentration and stable isotope analyses* [Preprint]. Biogeochemistry: Air - Land Exchange. https://doi.org/10.5194/bg-2022-124

McLagan, D. S., Stupple, G. W., Darlington, A., Hayden, K., Steffen, A., & Kamp, L. (2021). Where there is smoke there is mercury: Assessing boreal forest fire mercury emissions using aircraft and highlighting uncertainties associated with upscaling emissions estimates. *Atmos. Chem. Phys.*, 19.

Mercuri, A. M. (2015). Applied palynology as a trans-disciplinary science: The contribution of aerobiology data to forensic and palaeoenvironmental issues. *Aerobiologia*, *31*(3), 323–339. https://doi.org/10.1007/s10453-015-9367-5

Mitrakos, K. (1980). *A theory for Mediterranean plant life*.

Moriondo, M., Stefanini, F. M., & Bindi, M. (2008). Reproduction of olive tree habitat suitability for global change impact assessment. *Ecological Modelling*, *218*(1), 95–109.

Moriondo, M., Trombi, G., Ferrise, R., Brandani, G., Dibari, C., Ammann, C. M., Lippi, M. M., & Bindi, M. (2013). Olive trees as bio-indicators of climate evolution in the Mediterranean

Basin: Impact of climate change on olive tree distribution. *Global Ecology and Biogeography*, *22*(7), 818–833. https://doi.org/10.1111/geb.12061

Munksgaard, N. C., Wurster, C. M., Bass, A., & Bird, M. I. (2012). Extreme short-term stable isotope variability revealed by continuous rainwater analysis. *Hydrological Processes*, *26*(23), 3630–3634. https://doi.org/10.1002/hyp.9505

Munksgaard, N. C., Zwart, C., Kurita, N., Bass, A., Nott, J., & Bird, M. I. (2015). Stable Isotope Anatomy of Tropical Cyclone Ita, North-Eastern Australia, April 2014. *PLOS ONE*, *10*(3), e0119728. https://doi.org/10.1371/journal.pone.0119728

Naharro, R., Esbri, J., Amorós, J., & Higueras, P. (2018). *Atmospheric mercury uptake and desorption from olive-tree leaves*. *20*(EGU2018-2982,2018), 2.

Nassif, N., Jaoude, L. A., El Hage, M., & Robinson, C. A. (2016). Data Exploration and Reconnaissance to Identify Ocean Phenomena: A Guide for <i>In Situ</i> Data Collection. *Journal of Water Resource and Protection*, *08*(10), 929–943. https://doi.org/10.4236/jwarp.2016.810076

Neff, J. C., Chapin III, F. S., & Vitousek, P. M. (2003). Breaks in the cycle: Dissolved organic nitrogen in terrestrial ecosystems. *Frontiers in Ecology and the Environment*, *1*(4), 205–211. https://doi.org/10.1890/1540-9295(2003)001[0205:BITCDO]2.0.CO;2

Neumann, J. (1985). Climatic change as a topic in the classical Greek and Roman literature. *Climatic Change*, *7*(4), 441–454. https://doi.org/10.1007/BF00139058

Newton, C., Lorre, C., Sauvage, C., Ivorra, S., & Terral, J.-F. (2014). On the origins and spread of Olea europaea L. (olive) domestication: Evidence for shape variation of olive stones at Ugarit, Late Bronze Age, Syria—a window on the Mediterranean Basin and on the westward diffusion of olive varieties. *Vegetation History and Archaeobotany*, *23*(5), 567–575.

Niedermeyer, E. M., Forrest, M., Beckmann, B., Sessions, A. L., Mulch, A., & Schefuß, E. (2016). The stable hydrogen isotopic composition of sedimentary plant waxes as quantitative proxy for rainfall in the West African Sahel. *Geochimica et Cosmochimica Acta*, *184*, 55–70. https://doi.org/10.1016/j.gca.2016.03.034

Niu, Z., Zhang, X., Wang, Z., & Ci, Z. (2011). Field controlled experiments of mercury accumulation in crops from air and soil. *Environmental Pollution*, *159*(10), 2684–2689. https://doi.org/10.1016/j.envpol.2011.05.029

Novák, M., Buzek, F., Harrison, A. F., Přechová, E., Jačková, I., & Fottová, D. (2003). Similarity between C, N and S stable isotope profiles in European spruce forest soils: Implications for the use of δ34S as a tracer. *Applied Geochemistry*, *18*(5), 765.

Oakes, J., & Connolly, R. (2004). Causes of sulfur isotope variability in the seagrass, Zostera capricorni. *Journal of Experimental Marine Biology and Ecology*, *302*. https://doi.org/10.1016/j.jembe.2003.10.011

Obrist, D. (2007). Atmospheric mercury pollution due to losses of terrestrial carbon pools? *Biogeochemistry*, *85*(2), 119–123. https://doi.org/10.1007/s10533-007-9108-0

Obrist, D., Johnson, D. W., & Lindberg, S. E. (2009). *Mercury concentrations and pools in four Sierra Nevada forest sites, and relationships to organic carbon and nitrogen*. 13.

Obrist, D., Kirk, J. L., Zhang, L., Sunderland, E. M., Jiskra, M., & Selin, N. E. (2018a). A review of global environmental mercury processes in response to human and natural perturbations: Changes of emissions, climate, and land use. *Ambio*, *47*(2), 116–140. https://doi.org/10.1007/s13280-017-1004-9

Obrist, D., Kirk, J. L., Zhang, L., Sunderland, E. M., Jiskra, M., & Selin, N. E. (2018b). A review of global environmental mercury processes in response to human and natural perturbations: Changes of emissions, climate, and land use. *Ambio*, *47*(2), 116–140. https://doi.org/10.1007/s13280-017-1004-9

Obrist, M. K., Rathey, E., Bontadina, F., Martinoli, A., Conedera, M., Christe, P., & Moretti, M. (2011). Response of bat species to sylvo-pastoral abandonment. *Forest Ecology and Management*, *261*(3), 789–798. https://doi.org/10.1016/j.foreco.2010.12.010

O'Connor, D., Hou, D., Ok, Y. S., Mulder, J., Duan, L., Wu, Q., Wang, S., Tack, F. M. G., & Rinklebe, J. (2019a). Mercury speciation, transformation, and transportation in soils, atmospheric flux, and implications for risk management: A critical review. *Environment International*, *126*, 747–761. https://doi.org/10.1016/j.envint.2019.03.019

O'Connor, D., Hou, D., Ok, Y. S., Mulder, J., Duan, L., Wu, Q., Wang, S., Tack, F. M. G., & Rinklebe, J. (2019b). Mercury speciation, transformation, and transportation in soils, atmospheric flux, and implications for risk management: A critical review. *Environment International*, *126*, 747–761. https://doi.org/10.1016/j.envint.2019.03.019

Oflaz, A., Dörfler, W., & Weinelt, M. (2019). *An overview of olive trees in the eastern Mediterranean during the mid- to late Holocene: Selective exploitation or established arboriculture?* (pp. 131–165).

Ogaya, R., & Peñuelas, J. (2008). Changes in leaf δ13C and δ15N for three Mediterranean tree species in relation to soil water availability. *Acta Oecologica*, *34*(3), 331–338. https://doi.org/10.1016/j.actao.2008.06.005

Ozturk, M., Altay, V., Gönenç, T. M., Unal, B. T., Efe, R., Akçiçek, E., & Bukhari, A. (2021). An Overview of Olive Cultivation in Turkey: Botanical Features, Eco-Physiology and Phytochemical Aspects. *Agronomy*, *11*(2), 295. https://doi.org/10.3390/agronomy11020295

Pardo, L. H., Semaoune, P., Schaberg, P. G., Eagar, C., & Sebilo, M. (2013). Patterns in δ15N in roots, stems, and leaves of sugar maple and American beech seedlings, saplings, and mature trees. *Biogeochemistry*, *112*(1–3), 275–291. https://doi.org/10.1007/s10533-012-9724-1

Pardo, L. H., Templer, P. H., Goodale, C. L., Duke, S., Groffman, P. M., Adams, M. B., Boeckx, P., Boggs, J., Campbell, J., Colman, B., Compton, J., Emmett, B., Gundersen, P., Kjønaas, J.,

Lovett, G., Mack, M., Magill, A., Mbila, M., Mitchell, M. J., … Wessel, W. (2006). Regional Assessment of N Saturation using Foliar and Root $$\varvec {\delta}^{\bf 15}{\bf N}$$. *Biogeochemistry*, *80*(2), 143–171. https://doi.org/10.1007/s10533-006-9015-9

Park, R., & Epstein, S. (1960). CARBON ISOTOPE FRACTIONATION DURING PHOTOSYNTHESIS. *Geochim. et Cosmochim. Acta, Vol: 21*. https://doi.org/10.1016/S0016-7037(60)80006-3

Patra, M., & Sharma, A. (2000). Mercury toxicity in plants. *The Botanical Review*, *66*(3), 379–422. https://doi.org/10.1007/BF02868923

Peñuelas, J., Filella, I., Lloret, F., Piñol, J., & Siscart, D. (2000). Effects of a severe drought on water and nitrogen use by Quercus ilex and Phyllyrea latifolia. *Biologia Plantarum*, *43*(1), 47–53.

Pereira, J. S., & Chaves, M. M. (1995). Plant responses to drought under climate change in Mediterranean-type ecosystems. In *Global change and Mediterranean-type ecosystems* (pp. 140–160). Springer.

Peuke, A. D., Gessler, A., & Rennenberg, H. (2006). The effect of drought on C and N stable isotopes in different fractions of leaves, stems and roots of sensitive and tolerant beech ecotypes. *Plant, Cell and Environment*, *29*(5), 823–835. https://doi.org/10.1111/j.1365-3040.2005.01452.x

Pingyuan, W., Liu, W., & Li, J.-T. (2010). Water use strategy of Ficus tinctoria in tropical rainforest region of Xishuangbanna, South-western China. *Chinese Journal of Applied Ecology*, *21*, 836–842.

Pleijel, H., Klingberg, J., Nerentorp, M., Broberg, M. C., Nyirambangutse, B., Munthe, J., & Wallin, G. (2021). *Mercury accumulation in leaves of different plant types – the significance of tissue age and specific leaf area* [Preprint]. Biogeochemistry: Air - Land Exchange. https://doi.org/10.5194/bg-2021-117

Pokharel, A. K., & Obrist, D. (2011). Fate of mercury in tree litter during decomposition. *Biogeosciences*, *8*(9), 2507–2521. https://doi.org/10.5194/bg-8-2507-2011

Rea, A. W., Keeler, G. J., & Scherbatskoy, T. (1996a). The deposition of mercury in throughfall and litterfall in the lake champlain watershed: A short-term study. *Atmospheric Environment*, *30*(19), 3257–3263. https://doi.org/10.1016/1352-2310(96)00087-8

Rea, A. W., Keeler, G. J., & Scherbatskoy, T. (1996b). The deposition of mercury in throughfall and litterfall in the lake champlain watershed: A short-term study. *Atmospheric Environment*, *30*(19), 3257–3263. https://doi.org/10.1016/1352-2310(96)00087-8

Rea, A. W., Lindberg, S. E., Scherbatskoy, T., & Keeler, G. J. (2002). *Mercury Accumulation in Foliage over Time in Two Northern Mixed-Hardwood Forests*. 19.

Rennenberg, H., Brunold, C., Rijksuniversiteit Groningen, & Rijksuniversiteit (Eds.). (1990). *Sulfur nutrition and sulfur assimilation in higher plants: Fundamental, environmental and*

*agricultural aspects ; proceedings of a workshop organized by the Department of Plant Physiology, University of Groningen ... Haren, 28 - 31 March 1989*. SPB Adacemic Publ.

Richardson, J. B., Friedland, A. J., Engerbretson, T. R., Kaste, J. M., & Jackson, B. P. (2013). Spatial and vertical distribution of mercury in upland forest soils across the northeastern United States. *Environmental Pollution (Barking, Essex : 1987)*, *182*, 127–134. https://doi.org/10.1016/j.envpol.2013.07.011

Rossi, L., Sebastiani, L., Tognetti, R., d'Andria, R., Morelli, G., & Cherubini, P. (2013). Tree-ring wood anatomy and stable isotopes show structural and functional adjustments in olive trees under different water availability. *Plant and Soil*, *372*(1–2), 567–579. https://doi.org/10.1007/s11104-013-1759-0

Royer, D. L. (2001). Stomatal density and stomatal index as indicators of paleoatmospheric CO2 concentration. *Review of Palaeobotany and Palynology*, *114*(1–2), 1–28. https://doi.org/10.1016/S0034-6667(00)00074-9

Saad, Z., Slim, K., Ghaddar, A., Nasreddine, M., & Kattan, Z. (2000). Chemical composition of rain water in Lebanon. *Journal Européen d'hydrologie*, *31*(2), 223–238. https://doi.org/10.1051/water/20003102223

Saliendra, N., Meinzer, F., Perry, M., & Thom, M. (1996). Associations between partitioning of carboxylase activity and bundle sheath leakiness to CO2, carbon isotope discrimination, photosynthesis, and growth in sugarcane. *Journal of Experimental Botany*, *47*. https://doi.org/10.1093/jxb/47.7.907

Sanchez-Bragado, R., Serret, M. D., Marimon, R. M., Bort, J., & Araus, J. L. (2019). The Hydrogen Isotope Composition $\delta^{2}$H Reflects Plant Performance. *Plant Physiology*, *180*(2), 793–812. https://doi.org/10.1104/pp.19.00238

Sanz-Cortés, F., Martinez-Calvo, J., Badenes, M. L., Bleiholder, H., Hack, H., Llacer, G., & Meier, U. (2002). Phenological growth stages of olive trees (Olea europaea). *Annals of Applied Biology*, *140*(2), 151–157. https://doi.org/10.1111/j.1744-7348.2002.tb00167.x

Schaefer, K., Elshorbany, Y., Jafarov, E., Schuster, P. F., Striegl, R. G., Wickland, K. P., & Sunderland, E. M. (2020). Potential impacts of mercury released from thawing permafrost. *Nature Communications*, *11*(1), Article 1. https://doi.org/10.1038/s41467-020-18398-5

Schicchi, R., Speciale, C., Amato, F., Bazan, G., Di Noto, G., Marino, P., Ricciardo, P., & Geraci, A. (2021). The Monumental Olive Trees as Biocultural Heritage of Mediterranean Landscapes: The Case Study of Sicily. *Sustainability*, *13*(12), 6767. https://doi.org/10.3390/su13126767

Schmidt, H.-L., Werner, R. A., & Eisenreich, W. (2003). Systematics of 2H patterns in natural compounds and its importance for the elucidation of biosynthetic pathways. *Phytochemistry Reviews*, *2*(1–2), 61–85. https://doi.org/10.1023/B:PHYT.0000004185.92648.ae

Schneider, L., Allen, K., Walker, M., Morgan, C., & Haberle, S. (2019). Using Tree Rings to Track Atmospheric Mercury Pollution in Australia: The Legacy of Mining in Tasmania.

*Environmental Science & Technology*, *53*(10), 5697–5706. https://doi.org/10.1021/acs.est.8b06712

Scholl, M. A., Giambelluca, T. W., Gingerich, S. B., Nullet, M. A., & Loope, L. L. (2007). Cloud water in windward and leeward mountain forests: The stable isotope signature of orographic cloud water: ISOTOPE SIGNATURE OF CLOUD WATER. *Water Resources Research*, *43*(12). https://doi.org/10.1029/2007WR006011

Schubert, B. A., & Jahren, A. H. (2011). Fertilization trajectory of the root crop Raphanus sativus across atmospheric pCO2 estimates of the next 300 years. *Agriculture, Ecosystems & Environment*, *140*(1–2), 174–181. https://doi.org/10.1016/j.agee.2010.11.024

Schubert, B. A., & Jahren, A. H. (2012). The effect of atmospheric CO2 concentration on carbon isotope fractionation in C3 land plants. *Geochimica et Cosmochimica Acta*, *96*, 29–43. https://doi.org/10.1016/j.gca.2012.08.003

Schwesig, D., & Krebs, O. (2003). The role of ground vegetation in the uptake of mercury and methylmercury in a forest ecosystem. *Plant and Soil*, 11.

Senesil, G. S., Baldassarre, G., Senesi, N., & Radina, B. (1999). Trace element inputs into soils by anthropogenic activities and implications for human health. *Chemosphere*, *39*(2), 343–377. https://doi.org/10.1016/S0045-6535(99)00115-0

Sghaier, A., Perttunen, J., Sievaènen, R., Boujnah, D., Ouessar, M., Ben Ayed, R., & Naggaz, K. (2019). Photosynthetical activity modelisation of olive trees growing under drought conditions. *Scientific Reports*, *9*(1), 15536. https://doi.org/10.1038/s41598-019-52094-9

Sheil, D. (2018). Forests, atmospheric water and an uncertain future: The new biology of the global water cycle. *Forest Ecosystems*, *5*(1), 19. https://doi.org/10.1186/s40663-018-0138-y

Sidorova, O. V., Siegwolf, R. T. W., Saurer, M., Naurzbaev, M. M., & Vaganov, E. A. (2008). Isotopic composition (δ13C, δ18O) in wood and cellulose of Siberian larch trees for early Medieval and recent periods. *Journal of Geophysical Research: Biogeosciences*, *113*(G2). https://doi.org/10.1029/2007JG000473

Silva, L. C. R., & Horwath, W. R. (2013). Explaining Global Increases in Water Use Efficiency: Why Have We Overestimated Responses to Rising Atmospheric CO2 in Natural Forest Ecosystems? *PLoS ONE*, *8*(1), e53089. https://doi.org/10.1371/journal.pone.0053089

Singh, B. P. (2017). Original isotopic composition of water in precipitation by different methods. *Applied Water Science*, *7*(6), 3385–3390. https://doi.org/10.1007/s13201-016-0500-6

Swap, R. J., Aranibar, J. N., Dowty, P. R., Gilhooly III, W. P., & Macko, S. A. (2004). Natural abundance of 13C and 15N in C3 and C4 vegetation of southern Africa: Patterns and implications. *Global Change Biology*, *10*(3), 350–358. https://doi.org/10.1111/j.1365-2486.2003.00702.x

Tabaja, N., Amouroux, D., Chalak, L., Fourel, F., Tessier, E., Jomaa, I., El Riachy, M., & Bentaleb, I. (2022). Seasonal variation of mercury concentration of ancient olive groves of Lebanon. *EGUsphere*, *2022*, 1–25. https://doi.org/10.5194/egusphere-2022-174

Tang, Z., Xu, W., Zhou, G., Bai, Y., Li, J., Tang, X., Chen, D., Liu, Q., Ma, W., Xiong, G., He, N., Guo, Y., Guo, Q., Zhu, J., Han, W., Hu, H., Fang, J., & Xie, Z. (2017). *Patterns of plant carbon, nitrogen, and phosphorus concentration in relation to productivity in China's terrestrial ecosystems*. https://doi.org/10.1073/pnas.1700295114

Tatsumi, C., Hyodo, F., Taniguchi, T., Shi, W., Koba, K., Fukushima, K., Du, S., Yamanaka, N., Templer, P., & Tateno, R. (2021). Arbuscular Mycorrhizal Community in Roots and Nitrogen Uptake Patterns of Understory Trees Beneath Ectomycorrhizal and Non-ectomycorrhizal Overstory Trees. *Frontiers in Plant Science*, *11*. https://www.frontiersin.org/articles/10.3389/fpls.2020.583585

Taylor, A. M., Renée Brooks, J., Lachenbruch, B., Morrell, J. J., & Voelker, S. (2008). Correlation of carbon isotope ratios in the cellulose and wood extractives of Douglas-fir. *Dendrochronologia*, *26*(2), 125–131. https://doi.org/10.1016/j.dendro.2007.05.005

Tcherkez, G., & Tea, I. (2013). 32S/34S isotope fractionation in plant sulphur metabolism. *New Phytologist*, *200*(1), 44–53. https://doi.org/10.1111/nph.12314

Teixeira, D. C., Lacerda, L. D., & Silva-Filho, E. V. (2017). Mercury sequestration by rainforests: The influence of microclimate and different successional stages. *Chemosphere*, *168*, 1186–1193. https://doi.org/10.1016/j.chemosphere.2016.10.081

*Telelis 2000.pdf*. (n.d.).

Templer, P. H., Arthur, M. A., Lovett, G. M., & Weathers, K. C. (2007). Plant and soil natural abundance δ 15N: Indicators of relative rates of nitrogen cycling in temperate forest ecosystems. *Oecologia*, *153*(2), 399–406. https://doi.org/10.1007/s00442-007-0746-7

Tenzin, K., & Dukpa, D. (2017). *Dendrochronological Manual*.

Terral, J.-F., Alonso, N., Capdevila, R. B. i, Chatti, N., Fabre, L., Fiorentino, G., Marinval, P., Jordá, G. P., Pradat, B., Rovira, N., & Alibert, P. (2004). Historical biogeography of olive domestication (Olea europaea L.) as revealed by geometrical morphometry applied to biological and archaeological material: Historical biogeography of olive domestication (Olea europaea L.). *Journal of Biogeography*, *31*(1), 63–77. https://doi.org/10.1046/j.0305-0270.2003.01019.x

*The water cycle (article) | Ecology | Khan Academy*. (n.d.). Retrieved March 21, 2022, from https://www.khanacademy.org/science/biology/ecology/biogeochemical-cycles/a/the-water-cycle

Tognetti, R., d'Andria, R., Morelli, G., & Alvino, A. (2005). The effect of deficit irrigation on seasonal variations of plant water use in Olea europaea L. *Plant and Soil*, *273*(1–2), 139–155. https://doi.org/10.1007/s11104-004-7244-z

Tognetti, R., d'Andria, R., Morelli, G., Calandrelli, D., & Fragnito, F. (2004). Irrigation effects on daily and seasonal variations of trunk sap flow and leaf water relations in olive trees. *Plant and Soil*, *263*(1), 249–264. https://doi.org/10.1023/B:PLSO.0000047738.96931.91

Tognetti, R., Giovannelli, A., Lavini, A., Morelli, G., Fragnito, F., & d'Andria, R. (2009). Assessing environmental controls over conductances through the soil–plant–atmosphere continuum in an experimental olive tree plantation of southern Italy. *Agricultural and Forest Meteorology*, *149*(8), 1229–1243. https://doi.org/10.1016/j.agrformet.2009.02.008

Tomiyasu, T., Matsuo, T., Miyamoto, J., Imura, R., Anazawa, K., & Sakamoto, H. (2005). Low level mercury uptake by plants from natural environments—Mercury distribution in Solidago altissima L.-. *Environmental Sciences: An International Journal of Environmental Physiology and Toxicology*, *12*(4), 231–238.

Tormo-Molina, R., Gonzalo-Garijo, M., Silva-Palacios, I., & Muñoz, A. (2010). General Trends in Airborne Pollen Production and Pollination Periods at a Mediterranean Site (Badajoz, Southwest Spain). *J Investig Allergol Clin Immunol*, *20*, 8.

Trumbore, S. (2009). Radiocarbon and soil carbon dynamics. *Annual Review of Earth and Planetary Sciences*, *37*(1), 47–66.

Trust, B. A., & Fry, B. (1992). Stable sulphur isotopes in plants: A review. *Plant, Cell and Environment*, *15*(9), 1105–1110. https://doi.org/10.1111/j.1365-3040.1992.tb01661.x

Tu, K., & Dawson, T. (2005). Partitioning ecosystem respiration using stable carbon isotope analyses of CO2. *Flanagan, LB, Ehleringer, JR, and Pataki, DE, Physiological Ecology, Elsevier Academic Press, London, UK*, 125–153.

Tuel, A., & Eltahir, E. A. B. (2020). Why Is the Mediterranean a Climate Change Hot Spot? *JOURNAL OF CLIMATE*, *33*, 15.

UNEP. (2019). *Technical Background Report to the Global Mercury Assessment 2018*. IVL Svenska Miljöinstitutet.

Wallander, H., Nilsson, L. O., Hagerberg, D., & Rosengren, U. (2003). Direct estimates of C:N ratios of ectomycorrhizal mycelia collected from Norway spruce forest soils. *Soil Biology and Biochemistry*, *35*(7), 997–999. https://doi.org/10.1016/S0038-0717(03)00121-4

Wang, X., Lin, C.-J., Lu, Z., Zhang, H., Zhang, Y., & Feng, X. (2016). Enhanced accumulation and storage of mercury on subtropical evergreen forest floor: Implications on mercury budget in global forest ecosystems: HG STORAGE ON SUBTROPICAL FOREST FLOOR. *Journal of Geophysical Research: Biogeosciences*, *121*(8), 2096–2109. https://doi.org/10.1002/2016JG003446

Wigley, T. M. L., Ingram, M. J., & Farmer, G. (1981). *Climate and History: Studies in Past Climates and their Impact on Man*. CUP Archive.

Winner, W. E., & Bewley, J. D. (1978). Contrasts between bryophyte and vascular plant synecological responses in an SO2-stressed white spruce association in central Alberta. *Oecologia*, *33*(3), 311–325. https://doi.org/10.1007/BF00348116

Wofsy, S. C., Goulden, M. L., Munger, J. W., Fan, S.-M., Bakwin, P. S., Daube, B. C., Bassow, S. L., & Bazzaz, F. A. (1993). Net Exchange of $CO_2$ in a Mid-Latitude Forest. *Science*, *260*(5112), 1314–1317. https://doi.org/10.1126/science.260.5112.1314

Wohlgemuth, L., Rautio, P., Ahrends, B., Russ, A., Vesterdal, L., Waldner, P., Timmermann, V., Eickenscheidt, N., Fürst, A., Greve, M., Roskams, P., Thimonier, A., Nicolas, M., Kowalska, A., Ingerslev, M., Merilä, P., Benham, S., Iacoban, C., Hoch, G., … Jiskra, M. (2021). *Physiological and climate controls on foliar mercury uptake by European tree species* [Preprint]. Biogeochemistry: Air - Land Exchange. https://doi.org/10.5194/bg-2021-239

Wright, L. P., Zhang, L., & Marsik, F. J. (2016). Overview of mercury dry deposition, litterfall, and throughfall studies. *Atmospheric Chemistry and Physics*, *16*(21), 13399–13416. https://doi.org/10.5194/acp-16-13399-2016

Wynn, J. G., Bird, M. I., & Wong, V. N. L. (2005). Rayleigh distillation and the depth profile of 13C/12C ratios of soil organic carbon from soils of disparate texture in Iron Range National Park, Far North Queensland, Australia. *Geochimica et Cosmochimica Acta*, *69*(8), 1961–1973. https://doi.org/10.1016/j.gca.2004.09.003

Xoplaki, E. (2002). *Climate Variability over the Mediterranean*.

Yammine, P., Kfoury, A., El-Khoury, B., Nouali, H., El-Nakat, H., Ledoux, F., Courcot, D., & Aboukaïs, A. (2010). A PRELIMINARY EVALUATION OF THE INORGANIC CHEMICAL COMPOSITION OF ATMOSPHERIC TSP IN THE SELAATA REGION, NORTH LEBANON. *Lebanese Science Journal*, *11*(1), 18.

Yanai, R. D., Yang, Y., Wild, A. D., Smith, K. T., & Driscoll, C. T. (2020a). New Approaches to Understand Mercury in Trees: Radial and Longitudinal Patterns of Mercury in Tree Rings and Genetic Control of Mercury in Maple Sap. *Water, Air, & Soil Pollution*, *231*(5), 248. https://doi.org/10.1007/s11270-020-04601-2

Yanai, R. D., Yang, Y., Wild, A. D., Smith, K. T., & Driscoll, C. T. (2020b). New Approaches to Understand Mercury in Trees: Radial and Longitudinal Patterns of Mercury in Tree Rings and Genetic Control of Mercury in Maple Sap. *Water, Air, & Soil Pollution*, *231*(5), 248. https://doi.org/10.1007/s11270-020-04601-2

Yang, Y., Yanai, R. D., Driscoll, C. T., Montesdeoca, M., & Smith, K. T. (2018a). Concentrations and content of mercury in bark, wood, and leaves in hardwoods and conifers in four forested sites in the northeastern USA. *PLOS ONE*, *13*(4), e0196293. https://doi.org/10.1371/journal.pone.0196293

Yang, Y., Yanai, R. D., Driscoll, C. T., Montesdeoca, M., & Smith, K. T. (2018b). Concentrations and content of mercury in bark, wood, and leaves in hardwoods and conifers in four forested

sites in the northeastern USA. *PLOS ONE*, *13*(4), e0196293. https://doi.org/10.1371/journal.pone.0196293

Yazbeck, E. B., Rizk, G. A., Hassoun, G., El-Khoury, R., & Geagea, L. (2018). *Ecological characterization of ancient olive trees in Lebanon- Bshaaleh area and their age estimation*. *11*(2 Ver. 1), 35–44.

Yoneyama, T., Okada, H., & Ando, S. (2010). Seasonal variations in natural $^{13}$C abundances in $C_3$ and $C_4$ plants collected in Thailand and the Philippines. *Soil Science and Plant Nutrition*, *56*(3), 422–426. https://doi.org/10.1111/j.1747-0765.2010.00477.x

Z. Houlton, B., M. Sigman, D., A. G. Schuur, E., & Hedin, L. (2007). *A climate-driven switch in plant nitrogen acquisition within tropical forest communities*. https://doi.org/10.1073/pnas.0609935104

Zhang, J., He, N., Liu, C., Xu, L., Chen, Z., Li, Y., Wang, R., Yu, G., Sun, W., Xiao, C., & Reich, P. (2019). Variation and evolution of C:N ratio among different organs enable plants to adapt to N-limited environments. *Global Change Biology*, *26*. https://doi.org/10.1111/gcb.14973

Zhang, S., Wen, X., Wang, J., Yu, G., & Sun, X. (2010). The use of stable isotopes to partition evapotranspiration fluxes into evaporation and transpiration. *Acta Ecologica Sinica*, *30*(4), 201–209. https://doi.org/10.1016/j.chnaes.2010.06.003

Zhang, X., Aguilar, E., Sensoy, S., Melkonyan, H., Tagiyeva, U., Ahmed, N., Kutaladze, N., Rahimzadeh, F., Taghipour, A., Hantosh, T. H., Albert, P., Semawi, M., Karam Ali, M., Said Al-Shabibi, M. H., Al-Oulan, Z., Zatari, T., Al Dean Khelet, I., Hamoud, S., Sagir, R., … Wallis, T. (2005). Trends in Middle East climate extreme indices from 1950 to 2003. *Journal of Geophysical Research*, *110*(D22), D22104. https://doi.org/10.1029/2005JD006181

Zhang, Y., Mitchell, M. J., Christ, M., Likens, G. E., & Krouse, H. R. (1998). Stable sulfur isotopic biogeochemistry of the Hubbard Brook Experimental Forest, New Hampshire. *Biogeochemistry*, *41*(3), 259–275. https://doi.org/10.1023/A:1005992430776

Zhao, X., & Wang, D. (2010). Mercury in some chemical fertilizers and the effect of calcium superphosphate on mercury uptake by corn seedlings (Zea mays L.). *Journal of Environmental Sciences*, *22*(8), 1184–1188. https://doi.org/10.1016/S1001-0742(09)60236-9

Zheng, Y., Hu, Z., Pan, X., Chen, X., Derrien, D., Hu, F., Liu, M., & Hättenschwiler, S. (2021). Carbon and nitrogen transfer from litter to soil is higher in slow than rapid decomposing plant litter: A synthesis of stable isotope studies. *Soil Biology and Biochemistry*, *156*, 108196. https://doi.org/10.1016/j.soilbio.2021.108196

Zhou, J., Obrist, D., Dastoor, A., Jiskra, M., & Ryjkov, A. (2021). Vegetation uptake of mercury and impacts on global cycling. *Nature Reviews Earth & Environment*, *2*(4), 269–284. https://doi.org/10.1038/s43017-021-00146-y

Zhou, J., Wang, Z., & Zhang, X. (2018). Deposition and Fate of Mercury in Litterfall, Litter, and Soil in Coniferous and Broad-Leaved Forests. *Journal of Geophysical Research: Biogeosciences*, *123*(8), 2590–2603. https://doi.org/10.1029/2018JG004415

Zhou, Y., Grice, K., Chikaraishi, Y., Stuart-Williams, H., Farquhar, G. D., & Ohkouchi, N. (2011). Temperature effect on leaf water deuterium enrichment and isotopic fractionation during leaf lipid biosynthesis: Results from controlled growth of C3 and C4 land plants. *Phytochemistry*, *72*(2–3), 207.

Zohary, D., & Hopf, M. (2000). Domestication of plants in the Old World: The origin and spread of cultivated plants in West Asia, Europe and the Nile Valley. *Domestication of Plants in the Old World: The Origin and Spread of Cultivated Plants in West Asia, Europe and the Nile Valley.*, *Ed.3*. https://www.cabdirect.org/cabdirect/abstract/20013014838

Zohary, D., Hopf, M., & Weiss, E. (2012). *Domestication of Plants in the Old World: The origin and spread of domesticated plants in Southwest Asia, Europe, and the Mediterranean Basin* (4th ed.). Oxford University Press. https://doi.org/10.1093/acprof:osobl/9780199549061.001.0001